UNIVERSITY OF CALIFORNIA,
IRVINE

Characterizing Dry Weather Runoff, Sediment Resuspension and Associated Bacterial Loads into Newport Bay

DISSERTATION

submitted in partial fulfillment of the requirements
for the degree of

DOCTOR OF PHILOSOPHY

in Civil Engineering

by

Robert G. Stein

Dissertation Committee:
Professor Brett F. Sanders, Chair
Professor Stanley B. Grant
Professor John LaRue

2014

Table of Contents

Acknowledgements

First and foremost, I would like to thank my advisor Brett Sanders for giving me the opportunity to enter the Civil Engineering doctoral program at UCI and to see and participate in some of the groundbreaking scientific work being pursued by the department. I would like to express my heartfelt appreciation for his insights, advice and exceptional patience in guiding me through my research.

My co-advisor, Stanley Grant, very generously allowed me access to initial results of his field studies as well as draft manuscripts, and provided key suggestions at critical points in my work. During the year my advisor was on sabbatical, Professor Grant graciously invited me to attend and participate in his graduate seminars.

I would like to acknowledge Megan A. Rippy, Brett Sanders, Kristen Davis, Karen McLaughlin, Jack Skinner, John Kappeler and Stanley B. Grant, co-authors of the material in Chapter 4 which has been submitted as a manuscript for review to *Environmental Science & Technology* for possible publication.

Several professors were members of my various committees, agreeing to serve and provide insight on my research: Brett Sanders, Staley B. Grant, John LaRue, Sunny Jiang, Soroosh Sorooshian, Bisher Iman and William Cooper.

Special thanks are extended to Jochen Schubert for assistance with the numerical modeling; to Ying Poon, Craig Jones, John Kappeler, and Jack Skinner for assistance in defining and performing field studies key to this dissertation; and to Jong Ho Ahn for sharing important suspended sediment data.

Many individuals in the southern California government and scientific community took time to supply data for my research including Tom Rossmiller, Monica Mazur, Donna Ferguson, Chris Crompton, Jian Peng and Jamie Habben. I had long-term administrative support from Lorrie Aguirre and Yi-san Chang-Yen. I would also like to thank Fei Zhong and Weixia Jin who were the first to encourage me to embark on a doctoral program in engineering. Special thanks to my good friend and unofficial advisor Ying Poon who steered me to the engineering program at UCI and introduced me to my advisor Brett Sanders.

Finally, I am forever indebted to my wife, Marguerite Albanez whose belief in me never faltered.

List of Figures

List of Tables

Curriculum Vitae

Robert G. Stein

EDUCATION

Ph.D. in Civil Engineering **2014**
University of California, Irvine

M.S. in Civil Engineering **1995**
University of California, Irvine

B.S. in Civil Engineering **1982**
University of California, Irvine

B.A. in Physics **1977**
University of California, Santa Cruz

EXPERIENCE

Assistant City Engineer **1999–present**
City of Newport Beach Public Works Department *Newport Beach, California*

Senior Engineer **1995–1999**
Moffatt and Nichol Engineers *Long Beach, California*

Senior Engineer **1991–1995**
John Carollo Engineers *Santa Ana, California*

Project Manager **1987–1991**
RMS Engineering *Irvine, California*

Assistant Civil Engineer **1984–1987**
Los Angeles County Public Works Department *Los Angeles, California*

Assistant System Test Engineer **1982–1984**
Mare Island Naval Shipyard *Vallejo, California*

Peace Corps Volunteer **1977–1980**
Peace Corps *Gbinti, Sierra Leone*

Abstract of the Dissertation

Characterizing Dry Weather Runoff, Sediment Resuspension and Associated Bacterial Loads into Newport Bay

by

Robert G. Stein

Doctor of Philosophy in Civil Engineering

University of California, Irvine, 2014

Professor Brett F. Sanders, Chair

Fecal indicator bacteria (FIB) impairment of coastal water bodies is a wide-spread problem that impacts recreational water contact and shellfish harvesting. Storm water runoff is a major contributor to FIB during wet weather periods leading to beach closures or warnings to stay out of the water for several days after a storm event. However, FIB impairments also occur during the dry season when the levels of water-contact recreation are highest, especially at enclosed beaches. The causes and remedies of these problems can be difficult to identify.

This dissertation addresses the impacts of dry-weather runoff on FIB impairment in Newport Bay, California. The vast majority of runoff ($\sim 95\%$) enters the bay at two creeks located several kilometers from recreational waters, while only about 1% of the runoff enters the bay through over a hundred small drains located within the

recreational waters. This dissertation examines the relative impact of these large and small runoff sources based on bay-wide mixing and transport processes. Dry weather flow rates are reported as a function of drainage area based on limited field sampling and a regression analysis, and loads of FIB into the bay area estimated based on measured FIB concentrations in runoff and the volumetric flow rate. A 2D flow and scalar transport model is developed and calibrated for prediction of bay-wide salinity, and subsequently applied to simulate the relative impact of large and small drains on FIB impairment. Results show that small drains with minimal fresh water discharges contribute disproportionally to FIB impairment due to their proximity to recreational waters and minimal mixing therein. Further, a "trap-and-release" mechanism whereby runoff accumulates in drain pipes during rising tides and is released at low tide is modeled and shown to also contribute to the number of FIB exceedances.

This dissertation also presents analysis of the erosion thresholds and erosion rates for sediments in Newport Bay which indicate that sediment resuspension occurs only in the main channel and only during energetic spring tide conditions, during the dry weather months. This result suggests that resuspension of contaminated sediments is most likely not a significant contributor to FIB impairment during dry-weather periods.

Chapter 1

Introduction

1.1 Newport Bay and Watershed

Newport Bay, an 8-km^2 (3.1 square mile) tidal saltwater embayment located in Orange County, California is the receiving water for a 360 km^2 (139 square mile) watershed that has seen rapid development since the mid-1960s. Newport Bay is located approximately 32 km southeast of Los Angeles Harbor and 130 km northwest of La Jolla in San Diego County, and is divided into two distinct geographic regions. Upper Newport Bay, located north of Coast Highway (Highway 1), is oriented in a northeast direction and is about three miles long. It is an important salt marsh estuary and state ecological reserve and provides refuge, foraging areas, and a breeding ground for a number of threatened and endangered species. Upper Newport Bay is owned and managed by the California Department of Fish and Game and the County of Orange, and surrounded by property owned by the County of Orange and City of

Newport Beach (City of Newport Beach, 2009). Lower Newport Bay, south of Coast Highway, is sheltered from the open ocean by the 5.6 km Balboa Peninsula which is completely developed. The harbor (Newport Harbor) in Lower Newport Bay is 6.4 km long oriented in a northwest direction parallel to the coastline with the harbor entrance located at the south end of Balboa Peninsula. The harbor also encompasses a portion of the upper bay near Coast Highway and includes areas around Newport Dunes and Dover Shores. Contained within the protected harbor are seven developed islands which were stabilized as a result of dredging done in the 1920s. The three largest islands are Balboa Island and Little Balboa Island (Balboa Islands) and Lido Island. (See Figure 1.1.) The harbor area is a tourist attraction and one of the largest pleasure craft harbors in the United States.

Newport Bay was formed by the Santa Ana River which has meandered from geologic times. In the middle Pleistocene time, the river cut a trough which is now Newport Bay. A series of marine and estuarine deposits now fill the bay floor (Trimble, 1998).

Two principal creeks terminate in Upper Newport Bay: Santa Ana-Delhi Channel and San Diego Creek. These creeks account for approximately 95% of the freshwater flow into the bay. The hydraulic connection of the Santa Ana-Delhi Channel to Newport Bay is relatively recent. Historically, the Santa Ana-Delhi watershed drained to the west into the Santa Ana River. However, around 1900, farming intensified in the area and improved drainage was needed. It is probable that during the late 19th century, farming interests excavated a ditch to Upper Newport Bay to drain the

Figure 1.1: Major features of Newport Bay located in the City of Newport Beach, California.

land. In the 1960's, Orange County Flood Control District (OCFCD) converted these ditches into concrete channels (OCFCD, 1964). The Santa Ana-Delhi Channel and its tributaries now drain approximately 44 km^2 (17 square miles) from areas principally located in the Cities of Santa Ana and Costa Mesa (Trimble, 1998).

Changed Hydrology

The principal watercourse into Newport Bay is San Diego Creek whose tributary area accounts for approximately 316 km^2 (122 square miles) or about 80% of the Newport Bay Watershed area (U.S. Army Corps of Engineers, 1999). The history of the hydraulic connection of San Diego Creek to Upper Newport Bay is complicated and interesting. Before 1870, all of the San Diego Creek watershed streams and canyon washes terminated in a large marsh area called the Swamp of the Frogs in the Tustin Plain (in an area roughly bounded by Highway 55, Highway 405, Culver Drive and Highway 5 in what is now the City of Irvine) where the flat slopes decreased flow velocities allowing for rapid infiltration of water into the coarse sediments of the plain. Flood flows were blocked from flowing into Upper Newport Bay by a narrow ridge at the head of Newport Bay (Meixner, 2004). Beginning in 1890, drainage ditches were installed in the Tustin Plain to drain the shallow aquifer to allow for irrigated commercial crops and orchards. By 1928, the network of drainage channels had been significantly expanded by the Irvine Company for large-scale agricultural operations. It is reported that the groundwater table dropped by an average of 10 meters. By 1932, a channel had been dug towards upper Newport Bay and the ridge that had

historically dammed water in the Tustin Plain was breached. This connected a small portion of the watershed into a wetland at the head of Newport Bay where runoff could make its way to the bay (U.S. Army Corps of Engineers, 1972; Hoag, 1983).

Severe erosion around the drainage channels and concerns of flood damage constrained this area to only agricultural practices with virtually no residential or commercial development in the Swamp of the Frogs prior to the 1960's (USGS, 1965). In 1964, to create favorable conditions for residential and commercial development, OCFCD instituted a flood control program to convert the irrigation drainage ditches to trapezoidal channels and storm drains that drained to San Diego Creek or Peter's Canyon Wash, the primary tributary to San Diego Creek. Additionally, as part of this flood control program, and in cooperation with the Irvine Company, Peter's Canyon Wash and San Diego Creek were widened and deepened (OCFCD, 1967; Hibbs and Lee, 2000). In 1968, San Diego Creek was improved and extended downstream to MacArthur Boulevard to within about 1.6 km (one mile) of Upper Newport Bay (OCFCD, 1964). Before the final reach connecting San Diego Creek to Newport Bay could be constructed, a large storm in 1969 struck the watershed and the resultant storm flows conveyed down San Diego Creek blew through the interfering ridge and hydraulically linked the creek to Upper Newport Bay washing a massive amount of sediment into Upper Newport Bay (Trimble, 1998). As the upper bay continued to silt in, businesses joined with government in 1979 to create a standing sediment management committee to develop a plan to prevent the bay from completely filling with sediment. Trapping basins were constructed in the foothills, San Diego Creek and

Newport Bay to control sedimentation (Maurer and Rozengurt, 1997). The extensive flood control improvements created a climate for intense urbanization that began in the mid-60's, continues today, and transformed Orange County into the fifteenth urbanized area in the country. The remaining large tracts of agricultural land in the northeastern portion of the City of Irvine are now under development.

While upstream control measures and a large bay dredging operation in the 1990's eased sedimentation of Newport Bay, upstream erosion continues to be a problem. Severe winter storm seasons, such as the El Niño winter of 1997, carried several hundred thousand cubic meters of material from the foothills, along with material stored in the creeks and eroded from the earthen portions of the flood channels, into in-channel and in-bay sedimentation basins filling them nearly to capacity. In that year alone, channel erosion, including incising and loss of bank slopes, were clearly evident along Serrano Creek and other tributaries to the bay (Maurer and Rozengurt, 1997).

Water Quality Concerns

The massive release of sediment into Upper Newport Bay in 1969, immediately followed by a sharp increase in urbanization of the watershed, resulted in the introduction of large pollutant loads into the bay. Beginning in the 1970's, the County Health Care Department, County of Orange and the Regional Water Quality Control Board began regular monitoring of sediment, fecal indicator bacteria (FIB), nutrient, and toxic pollutant (metals and pesticides) loads. Newport Bay is now listed

as impaired for all of these constituents and subject to Total Maximum Daily Load (TMDL) requirements. A TMDL for a particular constituent is established such that the capacity of a water body to assimilate the pollutant load without deleterious impact to humans or the benthos is not exceeded (US EPA, 2002).

Of particular concern are enclosed beaches. Sheltered from the large waves and strong currents of open coastlines, these beaches are popular destinations for recreational bathers, particularly families with young children. Unfortunately, these enclosed beach sites also have among the highest rates of pollution-related closures and health advisories. In the 1970s, water samples at popular beaches in Newport Bay often found exceedences for FIB. During the summers of 1999 through 2004, 15% of water samples collected from enclosed beaches in Southern California exceeded marine bathing criteria for FIB, the water quality index used by public health officials to assess if beaches are safe to swim. By comparison, less than 3% of samples collected at open coastal beaches exceeded State criteria over the same time period (Largier *et al.*, 2006). At enclosed beaches, FIB can originate from beach-side sources (bather shedding, bird and dog feces, tidal washing of sediments, decaying vegetation, runoff from drains, and shallow groundwater discharge) and/or bay-side sources (sewage outfalls, creeks, and rivers) (Grant *et al.*, 2010).

Newport Bay is now a targeted watershed for priority water quality enhancement initiatives by the RWQCB (Lee *et al.*, 2001). Studies performed to identify upstream sources of constituents of interest have led to the implementation of projects and *best management practices* that have been successful in reducing constituent loads to

the bay. While substantial progress has been made in reducing loads from sediment, nutrients and FIB, no constituent has yet been delisted. A more rigorous understanding of pollutant sources and loading would facilitate cleanup of the constituents of interest. For instance, recent studies indicate that a significant fraction of the bay's pollution problem is thought to originate from dry-weather runoff that flows into the bay from numerous creeks and channels including San Diego Creek, Santa Ana Delhi Channel, Big Canyon Creek, and Santa Isabella Channel as well as over 200 storm drains that directly discharge into the bay (EOA, 2001; Pednekar *et al.*, 2005; Jeong *et al.*, 2005; Grant, 2008). Most urban areas in southern California have separate storm and sanitary sewer systems. Thus, dry weather runoff generated by over-irrigation of landscapes (generally consisting of non-native, ornamental plants) for example, is conveyed directly to receiving waters through the local storm drainage system. Dry weather runoff is a well-documented source of FIB at marine recreational beaches (Reeves *et al.*, 2004). Indeed, California's numerical criteria for FIB were motivated, in part, by an epidemiological study (the so-called Santa Monica Bay Study) that found bathers were at an increased risk of developing gastroenteritis if they recreated near storm drains discharging dry weather runoff (Haile *et al.*, 2009). Since the Santa Monica Bay Study, entrainment and alongshore transport of wet and dry weather runoff from storm drains and urban rivers has been studied at a number of open coastal beaches with relatively large wave-to-tide ratios (Wong *et al.*, 2013; Rippy *et al.*, 2013; Clark *et al.*, 2007; Grant *et al.*, 2005). However, insights from open coastal beaches are unlikely to apply at enclosed beaches, where breaking waves less influence

the transport of FIB along the shoreline. Furthermore, enclosed beaches are potentially impacted by dry weather runoff from tributaries and stormwater drainages of various sizes. Assessing the relative importance of these different dry weather runoff sources can be challenging, because it is not *a priori* obvious if water quality at a particular beach is most influenced by large sources of dry weather runoff located relatively far from the beach, or small sources of dry weather runoff discharging at the beach.

1.2 Challenges for Quantifying Sources and Loads to Newport Bay

Nationally, increasing attention is being paid to the impacts of dry-weather urban runoff on water quality in estuarine systems (State Water Resource Control Board, 2012; Regional Water Quality Control Board, 2008). For some constituents, loads associated with dry weather runoff may be more significant than loads associated with storm flows (Weston Solutions, 2007). Dry-weather flows, which are commonly fluctuating or intermittent, are generated from a various sources including over-irrigation and washdown activities, as well as dewatering operations and drainage from groundwater subdrains. These flows can mobilize constituents of concern present on roadways, on landscaped areas or in groundwater, and transport these pollutants into storm drain systems and then into a flood conveyance channel, creek, or embayment. The discharge point into a receiving water is potentially a compliance point where con-

formance with water quality standards is assessed. Under the current trend, federal and State agencies are moving forward by limiting allowable contaminant loads from upstream sources to receiving waters. Further, the basis for water quality improvement programs is typically an inventory of all pollutant loads to identify priorities for control measures. As there are no analytical methods for estimating dry-weather flows, field monitoring of flow and contaminant concentrations is currently the only option. But the scope of monitoring is prohibitively expensive for water bodies like Newport Bay which receive flows from hundreds of drains that experience intermittent flows as well as tidally influenced flows, which are difficult to measure. Attempts to extrapolate flows based on limited data have proven controversial.

Another important load arises from the resuspension, transport and settling of contaminated sediments. It has been widely documented (Preston *et al.*, 1972; Kirby and Parker, 1973; Hayter, 1986; Yan, 1995) that nutrients and pollutants are readily sorbed to fine-grained sediment tying water quality issues directly to the fate and transport of estuarine sediment. Contaminant loads in storm drains can be associated with particulate matter, and subjected to flocculation and possible deposition onto the bed sediments when freshwater flows enter the brackish water of an embayment. And beyond water quality considerations, erosion, transport and deposition of fine-grained sediment in estuarine waters can create significant problems including shoreline scour, channel shoaling problems and highly turbid waters that inhibit light penetration which in turn can negatively impact the biological productivity of the benthic community.

The manner in which estuarine cohesive sediment suspensions respond to hydrodynamic forcing is complex due to the interactions between the flow field and the high concentrations of suspended sediment near the bed which alters and links the fundamental transport processes of erosion, entrainment, eddy diffusion, flocculation/aggregation, settling, deposition and consolidation of cohesive sediments. Through sedimentation and resuspension cycles, fine sediment (<62.5 microns) cycles between a bed matrix, fluid mud layer, and the low concentration fluid suspension layer in the upper water column. Periods of low velocity promote settling of suspended sediments, formation of a near-bed fluid-mud layer, and consolidation of the bed matrix. Figure 1.2 illustrates the concept of a fluid mud layer in an estuarine system, essentially a thin, partly-consolidated soil layer or high concentration slurry at the interface between the sediment bed and the water column. As fifty to ninety percent of the sediment load may be transported as fluid mud (Kirby, 1986; Smith and Kirby, 1989; Kendrick and Derbyshire, 1985; van Leussen and van Velzen, 1989), numerical models that neglect the near bed fluid mud layer may yield unrealistic results in calculating the flux of the sediment transport over the water column making these models unsuitable tools for predicting changes based on proposed implementation of best management practices.

Many studies have shown that bacteria survive for long periods of time in estuarine sediments (Savage, 1905; Roper and Marshall, 1979; Labell *et al.*, 1980; Davies *et al.*, 1995). Bacteria in fluid suspensions may be either suspended or attached to particles or flocs. In water bodies with high suspended sediment concentrations, the majority

of bacteria are thought be attached to particles (Kirchman, 1983; Geesey and Costerton, 1979; Goulder, 1976). Lind and Lind (1991) found that the number of bacteria attached to suspended particles (attached bacteria) in a subtropical lake averaged four to seven times greater than the number of free-floating bacteria and that this relationship was strongest at high turbidity sites. The biomass of attached bacteria has been shown to increase with increasing suspended sediment concentration (Lind and Lind, 1991; Goulder, 1976). Koske *et al.* (1966) found in Kiel Bay a remarkable parallelism between the vertical distribution of suspended sediment and total bacteria (suspended plus attached). In the upper Bay of Fundy, in Southeastern Canada, the proportion of attached bacteria reached 94 percent of the total bacterial numbers with a strong correlation to turbidity (Cammen and Walker, 1982). And Ferguson *et al.* (1996) found a significant positive correlation between turbidity (caused by suspended sediment) and enteric bacteria concentrations in the Georges River estuary. Recent studies have shown that regrowth occurs in estuarine sediments (Desmarais *et al.*, 2002), sediment cycling may contribute significantly to concentrations of bacteria within the upper water column. This hypothesis is supported by several studies that have reported strong linkages between suspended sediment and bacteria concentrations (Ferguson *et al.*, 1996), but not by others where only a weak correlation has been observed (Jensen *et al.*, 1979). An understanding of the vertical structure of the sediment, especially the near bed fluid mud layer, would assist in assessing contributions of contaminants into the water column and formulating effective monitoring and mitigation programs.

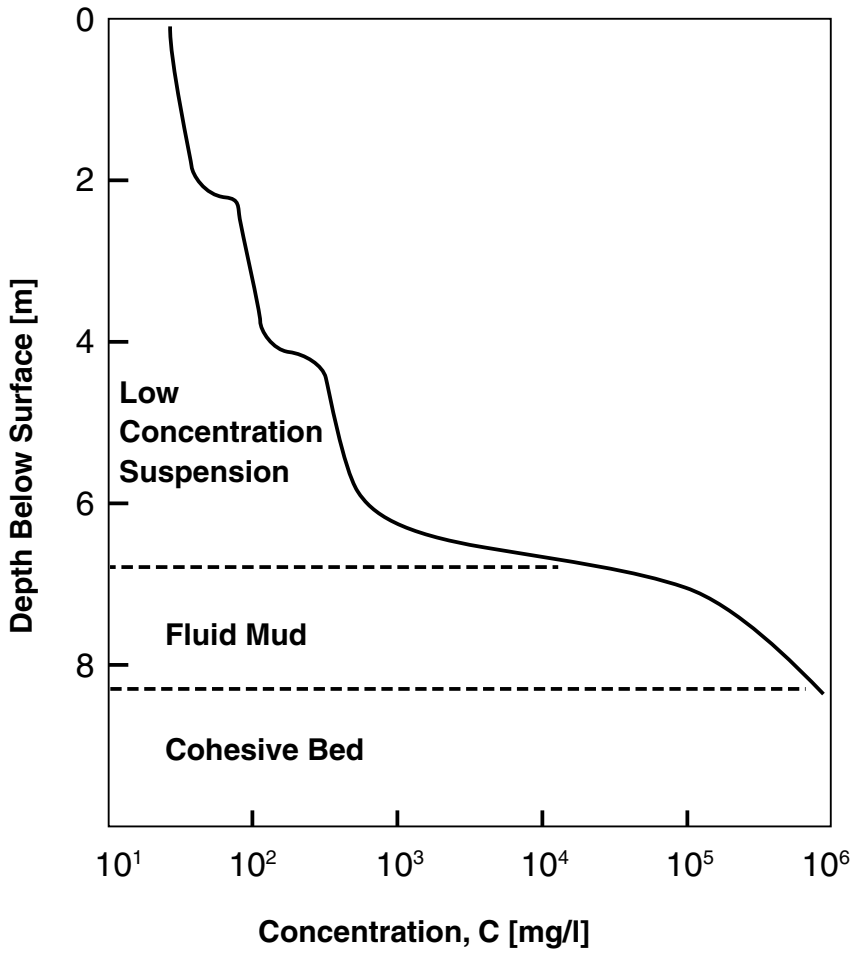

Figure 1.2: Vertical structure of sediment illustrating the concept of a fluid mud layer at the interface between the sediment bed and the water column.

1.3 Dissertation Objective and Outline

The objective of this dissertation is to advance a better understanding of two dry-weather distributed loading mechanisms in Newport Bay that will be central to future water quality management: (1) The magnitude of dry weather urban runoff from the hundreds of small to medium-sized storm drains that empty into Newport Bay; these flows are very difficult to measure directly but potentially important given their vast numbers, and (2) the magnitude and spatial distribution of sediment resuspension during dry-weather periods, in response to tidal currents. In addition to investigating these two dry-weather loading mechanisms, another objective of this dissertation is to improve the characterization of tidal circulation to better understand how this process acts to redistribute loads from storm drains and resuspended sediment.

To pursue these objectives, this dissertation presents analysis of dry weather flows from storm drains, tidal circulation, and tidally forced sediment resuspension and transport. Data from several field studies conducted in Newport Bay are used:

1. Measurements of dry-weather flows in the five largest storm drains emptying into Newport Bay in coordination with the City of Newport Beach (Everest International Consulting, 2006).

2. Measurements of dry-weather flows from ten small storm drains emptying into Newport Bay (City of Newport Beach, 2009).

3. Measurements of bay salinity at the outlets of 86 storm drains under dry-weather

conditions (Grant *et al.*, 2008).

4. Measurements of salinity and sediment concentrations at eight transects along the length main channel of the Newport Bay including a transect at the western end of the harbor (Grant *et al.*, 2008).

5. Measurements of FIB in drainage conveyances and in the Bay (Grant *et al.*, 2008).

6. Measurements of sediment properties and erosion rates from cores collected from the sediment bed in coordination with the City of Newport Beach (Sea Engineering, Inc., 2007).

This dissertation presents an original model to predict the intermittent release of fresh water from tidally flooded storm drains, a vertical one-dimensional (1D) model to investigate the vertical structure of sediment concentrations in Newport Bay, and the application of a two-dimensional (2D) numerical model to predict transport of both fresh water and sediment. Numerical models have been used successfully to predict constituent concentrations in coastal waters and embayments (Kashefipour *et al.*, 2002; Fiandrino *et al.*, 2003; Steets and Holden, 2003) and have been used to identify the relative impact of various sources (e.g., tributary creek loads versus storm drain loads), characterize the mechanisms governing the fate of these organisms (e.g., flushing versus die-off) and predict the efficacy of a range of potential management measures (Sanders *et al.*, 2005). Newport Bay is stratified episodically with storm

water input, but during dry-weather conditions, a 2D model provides a basic description of how well-mixed constituents (fresh water, sediment, etc.) can be transported laterally around the water body.

The dissertation is divided into two sections each consisting of three chapters. In the first section, Chapter 2 presents the formulation and calibration of the 2D model. Chapter 3 presents an analysis of dry-weather flows from storm drains, including the synthesis of field data and the presentation of an original model to describe the intermittent trap-and-release of runoff from tidally influenced storm drains. In Chapter 4, the impact of FIB loads in dry weather runoff from small drains on nearshore water quality in Lower Bay is examined providing validation for the trap-and-release model.

In the second section, Chapter 5 reviews basic properties of cohesive sediment including settling velocity, flocculation, and entrainment of cohesive bed sediment and the overlying fluid mud. In Chapter 6, a vertical, 1D model was developed to analyze near-bed sediment dynamics with the goal of determining whether a fluid mud layer in Newport Bay may be an important feature relative to sediment (and FIB) transport. Chapter 7 presents the analysis of four bed cores from Newport Bay which support the development of a quantitative model of erosion rates for Newport Bay. The 2D model is then run to predict the spatial and temporal distribution of resuspended sediment, which is compared with measurements to reveal the potential significance of sediment resuspension as a contributor to bay-wide water quality impairment.

Chapter 2

Newport Bay Hydraulic Model

This chapter presents the formulation, calibration and evaluation of a 2D numerical model that is applied in Chapter 3 for estimating dry-weather flows and characterizing bay-wide salinity transport, in Chapter 4 for characterizing bacterial loads associated with dry-weather flows, and again in Chapter 7 for characterizing bay-wide sediment transport. Following preliminary sections on model formulation, parameterization, and calibration, an evaluation of the model is presented to characterize uncertainties in model predictions and identify a model configuration (choice of boundary conditions, inputs, etc.) that is suitable for advancing an improved understanding of bay-wide salinity (Sections 2.4 to 2.6). Factors considered include the tidal forcing time series, the fresh water input time series, and the required modeling duration. Attention to these factors is motivated by the unsteadiness of the tidal forcing and the intermittency of fresh water inputs. The descriptive skill of the model is evaluated by a comparison to salinity measurements at nine channel sites spanning

the length of Newport Bay, including a station in the western part of lower bay which does not fall along the primary axis of the estuary. The chapter closes with several modeling scenarios revealing bay-wide 2D circulation patterns that bear on salinity, sediment and pollutant transport.

2.1 Model Formulation and Parameterization

The 2D model is based on the assumption of hydrostatic flow and rapid vertical mixing of salinity and sediment. The 2D model does not resolve stratified flow conditions which have been observed near the outlet of San Diego Creek, particularly during and after storm events (Grant *et al.*, 2008), but can be expected to provide a basic description of lateral scalar transport in lower bay and the parts of upper bay that are well-mixed. Use of a 2D model also allows a finer resolution mesh (as fine as 1.5 meters) than would otherwise be possible with a three-dimensional (3D) model for the same computational effort, enabling greater resolution of fine scale details such as small upper bay channels and nearshore mixing in lower bay.

The 2D model solves depth-integrated flow and transport equations using an unstructured-grid Godunov-type finite volume scheme (Begnudelli and Sanders, 2006). A structured-grid version of the model was successfully applied to simulate tidal dynamics, salinity transport, transport of a unit impulse load of dye, and transport of fecal indicator bacteria in nearby Talbert Marsh (Arega and Sanders, 2004; Sanders *et al.*, 2005). Importantly, the model was successfully applied to simulate fecal indicator bacteria dynamics at tidal time scales in response to sediment resuspension (Sanders

et al., 2005). A key advantage of the model is a robust treatment of wetting and drying fronts including the ability to track scalar concentrations without artificially adding or losing scalar mass (Begnudelli and Sanders, 2006). The primary drawback of the model is that it cannot resolve stratified flow. Previous work has indicated that the main channels of Newport Bay are vertically mixed during dry weather periods, but that stratified conditions may occur locally in response to fresh water inputs (Grant and Sanders, 2010). The model is conditionally stable in accordance with the Courant, Friedrichs, Lewy condition (Begnudelli and Sanders, 2006) which mandates a time step of less than a second due to the fine resolution mesh. In turn, millions of time steps are required to integrate the solution over tidal time scales, but an advantage of a small time step is accuracy including the ability to resolve sharp fronts in scalar concentrations.

The full system of governing equations can be found in Arega and Sanders (2004) and Sanders *et al.* (2005). Here, the transport equation for salinity per unit volume of water, c_s, is presented to introduce key model parameters:

$$\begin{aligned} \frac{\partial}{\partial t}(hc_s) + \frac{\partial}{\partial x}(\bar{u}hc_s) + \frac{\partial}{\partial y}(\bar{v}hc_s) &= \frac{\partial}{\partial x}\left(hE_{xx}\frac{\partial c_s}{\partial x} + hE_{xy}\frac{\partial c_s}{\partial y}\right) \\ &\quad + \frac{\partial}{\partial y}\left(hE_{yx}\frac{\partial c_s}{\partial x} + hE_{yy}\frac{\partial c_s}{\partial y}\right) \\ &\quad + \sum_{k=1}^{N_{ps}} \mathcal{L}_k\, \delta(x - x_s^k, y - y_s^k) \end{aligned} \tag{2.1}$$

where h equals the depth, $\bar{u}$ and $\bar{v}$ are the components of the depth-averaged velocity, E_{xx}, E_{xy}, E_{yx}, and E_{yy} are the elements of the dispersion tensor, and $\mathcal{L}_k$= freshwater

loading rate at the k^{th} point sources, where N_{ps} is the number of point sources, x_s^k and y_s^k= coordinates of the point source, and δ= Dirac delta function. Attention is given to point sources because these are used to model the input of runoff from storm drains.

The first term on the left hand side of Eq. 2.1 accounts for local changes in salinity concentration, the second two terms account for advection by depth-averaged currents, and the diffusive terms on the right-hand side account for shear flow dispersion and turbulent diffusion. The diffusion/dispersion parameters (E_{xx}, etc.) are computed locally based on currents in accordance with an internally computed shear velocity $u_*=(\tau_o/\rho)^{1/2}$ and experimentally observed correlations for the rates of turbulent diffusion and shear flow dispersion (Arega and Sanders, 2004), where τ_o represents the shear stress on the bed of the estuary and ρ is the fluid density. The final term on the right-hand side accounts for sources of fresh water from creek and storm drain flows.

The model domain covers the entirety of Newport Bay up to the high water line and extends several kilometers offshore (into coastal ocean surrounds). The numerical model runs on a unstructured mesh of triangular cells that is constrained in extent by the high water line of the system and locally refined to resolve narrow channels and nearshore transport. The model domain extends inland to Jamboree Road, the head of Newport Bay, and offshore to a depth a depth of approximately 100 meters where the model is externally forced by a time series of total water level. By specifying a deep water tidal boundary condition, the model resolves the flood and ebb of the tide

Dataset	Data Provider	Date	Resolution [meter]	Datum	Vertical Accuracy
LiDAR	Merrick	2006	3	NAVD88	<0.2 m
Lower Bay Bathymetry	Corps Contractor	2005	3	NAVD88	0.03-0.09 m
Upper Bay Bathymetry	Corps Contractor	2002-2003	1	NAVD88	0.03-0.09 m
Offshore Bathymetry	National Ocean Service		100	MLLW	0.3 m

Table 2.1: Summary of Terrain Data

through Newport Bay and associated transport and mixing. The model is also forced by point sources of runoff including two point sources that account for flows from San Diego Creek and Santa Ana Delhi Channel, as well as 12 large drains and 207 smaller drains that flow directly into the bay.

During dry weather conditions, these inputs have a negligible impact on water levels and tidal currents, but an important impact on the salinity distribution. The mesh resolution is varied from 1.5 meters to 100 meters to support localized refinement, in particular modeling of flow through narrow upper bay channels and nearshore transport along the banks of lower bay. The coarsest mesh resolution is used offshore of the harbor mouth.

Several sources of terrain data were obtained and organized to define the bathymetry of the bay. The data sources are summarized in Table 2.1:

1. Upper Bay bathymetric data from an ultra-beam survey by an unknown contractor for the U.S Army Corps of Engineers, Los Angeles District.

2. Lower Bay bathymetric data from an ultra-beam survey by an unknown contractor for the U.S Army Corps of Engineers, Los Angeles District.

3. Light Detection and Ranging (LiDAR) topographic data by Merrick and Company for the City of Newport Beach. This data is important for resolving intertidal topographic heights, including channel banks.

4. Offshore bathymetric data from the National Geophysical Data Center 3 arc-second coastal relief model access from the Southern California Coastal Ocean Observing System website.

To parameterize elevation, a 3-meter Digital Terrain Model (DTM) representing both bathymetry and topography was created from a combination of data sources including aerial LIDAR data and sonar data (Gallien *et al.*, 2011). Elevation was assigned to vertices of the computational mesh from the DTM by inverse-distance weighted interpolation. In the region of interest, along the banks of Lower Bay channels, vertical accuracies of 0.18 cm RMSE (root-mean-square error) are expected based on the accuracy of the aerial LIDAR data (Gallien *et al.*, 2011). Use of accurate topographic data, a numerical model designed for wetting and drying fronts, and a fine mesh resolution along channel banks promotes accurate predictions of shoreline mixing of FIB from runoff under the influence of tidal currents resolved by the model and observed ambient turbulence.

Water level measurements from the Los Angeles NOAA Tide Gage (NOAA, 2006) were used to specific the offshore water level boundary condition. The timing and

duration of the time series is discussed later. All terrain and water level data were placed in metric units and heights were referenced to the North American Vertical Datum of 1988 (NAVD88). Required discharge data were obtained from the County of Orange, which maintains gaging stations along San Diego Creek at Campus Drive and along Santa Ana Delhi Channel near Irvine Avenue at Mesa Street. County discharge data include four measurements per hour (every 15 minutes).

2.2 Dispersion Coefficients

The dispersion coefficients E_{xx}, E_{xy}, E_{yx} and E_{yy} are computed in the model in accordance with the flow direction and the principal components of dispersion known as the longitudinal and transverse dispersion coefficients, ε_L and ε_T, respectively. The longitudinal dispersion coefficient is aligned with the flow and accounts for the diffusive mass flux associated with surface currents moving faster than the mean flow, and bed currents moving slower than the mean flow, a mechanism known as shear-flow dispersion. The transverse dispersion coefficient is aligned normal to the flow direction and accounts for lateral mixing by turbulent eddies. Formally, it represents a depth-averaged turbulent diffusion mechanism.

The longitudinal dispersion for an open channel flow is well-known and given by (Fischer, 1979)

$$\varepsilon_L = 5.93 u_* d$$

where d is the depth and $u_* = (\tau_o/\rho)^{1/2}$ is the shear velocity, the rate of shear in the water column with dimensions of velocity. The transverse dispersion coefficient

is given in a general form as follows (Fischer, 1979),

$$\varepsilon_T = \alpha u_* d$$

where α is a dimensionless turbulent diffusivity which generally varies from 0.1 to 1.0 in shear flows and is estimated to be 0.3 for Newport Bay (see Section 4.3 - Nearshore Turbulence Measurements).

2.3 Manning Roughness Coefficient

The hydrodynamic model accounts for flow resistance with a quadratic drag law for the shear stress at the bed as follows,

$$\tau_o = c_D \rho (\bar{u}^2 + \bar{v}^2)^{1/2} \tag{2.2}$$

and the drag coefficient c_D is scaled by a Manning roughness coefficient n as follows (Begnudelli and Sanders, 2006):

$$c_D = g \frac{n^2}{h^{1/3}} \tag{2.3}$$

The roughness coefficient n can be expected to fall within a range of possible values based on the surface roughness, but it cannot be prescribed precisely. Consequently, calibration of n is common in modeling studies. To calibrate n for Newport Bay, the model was run using n values ranging from 0.015 to 0.100 $\mathrm{m}^{-1/3}\mathrm{s}$ and predicted water levels and velocities were compared to measurements from an S4 directional current meter (InterOcean Science, San Diego, California) at two locations, a mid-channel location near Balboa Yacht basin in lower bay, and a mid-channel location near Newport Dunes in upper bay (Grant, 2004). Figure 2.1 shows that model predictions for

current direction are not sensitive to roughness coefficient n, presumably due to the channelized flow. Additionally, Figure 2.2 shows that current speeds are insensitive to n values ranging from 0.015 to 0.050 $m^{-1/3}s$, while n=0.1 $m^{-1/3}s$ notably attenuates peak speeds. These results indicate there is no optimal n value, so n=0.020 $m^{-1/3}s$ was adopted based on the relatively smooth channel bottom and a previous application in nearby Talbert Marsh where n=0.020 $m^{-1/3}s$ was optimal considering its impact on predicted flow and turbulent dispersion (Arega and Sanders, 2004).

Figure 2.4 shows model predictions of water surface elevation at Station BTO9, a mid-bay location, alongside the water surface elevation specified at the off-shore boundary (measurements in Los Angeles Harbor, taken in 2006). This shows a short spin-up period of less than one tide cycle, and minimal tidal amplification. Gallien *et al.* (2011) report that spring tides are amplified as much as 3 to 4 cm in the bay, compared with off-shore forcing, and that differences between the Newport Bay and Los Angeles Harbor water surface elevations are typically less than 10 cm at any given time. While the differences in Los Angeles Harbor and Newport Bay Harbor water surface heights can be significant from a flooding perspective, because overtopping of just a few centimeters can cause, these differences are far less important for the purpose of modeling tidal currents and circulation. Consequently, Los Angeles water surface measurements are taken here as a reasonable proxy for the water elevation offshore of Newport Harbor, one that is suitable for modeling tidal circulation and transport.

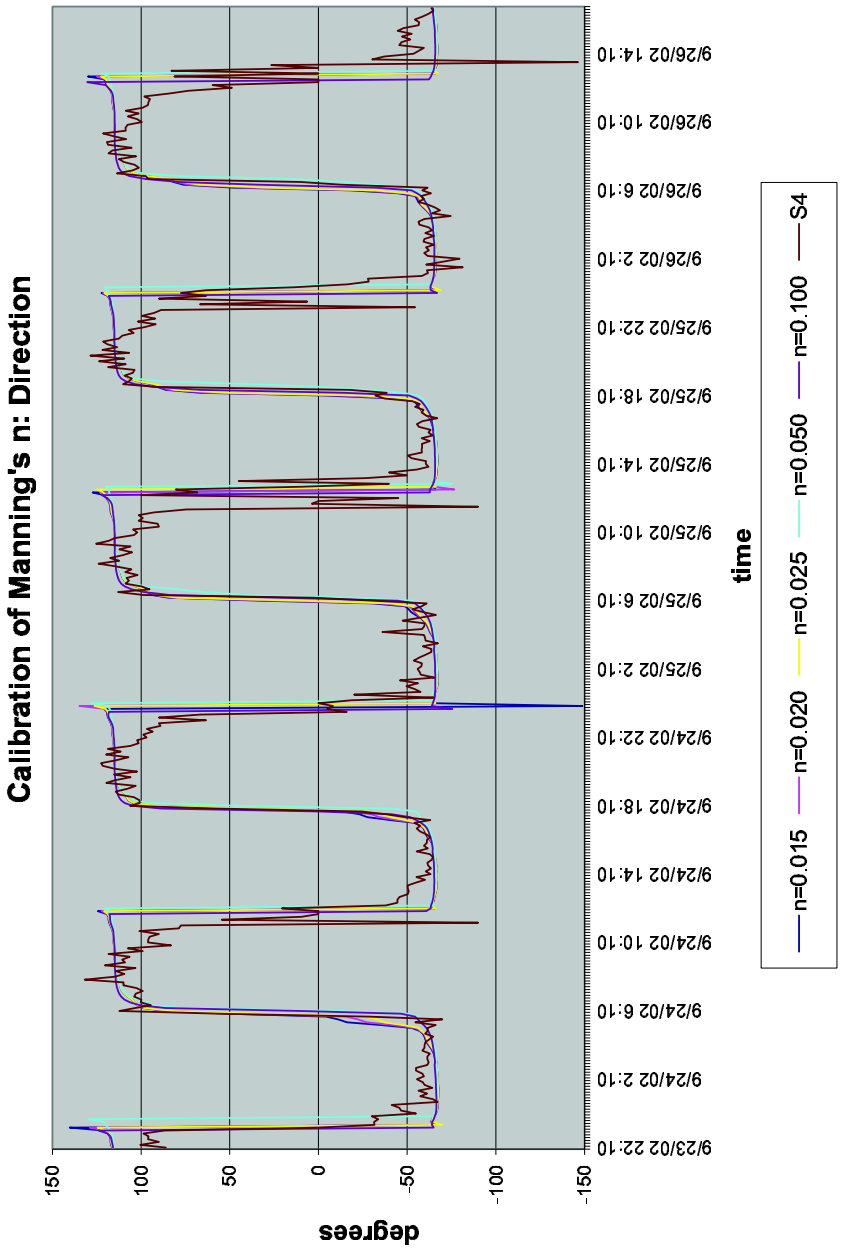

Figure 2.1: Measured and predicted tide direction near the Balboa Yacht Basin using n values ranging from 0.015 to 0.100 $\mathrm{m}^{-1/3}\mathrm{s}$.

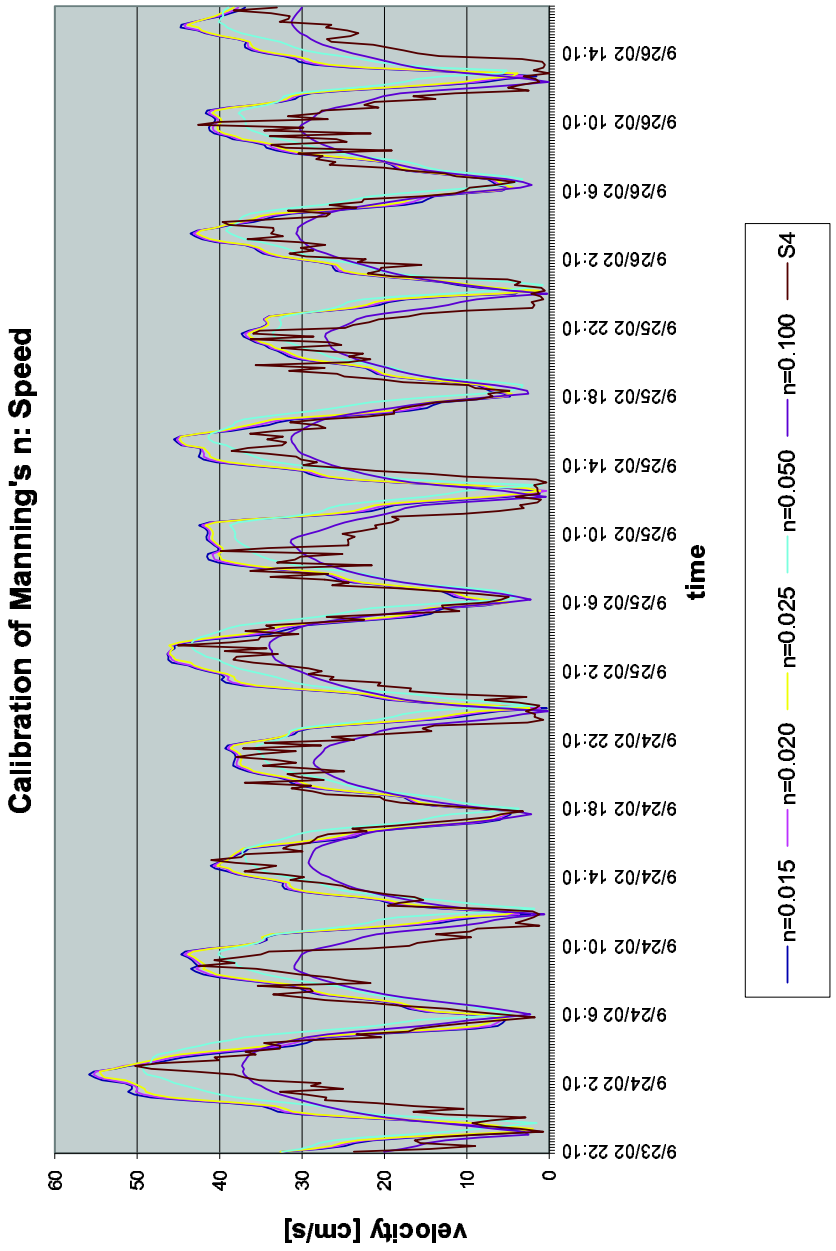

Figure 2.2: Measured and predicted tide speed near the Balboa Yacht Basin using n values ranging from 0.015 to 0.100 $\mathrm{m}^{-1/3}\mathrm{s}$.

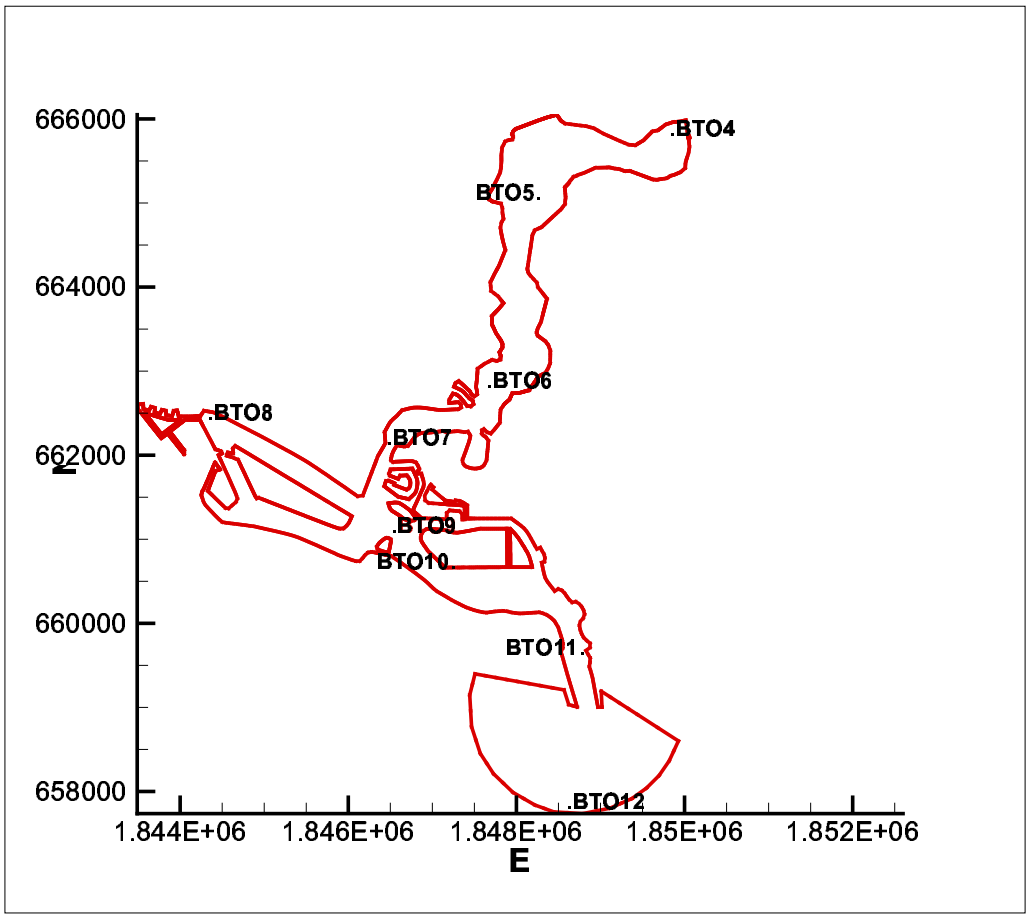

Figure 2.3: Location of BTO Stations

2.4 Modeling Duration Requirements for Tide Dynamics

To estimate the modeling duration needed to capture representative tidal dynamics in the bay, predicted water surface elevations at Station BTO9 for durations of 28,

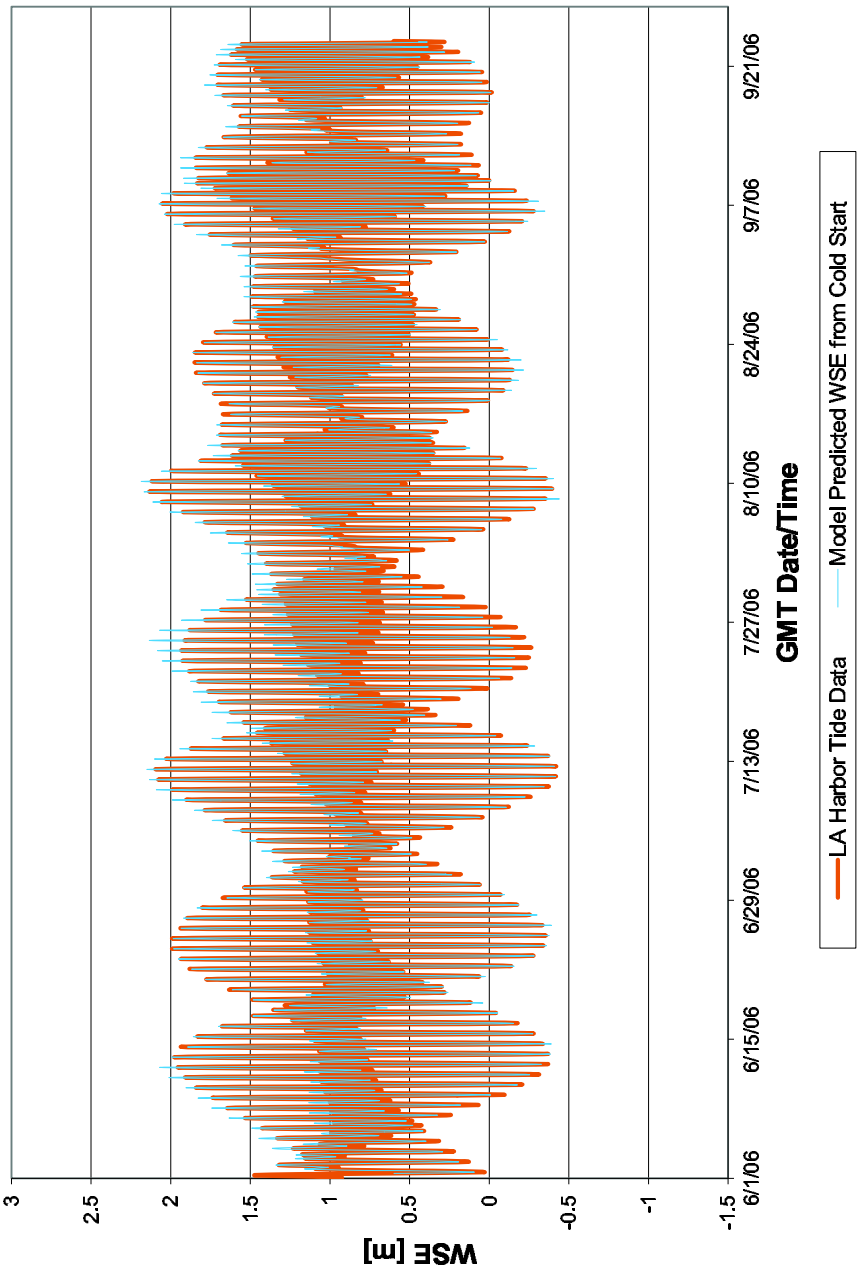

Figure 2.4: Model predicted water surface elevations at Station BTO9 versus tide forcing outside the harbor entrance.

42, and 56 days were compared to a model predictions for a duration of 112 days. For each duration, the probability distribution (or more formally, the cumulative mass function) for that water surface elevation data set is generated by sorting the data set from low to high values and then assigning a proportional frequency (probability) from 0.0 to 1.0. The probability distributions for these four modeling durations are plotted in Figure 2.5. As an example how a probability distribution is interpreted, for a specific tide height, say 0.5 meters, a probability of about 20% can be read on the vertical axis. This means that there is a 20% chance that a randomly measured tide height will be 0.5 meters or less. Conversely, there is an 80% chance that the measured tide height will be greater than 0.5 meters.

In Figure 2.5, it can be seen that with longer modeling durations, there is a convergence of the shorter duration probability distributions toward the reference duration of 112 days. The root-mean-square deviations of the 28-, 42- and 56-day durations with respect to the reference are 6.4%, 4.0% and 2.5% respectively. Consequently, modeling duration of 56 days was considered adequate for representing the tide climate in the harbor.

2.5 Modeling Duration Requirements for Salinity Dynamics

This section presents a similar analysis aimed at understanding the required model duration to capture representative salinity dynamics. In this case, probability distri-

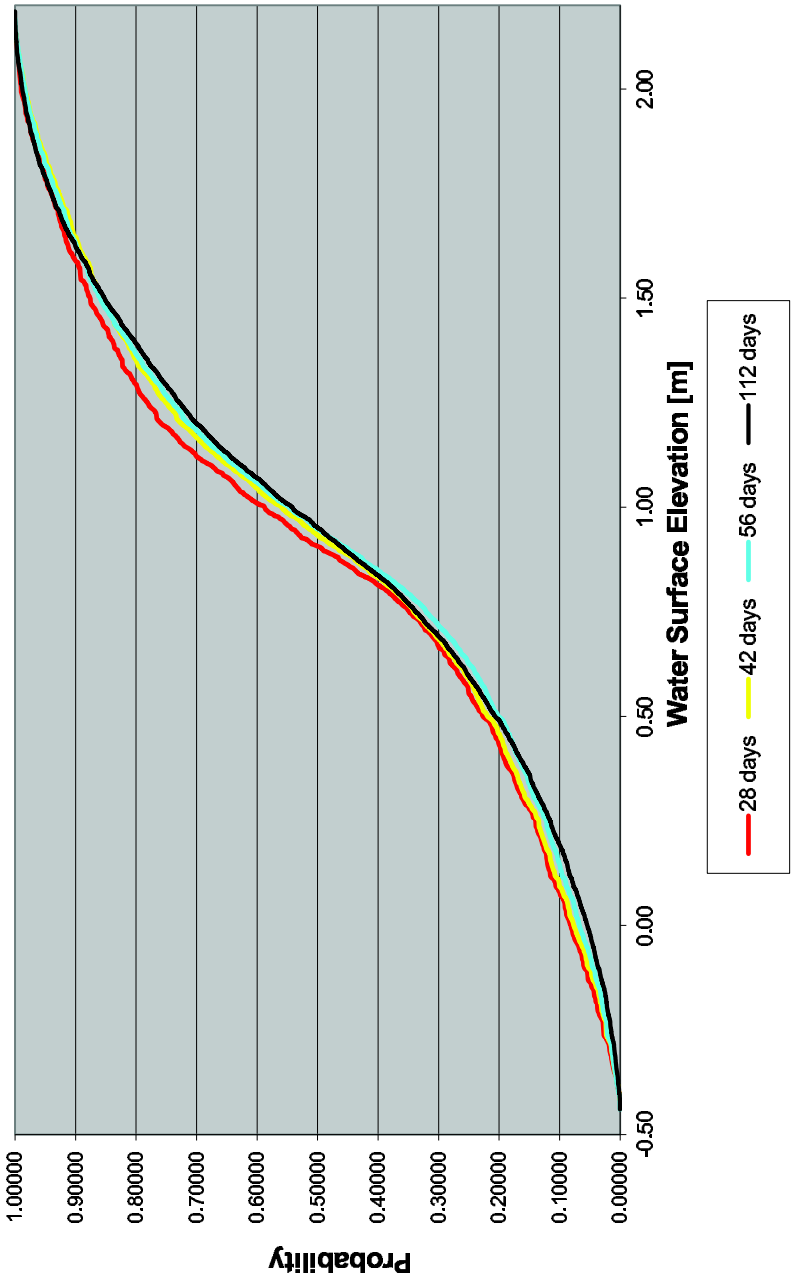

Figure 2.5: Comparison of probability distributions for different modeling durations to approximate tide dynamics.

butions of salinity at numerous stations are compared to field measurements described next.

Bay Salinity Data

Bay salinity data collected in the "Bay-To-Ocean" (BTO) study of Newport Bay (Grant *et al.*, 2008) were used to evaluate the predictive skill of the 2D model with respect to salinity, and to determine a reasonable model duration for studies of bay-wide salinity transport. The BTO study measured salinity along the bay's main axis at seven locations (BTO4, BTO5, BTO6, BTO7, BTO9, BTO10 and BTO11) from the upper bay to the harbor jetty entrance (Figure 2.3). An additional transect, BTO8, was located in the far western part of the bay in the so-called Turning Basin. Along each transect, samples were taken at each bank and at mid-channel. At each sampling point, salinity was measured at the surface and near the sediment bed. The top and near-bottom measurements were used to calculate an *averaged* salinity over the depth of the water column. A separate, *integrated* salinity measurement, was made using a sampling device that collects samples over the depth of the water column. Salinity measurements were collected three or four times per month over a year period. However, for this study, only dry-weather salinity data are used corresponding to the period from April 15, 2006 to November 30, 2006. Samples were generally taken in the late morning before noon with sampling dates and times selected to try and capture tides that would be representative of the dry season period. Figure 2.6 shows the water surface elevation at the time of salinity sampling at Station BTO9 in

relation to the measured water surface elevation during the *dry season* at Los Angeles Harbor. The figure indicates that the samples were obtained over a wide range of tides at different ebb and flood stages, with a slight bias towards ebb tides and low tides.

Salinity Predictions at BTO Stations

To predict salinity, the 2D model was applied with inflow specified at San Diego Creek, Santa Ana-Delhi Channel, and the five largest storm drains emptying into the harbor. These flows were modeled as fresh water: 0.0 ppt salinity. A salinity of 32 ppt was specified at the offshore boundary, which corresponds to the high end of concurrent salinity measurements taken at the harbor mouth which ranged from 30.1-32.1 ppt (Grant *et al.*, 2008). To compare model predictions of salinity with measurements, model predictions were sampled at the centerline of the channel at the time for which the sample was recorded. Salinity probability distributions were then generated for the predicted salinity at each BTO station.

Predicted salinity probability distributions compare with measurements best at mid-bay locations: BTO6, BTO7, BTO9 and BTO10. In Figure 2.7, the probability distributions at BTO6 are plotted for modeling durations of 56, 84 and 103 days and appear to be converging toward the averaged measured salinity. Figures 2.8 and 2.9, respectively, show that probability distributions of BTO7 and BTO9 salinity predictions are converging for longer modeling durations and nicely mimicking the probability distribution of integrated salinity measurements. At Station BTO10

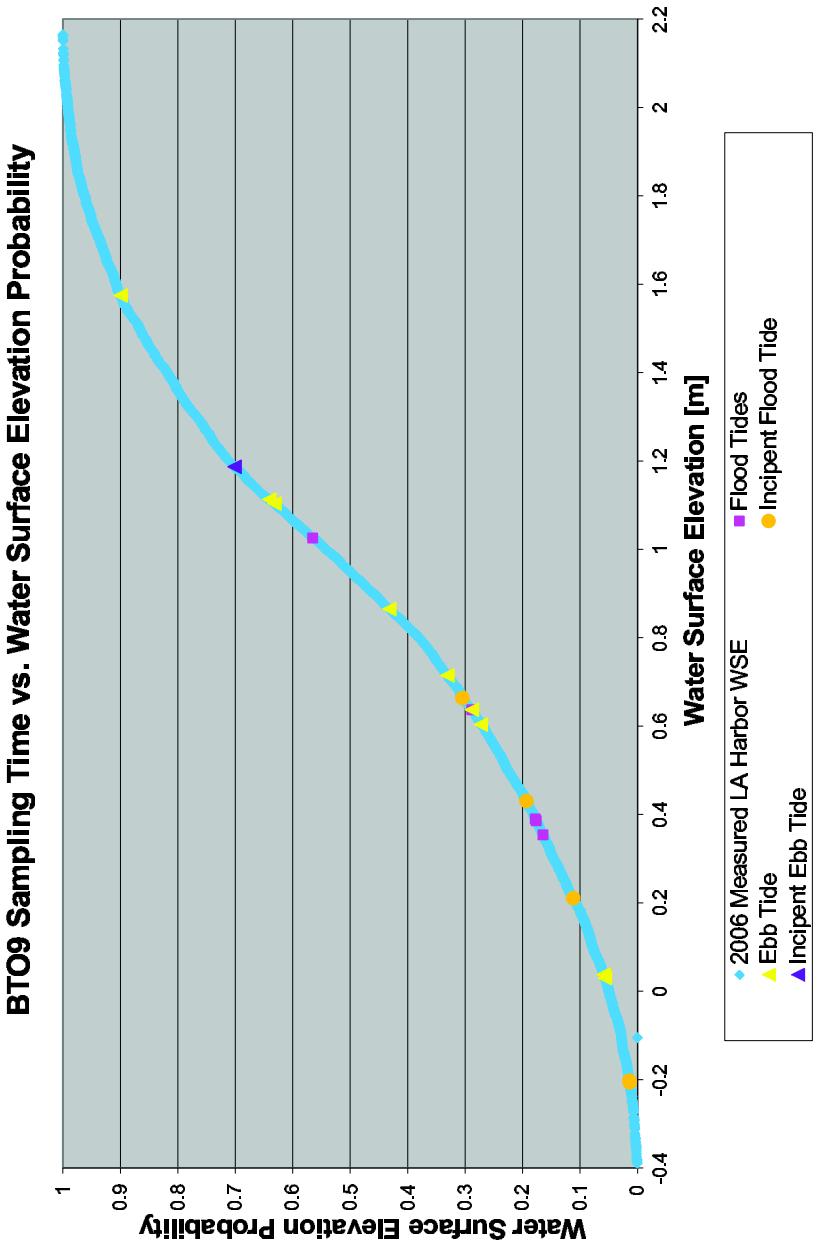

Figure 2.6: Salinity samples taken at BTO9 were obtained over a range of tide conditions.

(Figure 2.10), the longer duration probability distributions converge toward the probability distribution of averaged measured salinity with a lateral offset by about 0.25 ppt.

Figure 2.11 shows that probability distributions of salinity predictions at Station BTO11, located in the harbor jetty entrance, approximate the shape of the probability distribution of salinity measurements but with higher predicted salinities varying from 0.5 to 1.5 ppt. The offset is attributed to differences in ocean salinity that are not captured by the model, which assumes a constant value of 32 ppt.

At Stations BTO4 and BTO5 located in Upper Bay, there is a noticeable difference between probability distributions of predicted and measured salinity (see Figures 2.12 and 2.13, respectively). This is likely because of salinity stratification from San Diego Creek and the Santa Ana Delhi Channel (Grant *et al.*, 2008). Further, this indicates that 2D model predictions of salinity need to be interpreted cautiously at these upper bay locations.

2.6 Sensitivity of Salinity at BTO Stations to Freshwater Inputs

Previous work by Azevedo *et al.* (2009) suggest that both the magnitude and variability of stream flow inputs needs to be considered to accurately model estuarine salinity. Model predictions thus far are based on 15 minute intervals of stream flow data, and here the sensitivity of predicted salinity to streamflow variability is

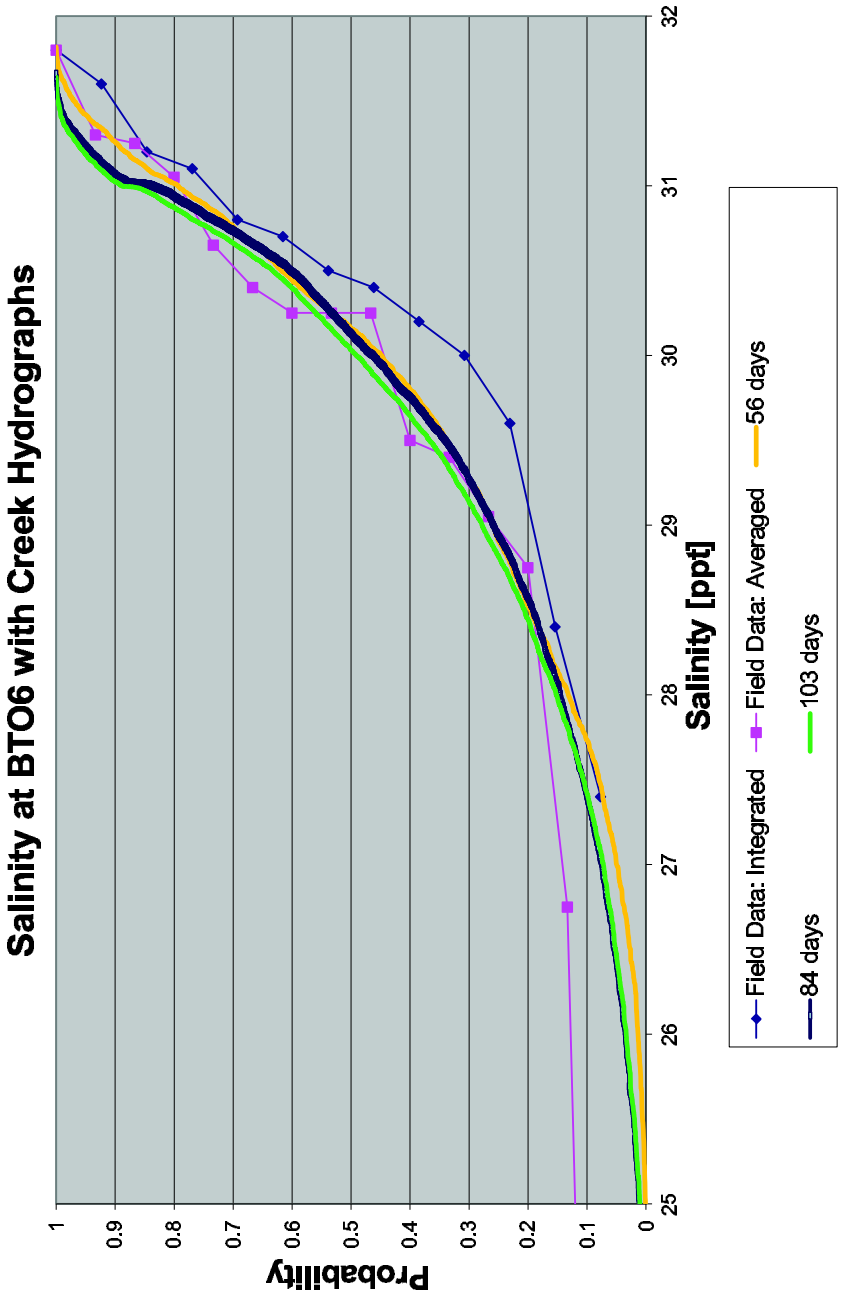

Figure 2.7: Salinity probabilities at BTO6 using hydrographs for flows from San Diego Creek, Santa Ana-Delhi Channel and the five largest harbor storm drains.

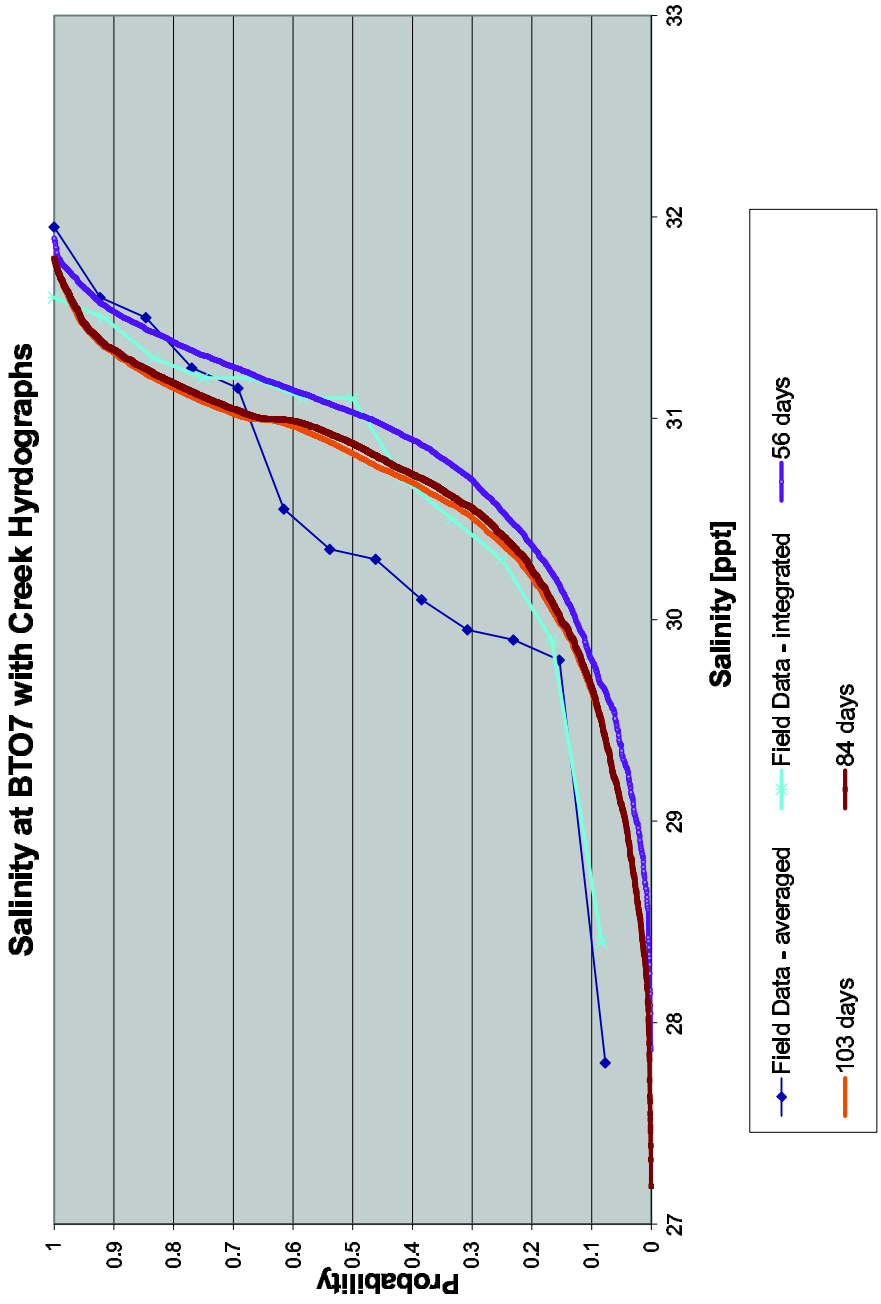

Figure 2.8: Salinity probabilities at BTO7 using hydrographs for flows from San Diego Creek, Santa Ana-Delhi Channel and the five largest harbor storm drains.

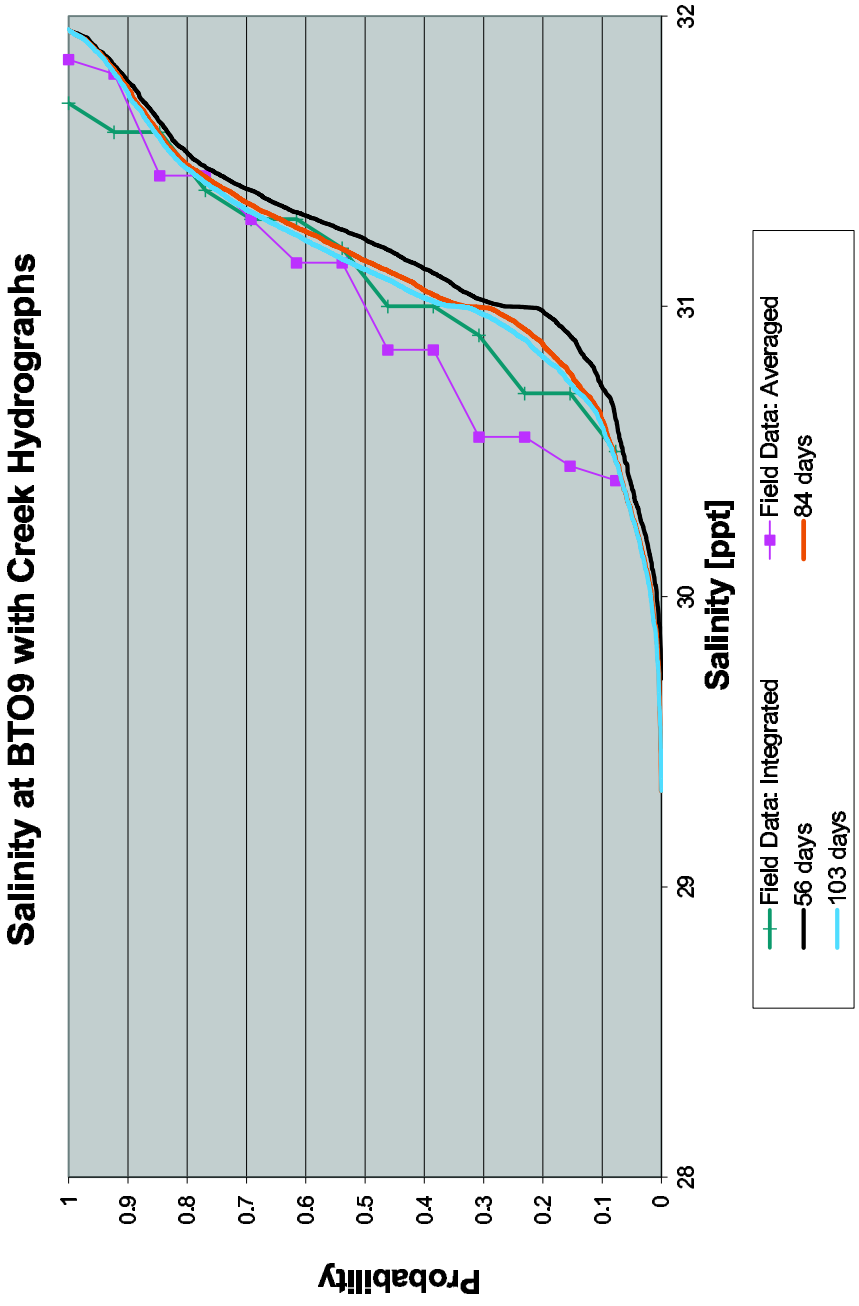

Figure 2.9: Salinity probabilities at BTO9 using hydrographs for flows from San Diego Creek, Santa Ana-Delhi Channel and the five largest harbor storm drains.

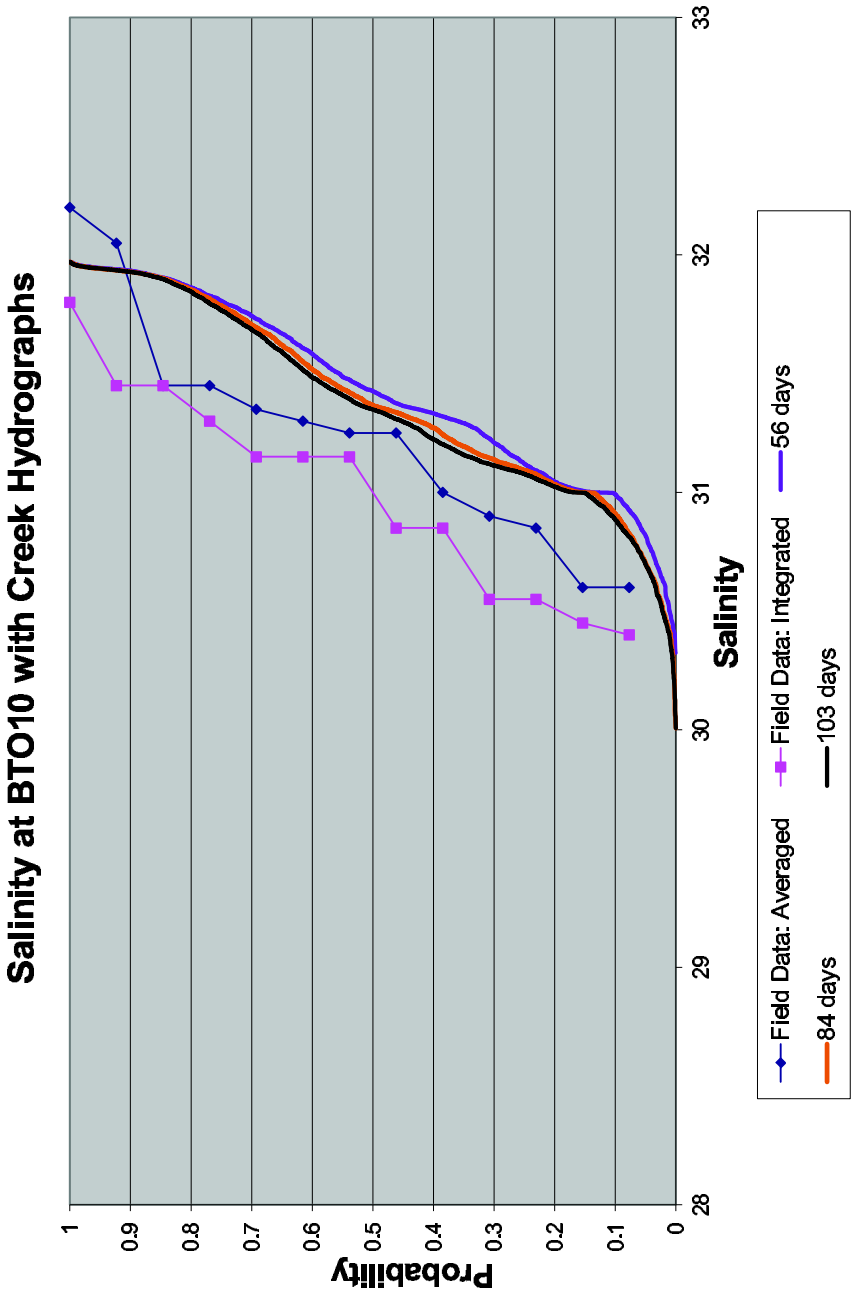

Figure 2.10: Salinity probabilities at BTO10 using hydrographs for flows from San Diego Creek, Santa Ana-Delhi Channel and the five largest harbor storm drains.

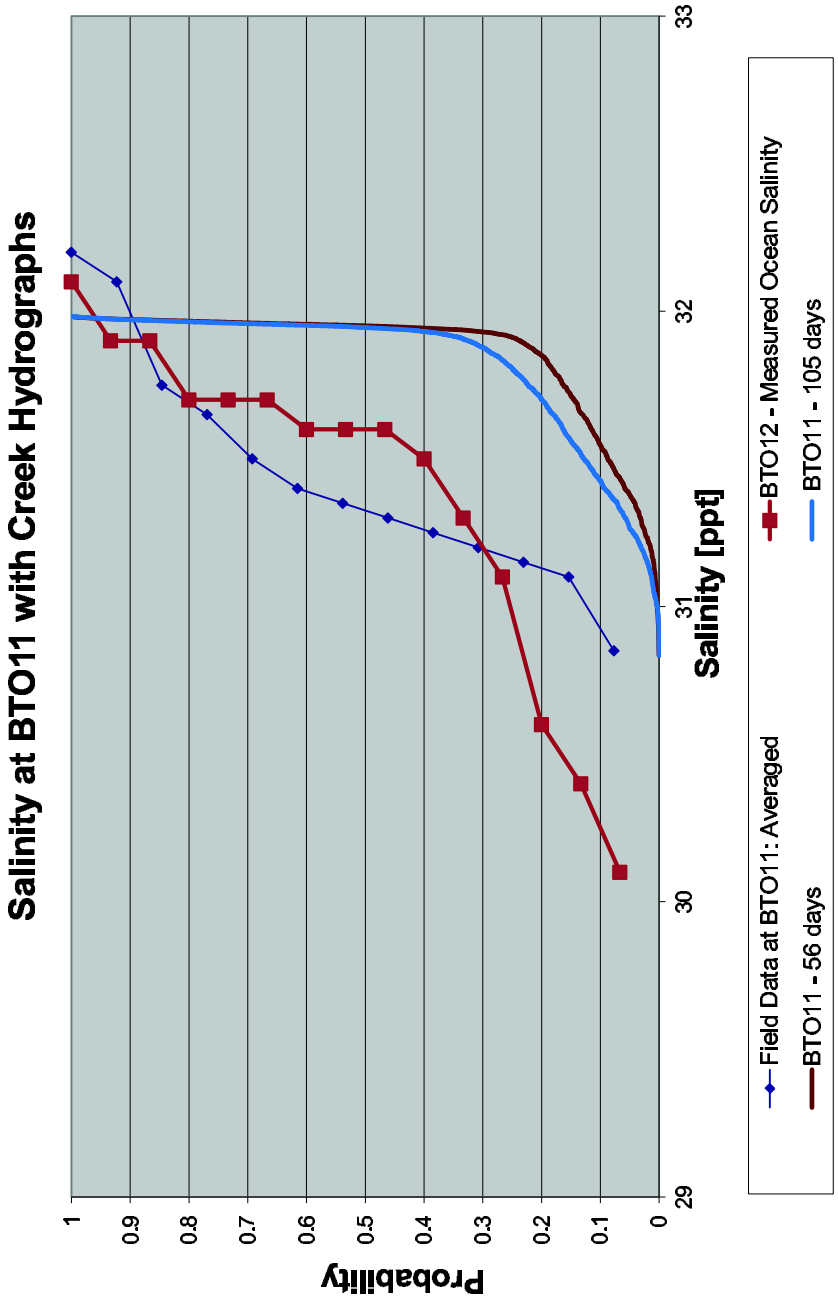

Figure 2.11: Salinity probabilities at BTO11 using hydrographs for flows from San Diego Creek, Santa Ana-Delhi Channel and the five largest harbor storm drains.

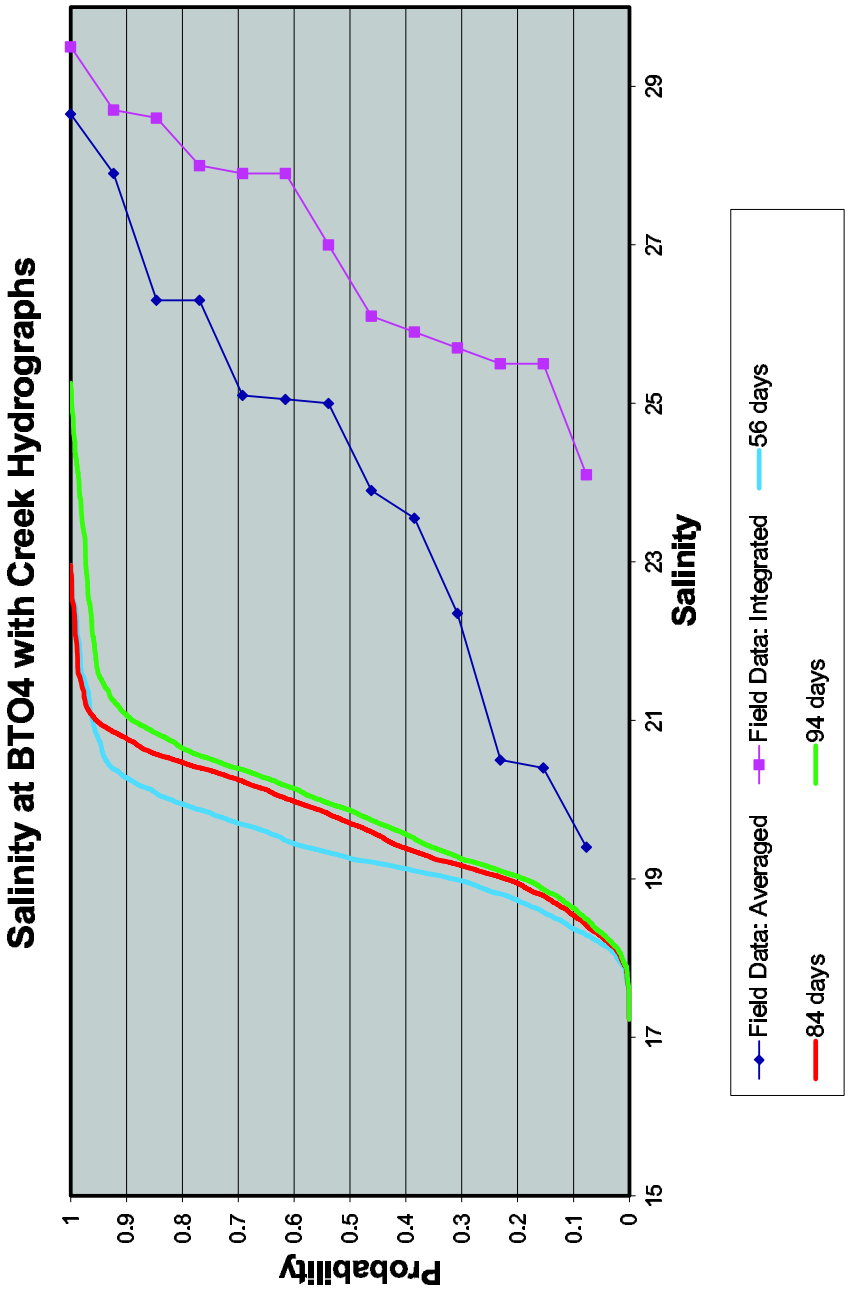

Figure 2.12: Salinity probabilities at BTO4 using hydrographs for flows from San Diego Creek, Santa Ana-Delhi Channel and the five largest harbor storm drains.

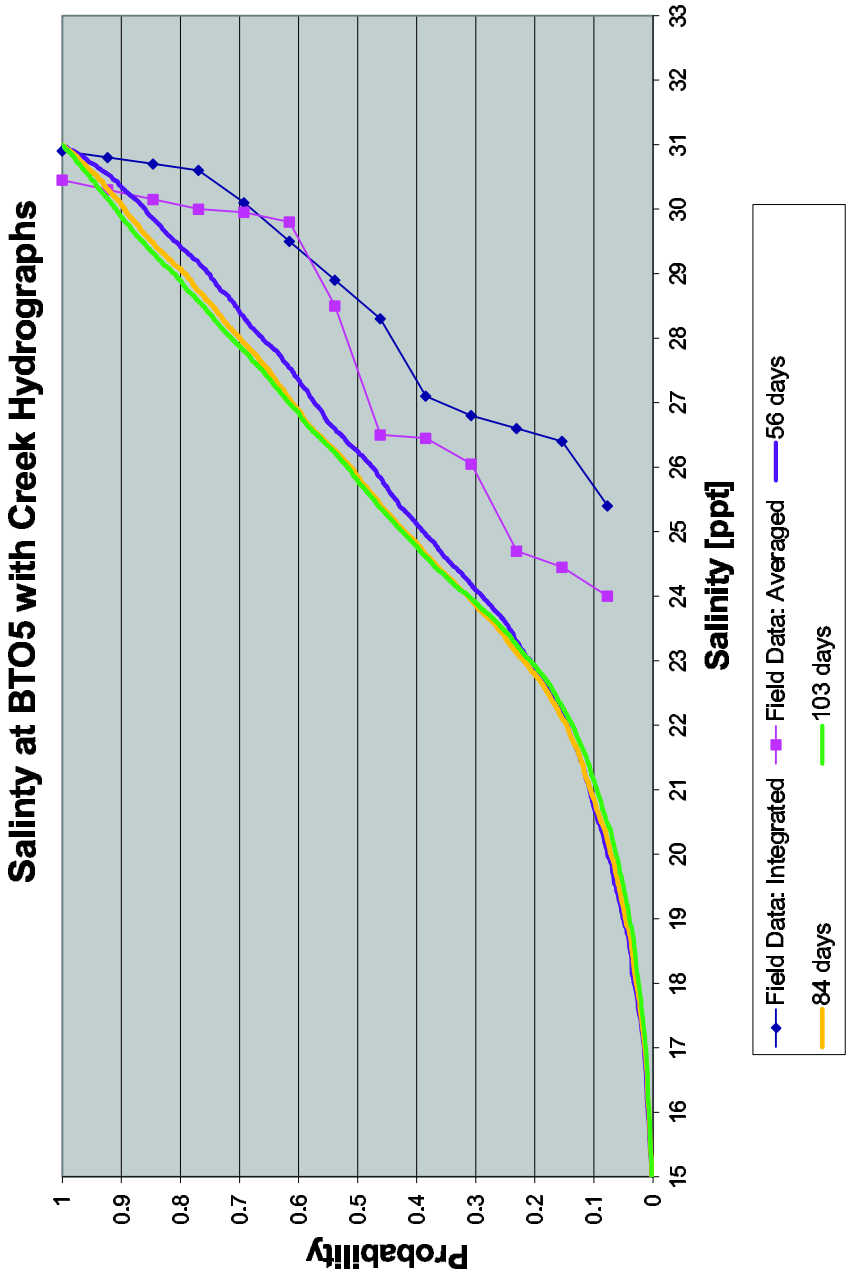

Figure 2.13: Salinity probabilities at BTO5 using hydrographs for flows from San Diego Creek, Santa Ana-Delhi Channel and the five largest harbor storm drains.

examined with additional scenarios that assume constant streamflow inputs based on mean or median flows. Additionally, another set of scenarios that omit the five large harbor storm drains is also considered. These scenarios are motivated by an interest in understanding the level of complexity in fresh water inputs that is needed for the model to predict salinity at the level of accuracy required for this study of tidal circulation and transport.

Results indicate that salinity is under predicted when a constant stream flow is used based on the mean or median value, instead of flow data at 15 minute intervals. Figures 2.14, 2.15, and 2.16 show salinity for BTO6, BTO7 and BTO9, respectively, based on median streamflows of 0.24 m^3/s for San Diego Creek and a flow rate of 0.068 m^3/s for the Santa Ana-Delhi Channel. Median flows are slightly smaller than mean flows, so the offset would be even greater with mean flows. These results echo findings by Azevedo *et al.* (2009) who showed that flow magnitude and variability both play a role in determining estuarine salinity concentrations. Flow rates in San Diego Creek and the Santa Ana Delhi Channel therefore should be modeled as hydrographs.

To test the localized importance of the five largest storm drains that were modeled in the first series of runs, additional modeling scenarios were run using 15 min streamflow data with and without the input from five large lower bay storm drains (Carnations, El Paseo, Polaris, Arches and Dover Drains). Figure 2.18 shows probability distributions of salinity predictions and measurements at the mid-bay station, BTO9. At the a probability of 50%, the salinity is reduced from 31.40 to 31.34 ppt. This indicates that lower bay storm drains exhibit a very small influence, overall, on

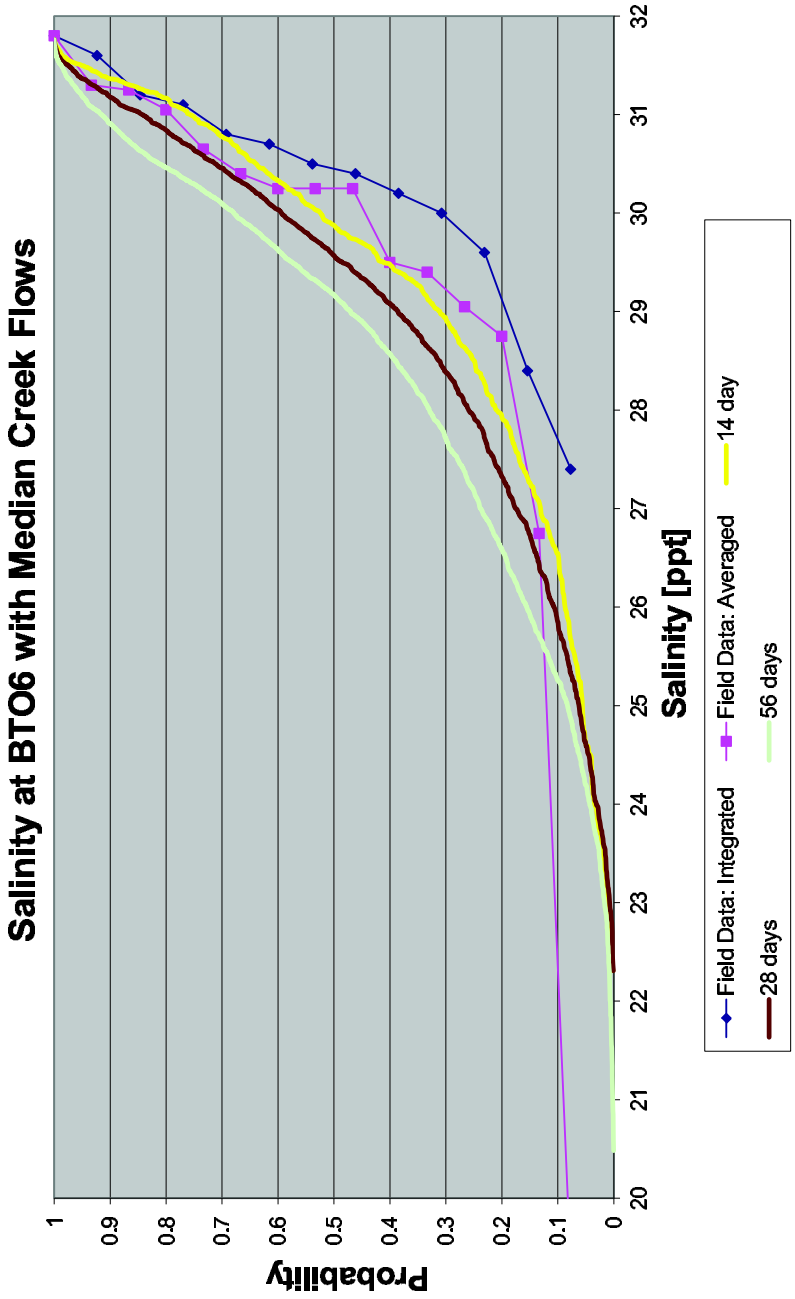

Figure 2.14: Salinity probabilities at BTO6 with Median Flows From San Diego Creek and Santa Ana-Delhi Channel.

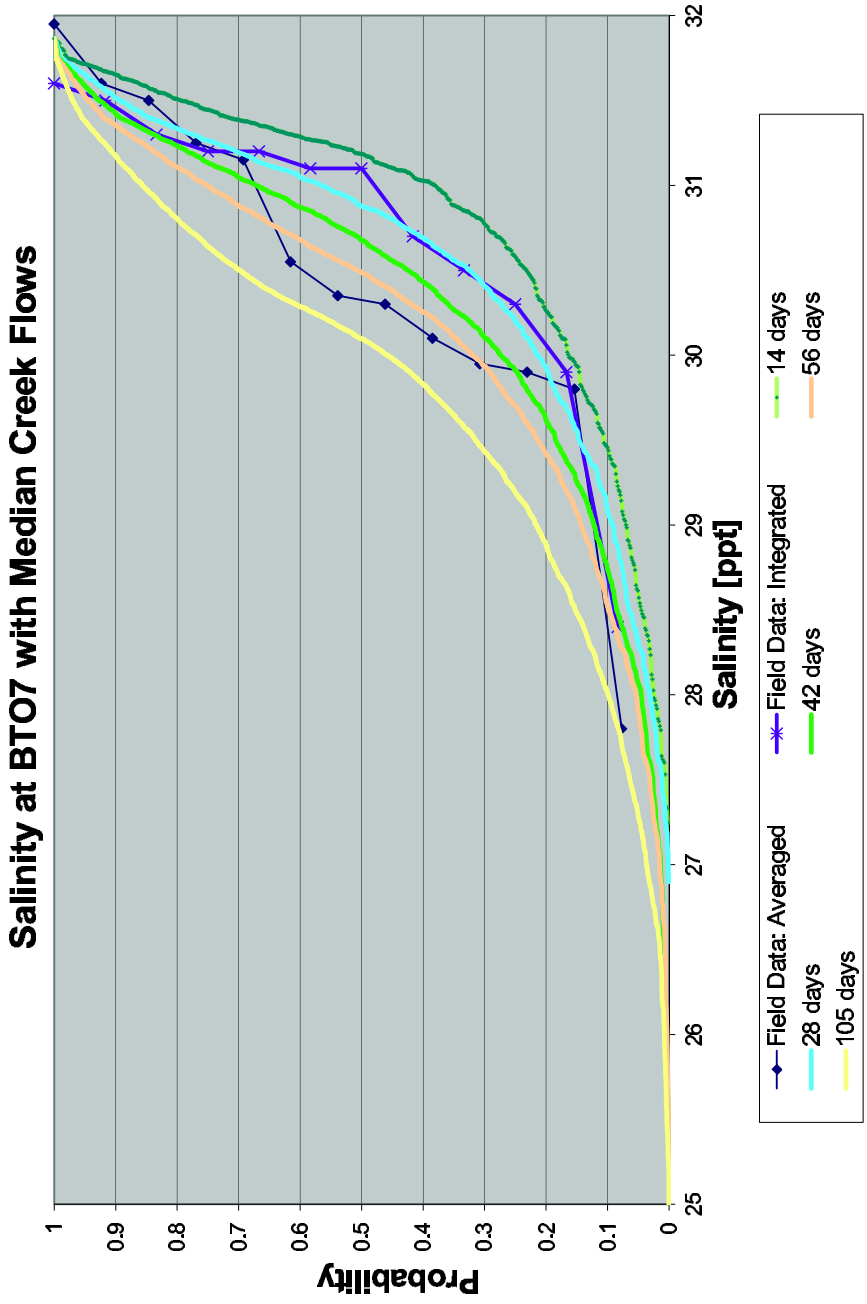

Figure 2.15: Salinity probabilities at BTO7 with Median Flows From San Diego Creek and Santa Ana-Delhi Channel.

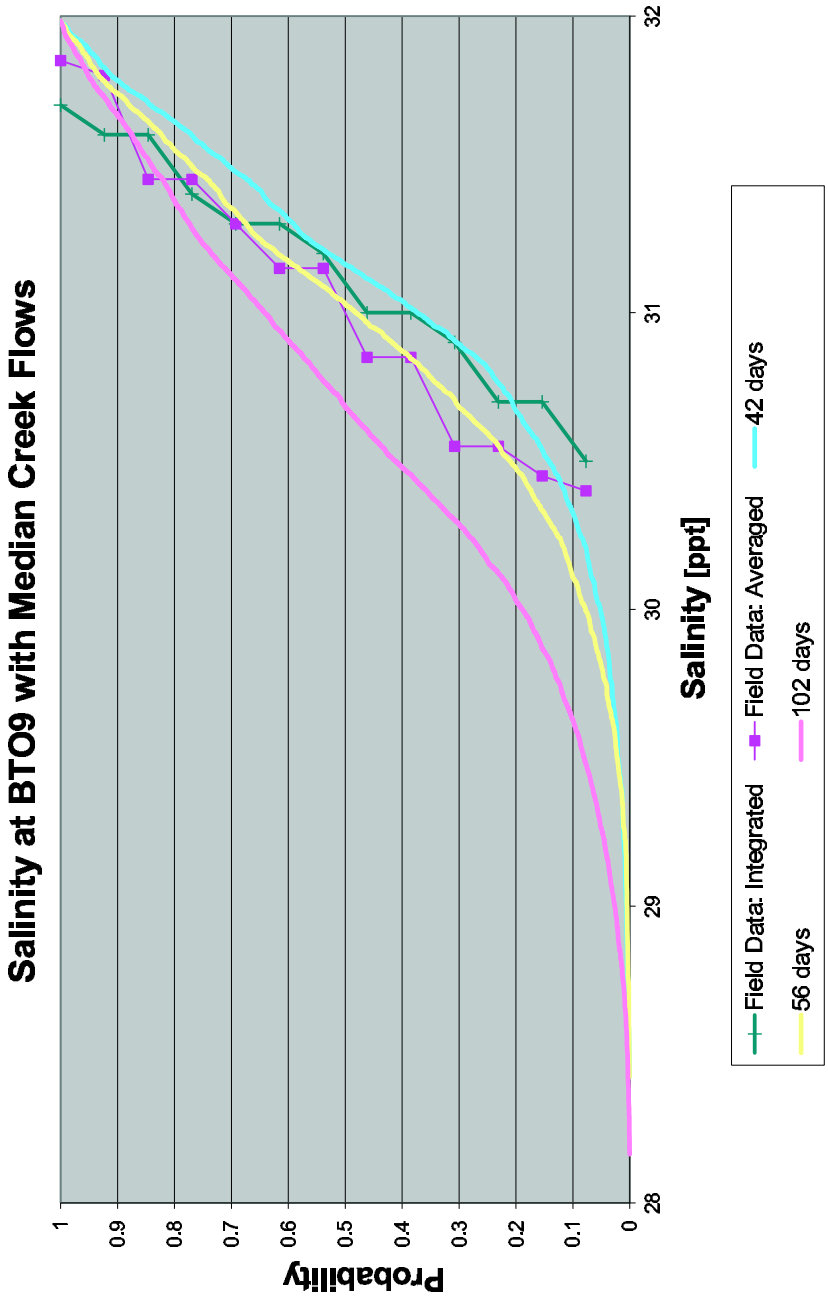

Figure 2.16: Salinity probabilities at BTO9 with Median Flows From San Diego Creek and Santa Ana-Delhi Channel.

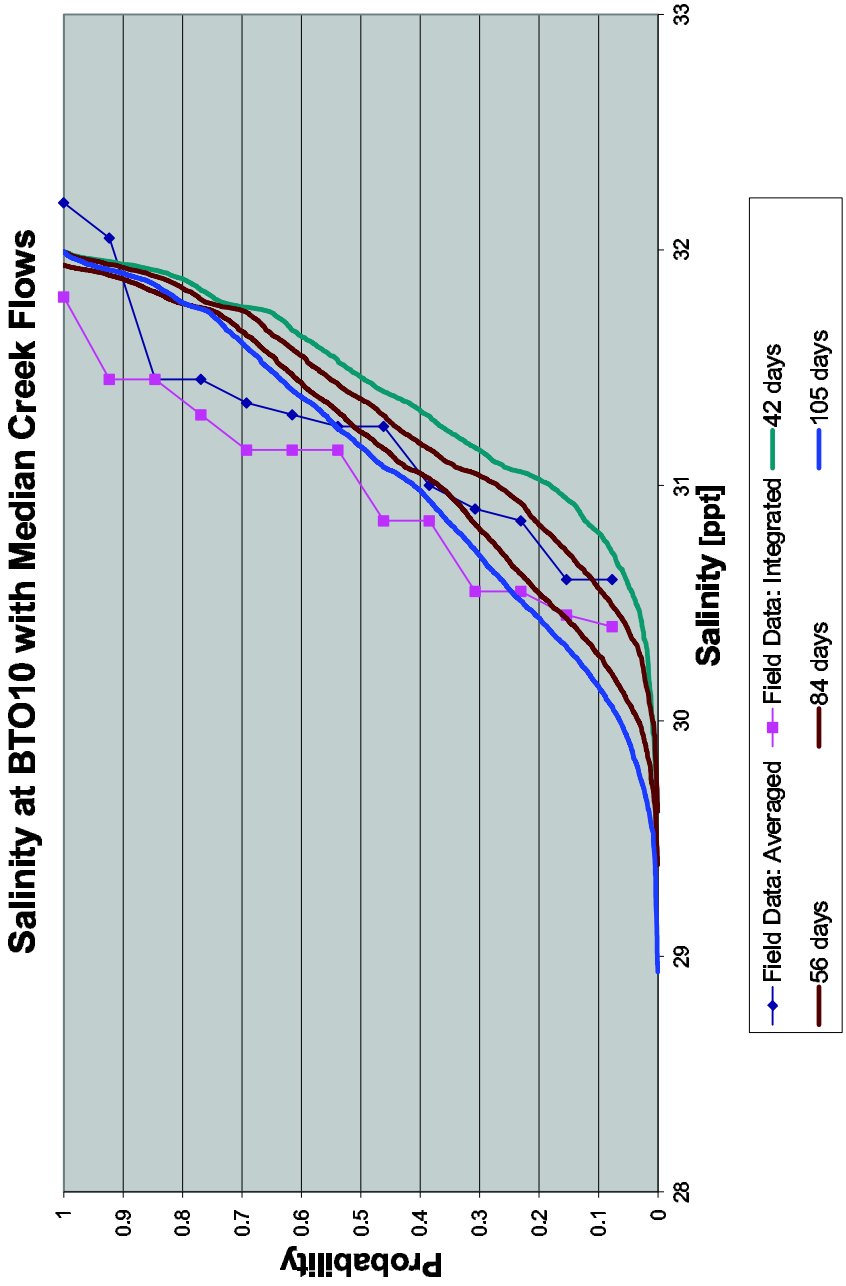

Figure 2.17: Salinity probabilities at BTO10 with Median Flows From San Diego Creek and Santa Ana-Delhi Channel.

the bay-wide salinity distribution, although the storm drains can have a significant local effect on salinity in the vicinity of a storm drain outlet.

The preceding scenarios show that the 2D model reproduces salinity distributions at mid-bay locations, BTO6-BTO10, with an average accuracy of about 0.5 ppt or less when 15 minute streamflow data are used. Secondly, runoff from lower bay storm drains exert a relatively small influence on bay-wide salinity distributions, less than 0.1 ppt, although these inputs can exert a strong local influence on salinity as will be shown later. Third, the model under predicts salinity at mid-bay locations when 15 minute streamflow time series are replaced by constants representing the mean or even the smaller median flows. This finding is consistent with previous work by Azevedo *et al.* (2009). Fourth, results show that the model poorly captures salinity at upper bay stations near the outlets of San Diego Creek and Santa Ana-Delhi Channel, which is taken as a limitation of the 2D modeling approach, and at the entrance to the bay which is attributed to variability in ocean salinity that is not captured in the boundary forcing data (assumed constant salinity of 32 ppt).

2.7 Tidal Pumping in Lower Bay

Figure 2.19 shows an interesting circulation pattern in the west end of the harbor predicted by the 2D model. The pattern involves the exchange of water from the main stem of the estuary and the channel loop around Lido Island, on the western side of the bay. In this example, towards the end of an ebb tide, a low salinity parcel of water from Upper Bay is advected seaward under Coast Highway, enters the harbor and

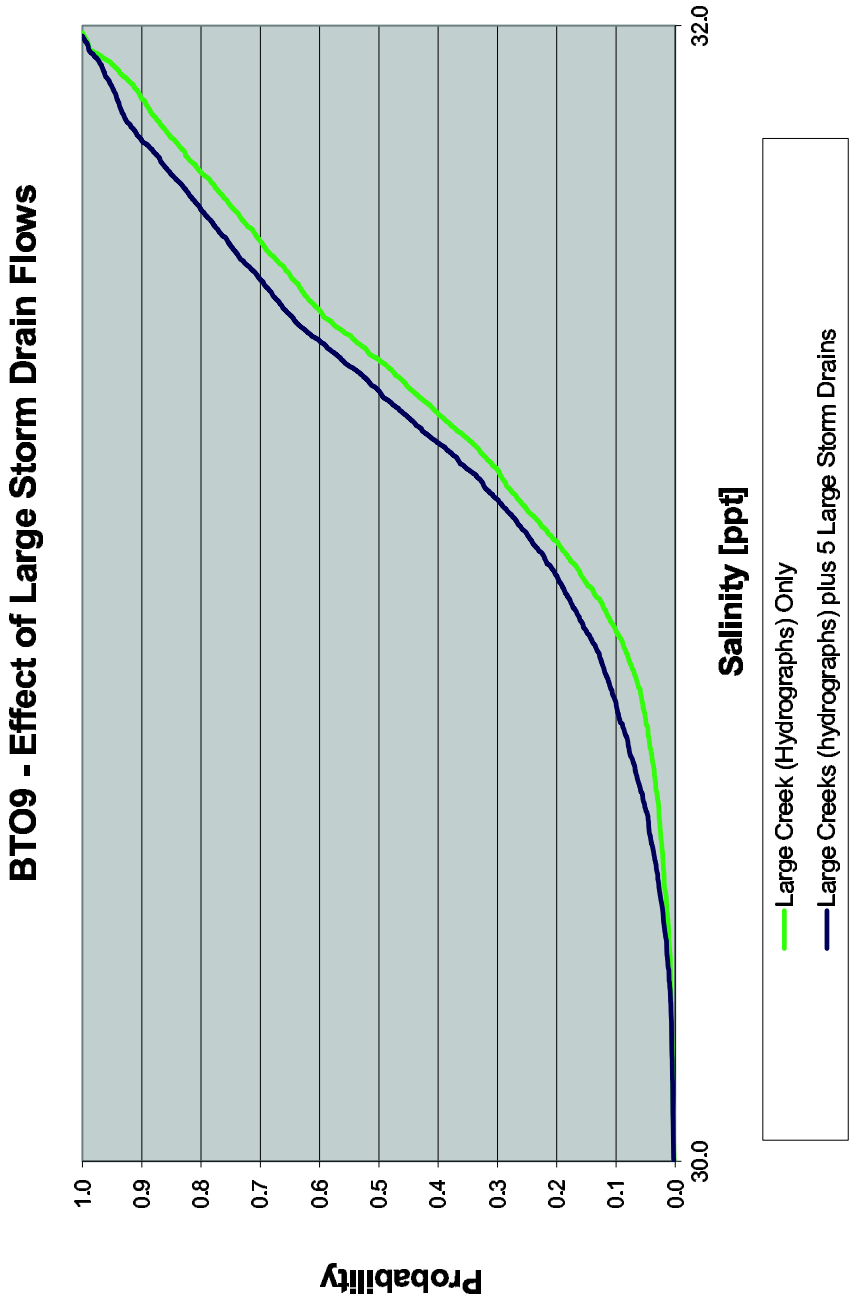

Figure 2.18: Additional salinity dilution is observed at BTO9 when flows from the five large storm drains are included in the modeling.

begins to skirt the south side of Balboa Island (Hour 0). Next, upon commencement of the flood tide, higher salinity water from the ocean floods into the harbor pushing the low salinity parcel back toward Coast Highway (Hour 2) but here the flow splits: a portion flows (1) north under Coast Highway and back into the upper bay and (2) west along the north side of Lido Islands. As the flood tide continues, low salinity water continues west along the north side of Lido Island followed by high salinity ocean water (Hour 4). With the ebb tide, these parcels reverse direction but do not cover the same distance as in the flood tide. Hence, tidal forcing creates a residual circulation in the counter-clockwise direction around Lido Island, a phenomena known as tidal pumping (Fischer *et al.*, 1979). This gives rise to a pattern of low and high salinity water parcels wrapped around Lido Island (Hour 7).

Figures 2.20 and 2.21 shows that one counter-clockwise cycle around Lido Island takes about three days under Spring Tide conditions. The flood tide commences at Hour 0 which pushes a low salinity parcel on the north side of Lido Island westerly (Hour 2). By Hour 7, the parcel has almost reached the Turning Basin at the west end of the Harbor. At Hour 30, the low salinity parcel has mixed within the Turning Basin, lowering the salinity and begins to head South. By Hour 42, a low salinity plume can be seen along the length of the west side of Lido Island. At Hour 46, the plume can be seen starting to turn easterly along the south side of Lido Island. Notice that the plume skirts past the Rhine Channel. The plume continues to migrate easterly (Hour 60) and finally begins to re-enter the center of the harbor near Station BTO9 at Hour 74.

Tidal pumping is also observed around Balboa Islands, and may occur on a faster time scale. Modeling indicates that the predominant circulation pattern is a back-and-forth sloshing of the flood and ebb tides, which moves water along the north and south sides of the islands. However, on a strong flood tide, a high salinity parcel can move along the north side of Balboa Islands and just reach the western edge of Balboa Island, enabling subsequent transport along the southern side of Balboa islands with the ebb tide. This corresponds to counter-clockwise transport of water around the Islands. The reverse can happen on a strong ebb tide where a low salinity parcel advects easterly along the north side of Balboa Islands just reaching the southern point of Little Balboa Island. With the following flood tide, this water is transported in the main channel along the south side of Balboa Islands back toward Upper Bay to complete a clockwise transport around the islands.

2.8 West Bay Salinity Dynamics

The predicted tidal pumping phenomena around Lido Island is validated with salinity measurements in the BTO study (Grant *et al.*, 2008). Figure 2.22 shows probability distributions of the predicted and measured salinity at BTO8, located in western part of lower bay. Both probability distributions exhibit a step-like pattern that is unlike probability distributions at other BTO stations. The step-wise change in salinity is attributed to the passage of alternating parcels of relatively low and high salinity water. With the longer modeling durations, model predictions appear to be converging toward the measured results as shown in Figure 2.22.

As a final modeling run, Figure 2.23 shows the influence of the Arches Drain on salinity at Station BTO8. At p=0.50, one can see that the freshwater flows from the Arches Drain reduces salinity by about 0.1 ppt.

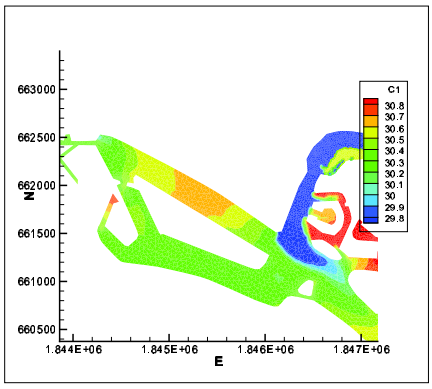

(a) Beginning of the Flood Tide

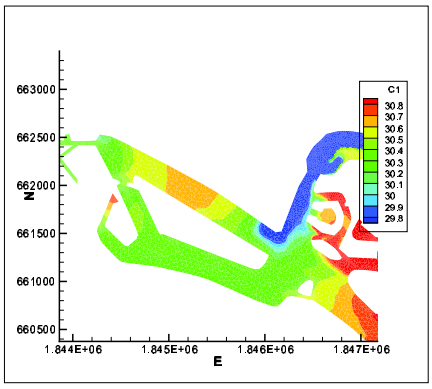

(b) The flood tide pushes a lower salinity parcel of water into the channel North of Lido Island.

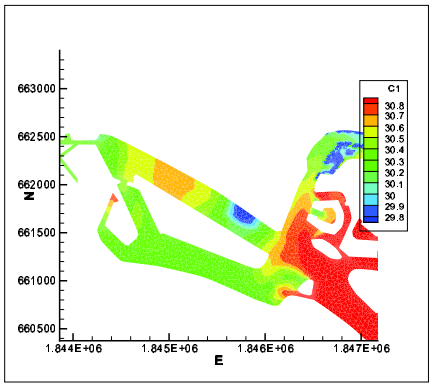

(c) The flood tide continues to push the lower salinity parcel along the north side of Lido Island.

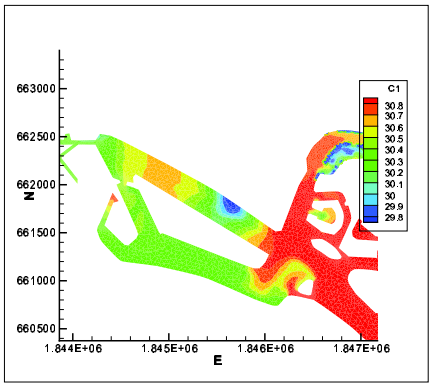

(d) End of the Flood Tide

Figure 2.19: Tidal pumping creates parcels of differing salinity in the channel on the north side of Lido Island.

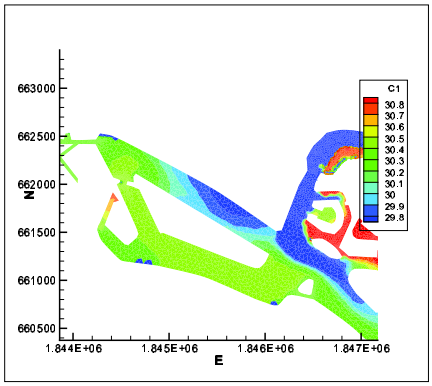

(a) Hour 0: Begin Flood Tide

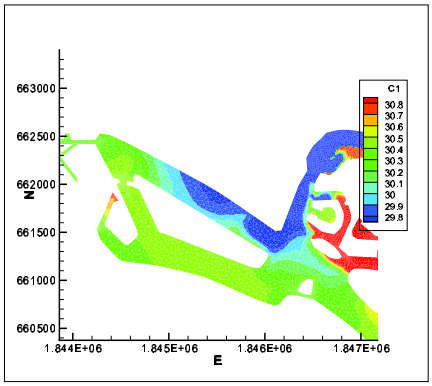

(b) Hour 2

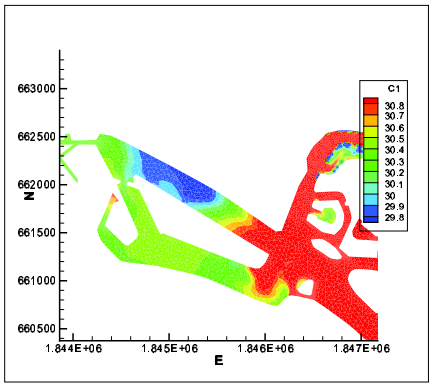

(c) Hour 7

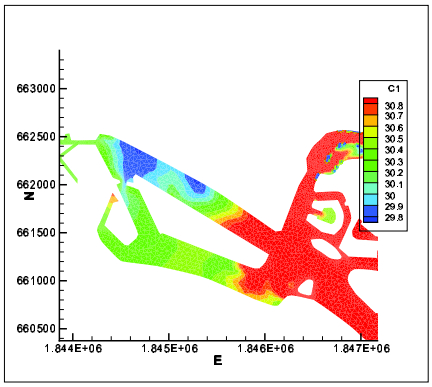

(d) Hour 30

Figure 2.20: A low salinity parcel migrates in a net counter-clockwise manner along the north side of Lido Island.

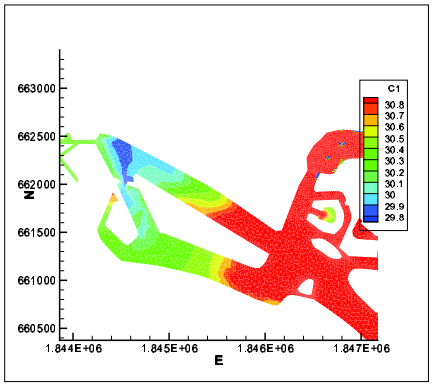

(a) Hour 42

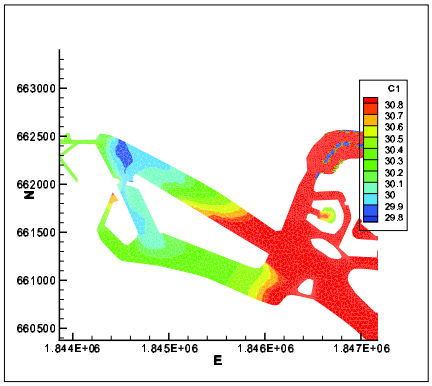

(b) Hour 46

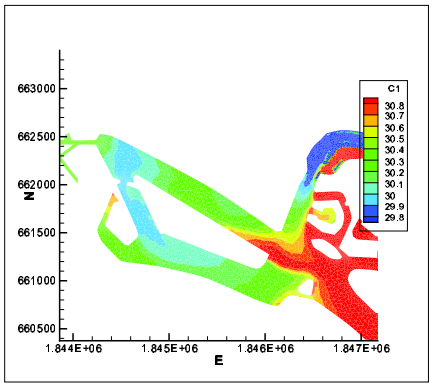

(c) Hour 60

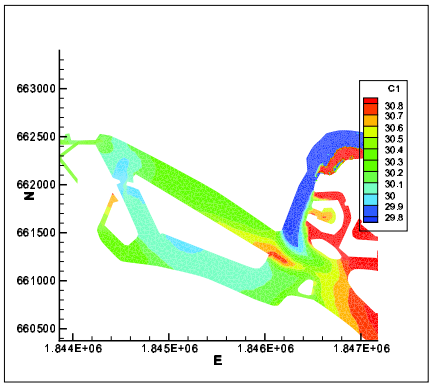

(d) Hour 74

Figure 2.21: A low salinity plume migrates in a net counter-clockwise manner along the south side of Lido Island.

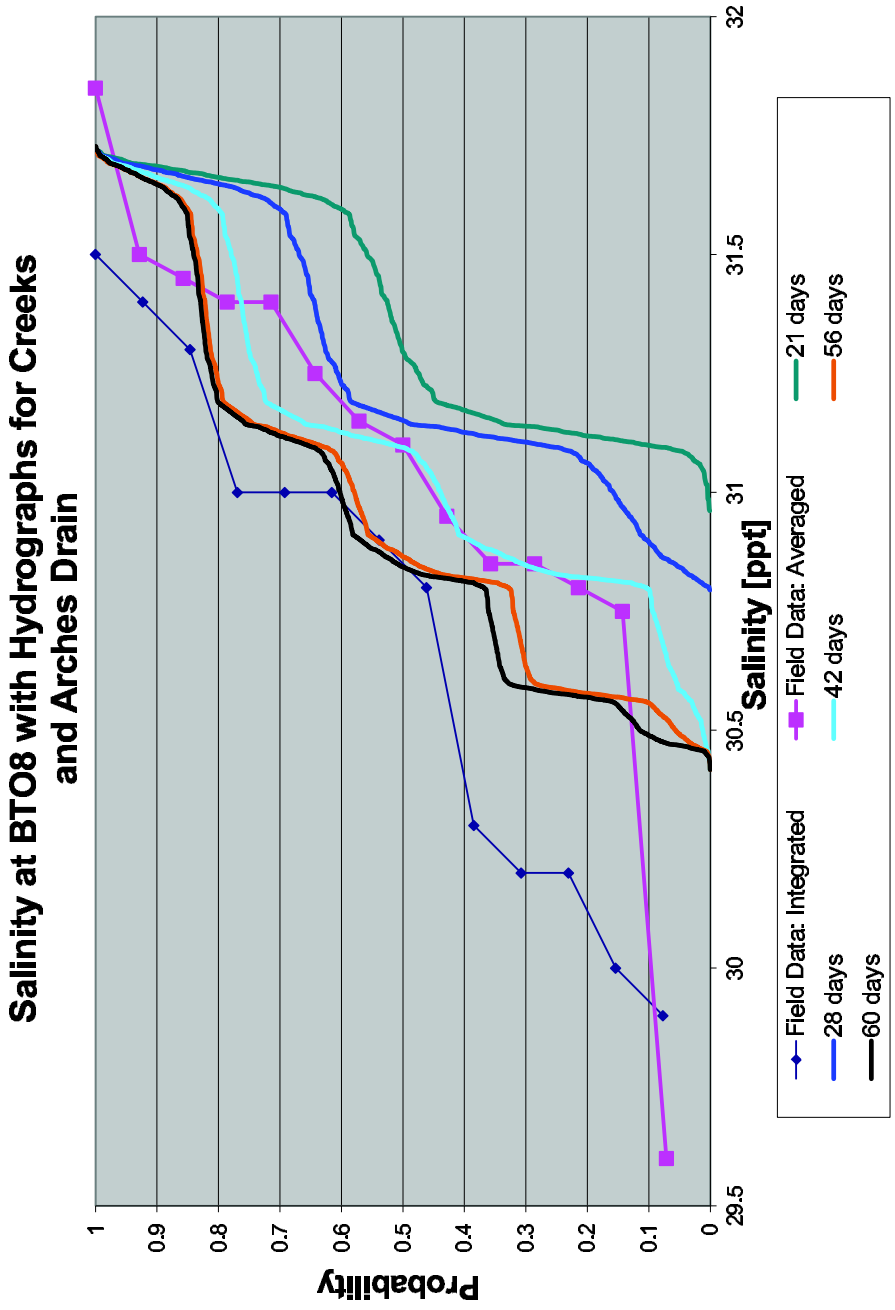

Figure 2.22: Salinity probabilities at BTO8 using flow hydrographs for San Diego Creek, Santa Ana-Delhi Channel and the five largest harbor storm drains.

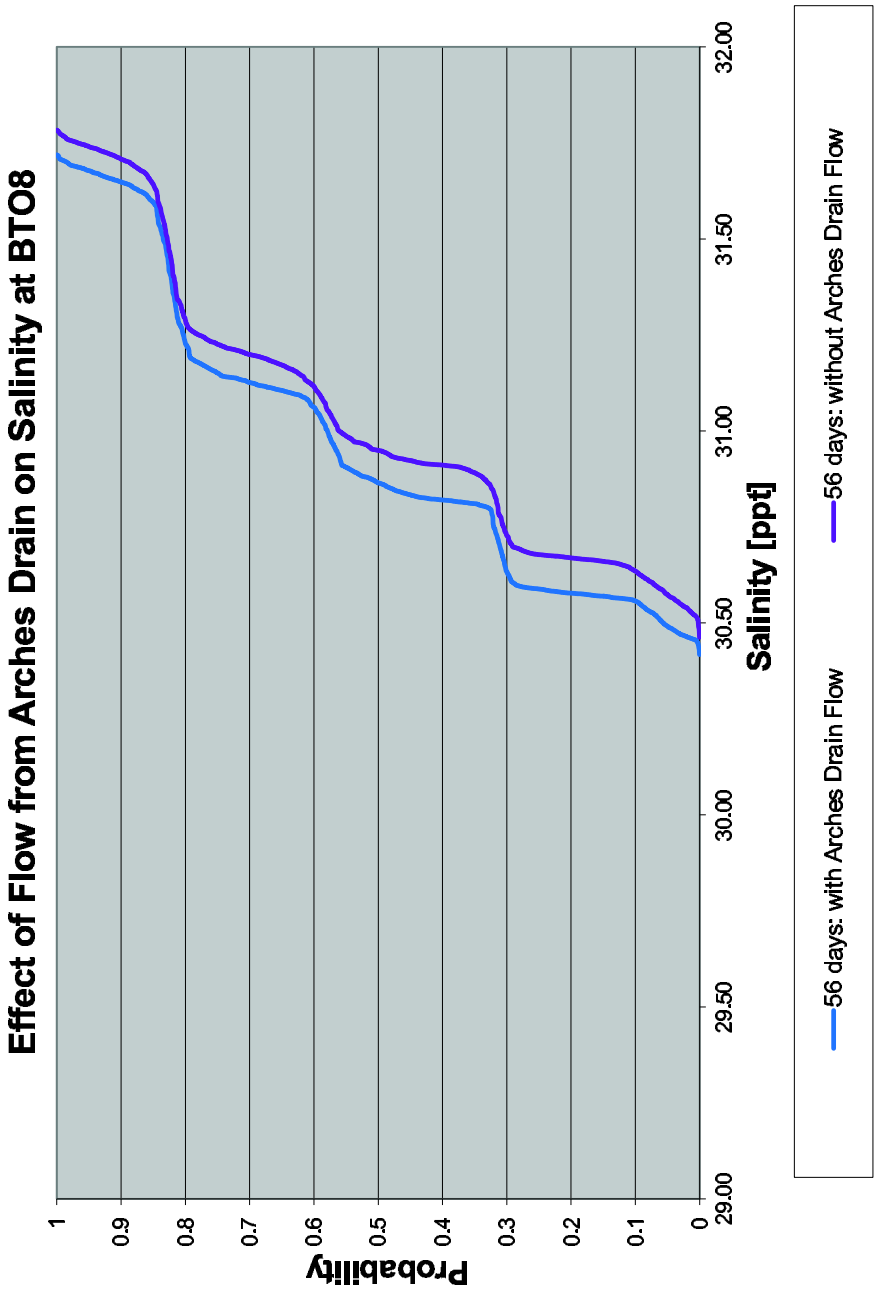

Figure 2.23: Additional salinity dilution is observed at BTO8 when flow from the Arches Drain is included in the modeling.

Chapter 3

Estimating Dry Weather Urban Runoff

As discussed in the introduction, urban runoff is likely responsible for loading contaminants and thus storm drain discharges must be addressed in any water quality improvement program. However, little is known about the magnitude of these flows. This chapter is focused on the development of an empirical model (formula) for estimating the magnitude of dry-weather flows from storm drains as a function of drainage area along with a characterization of model uncertainties. The empirical model is developed from a combination of storm drain flow measurements and a unique study of nearshore salinity using the 2D salinity transport model described in Chapter 2. The 2D model uses an original model describing the intermittent release of urban runoff from tidally flooded storm drains ("trap-and-release" model) described in this chapter, to back-calculate discharge rates from individual storm drains. Hence,

an empirical regression for urban runoff discharge rates is developed from a combination of direct and indirect measurements. Practicing engineers will find this model useful for preparing preliminary estimates of constituent loadings to a receiving water and assisting in prioritizing storm drains for further monitoring investigations. In this chapter, the development and the results of the model are done in English units, the customary system of units for practicing engineers in Orange County (and in the U.S.). The text also includes the S.I. equivalents.

Urban runoff terminology can be confusing. For clarity, *storm drain*, *storm sewer* or *drain* are used here when referring to the physical infrastructure, including catch basins and pipes. Additionally, *drainage* is used when referring to the process of urban runoff flowing into the storm drain, and *discharge* is used when referring to the flow of runoff from a storm drain and into Newport Bay.

3.1 Field Studies Monitoring Dry Weather Flows

There are 219 storm drains that discharge directly into Newport Bay. Figure 3.1 shows the location of storm drain outlets around the harbor. Two field studies were performed to measure dry weather storm drain discharges, one focusing on the five largest storm drains (Large Drain Study) and one focused on a sampling of the smallest drains (Small Drain Study).

Figure 3.1: Locations of storm drains discharging into Newport Harbor.

Large Drainage Areas Study

In 2004, dry-weather discharges were monitored from the five largest storm drains discharging to Newport Harbor: Carnation (S91), El Paseo (S88), Polaris (S41), Arches (S178) and Dover (S189) (see Figure 3.1). Note that the Polaris Drain is North of Coast Highway opposite Newport Dunes. Discharge was measured by installing a weir-type flow meter in each drain at the closest manhole to the outlet. Depths were sampled hourly over a two-week period in August that provided a time series of hourly discharge (City of Newport Beach, 2004). The study found that the storm drains with the largest tributary areas, Carnation (805 acres or 326 hectares), El Paseo (523 acres or 212 hectares), Arches (400 acres or 162 hectares) and Polaris (384 acres or 155 hectares), had continuous flows. The Dover Drain, with a watershed drainage area of 94 acres (38 hectares), had intermittent flow. The mean dry-weather flow rates for these storm drain, along with the mean discharge rates for San Diego Creek and Santa Ana-Delhi Channel (County of Orange, 2006) are plotted in Figure 3.2. The creeks have continuous flow. The regression of the mean dry-weather discharge into the bay (in units of gallons per day) from these large conveyances with continuous flow, e.g., the Dover drain is not included, scales nearly linearly with the drainage area, A (in units of acres), as follows:

$$Q_{large} = 135.5A^{0.988}, \qquad R^2 = 0.95 \quad (p = 0.0005) \tag{3.1}$$

the low p-value (level of significance) indicating that the correlation is highly significant. It should be noted that San Diego Creek, which accounts for nearly 75% of the

Storm Drain	Drainage Area [acre]	Flow Rate [gpd]
Adams/Edgewater	6.51	10.4
Cypress/Edgewater	5.06	12.4
Fernando/Edgewater	3.98	10.4
Coronado/Edgewater	5.19	14.6
Alvarado/Edgewater	2.41	0.64
Opal/S. Bayfront	2.12	34.5
Emerald/S. Bayfront	1.24	0.0
Pearl/N. Bayfront	1.46	0.0
Diamond/N. Bayfront	3.35	15.9
Sapphire/N. Bayfront	5.21	0.13

Table 3.1: Flow Rates from drains with small tributary watersheds on Balboa Peninsula and Balboa Island.

flow into Newport Bay, is somewhat remote as compared to the other flow rates, so its flow rate leverages the slope of the trend line.

Small Drainage Areas Study

In a separate study, the City of Newport Beach measured dry-weather flows and salinity concentrations from ten storm drains with small tributary areas (1.2 to 6.5 acres or 0.5 to 2.6 hectares) on Lido Island and Balboa Peninsula by closing tide gates at these outlets, allowing runoff to accumulate in the tide gate vault of know dimensions for 24 hours and then measuring the depth of accumulated water (City of Newport Beach, 2008). Table 3.1 summarizes the measurements, which are also plotted in Figure 3.2. A mild, but significant correlation between tributary watershed area and drainage rate into a storm drain is described by the power law:

$$Q_{small} = 0.0278 A^{3.74}, \qquad R^2 = 0.40 \quad (p = 0.025) \tag{3.2}$$

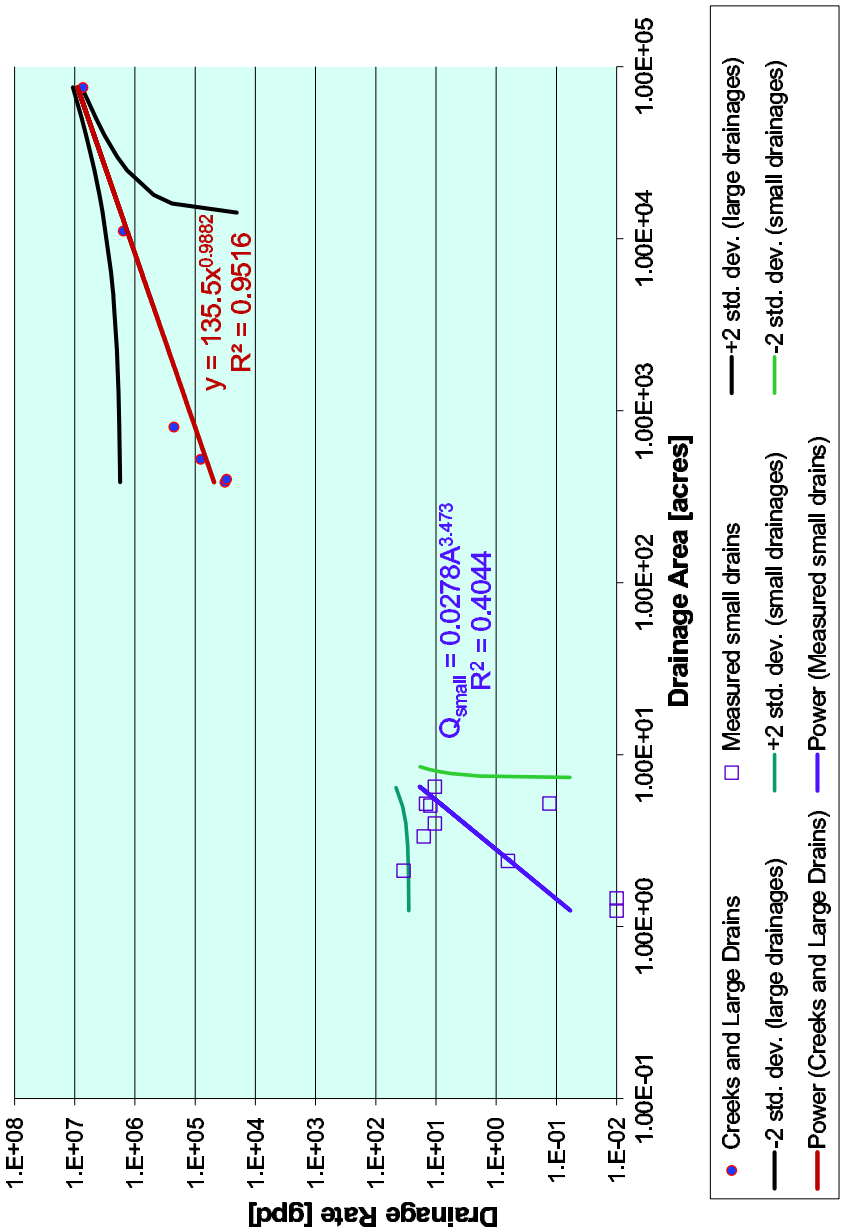

Figure 3.2: Expected Values and Variance for Small and Large Drainage Areas .

The 95% confidence intervals of the large and small measured drainages are shown in Figure 3.2.

Drainage Rate - Drainage Area Regression

Generally, the rate of dry-weather runoff shed from the small drainage areas around the harbor is smaller than what is predicted by the large drainage area regression (Eq. 3.1). It is suspected that this is due to differences in residential development and subwatershed slope. That is, the small drainage areas are associated with low lying and flat harbor terrain that is more densely developed, and therefore less vegetated, than the surrounding hill slopes and mesas where there is more extensive landscaping and requisite irrigation.

By analogy to the parallel arrangements of resistors in an electrical circuit, the small- and large-drainage area models can be combined to arrive at a model that may apply to all drainage areas as follows,

$$Q' = [(1/Q_{\text{large}} + 1/Q_{\text{small}})]^{-1} \tag{3.3}$$

or

$$Q' = \left[\frac{Q_{\text{large}}Q_{\text{small}}}{(Q_{\text{large}} + Q_{\text{small}})}\right] = \left[\frac{(135.5A^{0.988})(0.0278A^{3.74})}{(135.5A^{0.988} + 0.0278A^{3.74})}\right] \tag{3.4}$$

Note that this model converges to the small- and large-drainage area models in the limit of small and large A, respectively, and smoothly transitions between the two models for intermediate values of A. Figure 3.3 plots the curve represented by the Eq. 3.4. As a first check of this regression, the measured flow rate for the Dover Drive

storm drain, which drains an intermediate-sized watershed of 94 acres (38 hectares), plots closely (green triangle) to the regression in Figure 3.3.

Two important objectives remain: Validate the proposed model (Eq. 3.4) with additional data from intermediate-sized drainage areas, and characterize the uncertainty of discharge estimates. Validation of the model for intermediate-sized drainage areas is important because small and large drainage areas differ by more than two orders of magnitude. Hence, there is a large data gap, as shown in Fig. 3.2.

3.2 Filling the Data Gap: Estimation of Drainage Rate by Inverse Modeling

In August 2006, over 320 samples of bay water were collected near the outlets of 86 storm drains discharging to Newport Bay and tested for salinity (Grant, 2008). Sampling was carried out at low tide over a four-hour period on two consecutive nights on August 3 and 4, 2006 between 4:30 AM and 8:30 AM local time. The east side of the harbor was sampled the first night and the west side of the harbor the second night. The weather was typical of summers in Southern California: dry and warm. The only recorded rain at Newport Beach was 0.02 inches (0.51 mm) that fell three weeks prior to the start of the sampling. Sampling locations were chosen to provide relatively uniform coverage of the harbor shoreline and to be proximal to locations of storm drains discharging to the bay. Two samples were collected at each site, one near the water's edge in a depth of about 2 feet (0.6 meters) (typically directly in front of a

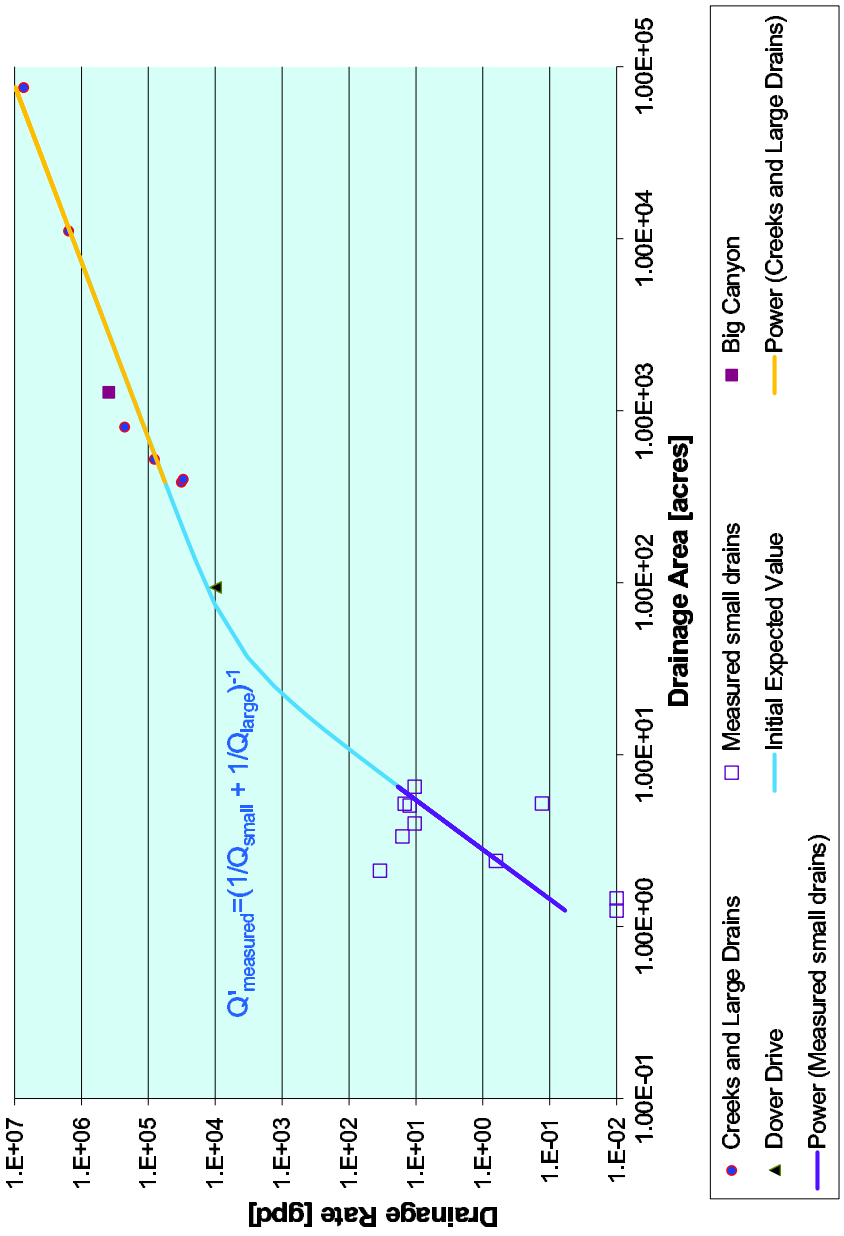

Figure 3.3: Correlation Between Small and Large Drainage Areas.

storm drain) and one approximately 100 feet (30 meters) bayward of the storm drain outlet. The nearshore samples were collected from a kayak; bay-ward samples were collected from a small motor boat. All water samples were collected from the surface of the water column in 500 mL sterilized HDPE bottles. After sampling, bottles were immediately capped and then transported back to the laboratory at UCI where they were analyzed for numerous analytes including salinity. See Attachments A and B for the coordinates of each of the sampling points and the corresponding salinity measurements. Of the 86 drains monitored, a salinity dilution at the storm drain outlet was registered at 59 locations, i.e., the bayward sample had a higher salinity concentration than the nearshore sample. This is taken to indicate a source of fresh water from the adjacent storm drain. Chapter 2 modeling shows that the residual tidal circulation in lower bay moves large scale parcels of upper bay water (relatively low salinity) and lower bay water (relatively high salinity) around Lido Island in the western part of lower bay and Balboa Island in the eastern portion of lower bay. Hence, the background salinity at a channel monitoring station can be expected to vary by as much as 1 ppt as parcels of upper and lower bay water are transported by tidal circulation. By measuring the difference in salinity between a bayward and shoreline location, this variability in background salinity does not interfere with storm drain discharge estimation.

Estimation of dry-weather runoff is approached here as an inverse-problem: determine the storm drain discharge that leads to a 2D model prediction of a salinity dilution (difference between bayward and shoreline salinity) that compares best with

observed salinity dilution. To complement the 2D transport model, and account for the effect of tides on the release of fresh water from tidally flooded storm drains, a loading model is developed to convert an assumed, constant, *drainage* rate into a time-dependent *discharge* rate. This approach focuses attention on intermediate-sized drainage areas defined as watersheds greater than about six acres (2.4 hectares) and less than 100 acres (40 hectares).

Loading Model

The tidal exit condition of lower-bay storm drains results in time-dependent discharge of fresh water even in the presence of steady drainage into storm sewers. Essentially, under dry weather conditions when drainage rates are small compared to storm drain design flows (for storm water), urban runoff accumulates in the storm drain while the tide is rising, and at some point during a subsequent falling tide, a slug of runoff is released into the bay. This process is shown conceptually in Figure 3.4. In Subfigure 3.4A, urban runoff drainage is trapped within the storm drain when the tide height is above the pipe soffit (the point at the top of pipe on the inside of the pipe). Buoyancy and limited mixing inhibit fresh water from reaching the submerged outlet, so the fresh water layer increases in thickness in response to drainage. As the tide begins to fall, however, the bottom of the fresh water layer approaches the pipe soffit as shown in Subfigure 3.4B. Fresh water is subsequently released when the bottom of the freshwater layer falls below the soffit, as shown in Subfigures 3.4C and 3.4D. It is assumed that buoyancy will dominate inside the storm sewer, so fresh

water will immediately escape the sewer as it drops below the soffit elevation and the storm sewer draws in an equal volume of relatively dense bay water.

A loading model was developed to predict the discharge rate in accordance with the pipe diameter, slope and soffit elevation and the conceptual model described above. The accumulation of fresh water inside a storm drain is described by,

$$\frac{d\mathcal{V}}{dt} = Q_{\text{drainage}} - Q_{\text{discharge}} \tag{3.5}$$

where $\mathcal{V}$ represents the freshwater volume in the storm drain, Q_{drainage} represents the drainage rate into the storm drain (assumed constant) and $Q_{\text{discharge}}$ represents the freshwater discharge rate. After a low tide that empties the storm drain, freshwater volume increases in the pipe once tide rises above the pipe soffit so,

$$\mathcal{V}(t) = Q_{\text{drainage}}(t - t_1) \tag{3.6}$$

where t represents time and t_1 represents the moment when the tide surpasses the soffit elevation. The above volume is assumed to layer in the storm drain horizontally above denser bay water in a lens of thickness h_{layer}. The volume is related to the layer thickness as follows,

$$\mathcal{V} = A_{layer} h_{\text{layer}} \tag{3.7}$$

where A_{layer} represents the cross-sectional area of the ellipsoid that corresponds to a horizontal slice through a sloping storm drain pipe (see Figure 3.5). The free surface elevation inside the storm drain is predicted based on hydrostatic equilibrium with the bay water elevation, i.e., the model accounts for the density difference between

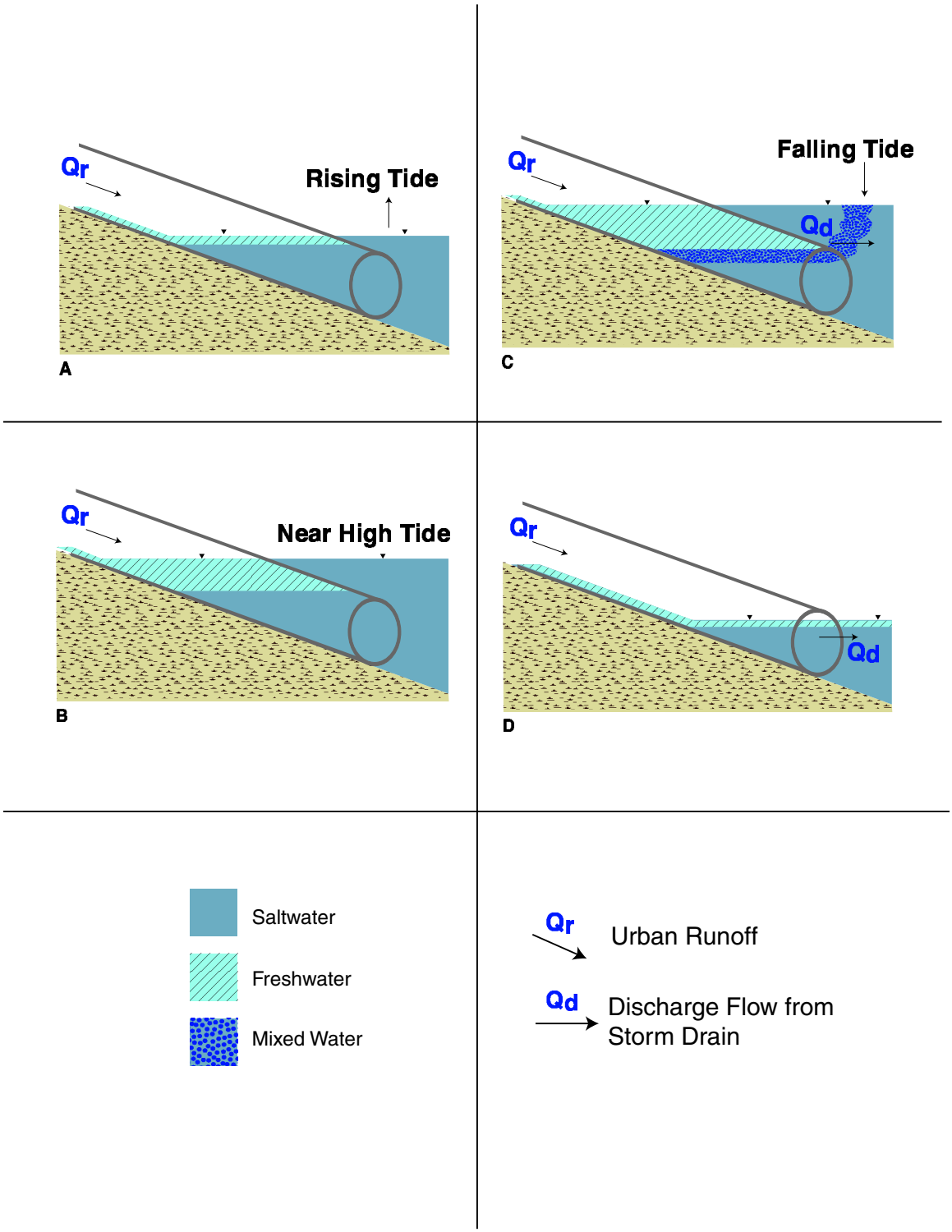

Figure 3.4: Illustration of fresh water accumulating in a tidally submerged storm drain and discharging as the bottom of the freshwater layer falls below the pipe soffit.

bay water and the freshwater in the storm drain. The potential for energy losses in the pipe due to fluid flow is assumed not to be significant. Given the time-dependent bay water elevation η and a layer thickness h_{layer}, discharge will commence (usually during a falling tide) once the freshwater head exceeds the bay head:

$$\alpha h_{\text{layer}} > \eta - z_{\text{soffit}} \tag{3.8}$$

where α is the ratio of the specific gravity of seawater to that of freshwater. The corresponding discharge rate is given by,

$$Q_{\text{discharge}} = A_{layer} \left| \frac{d\eta}{dt} \right| + Q_{\text{drainage}} \tag{3.9}$$

Eq. 3.9 holds until the tide elevation reaches the soffit elevation completing the release of the fresh water layer trapped in the storm drain. The trap-and-release of the slug of freshwater runoff occurs relative quickly in the field, in a matter of minutes to hours. After the release the discharge rate is assumed to equal the drainage rate until the tide rises once again to trap freshwater above the soffit elevation.

A review of City of Newport Beach *As-Built* documents provided information on sizes and outfall locations for the 219 storm drains draining directly to the bay, which allowed the above model to be parameterized and integrated using tide measurements at the Los Angeles gage as a proxy for η. City data indicate that pipe diameters range from 4 to 144 inches (0.13 to 3.66 meters) with a median diameter of 18 inches (0.46 meters). As-Built drawings, some dating from the 1930's, typically do not provide sufficient information to determine the pipe slope or elevations at the pipe outlet. Data that are available suggests that drains are commonly constructed with pipe

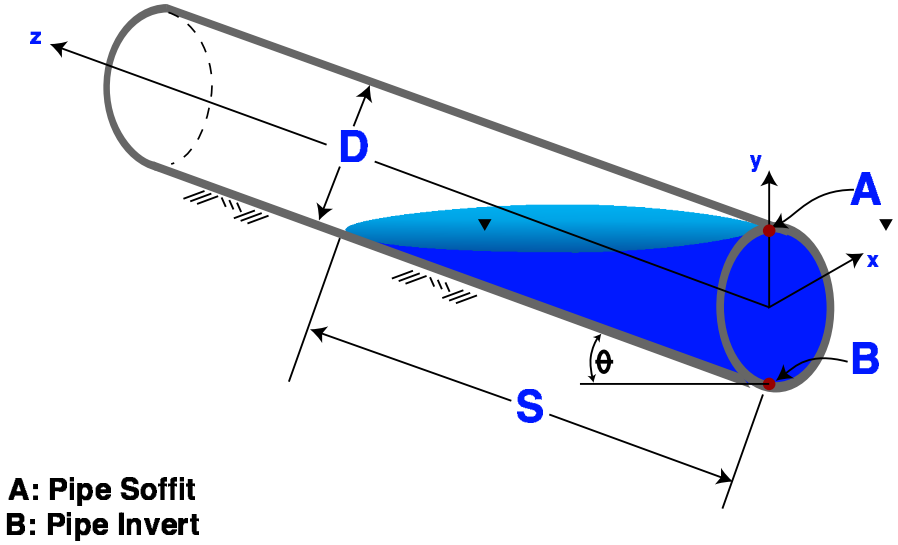

Figure 3.5: Free surface in an inclined pipe.

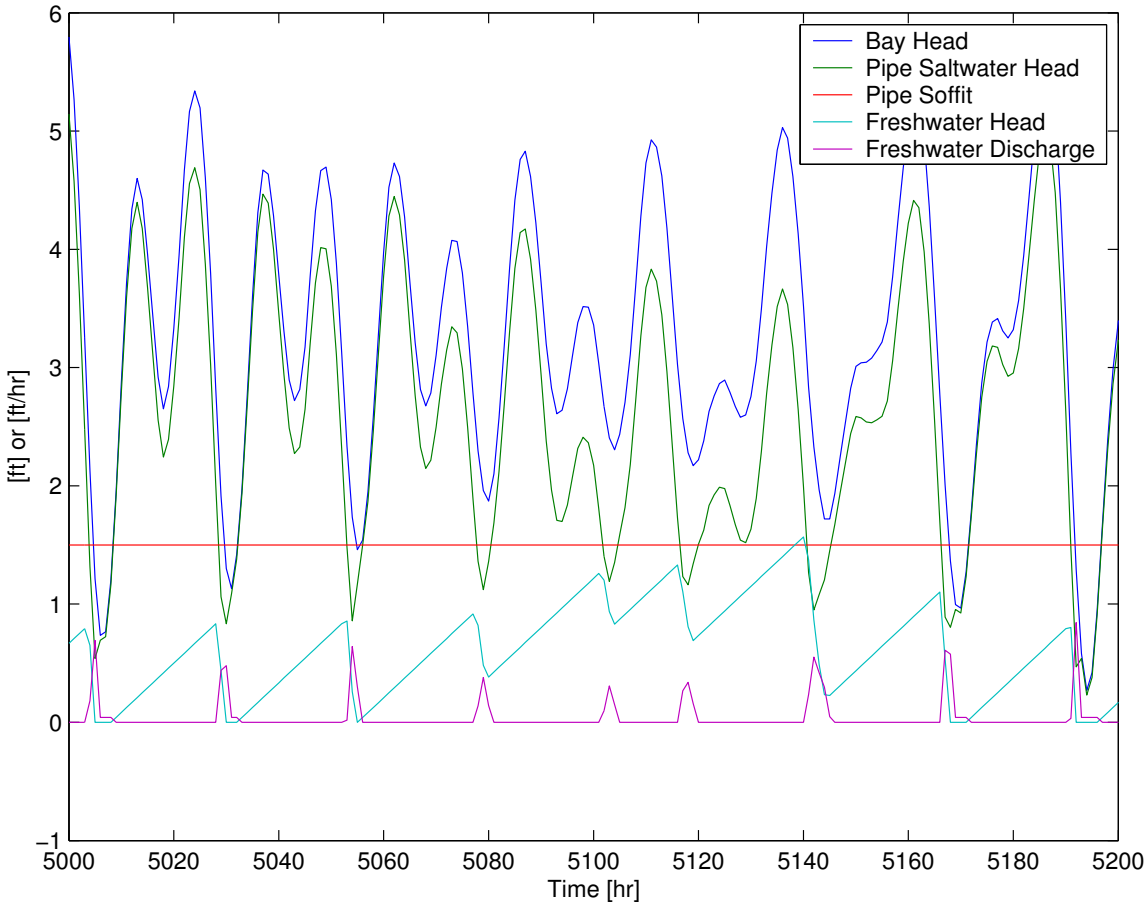

Figure 3.6: Time series of freshwater accumulation and subsequent discharge from Storm Drain S-183 as a function of tide variation.

slopes typically in the range of one-half to four percent. For this analysis, storm drains were assumed to have a one percent slope. Elevations of the storm drain at the outlet varies considerably. To simplify the analysis, the pipe soffit was set at Elevation 2.0 feet (0.61 meters) relative to Mean Lower Low Water (MLLW) datum regardless of the pipe diameter.

Figure 3.6 shows a discharge hydrograph for drain S-183 assuming a drainage rate of 300 gallons per hour (gph) (0.315 L/s). The figure shows the bay water surface elevation, seawater level in the pipe, accumulated freshwater in the pipe,

and freshwater discharge pulses. Consider the freshwater discharge that occurs at Hour 5030: Just prior to release of the freshwater pulse, the head of the freshwater accumulated in the pipe is 0.87 feet (0.27 meters). At that time, the elevation of the saltwater in the pipe is at the pipe soffit. Then at Hour 5030, the saltwater in the pipe drops below the soffit and 0.43 feet of head (0.13 meters) of freshwater is released. Over the following hour another 0.43 feet of accumulated freshwater head is released plus the additional drainage head entering the pipe of 0.04 feet (0.012 meters) (equivalent to 300 gph). From Hour 5031 to 5032, drainage into the pipe directly discharges into the bay (0.04 feet of head). At Hour 5033, the tide rises sealing off the pipe and the freshwater again begins to accumulate in the pipe.

Figure 3.7 shows the freshwater discharge hydrograph in greater detail at Hour 5166 (August 4, 2006, 5:00 AM local time), with a majority of the pulse occurring over a two hour period. Freshwater continues to flow unimpeded from the pipe into the bay at a rate equal to drainage into the pipe (300 gph) until Hour 5173 (11:00 AM) when the rising tide once again seals the end of the pipe.

2D Salinity Transport Modeling and Drainage Rate Estimation

Discharge hydrographs predicted by the loading model were input into the 2D model (Chapter 2) to simulate salinity at sampling sites and support inverse modeling of the dry-weather drainage rate. Local mixing of a pulse of fresh water in saline receiving waters is a complex three-dimensional, time-dependent process. The 2D

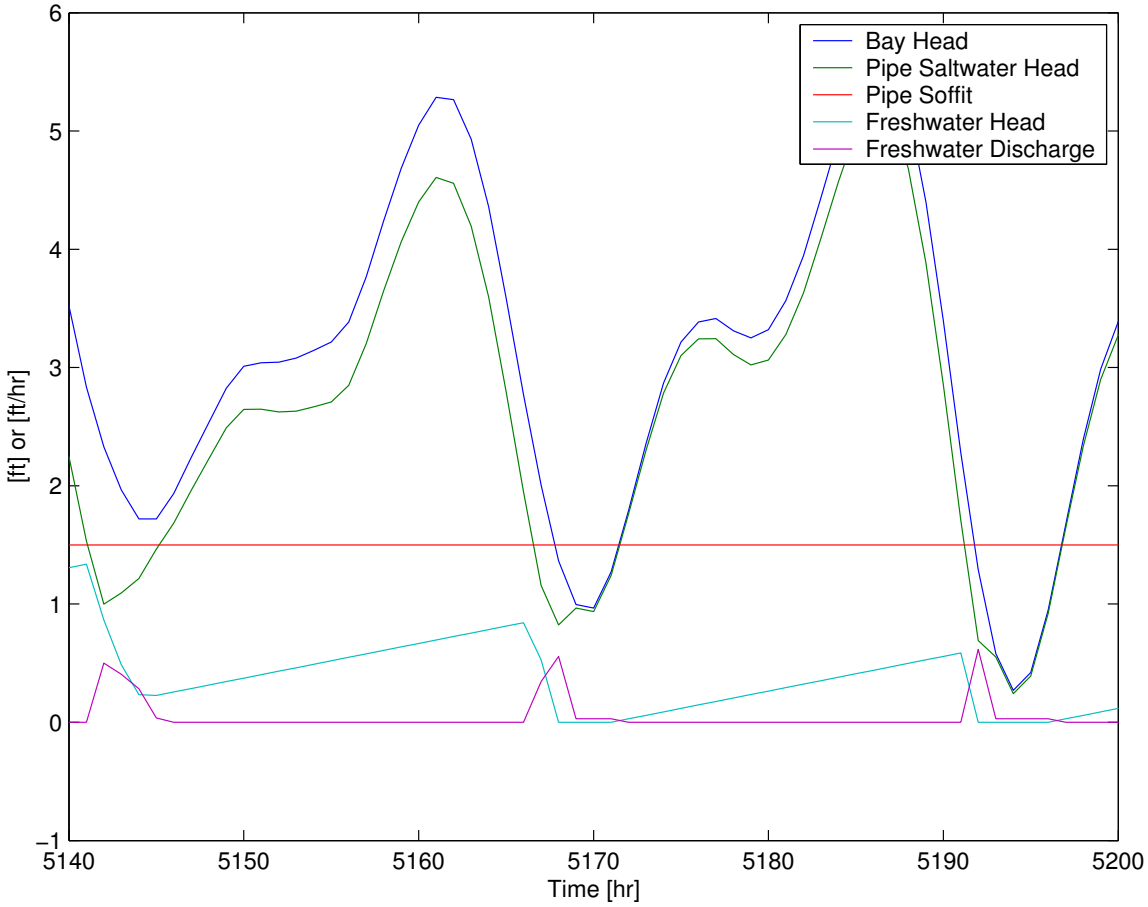

Figure 3.7: Detail of freshwater accumulation in and discharge from Storm Drain S-183.

model used here assumes instantaneous vertical mixing, which introduces uncertainty to the estimated storm drain discharges, but this is not viewed as a major drawback in this study because there are other large sources of uncertainty which affect our ability to estimate discharge. Namely, dry-weather drainage rates are highly variable as a consequence of intermittent and sporadic runoff generation mechanisms linked to human behavior (wash down activities, irrigation, etc.). Figure 3.2 shows that discharges from two drains of similar size can vary by an order of magnitude or more. The uncertainty associated with using a 2D model instead of a 3D model is estimated to be less than one order of magnitude.

A range of drainage rates were considered for each storm drain, and after applying the loading model to determine the time-dependent discharge rate, this was input to the 2D model to predict salinities at the location and time of sampling within the bay. Subsequently, predicted salinity dilutions were compared to measurements to determine the drainage rate that matches the observed salinity dilutions. Cases of over-prediction and under-prediction of the salinity dilution were identified, and the final estimate of the drainage rate was computed by interpolation as shown in Table 3.2. This approach was selected over formal optimization approaches because the 2D model is computationally expensive, given its fine resolution along the shoreline, and because precise discharge estimation was not necessary given other sources of uncertainty.

The above process was repeated for the fifty-nine intermediate-sized drainage areas in Lower Bay where a salinity difference was measured (Grant *et al.*, 2008), and

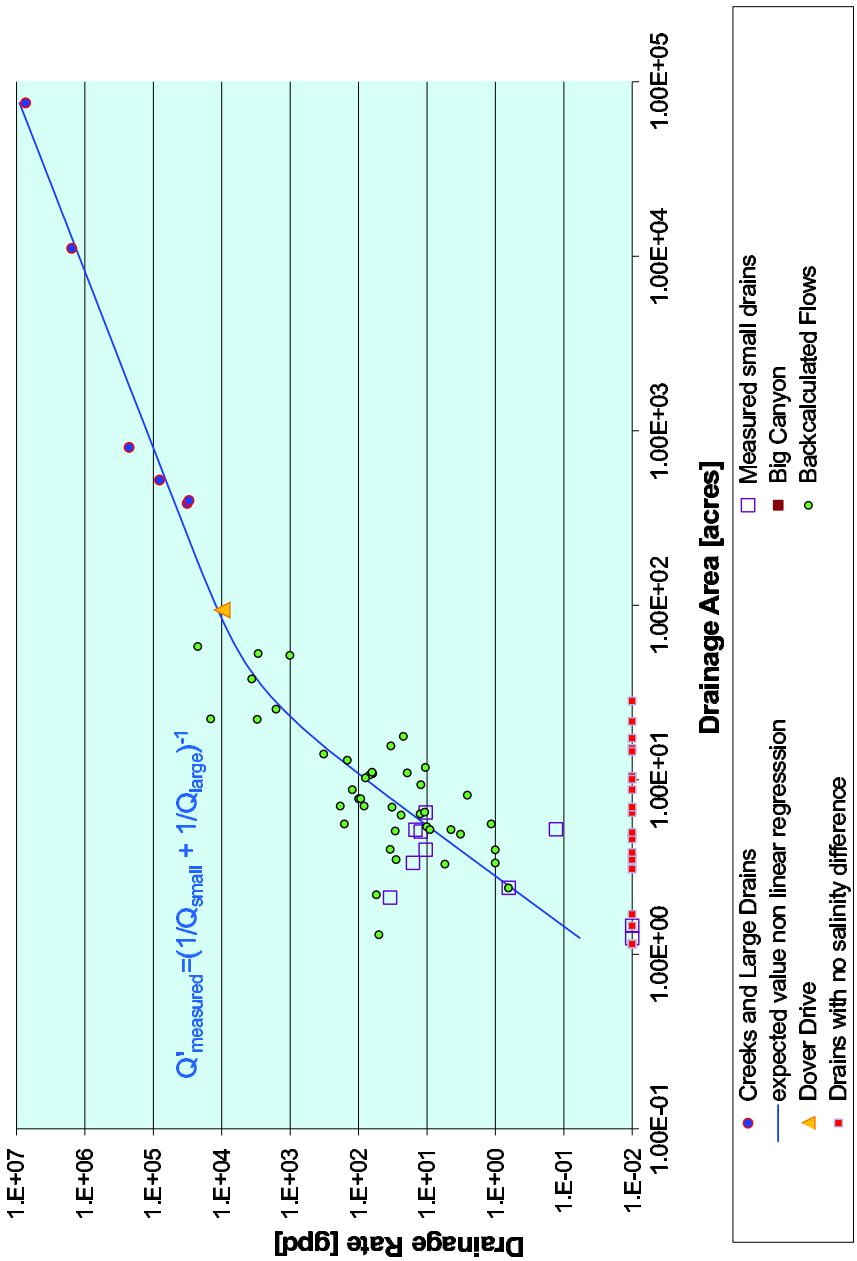

Figure 3.8: Calculated flow rates from intermediate-sized drainage areas overlaid on the *Small/Large Drainage Area* correlation.

Drainage Rate [gph]	**Average Salinity Delta [ppt]**
2400 (assumed)	0.15 (modeled)
2914 (interpolated)	**0.30 (measured)**
3600 (assumed)	0.50 (modeled)

Table 3.2: Interpolating Drainage Flow Rate for Storm Drain S-183

after determining watershed areas for each storm drain from drainage maps and topographic data (City of Newport Beach, 2006), the estimated drainage rates were plotted as a function of drainage area, as shown in Figure 3.8. These results show excellent agreement with the previously reported small- and large-drainage area data: the intermediate-sized drainage area data cluster around the trend line given by Eq. 3.4.

Note that the twenty-five drainage areas where no salinity difference was measured in the Grant *et al.* (2008) study are also shown in Figure 3.8. It cannot be ascertained from the data if the lack of a measured salinity difference is because there was no freshwater flow in these drains or because the sampling occurred before or after a freshwater plume manifested itself.

3.3 Drainage Rates from Different Classes of Conveyance Systems

One of the motivations for this study was to derive an analytical expression for dry weather flows that would assist in evaluating pollutant loads outletting to the bay. As an example, Eq. 3.3 was used to assess the relative importance of the different

classes of conveyance systems outletting to the bay. Table 3.3 tabulates the measured flow rates for San Diego Creek, the Santa Ana-Delhi Channel and Big Canyon Creek and predicted storm drain flow rates. From the table, the two largest creeks, San Diego Creek and the Santa Ana-Delhi Channel, account for over 94% of the urban runoff entering the bay. The twelve largest local drainage systems, which include Big Canyon Creek and the Santa Isabella Channel, all with tributary watershed areas larger than 100 acres (40 hectares), contribute about one-third the flow of the Santa Ana-Delhi Channel. The 207 storm drains draining the small and intermediate tributary watersheds, contribute less than one percent of the total flow.

San Diego Creek, which is the primary drainage conveyance into Newport Bay, has a unit flow rate of 96 gpd per acre (910 L/day per hectare), about 30% less than the unit flow rate conveyed by the Santa Ana-Delhi Channel (139 gpd per acre or 1,300 L/day per hectare). As mentioned in the previous section, the drainage from San Diego Creek watershed can be expected to increase as the efficiently irrigated agricultural areas are developed into residential areas due to the increase in impervious areas. A small part of the difference between the two largest tributary watersheds may be explained by the long reaches of soft bottom in San Diego Creek that allow for infiltration as opposed to the concrete-lined Santa Ana-Delhi Channel. Also, the difference in sizes of the two watersheds may also be a factor as increased evapotranspiration likely occurs with the longer conveyance time for drainage in the San Diego Creek watershed.

From Table 3.3, the unit flow rate for the twelve storm drains with tributary

Drainage Conveyance	**Drainage Area [acre]**	**No. of Storm Drains**	**Total Flow Rate [gpd]**	**Unit Flow Rate [gpd/acre]**	**Percent of Total Discharge**
San Diego Creek (measured)	75,822		7,300,000	96	77.66%
Santa Ana-Delhi Channel (measured)	11,114		1,550,000	139	16.49%
Large-Sized Watersheds ($A \geq 100$ acres) Drained by Storm Drain (calculated)	3,674	12	458,900	125	4.87%
Intermediate-Sized Watersheds ($10 \leq A < 100$ acres) Drained by Storm Drain (calculated)	2,020	71	90,600	45	0.96%
Small-Sized Watersheds ($A < 10$ acres) Drained by Storm Drain (calculated)	626	136	1620	3	0.02%
TOTAL	**93,258**	**219**	**9,400,000**	**101**	**100%**

Table 3.3: Total and unit flow rates of creeks and storm drains flowing into Newport Bay.

drainage area greater than 100 acres (40 hectares) conveying flow directly to the bay is 125 gpd per acre (1,180 L/day per hectare). The unit flow rate from these large-diameter, concrete storm drains is somewhat lower than the unit flow rate from the concrete-lined Santa Ana-Delhi Channel.

The calculated unit flow rate of 3 gpd per acre (28 L/day per hectare) for the small drainage areas is in line with the findings of the City of Newport Beach field study (2008). Most of the small watersheds are found on the Balboa Peninsula and on the islands in the harbor. House densities are high and garden areas are limited. General

observations in the area confirm that over-irrigation runoff conveyed in the street is low. The very flat street grades create long times of concentration that allow for more evaporation as well as increased infiltration of the intermittent flows. Discharge volumes from this limited runoff may be further muted due to imperfections in the gutter that tend to trap small flows.

3.4 Discussion

Dry-weather flow rates from a storm drain or channel can be directly estimated from Eq. 3.3 based on a knowledge of tributary drainage area. The regression is based on field measurements of flow rates from large and small drainage conveyances. 2D model predictions of flow rates back-calculated from field measured salinity dilution at the outlet of 59 small- to intermediate-sized storm drains, provide some assurance that the measured small and large drain data connect in a smooth way. This model of dry weather discharge rates is viewed as a major step forward toward understanding water quality impacts to the bay. Dry weather flows in other catchments in southern California should also be measured to evaluate whether the scaling of the regression is comparable.

A wide range of variability would be expected in dry-weather flow rates that is generated by individual properties from irrigation runoff and washdown activities. It is somewhat remarkable that a *snapshot* of salinity level data in the bay at storm drain outlets provided sufficiently accurate information to allow the 2D modeling approach to be successful. A lesson learned is that it is highly beneficial to sample

a large number of storm drains to capture the range of variability that is present. In the future, the effectiveness of field monitoring can be increased by using the trap-and-release model to estimate the timing of releases of dry weather pulses.

When looking at total constituent loads into a receiving water, loading from small drains can be expected to be very small with respect to creek and large drain inputs as demonstrated in Table 3.3. However, small drains could still have a local impact on water quality at the drain outlet. The impact of constituent loads, i.e. bacteria, from small drains in considered in the following chapter.

With characterization of dry-weather storm drain flow rates, constituent loads entering receiving waters can be predicted assuming constituent concentrations are measured. This in turn would provide a basis for assessing potential impacts from runoff to a receiving water that can then be compared to potential impacts from other source loadings, e.g., pollutant entrainment from bed sediments, aerial deposition, leaking sewer lines or direct inputs from water craft. This information could help in designing a water quality monitoring program or for prioritizing water quality improvement projects.

Chapter 4

Bacterial Impacts from Dry Weather Runoff from Small Drainages on Water Quality at Enclosed Beaches

Most of the material of chapter was co-written with Megan A. Rippy, Brett Sanders, Kristen Davis, Karen McLaughlin, Jack Skinner, John Kappeler and Stanley B. Grant, the co-authors of a manuscript submitted for review to *Environmental Science & Technology* for possible publication (available upon request). To present this work as a chapter in this dissertation, the submitted manuscript was modified slightly to allow for easier reading and to link with other chapters of the disserta-

tion. The results and conclusions remain unchanged. This chapter reports on field and modeling studies of fecal indicator bacteria (FIB) in Newport Bay. FIB groups such as total coliform, fecal coliform, *Escherichia coli* (EC), and enterococci (ENT) are utilized world wide to measure health hazards in bathing and shellfish harvesting waters (Thomann and Mueller, 1987).

Ten years ago, a number of beaches in Newport Harbor Lower Bay were often off-limits to the public due to the presence of elevated FIB concentrations in shoreline waters (Pednekar *et al.* 2005; Jeong *et al.*, 2005). To address this problem, bacterial Total Maximum Daily Loads (TMDLs) have been adopted for the Bay (SWRCB, 1999). While the number of posting has decreased significantly, this study was designed to assist with the TMDL planning process by determining the impact of FIB loads from dry weather runoff in storm drains on water quality in Lower Bay.

4.1 Fecal Indicator Bacteria Field Studies

Five field studies were performed investigating transport and fate of FIB discharged from storm drains around the harbor:

1. Irrigation Runoff Study
2. Lower Bay Shoreline Study
3. Cross-Shore Drain Study
4. Nearshore Turbulence Studies

5. Drain Dye Study

Irrigation Runoff Study

Over irrigation in the residential communities surrounding Lower Bay generates runoff that collects along street curbs, flows into the local drainage system, and discharges to the Bay through drain pipes that extend a short distance down the beach slope. To determine if FIB concentrations near Lower Bay drains are consistent with an irrigation runoff source, samples of irrigation runoff (N = 23), and water near drain outlets (N = 30) were collected from Lower Bay during dry weather on November 16 (2006) (open triangles, Figure 4.1 A). Irrigation runoff samples were collected at 7 AM local time, coincident with peak irrigation runoff from the surrounding landscape, and near-drain samples were collected at low tide (12 PM local time), when drainpipe outlets were exposed and accessible.

All samples of irrigation runoff were aspirated from street curbs into sterile 50 mL syringes, and then dispensed into sterile polypropylene bottles. Near-drain samples (also collected in sterile bottles) were obtained from storm sewer drainpipe outlets. Samples consisted of (1) drainpipe outflow water only (if the water level in the Bay was below the drainpipe outlet) or (2) a mixture of Bay water and drainpipe outflow (if the water level in the Bay was above the drainpipe outlet). All water samples collected were stored on ice and analyzed within six hours for conductivity and FIB concentrations. FIB were measured using the defined substrate test known commercially as IDEXX Colilert-18 (for EC) and Enterolert (for ENT), implemented in a

97 well quantitray format. Conductivity measurements were converted to salinity using the Practical Salinity Scale. No rainfall was recorded on the day of sampling (November 16th), and rainfall on the 14th and 15th was minimal (2.0 mm and 0.25 mm rain, respectively).

Lower Bay Shoreline Study

To characterize how nearshore FIB concentrations vary in space and time, 334 nearshore water samples were collected during dry weather (August, 2006) at 86 sites along the Lower Bay shoreline (open circles, Figure 4.1 A). Sampling was carried out at two cross-shore locations per alongshore site (shoreline and offshore (30 meter bay-ward)) over two consecutive low tides (4:30 - 8:30 AM on August 3 and 4, 2006) and two consecutive high tides (1:30 - 5:00 AM on August 8 and 2:30 - 6:00 AM on August 9, 2006). The east side of Lower Bay was sampled the first night and the west side the second night. It was not possible to sample the entire Lower Bay shoreline in one night and simultaneously keep sample holding times under the six hours required for bacterial testing. All shoreline samples were collected from a kayak. Bay-ward samples were collected simultaneously from an 5.5-meter research boat built specifically for this study (the "Granteater"). All water samples were collected in sterile polypropylene bottles and analyzed for conductivity, EC, and ENT (described above). Sampling was conducted at night to minimize solar effects on FIB concentrations (Rippy *et al.*, 2013; Sassoubre *et al.*, 2012).

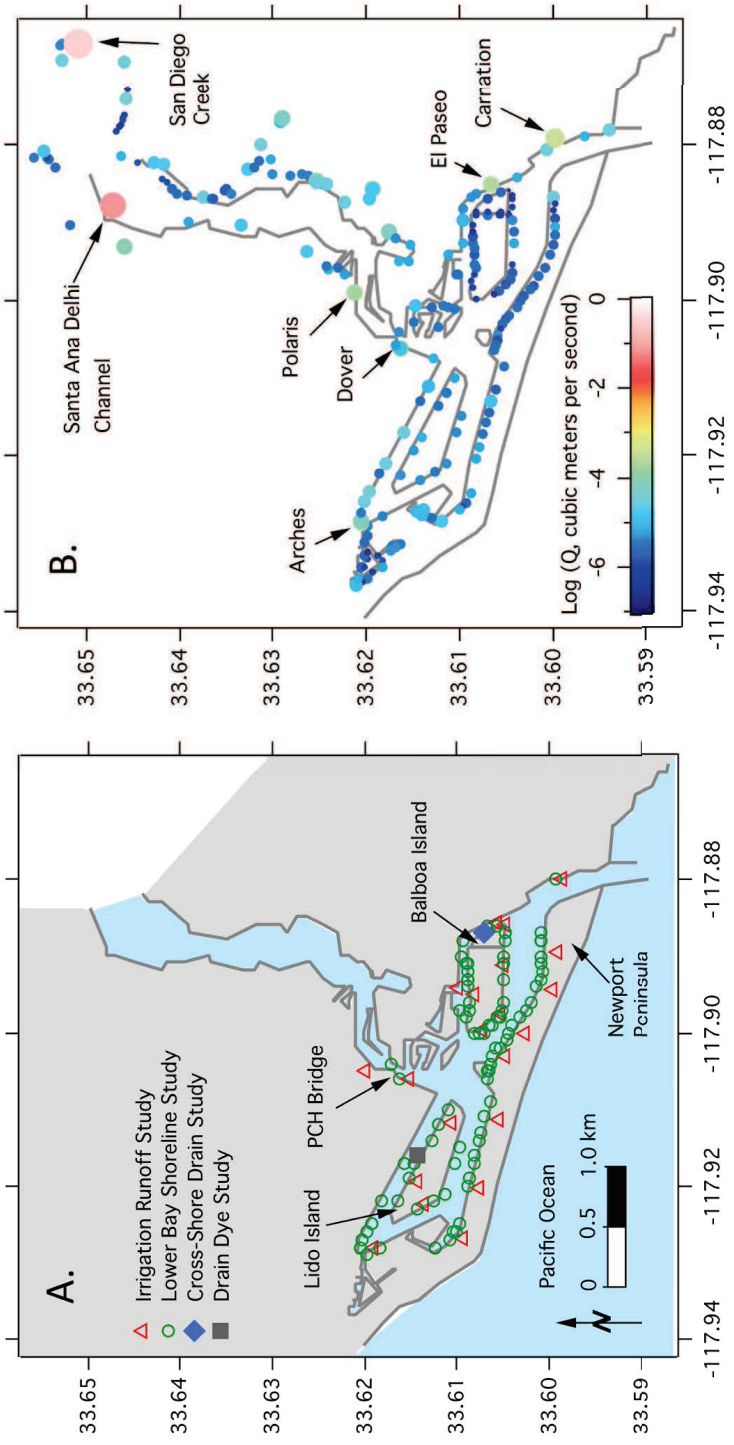

Figure 4.1: Sampling sites (A) and measured and calculated storm conveyance system drainage flow rates (B).

Cross-Shore Drain Study

Cross-shore transects of conductivity and FIB were performed on May 30 (2008) to evaluate cross-shore variability of these analytes bay-ward of small drains. The study was centered on a single drain at Park Avenue Beach, Balboa Island (solid blue diamond, Figure 4.1 A). The drain is adjacent to a public dock, which was used as a platform to collect water samples (N = 49: 9 stations, 2.2 to 3.7 meter spacing). Surface water was sampled at all stations using sterile polypropylene bottles. Bottom water samples were also collected using a Van Doren bottle (Wildco, Yulee, Florida) at stations where water depth exceeded 0.5 meter. All samples (surface and depth) were analyzed within six hours for conductivity, EC, and ENT (described above). Transect sampling occurred four times over a 24-hour period (6 AM, 12 PM, 5 PM, and 10 PM local time), roughly corresponding to low-high tide (LHT), high-low tide (HLT), high-high tide (HHT), and low-low tide (LLT), respectively.

Nearshore Turbulence Studies

Coincident with the Cross-Shore Drain Study, nearshore turbulence was measured using an Acoustic Doppler Velocimeter (ADV) (SonTek/YSI, Inc., San Diego, CA). The ADV was mounted on a metal frame and lowered over the side of the Park Avenue Beach Pier that crosses the Grand Canal between Balboa Island and Little Balboa Island until the frame came to rest on the sediment bed. The ADV measures three components of velocity (U, V, W) corresponding to along-shore, cross-shore, and vertical directions in a small sensing volume located approximately 25 cm above the

sediment bed.

The ADV was deployed eleven times at three sites (5, 6, and 8) near the end of the Park Avenue Beach Pier (see Figure 4.2 C). Deployments occurred at 0657, 1036, 1055, 1242, 1300, 1522, 1600, 1713, 1736, 2221 and 2236 local time on May 30, 2008. During each deployment, velocity measurements were carried out at 25 Hz for 10 minutes.

Prior to the calculation of turbulent statistics, the ADV data were examined to assess the signal strength and quality of the velocity measurements. Data used for analysis had instrument-reported correlation values greater than 90% and signal-to-noise ratios greater than 10 dB. The stationarity of each 10-minute deployment was determined using a non-parametric reverse arrangements test to look for non-stationary trends in the time-averaged and fluctuating quantities (Bendat and Piersol, 2000). This test evaluates whether a sequence of ordered data is derived from independent observations of some random variable by looking for underlying trends in the observations, making no assumptions about the probability distribution of the data. Lastly, despite careful positioning, spectra of the turbulent velocities indicate that data from nine of the ADV deployments collected on flood tide were contaminated by interference from frame or dock piling wakes and could not be used for analysis. The uncontaminated data were collected during deployments at Station 8, located at the end of the dock during ebb tide. Turbulent eddy diffusivity was estimated from ADV velocities that passed all quality control tests listed above. Turbulence intensity

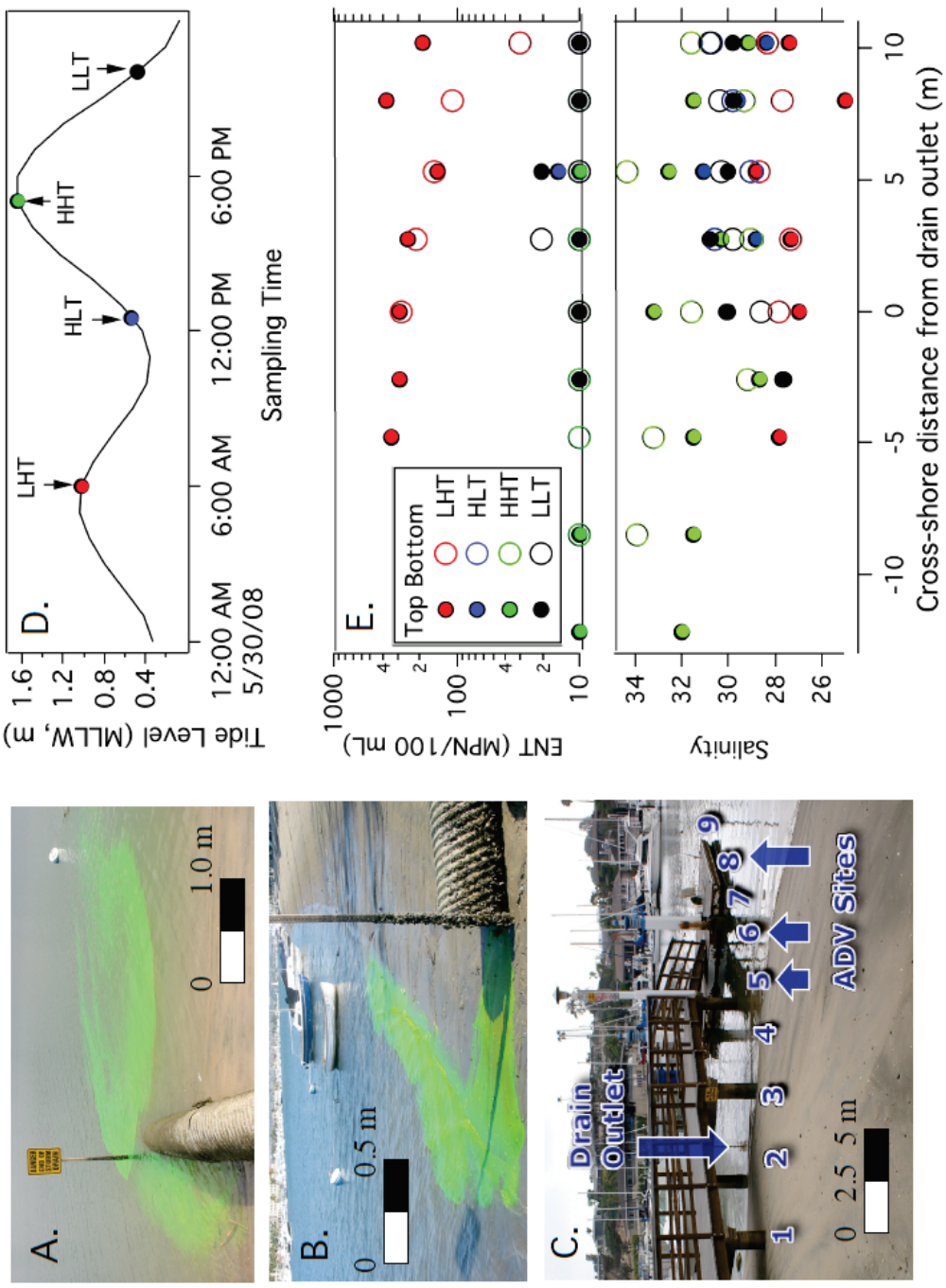

Figure 4.2: Dye Drain Study location at Genoa Beach Storm Drain (A and B) and Nearshore Turbulence Study location at Park Avenue Beach Pier (C).

I, a measure of the turbulent fluctuations in the velocity signal, and the Lagrangian time scale T_L, the time scale over which velocity fluctuations are de-correlated, were calculated for the cross-shore and along-shore directions:

$$I = [\langle u^2 \rangle]^{1/2} \tag{4.1}$$

$$T_L = \int_0^\infty R_x(s) ds \tag{4.2}$$

where u is the fluctuating component of the velocity, brackets denote a time average, and R_x is the autocorrelation function:

$$R_x(s) = \frac{\overline{u(x)u(x+s)}}{\langle u^2 \rangle} \tag{4.3}$$

The turbulent intensity is a measure of the turbulent fluctuations in the velocity signal for the Lagrangian time scale over which velocity fluctuations are de-correlated. Assuming a stationary and homogeneous turbulent field, estimates were obtained for the Lagrangian length scale (L=$I(T_L)$) and the turbulent eddy diffusivity ϵ=$L(I)$. A non-dimensional transverse mixing coefficient was also estimated:

$$\overline{\varepsilon} = \varepsilon/(u_* d) \tag{4.4}$$

where u_* is a measure of turbulent bed shear called shear velocity (estimated from the covariance of ADV velocities) and d is water depth (Fischer *et al.*, 1979). The

non-dimensional transverse mixing coefficient was used to parameterize horizontal diffusion in the Newport Bay flow and transport model described below.

Drain Dye Study

Three dye release experiments were conducted in Lower Bay (Genoa Beach, Lido Island) during dry weather conditions on February 25 (2010) (solid grey square, Figure 4.1 A). These experiments were qualitative, and used to determine (1) the timing of runoff released from small drainpipe outlets; and (2) the extent to which runoff plume dispersal is influenced by buoyancy, tidal currents, and wind.

The first two experiments evaluated freshwater release from small drainpipe outlets. Dye labeled freshwater (1700 L) (Acid Yellow 73, Norlab, Inc., Amherst, OH; specific gravity = 1.0) was pumped into a curbside gutter that drains into Lower Bay through a pipe. Experiment 1 was conducted during morning high tide when the drainpipe outlet was submerged, and Experiment 2 was conducted during afternoon low tide when the outlet was exposed. In both experiments, the flow rate of dye labeled freshwater was 0.50-0.63 L/s to mimic peak (early morning) dry weather runoff from neighboring residential communities. Experiment 3, in contrast to Experiments 1 and 2, evaluated dye dispersal offshore of drainpipe outlets. Here, approximately 5 mL of undiluted dye was poured off the end of the Genoa Beach Public Pier, forming an offshore dye patch. Dye plumes generated by all three experiments were observed and photo-documented for approximately 30 min after dye entered the Bay. Along-shore transport velocity was estimated during Experiment 2 using a series of

time-stamped photographs taken when the plume was traveling parallel to the shoreline.

4.2 2D Flow and Transport Modeling of ENT and EC

The two-dimensional flow and transport model presented in Chapter 2 was applied to quantify: (1) the relative impact of large drains and tributaries versus small drains on shoreline water quality in Lower Bay, and (2) the impact of point discharge dynamics on shoreline water quality, in particular the role of tidal backwater conditions which cause intermittent fresh water releases near low.

The model was used to simulate the spatio-temporal distribution of three scalars, salinity, ENT and EC, in Newport Bay. To evaluate the relative influence of runoff from large sources (tributaries and 12 large subwatersheds drained by storm drains) and smaller sources (207 small- and intermediate-sized subwatersheds drained by storm drains) on shoreline water quality in Lower Bay, three scenarios were evaluated with the discharge regime for the storm drains in Upper Bay and the Harbor defined as shown in Table 4.1.

In Scenario 1, runoff entered the Bay only from tributaries and large drains (i.e., inputs from small drains were "turned off"). In Scenario 2, runoff entered the Bay from a full inventory of inputs (tributaries, large and small drains) with small drains assumed to discharge runoff continuously throughout the tidal cycle. Scenario 3 is

	Upper Bay: Large Drains	**Harbor: Large Drains**	**Upper Bay: Small Drains**	**Harbor: Small Drains**
Scenario 1	H	H	off	off
Scenario 2	H	H	C	C
Scenario 3	H	H	C	H (trap-and-release)

Table 4.1: Types of Storm Drain Discharge to Bay where C indicates *Constant Discharge Rate* and H indicates means *Hydrograph Discharge* (tidally influenced)

.

similar to Scenario 2 except here point discharges from small drains occurred when the freshwater head in the drain exceeds the bay water head referenced to the storm drain soffit (usually on the approach to low tide). Hence, this scenario accounts for a so-called trap-and-release mechanism described in Chapter 3 that is informed by the field experimental studies described above. Model scenarios were determined to be different when the number of locations where model predictions of FIB exceeding a given FIB concentration was significantly different. Significance was evaluated at multiple FIB concentrations allowing scenarios to be compared across different recreational water quality standards including: (1) presence/absence (>or <10 EC or ENT per 100 mL); (2) geometric mean standard (GM: 35 ENT or 126 EC per 100 mL); (3) beach action value (BAV: 70 ENT or 235 EC per 100 mL); and (4) statistical threshold value (STV: 130 ENT or 410 EC per 100 mL) (USEPA, 2012).

Model Boundary Conditions: FIB and Salinity

Water entering the domain from the offshore boundary is assumed to be free of FIB. Dry weather runoff from storm drains is assumed to have FIB concentrations equal to the median values measured during field sampling, as indicated in Table 4.2.

Constituent	SDC [MPN/100 ml]	SAD [MPN/100 ml]	Storm Drains [MPN/100 ml]
ENT	159	3,165	1,500
EC	52	309	50

Table 4.2: FIB concentrations in storm drains.

SDC and SAD inputs are specified as time-dependent flows based on gage measurements, with FIB concentrations equal to dry-weather median concentrations as indicated in Table 4.2. FIB were assumed to die-off in accordance with first-order kinetics for sunlight exposed marine waters as described by Sinton *et al.* (2002), similar to previous studies in nearby Talbert Marsh (Sanders *et al.*, 2005).

Drainage Runoff Rates into Storm Drains

In Chapter 3, a drainage rate - drainage area regression was developed (Eq. 3.3):

$$Q' = [(1/Q_{\text{large}} + 1/Q_{\text{small}})]^{-1} \tag{4.5}$$

relating the rate of runoff (drainage) into drainage conveyance based on tributary area for small and large conveyances. The regression for drainage rates of small conveyances based on tributary watershed area is given by Eq. 3.2 with the conversion to SI units as:

$$Q_{large} = 0.25A^{3.47}, R^2 = 0.40 \quad (p = 0.25) \tag{4.6}$$

with drainage area in km^2 and drainage rate in m^3/s. For large drains, Grant *et al.* (2008) provided the following regression for drainage rate as a function of tributary

watershed area (SI units):

$$Q_{large} = 0.0013A, R^2 = 0.96 \quad (p < 0.0001) \tag{4.7}$$

based on an assumed linear regression of the mean drainage rates of San Diego Creek and Santa Ana-Delhi, as well as the Carnation, El Paseo, Polaris, Arches and Dover storm drains. The drainage rate - drainage area regression is shown in Figure 4.3.

Horizontal Mixing Parameterization

The model was updated to account for horizontal mixing with a horizontal diffusivity that is consistent with turbulence measurements made during the ADV Study described in the Nearshore Turbulence Measurements subsection that follows. Horizontal diffusivity was computed and iteratively updated as $\varepsilon = 0.3u_*d$ based on the ADV studies. The model was spun up for a 28-day antecedent period prior to comparison with water samples collected in August, 2006. The simulation time period (August, 2006) was chosen to coincide with the Lower Bay Shoreline Study described above.

4.3 Field Study and 2D Modeling Results

Permutation-based and Bootstrap-based Statistical Techniques

Non-parametric permutation tests were used to compare FIB concentrations or salinities amongst water samples collected during the (1) Irrigation Runoff Study or (2) Lower Bay Shoreline Study. Additional bootstrapped-based analyses were

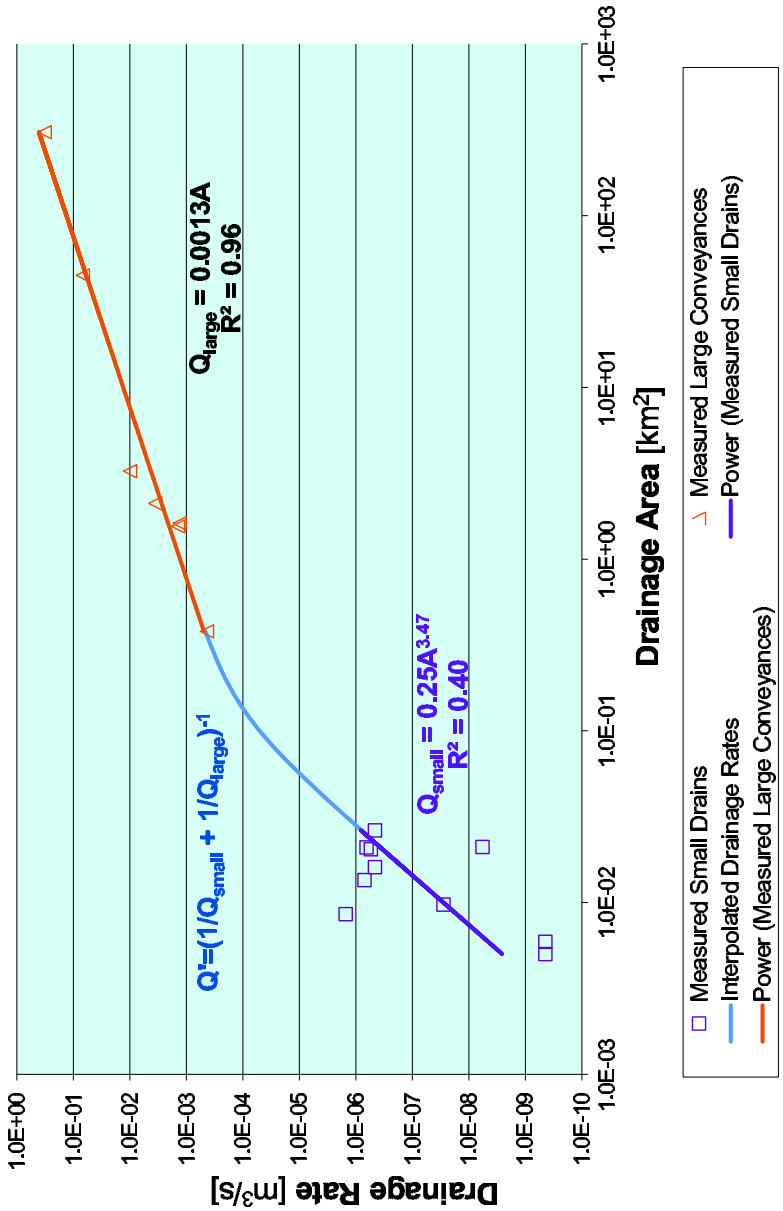

Figure 4.3: Drainage rate/drainage area regression for small and large conveyances.

used to compare model scenarios performed during the Flow and Transport Modeling Study and to identify those that produced significantly different FIB contamination signatures along the Lower Bay shoreline.

Nonparametric methods do not rely on the estimation of parameters such as the mean or the standard deviation to describe the distribution of the variable of interest in the population. Permutation tests are a subset of non-parametric statistics. The basic idea behind permutation methods is to generate a reference distribution by recalculating a statistic for many permutations of the data.

Bootstrapping is a statistical method for estimating the sampling distribution of an estimator by sampling with replacement from the original sample. The idea behind bootstrap is to use the data of a sample study at hand as a *surrogate population*, for the purpose of approximating the sampling distribution of a statistic; i.e. to resample (with replacement) from the sample data at hand and create a large number of *phantom samples* known as bootstrap samples. The sample summary is then computed on each of the bootstrap samples (usually a few thousand). A histogram of the set of these computed values is referred to as the bootstrap distribution of the statistic. In bootstraps most elementary application, one produces a large number of *copies* of a sample statistic, computed from these phantom bootstrap samples. Then, a small percentage, say 100(a/2)% (usually a=0.05), is trimmed off from the lower as well as from the upper end of these numbers. The range of remaining 100(1-a)% values is declared as the confidence limits of the corresponding unknown population summary number of interest, with level of confidence 100(1-a)%.

Irrigation Runoff Study

For the Irrigation Runoff Study, a paired, non-parametric t-test was used to determine if ENT or EC concentrations differed across irrigation runoff (IR) and near drain water (ND) samples. A second, non-paired t-test was used subsequently to determine if ENT or EC concentrations were different in near drain water samples with salinity greater than 30 ppt *saline* or less than 30 ppt *brackish*.

The paired, non-parametric t-test was performed as follows. First, reciprocal differences between near drain water and irrigation runoff sample pairs were calculated (e.g., ND-IR and IR-ND). Subsequently, these two sets of reciprocal differences were pooled, shuffled, and used to calculate a t-statistic. This procedure was performed 10,000 times, generating a t-distribution expected under the null hypothesis that irrigation runoff and near drain water sample groups were not significantly different. This t-distribution was then compared to t-values calculated for the original (non-shuffled) data difference scores. Irrigation runoff and near drain water data sets were determined to be significantly different when $<5\%$ of shuffling events resulted in t-values more extreme than the original data t-value.

The non-paired t-test used to compare EC and ENT concentrations in saline vs. brackish near drain water samples was identical to the above described test save that it was performed on raw data values instead of differences between sets of paired values. This follows our assumption that saline and brackish near drain water sample groups are independent, making paired analysis inappropriate.

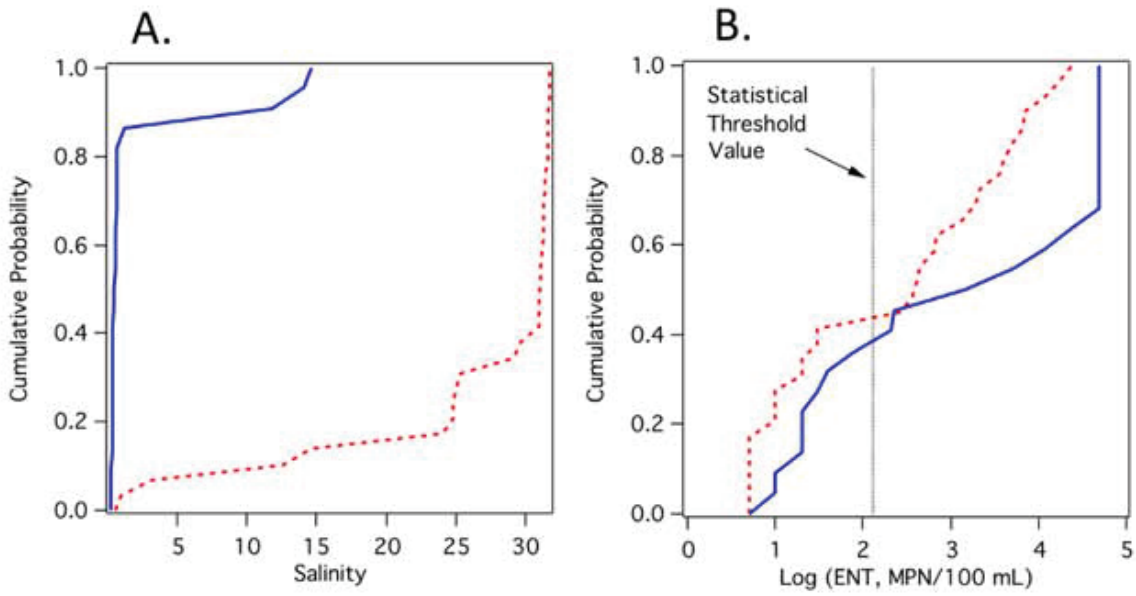

Figure 4.4: Cumulative probability plots of data collected during the Irrigation Runoff Study, including measurements of salinity (A) and ENT (B). IR and ND samples are distinguished with solid blue and dotted red lines, respectively. US EPA STV for ENT (130 MPN per 100 mL) is marked with black dotted lines. Note that FIB measurements above or below the detection limit (10 and 20,500 MPN per 100 mL, respectively) was set to twice the upper-limit of detection or one-half the lower-limit of detection.

	ENT t-statistic	ENT p-value	EC t-statistic	EC p-value
IR vs. ND[a]	1.85**	0.0069	-0.11	0.5600
ND brackish ND saline[b]	3.37**	0.0028	3.47**	00.0019

Table 4.3: Table S1: Irrigation Runoff Study - Permutation-based t-test. **: significant at a p <0.05 level. [a]: paired t-test. [b]: non-paired t-test.

Although irrigation runoff samples were fresh (median salinity: 0.5 ppt), drainpipe outlet samples had variable salinity ranging from fresh to oceanic (salinity: <0.7 to 32 ppt; median 31 ppt). (See Figure 4.4 A.) FIB concentrations were also variable, spanning four orders of magnitude in both irrigation and drainpipe outlet samples (<10 to >20,500 MPN per 100 ml, Figure 4.4 B).

ENT concentrations were significantly higher in irrigation runoff than drainpipe outlet samples, while EC concentrations were not significantly different (permutation-based paired t-test; p <0.05 level, Table 4.3). Amongst near drain samples, those with brackish water (salinity <30 ppt) had significantly higher FIB concentrations than those that were saline (salinity >30 ppt) (permutation-based t-test; p <0.05 level, Figure 4.5, Table 4.3).

Median FIB concentrations in irrigation runoff samples were 30 MPN per 100 ml for EC, and 1,455 MPN per 100 mL for ENT (Figure 4.4 B). These values were rounded to the nearest 50 MPN per 100 ml and adopted as the runoff source concentrations in the Flow and Transport Modeling Study (EC: 50 MPN per 100 mL, ENT: 1,500 MPN per 100 mL).

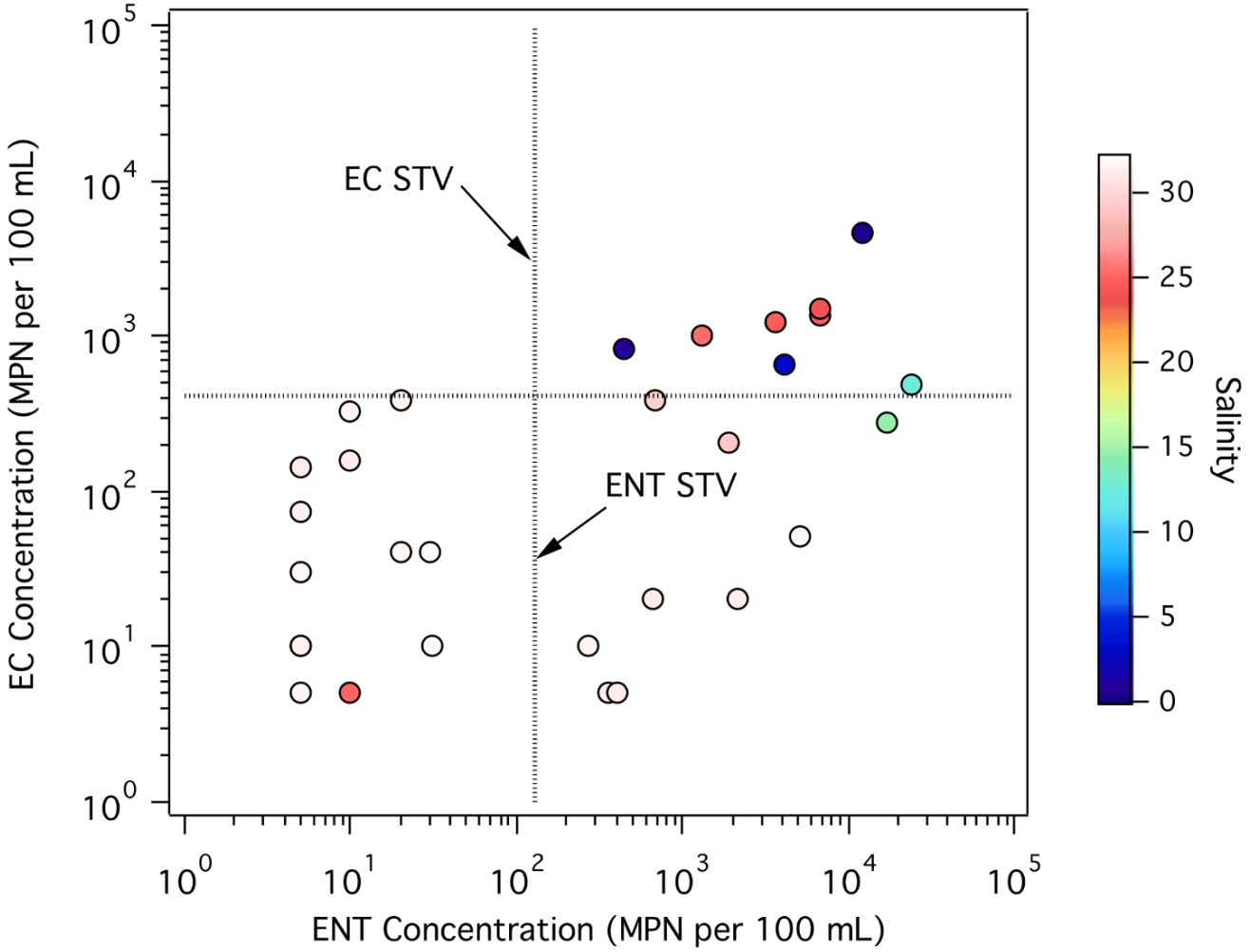

Figure 4.5: Cross plots of ENT (x-axis) and EC (y-axis) concentrations in ND samples collected during the Irrigation Runoff Study. The STVs for EC and ENT are marked with black dotted lines. The colormap shows sample salinity. Note that most samples exceeding the STV for both EC and ENT had salinities <30 ppt.

Lower Bay Shoreline Study

For the Lower Bay Shoreline Study, two-way non-parametric ANOVAs (analysis of variance) were used to determine if salinity, ENT, or EC were different in samples collected onshore vs. offshore, and at high tide vs. low tide. These tests were performed as recommended by Manly (2007). Briefly, samples were shuffled across groups (high tide, low tide, onshore, and offshore), and re-assigned at random. Three F-statistics were calculated for each shuffled dataset: 2 main effects (F_{tide} and $F_{location}$) and their interaction ($F_{tide:location}$). This process was repeated 10,000 times, producing distributions of F_{tide}, $F_{location}$, and $F_{tide:location}$ expected under the null hypothesis that water samples are statistically indistinguishable across groups. No distributions were bimodal, suggesting that residual based resampling techniques were not required. The F distributions generated were compared to values of F_{tide}, $F_{location}$, and $F_{tide:location}$ estimated using the original (non-shuffled) data. As for the above described t-tests, main effects (F_{tide} and $F_{location}$) and effect interactions ($F_{tide:location}$) were determined to be significant when less than 5% of shuffling events resulted in F-values more extreme than those calculated for the original data.

Permutation-based multiple comparison tests were performed subsequent to all non-parametric ANOVAs. These tests are analogous to the non-paired t-test described in the Irrigation Runoff Study section (see above). Four combinations of high tide, low tide, onshore and offshore datasets were evaluated (high tide onshore vs. high tide offshore, low tide onshore vs. low tide offshore, high tide onshore vs. low

tide onshore, and high tide offshore vs. low tide offshore). Data sets were determined to be significantly different at a Bonferroni-Holms corrected $p < 0.05$ level. Marginal significance was also evaluated at a Bonferroni-Holms corrected $p < 0.10$ level. The Bonferroni-Holms correction adjusts for multiple comparisons (Holm, 1979). The correction is performed as follows: $\rho_{BH} = p_{sig} / (n - c)$, where p_{sig} is the significance threshold desired ($p < 0.05$ or 0.10), n is the number of comparisons evaluated (4), c is the number of comparisons that have already been performed (0 for the first comparison), and ρ_{BH} is the new significance threshold that must be met for a comparison to be significant at the p_{sig} level. This test is always applied to the comparison with the largest t-value first (c = 0), and to other comparisons in order of decreasing t-value (c = 1 to 3). Note that c only advances when comparisons are significant (e.g., all comparisons with smaller t-values than the first non-significant comparison will also be non-significant).

During early morning low tide, 24% of shoreline samples and 12% of offshore samples (collected 30m bay-ward) exceeded the statistical threshold value (STV) for EC and/or ENT (Figure 4.6 B). Fewer samples exceeded the statistical threshold value for either FIB group during high tide (1% of shoreline or offshore samples; Figure 4.6 A). Consistent with this finding, overall FIB concentrations were significantly higher during low tide than high tide (permutation-based ANOVA; $p < 0.05$, Tables 4.4 and 4.5, Figure 4.7 B,C). Nearshore contamination was variable along-Bay and was highest (7 samples exceeded the statistical threshold value for EC, ENT, or both FIB groups) in a $\sim$ 1 km region along the Newport Bay peninsula (black dashed box, Figure 4.6

	ENT t-statistic	ENT p-value	EC t-statistic	EC p-value	Salinity t-statistic	Salinity p-value
$\mathbf{F}_{tide}$	22.8**	0.0000	50.78**	0.0000	0.89	0.3783
$\mathbf{F}_{location}$	2.40	0.1169	5.89**	0.0152	2.69*	0.0972
$\mathbf{F}_{tide:location}$	1.50	0.2311	0.71	0.4059	1.11	0.3215

Table 4.4: Table S2: Lower Bay Shoreline Study - 2 Way Permutation-based ANOVAs. **: significant at a p <0.05 level. *: marginally significant at a p <0.10 level.

A).

Cross-shore differences in FIB concentration were less pronounced than tidal differences. That said, at low tide FIB concentrations were generally higher at the shoreline than 30 meter bayward (Figure 4.7 B,C). This pattern was marginally significant for EC (Bonferroni-Holms corrected p <0.10 level) and was not significant for ENT (permutation-based multiple comparison test, Table 4.5). Salinity was also cross-shore variable during low tide with lower salinities measured at the shoreline (Figure 4.7 A). This pattern was marginally significant at a Bonferroni-Holms corrected p <0.10 level (permutation-based multiple comparison test, Table 4.5). Both FIB groups exceeded the STV in 20% of brackish samples (salinity <30 ppt) and 1.5% of saline samples (salinity >30 ppt) (Figure 4.8). In summary, FIB concentrations are generally higher: (1) at low tide, (2) close to shore, and (3) in samples with salinity <30 ppt.

Cross-Shore Drain Study

EC concentrations were below the STV in water samples from all transects (data not shown). ENT concentrations were also frequently below the STV, although ex-

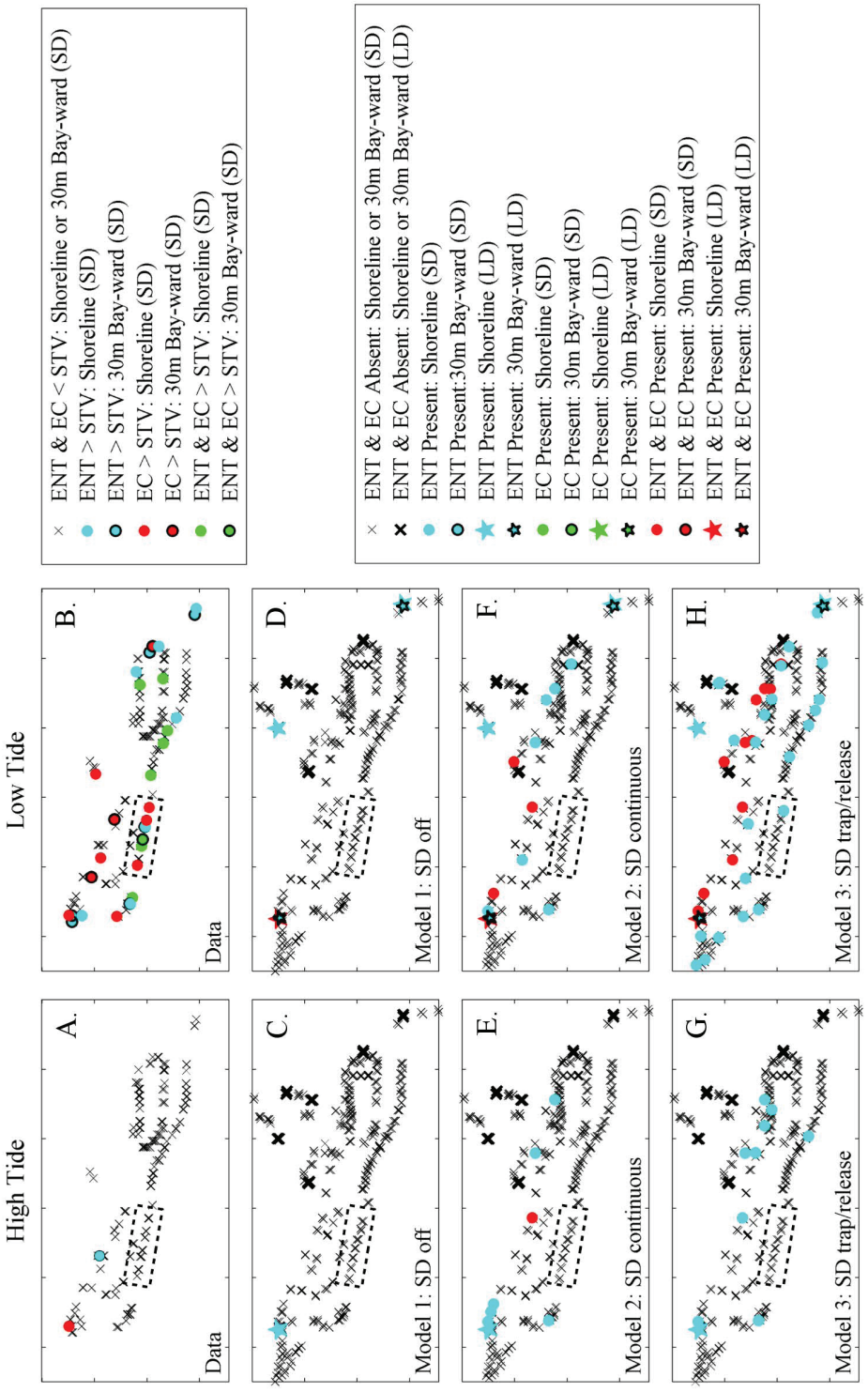

Figure 4.6: Predicted ENT and EC under three scenarios vs. measured.

	ENT t-statistic	**ENT p-value**	**ENT ρ_{BH} at p_{sig}=0.10**[e]	**ENT ρ_{BH} at p_{sig}=0.05**[f]	**EC t-statistic**	**EC p-value**
HT[a] **ON**[c] **LT**[b] **ON**	3.58**	0.0002	0.0250	0.0125	5.25**	0.0000
HT OFF[d] **LT OFF**	3.26**	0.0014	0.0333	0.0167	4.82**	0.0000
LT ON LT OFF	1.51	0.1280	0.0500	0.0250	2.00*	0.0462
HT ON HT OFF	0.42	0.6732	0.0500	0.0250	1.37	0.1702

	EC ρ_{BH} at p_{sig}=0.10[c]	**EC ρ_{BH} at p_{sig}=0.05**	**Salinity t-statistic**	**Salinity p-value**	**Salinity ρ_{BH} at p_{sig}=0.10**[c]	**Salinity ρ_{BH} at p_{sig}=0.05**
HT[a] **ON**[c] **LT**[b] **ON**	0.0250	0.0125	1.06	0.4288	0.0333	0.0125
HT OFF[d] **LT OFF**	0.0333	0.0167	0.16	0.8952	0.0333	0.0125
LT ON LT OFF	0.0500	0.0250	1.76*	0.0152	0.0250	0.0125
HT ON HT OFF	0.1000	0.0250	0.46	0.7692	0.0333	0.0125

Table 4.5: Lower Bay Shoreline Study - 2 Way Permutation-based ANOVAs. **: significant at a Bonferroni-Holms corrected p <0.05 level. *: marginally significant at a at a Bonferroni-Holms corrected p <0.10 level. [a]: HT=high tide, [b]: LT=low tide, [c]: ON=onshore, [d]: OFF=offhsore, [e,f]: Bonferroni-Holms corrected for p <0.10 and 0.05 significance level, respectively.

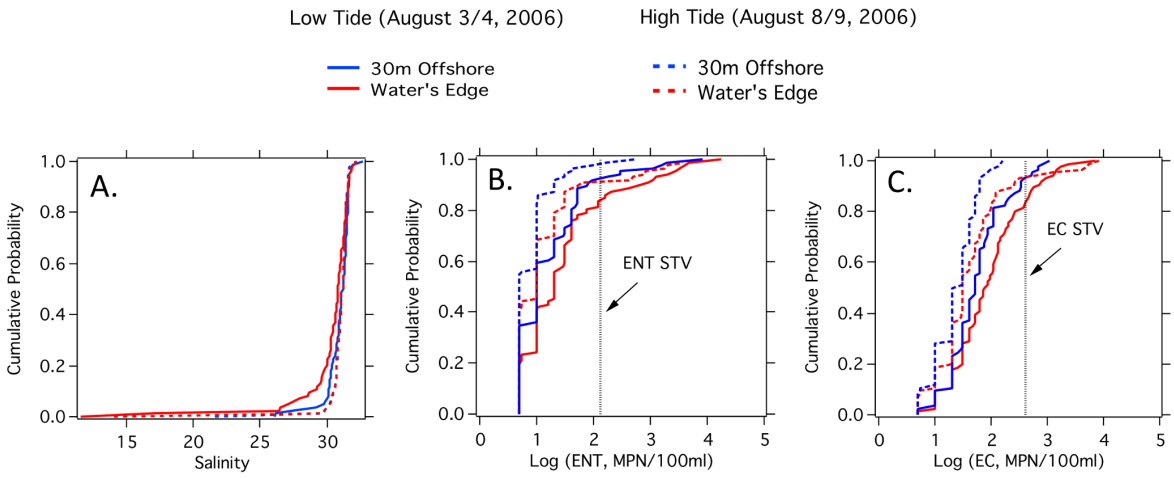

Figure 4.7: Cumulative probability plots of data collected during the Lower Bay Shoreline Study, including measurements of salinity (A), ENT (B), and EC (C). Shoreline samples and offshore samples are marked with red and blue lines, respectively. Dashed lines correspond to high tide samples and solid lines to low tide samples. US EPA STVs for EC and ENT are marked with black dotted lines. As for the Irrigation Runoff Study, FIB measurements above or below the detection limit were set to twice the upper-limit of detection or one-half the lower-limit of detection, respectively.

ceedances were observed during the early morning low-high tide (LHT, Figure 4.2 D,E). The average salinity was lowest during LHT (27.6 +/- 1.0), intermediate during HLT and LLT (29.8 +/- 0.9 ppt and 29.8 +/- 1.0 ppt, respectively), and highest during HHT (31.3 +/- 1.8 ppt) (Figure 4.2 D,E). In short, samples collected during LHT had the lowest salinity (max <29 ppt) and the highest ENT concentrations (11 of 12 samples exceeded the STV, Figure 4.2 D,E).

The vertically resolved samples collected during LHT reveal two patterns: (1) samples collected near the drain outlet are well-mixed over the vertical (see open and filled red circles for stations located <5.2 meter from the drain, Figure 4.2 E), and (2) surface water samples collected at the end of the dock are fresher and have higher ENT concentrations than deep water samples (see open and filled red circles

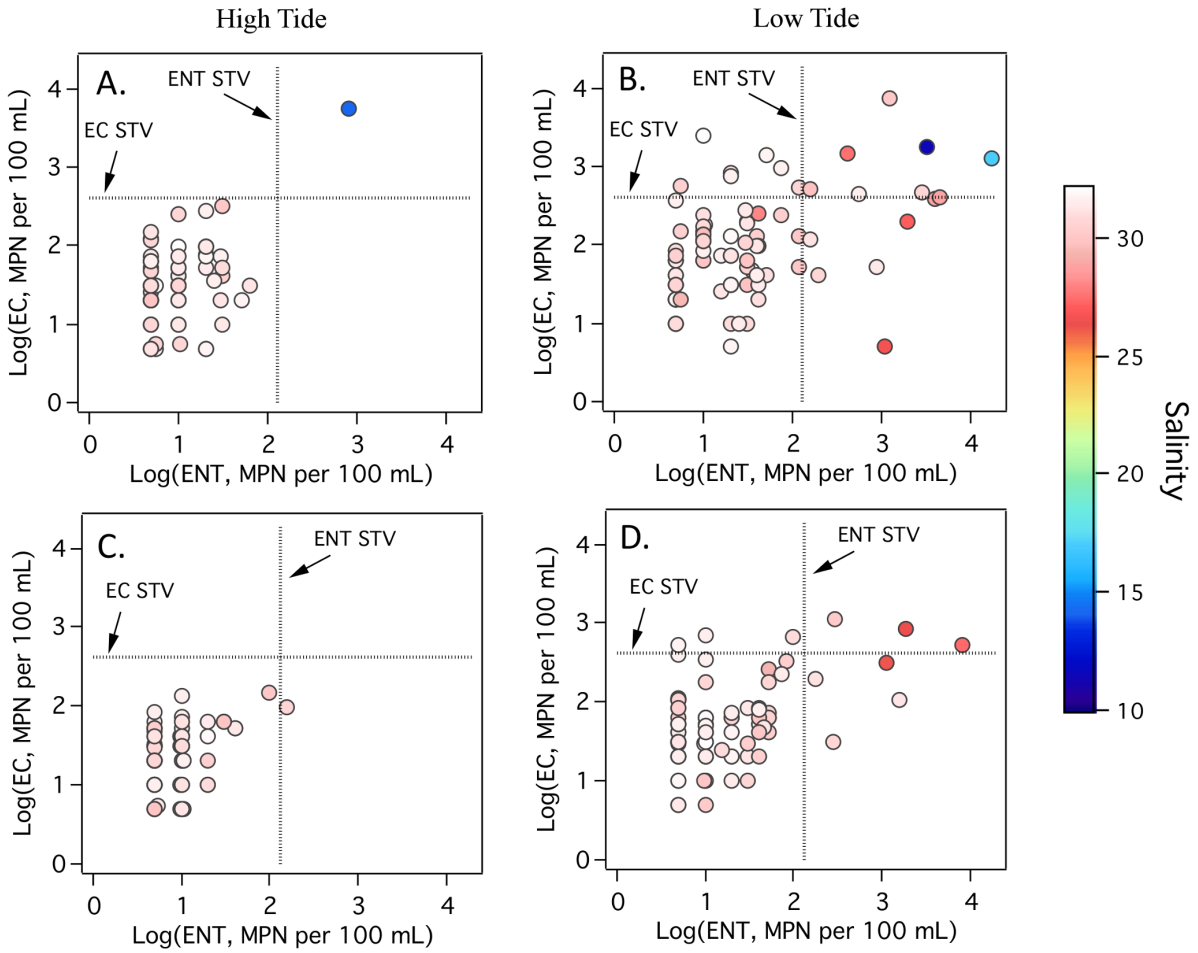

Figure 4.8: Cross plots of ENT (x-axis) and EC (y-axis) concentrations in samples collected during the Lower Bay Shoreline Study: A) shoreline stations at high tide, B) shoreline stations at low tide, C) offshore stations at high tide, D) offshore stations at low tide. For all panels, the colormap indicates sample salinity and the STVs for EC and ENT are marked with black dotted lines. While most samples exceeding the STV for EC and ENT at low tide had salinities <30 ppt, few exceedances were observed at high tide, irrespective of salinity.

for stations located >7 meters from the drain, Figure 4.2 E).

Nearshore Turbulence Measurements

Turbulent velocity spectra indicate that the nine ADV deployments collected on flood tide were contaminated by interference from frame or dock piling wakes and could not be used for analysis. Uncontaminated data were collected during a single ebb tide deployments at Station 8 were used to estimate alongshore (ε_x = 0.003 m^2/s) and across-shore (ε_y = 0.001 m^2/s) turbulent eddy diffusivities, a quantity which parameterizes the bulk dispersal effects of turbulent velocities. The associated Lagrangian length scales along- and across-shore were 30 cm and 16 cm, respectively. A value of 0.3 was estimated for the non-dimensional transverse mixing coefficient, which falls within the range of values observed for natural channels (Fischer, 1979).

Drain Dye Study

During Experiment 1 (performed on falling tide), no dye was observed leaking from the drainpipe outlet when it was flooded with bay water (dye trapped: 0 - 1.75 hours after addition to the curbside gutter). Dye began leaking from a small crack near the end of the pipe when the tide level was even with the top of the outlet (initial dye release: 1.75 hours after addition to the curbside gutter), and a large dye plume was discharged (moving offshore and down-Bay (east) with the falling tide) when the tide level fell below the top of the outlet (bulk dye release: several minutes post-discharge from the crack). The two dye plumes (crack and outlet) are visible in the photo taken $\sim$ 2 hours after the dye was added to the curbside gutter (Figure 4.2

A).

During Experiment 2 (performed during a low, flood tide) the drainpipe outlet was exposed, and located several meters above the water line. Within minutes of addition to the curbside gutter, dye tagged freshwater flowed out of the drain and down the beach. Upon entering the Bay, the dye plume hugged the shoreline and traveled down-Bay at approximately 0.07 m/s (Figure 4.2 B). The direction of transport opposed the average tidal current (up-bay Bay on flood tide), but was consistent with prevailing winds (out of the northwest).

During Experiment 3, the dye bolus released from the end of the Genoa Beach pier formed a vertically sheared plume. Tide and wind conditions were the same as in Experiment 2. The upper portion (top 20 cm) of the plume moved down-Bay and shoreward (parallel to the prevailing wind direction), and the bottom portion moved up-Bay (parallel to the average tidal current).

Flow and Transport Modeling

Bootstrap-based statistical techniques were used to determine if the different model scenarios simulated during the Flow and Transport Modeling Study produced significantly different FIB concentrations at storm drain outlets. Briefly, data were thresholded at all possible FIB concentrations from 10 to 1,500 MPN per 100 ml, resulting in 1,490 binary datasets for each scenario. This allowed model scenarios to be evaluated at multiple thresholds, reflecting different US EPA FIB criteria. Each dataset was sampled with replacement 1,000 times, and the number of drains ex-

ceeding the FIB threshold for that dataset was determined. Global averages and associated 95% bias-corrected bootstrap confidence intervals were calculated across all 1000 realizations for each scenario. Model scenarios were determined to be significantly different ($p < 0.05$) for all FIB concentrations where the confidence interval bounds of one scenario did not intersect the bounds of another scenario.

The three model scenarios control for differences in fresh water inputs as follows: Scenario 1 accounts for only tributaries and large drains only, Scenario 2 accounts for continuous small drain discharges in addition to tributaries and large drains, and Scenario 3 accounts for trap-and-release small drain discharges in addition to tributaries and large drains. Distinct spatial and temporal FIB patterns are found by comparing the scenarios. The number of detection events predicted in Lower Bay (>10 EC or ENT per 100 mL) was highest under Scenario 3, and lowest under Scenario 1 (Figure 4.6). FIB were only detected along the entire Lower Bay perimeter (consistent with experimental measurements) under Scenario 3 (Figure 4.6 B,H). Note that all scenarios underestimated FIB concentrations, especially at stations bay-ward of small drains, where simulated FIB were always below the detection limit (Figures 4.6, 4.7 and 4.9). All scenarios also failed to reproduce the region of the Newport Peninsula with the highest concentration of FIB exceedences identified during the Lower Bay Shoreline Study (black dashed box, Figure 4.6).

FIB concentrations exhibited the strongest tidal signature under Scenario 3 (Figure 4.9), although both scenarios with small drain discharge predicted more FIB detects at low vs high tide, consistent with experimental measurements (Figure 4.6

A,B and E-H). No significant differences were observed between model scenarios at high tide (Figure 4.10 A,C). At low tide, however, the trap and release mechanism simulated in Scenario 3 resulted in significantly more stations exceeding both detection limits and recreational standards for ENT (GM, BAV, and STV) than Scenario 1 (Figure 4.7 B). Significantly more stations also exceeded ENT detection limits and GM standards under Scenario 3 than Scenario 2, where FIB release from drains was continuous (Figure 4.10 B). Lastly, Scenarios 1 and 2 were also significantly different, but only at ENT concentrations below recreational standards (<20 MPN per 100 ml, Figure 4.10 B).

Differences between model Scenarios were less distinct for EC reflecting the low initial concentrations of EC in modeled drain discharge (50 MPN per 100 mL). Only Scenarios 1 and 3 were significantly different, and only at EC concentrations below recreational standards (<20 MPN per 100 ml, Figure 4.10 D).

4.4 Discussion

Small drains account for $\sim$ 1.0 of the total freshwater volumetric flow to Newport Bay on a typical dry weather day. Nevertheless, the field and modeling results presented here suggest that irrigation runoff from small drains could be a significant source of episodic fecal pollution at Lower Bay beaches during dry weather conditions. This conclusion is supported by the following: (1) FIB concentrations in Lower Bay are typically high at the shoreline and low offshore, consistent with a beach-side bacterial source (Lower Bay Shoreline Study, Cross-Shore Drain Study, Flow

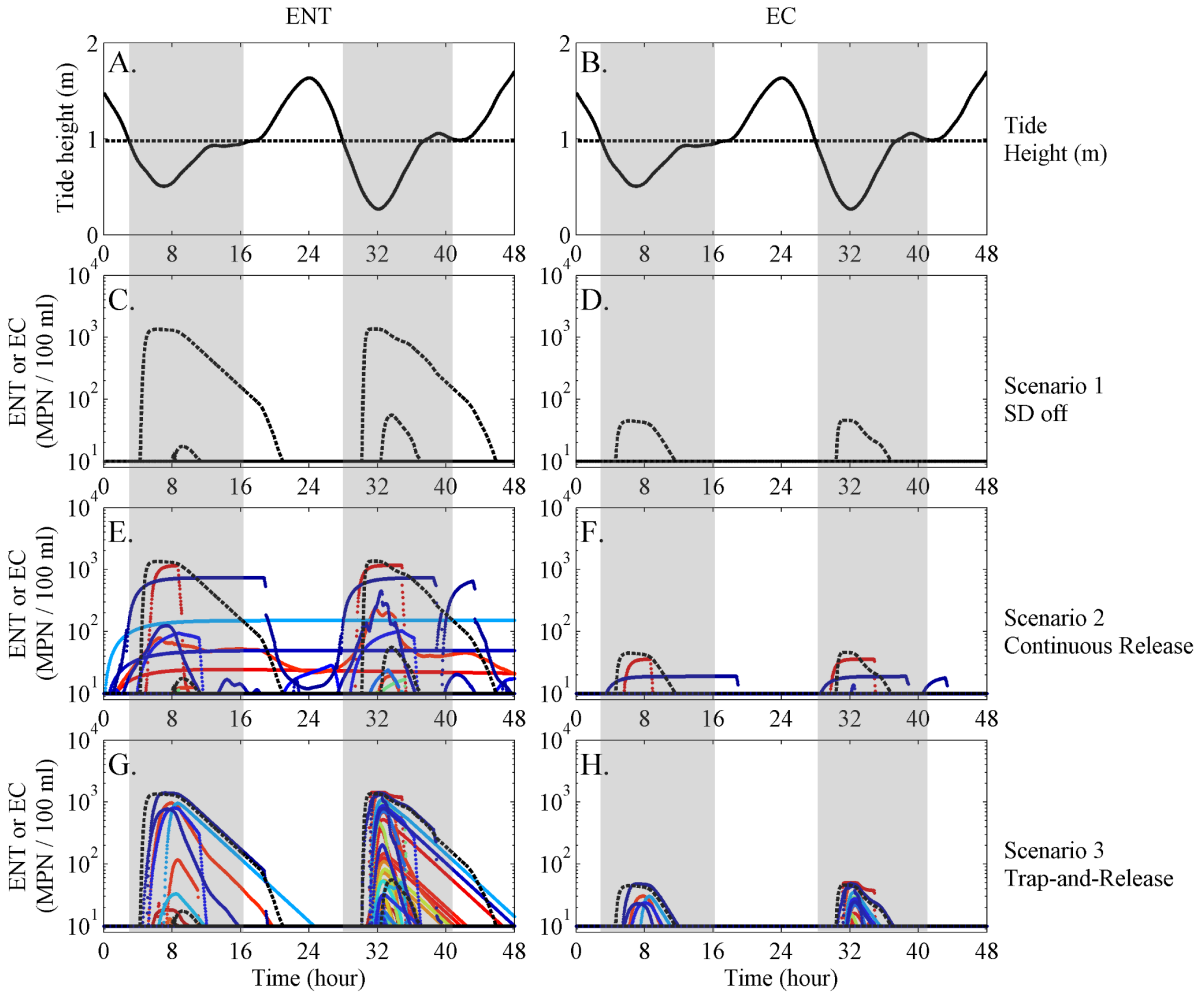

Figure 4.9: ENT (left) and EC (right) concentrations from three model scenarios (Scenario 1: C, D, Scenario 2: E, F, Scenario 3: G, H) simulated as part of the 2D Flow and Transport Modeling Study. Results are shown over two tidal cycles (low tide: shaded grey), with tide height (m) reported in panels A and B. Colored lines show the FIB concentrations released from small drains and black dashed lines show the FIB concentrations released from large drains. Note that predicted FIB concentrations are most strongly tidal under Scenario 3.

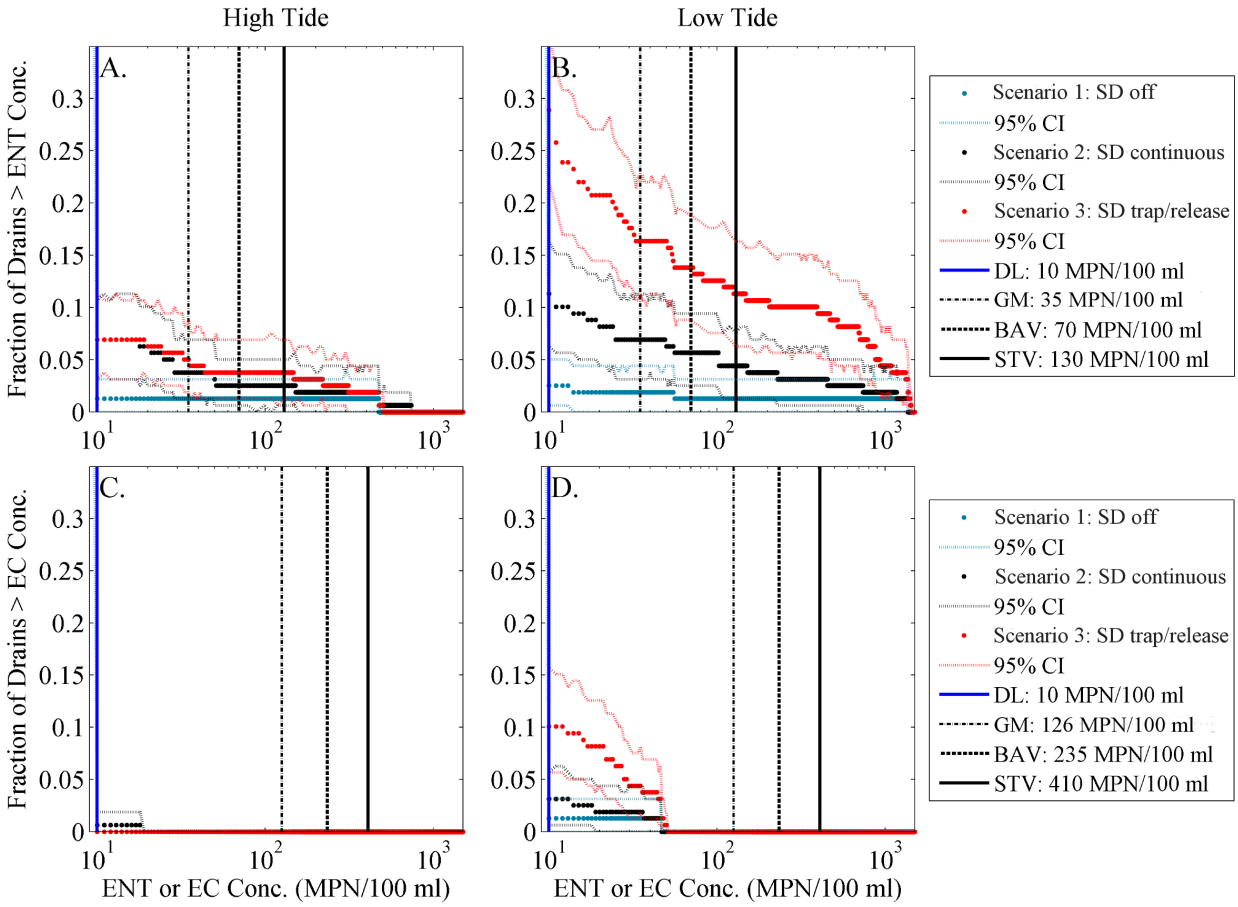

Figure 4.10: Statistical evaluation of model scenarios simulated as part of the 2D Flow and Transport Modeling Study. The x-axis is ENT (A, B) or EC (C, D) concentration, and the y-axis is the fraction of drains exceeding any given EC or ENT concentration on the x-axis. Model scenarios are evaluated at high tide (HT: A, C) and low tide (LT: B, D). The different model Scenarios (and bootstrapped 95% confidence intervals) are marked by colored circles and dotted lines, respectively: Scenario 1 (light blue), Scenario 2 (black), Scenario 3 (red). US EPA recreational criteria are indicated by vertical lines: solid blue (detection limit: DL), black dash-and-dot (geometric mean standard: GM), black dashed (beach action value: BAV), and solid black (statistical threshold value: STV).

and Transport Modeling Study); (2) FIB concentrations in Lower Bay are highest when salinity is <30 ppt, consistent with a freshwater bacterial source such as irrigation runoff (Irrigation Runoff Study, Lower Bay Shoreline Study, and Cross-Shore Drain Study); and (3) FIB patterns are modeled most accurately when small drains trap-and-release runoff (Scenario 3), consistent with episodic small drain discharge as a significant contributor to FIB contamination in Lower Bay (Flow and Transport Modeling Study).

Because most drainpipe outlets are located near mean tide line, they are typically submerged at high tide and exposed at low tide. One consequence of this outlet design is that FIB can accumulate in the drainpipe when the outlet is flooded at high tide and are discharged to the Bay when outlet is exposed at low tide; in other words, the drain pipes trap-and-release dry weather runoff to Lower Bay. This trap-and-release process was directly observed during the Drain Dye Study at Genoa Beach (Figure 4.2 A). Furthermore, its tidal signature is consistent with field and modeling studies of Lower Bay: (1) more stations exceeded statistical threshold value criteria during the Lower Bay Shoreline Study at low tide (outlets exposed) than high tide (outlets submerged) (Figure 4.6 A,B); and (2) model predicted FIB concentrations and shoreline distributions had the strongest tidal signature when trap-and-release discharge was simulated (Scenario 3, Figure 4.9 and Figure 4.6 G,H).

Although FIB pollution in Lower Bay is largely consistent with a trap-and-release process, some exceptions were observed: (1) model simulations including trap-and-release discharge were unable to reproduce observed FIB contamination along the

western portion of the Newport Bay Peninsula (black box in Figure 4.6), and (2) FIB concentrations measured during the Cross-Shore Drain Study were higher at low-high tide (LHT; 6 AM) than low-low tide (LLT; 10 PM) (Figure 4.7 D,E). Relative to exception (1), it is notable that the western portion of the Newport Bay Peninsula has only two drainpipe outlets (located at either end of the black dashed box in Figure 4.6). Hence the elevated FIB concentrations measured there may reflect contributions from non-runoff sources such as bird or dog droppings, sediments, and/or contaminated shallow groundwater, and/or bather shedding (Grant *et al.*, 2010; Halliday *et al.*, 2011). Exception (2) likely reflects prevailing irrigation schedules in residential communities surrounding Lower Bay; yard irrigation often occurs during the night or early morning when evapotranspiration is low and yards are not in use (personal observation). Indeed, samples collected during LHT had lower salinity than those collected during LLT, suggesting a larger irrigation runoff signal during early morning LHT (Figure 4.7).

Upon release from small drains, FIB plumes are diluted by ambient turbulence and transported horizontally and vertically by tide- and wind-driven currents. Because the initial dilution step is characterized by relatively small eddy diffusivities (Nearshore Turbulence Measurements Study: $\sim$0.001 m^2/s), FIB released from small drains may linger at the shoreline, where they are more likely to trigger water quality exceedences (routine beach monitoring involves collecting water samples in ankle depth water). By comparison, tributaries (e.g., SDC and SAD, Figure 4.1 B) contribute relatively little to shoreline FIB pollution in Lower Bay (Scenario 1: Flow and Transport Modeling

Study, Figure 4.6 C,D). This may be due to: (1) large effective mixing coefficients (100 m^2/s) associated with estuarine scale mixing processes (tidal trapping, longitudinal shear dispersion, and baroclinic exchange) (Fischer *et al.*, 1979; Geyer *et al.*, 1992), and/or (2) long transit times which increase the opportunity for non-conservative processes (e.g., bacterial mortality) to attenuate FIB concentrations prior to reaching Lower Bay (Rippy *et al.*, 2013; Sassoubre *et al.*, 2012).

Because irrigation runoff (median salinity 0.5 ppt) is less dense than Bay water (median salinity >30 ppt) it can form a buoyant surface plume upon entering the Bay. Buoyant plumes are likely to be responsive to the speed and direction of local winds given their location near the air-water interface. Wind-driven plume transport was observed in the Drain-Dye Study at Genoa Beach, with dye tagged freshwater traveling in the direction of local winds (and in opposition to tidal currents; Experiments 2 and 3, Figure 4.2 A). It is also likely that an ENT-laden freshwater plume was present during the LHT transect of the Cross Shore Drain Study, as offshore surface water (Stations 8 and 9, 4.6 C) had higher ENT concentrations and lower salinities than subsurface water. Notably, ENT was well mixed over the vertical in samples collected closer to shore (<5.2 m Bay-ward, Figure 4.2 E), highlighting the three-dimensional (and no doubt temporal) complexity associated with FIB in nearshore waters of Lower Bay. Because bacterial die-off is a function of both salinity (low in surface plumes, (Rozen and Belkin, 2001)) and light intensity (high at the air-water interface (Sinton *et al.*, 2002)), runoff plumes could have implications for FIB survival as well as transport and mixing in the Bay. In summary, buoyant freshwater plumes

are an important but poorly understood feature of FIB fate and transport at enclosed saltwater beaches.

Model-predicted FIB concentrations in Lower Bay were generally below measured concentrations (Figure 4.6). This could be a consequence of model oversimplification of biology or fluid dynamics (e.g., our model does not consider the possibility of wind-driven buoyant plume transport, as noted above) and/or the way in which source concentrations were parameterized. Field measured FIB concentrations in irrigation runoff were highly variable (<10 to 20,762 MPN per 100 ml), yet the model was run assuming they were fixed (EC: 50 and ENT: 1,500 MPN per 100 ml) (Figures 4.6, 4.7 and 4.9). FIB monitoring data are often log normally distributed, with concentrations spanning several orders of magnitude (Noble *et al.*, 2003). Given the highly variable nature of FIB concentrations in source waters (and irrigation runoff in particular), a direct comparison between model-predicted and observed FIB concentrations in Newport Bay might best be performed using a probabilistic framework, e.g., generating FIB concentration distributions at sites throughout the Bay using Monte Carlo sampling techniques (Beck *et al.*, 1987). Given that the present study focused on evaluation of spatial and temporal patterns in FIB (not model-data comparison of absolute concentrations), this method was not employed here. As performed, our model provides insights into the trap-and-release mechanism and the relative influence of small drains, large drains, and tributaries on nearshore water quality; it does not allow for robust model-data comparisons of FIB concentration.

From an urban infrastructure perspective, the design of small drains in Lower

Bay is (unintentionally) optimized to impact nearshore water quality and expose beachgoers to dry weather runoff. The human health risk posed by this engineering design will ultimately depend on the nature of contaminants entering and exiting the local storm drain system. Numerous studies support a dose-response relationship between ENT concentrations in sewage-impacted waters and recreational waterborne illness (Wade *et al.*, 2003). The dose-response relationship weakens, however, when FIB have non-sewage sources including non-human feces (e.g., birds and animals) and environmental re-growth (on vegetation, sediments, and storm drain piping) (Colford *et al.*, 2007). Multiple lines of evidence suggest that dry weather runoff in the region surrounding Newport Bay contain FIB from non-sewage sources (Ferguson *et al.*, 2009; Skinner *et al.*, 2010). Thus, storm drain discharge of irrigation runoff may not contribute significantly to recreational waterborne illness, even if it is (as our study suggests) a significant source of FIB pollution in Lower Bay. This is not meant to imply that storm drain discharge is "safe", as storm drains may occasionally contain untreated sewage from illicit cross-connections, sanitary sewer exfiltration, and/or sewage spills and overflows (Mallin *et al.*, 2007; Sercu *et al.*, 2009; Noble *et al.*, 2006). Furthermore, the storm sewer system is a conduit through which illicitly disposed chemicals (e.g., motor oil, detergents) can enter the Bay.

This suggests that Lower Bay water quality might be improved by re-engineering the drainage system and/or drainpipe outlets. For example, drainpipe outlets could be extended bay-ward to minimize human contact with runoff plumes. Alternatively, management strategies aimed at collecting, retaining, evapotranspiring, treat-

ing, and/or reusing dry weather runoff (e.g., biofilters, porous pavement, swales) have proven efficacy and many co-benefits (Grant *et al.*, 2012; Fletcher *et al.*, 2008; Dorsey, 2010). A number of large-scale studies are currently underway to evaluate the performance (and incentivize the adoption) of green infrastructure for capturing both dry and wet weather runoff in urban streams (Fletcher *et al.*, 2011). The results of these studies may prove useful for managing dry weather runoff at enclosed beaches, as technologies and incentive strategies that are effective in riparian systems may also be successful in urban-impacted coastal embayments.

Chapter 5

Fluid Mud Characteristics and Processes

In estuaries subject to tidal forcing, the interaction between the flow field and suspended particulates is complex and may give rise to a vertical structure involving several distinct layers as shown in Figure 5.1 (Ross, 1988). Particles are in suspension in the upper part of the water column, and as particle concentrations increase with increasing depth, the suspension may transition into a fluid mud and then a stationary mud. As shown in Figure 5.1, the interface between the suspension and the fluid mud is termed the lutocline and is characterized by a strong vertical gradient in buoyancy which acts to stabilize the profile against the influence of turbulent mixing.

Fluid mud is composed primarily of water and clay- and silt-sized particles, typically defined as particles less than 62.5 μm in diameter, and is commonly found in many estuaries, bays and channels (ASCE, 2005). Whereas turbulent eddies (e.g.,

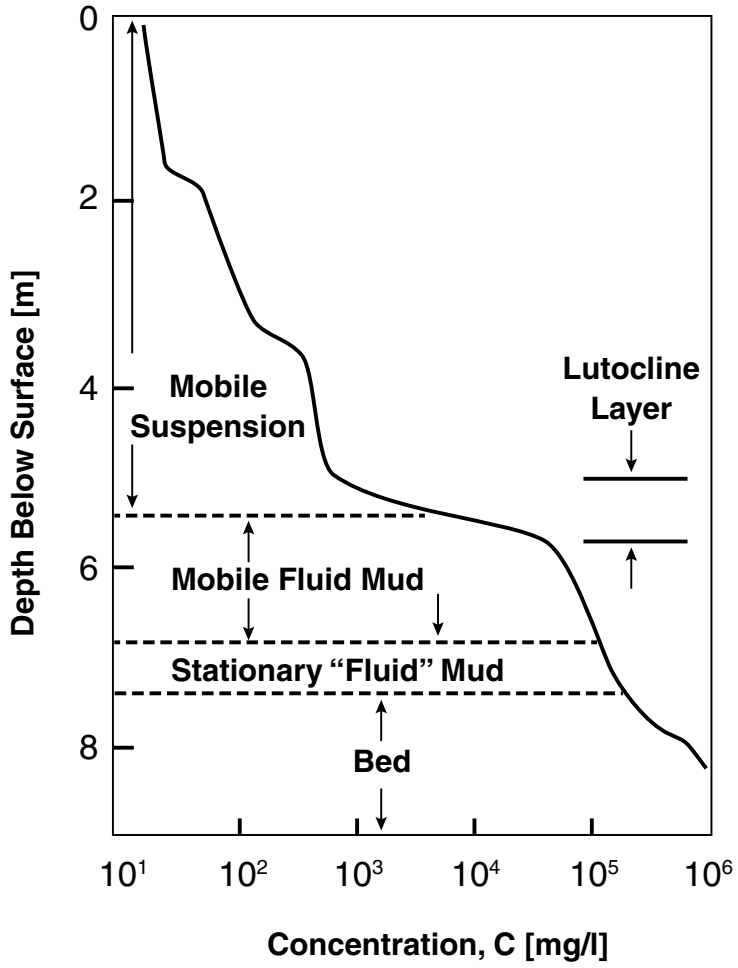

Figure 5.1: Suspended sediment concentration in a high concentration estuarine environment.

from tidal currents interacting with the bed) act to mix particles and maintain particles in suspension, the added density of particles promote stability and effectively dampen the mixing effects of turbulence. The effective viscosity of a fluid mud can be 10-100 times that of clear water (Einstein and Chien, 1955; Ross, 1988). Addition, the degree of vertical stratification has been attributed to asymmetric mixing over the region of high density gradients (Wolanski *et al.*, 1992; Scarlatos and Mehta, 1993; Kranenburg and Winterwerp, 1997; Jiang and Wolanski, 1998; Ross, 1988). High density sediment concentrations near the bed also affect settling velocities through flocculation and hindered settling. And opposed to cohesionless particles where deposition is primarily determined by particle size, deposition for cohesive sediment is controlled by bed shear stress, turbulence processes in the zone near the bed, settling velocity, type of sediment, depth of flow, suspension concentration and ionic substitution of the suspending fluid (Mehta and Partheniades, 1973).

The high density suspension of a fluid mud above the bed makes delineation of erosion and deposition processes more complicated. For example, fluidization of the cohesive bed and entrainment of fluid mud due to hydrodynamic forcing may both be thought of as erosion-type processes, while gravitational settling of sediment onto the fluid mud, as well as formation of the bed by dewatering of fluid mud, can be considered to be deposition-type phenomena (Mehta, 1989).

The importance of the fluid mud layer from a water quality perspective is that in some estuaries, fifty to ninety percent of the sediment load may be transported as fluid mud (Kirby, 1986; Smith and Kirby, 1989; Kendrick and Derbyshire, 1985;

Leussen and Velzen, 1989). The sediments themselves are sometimes a water quality concern as turbidity caused by sediment particles can restrict the penetration of sunlight and increase food availability, thus affecting aquatic life (Preston *et al.*, 1972; Kirby and Parker, 1973; Hayter, 1986; Yan, 1995). Perhaps more importantly, cohesive sediments, which are composed primarily of clay-sized material, have strong interparticle forces due to their surface ionic charges that adsorb heavy metals, pesticides and nutrients. Numerical models that neglect the near-bed fluid mud layer may yield unrealistic results in predicting dispersion of sediment into the water column and sediment advection through the water body making these models unsuitable tools for predicting pollutant fate and transport, developing water quality standards, or developing water quality mitigation measures and programs. Considerable advances in predicting cohesive sediment transport have been made in the past decades, however, one of the key difficulties in making accurate predictions is the difficulty of assessing the critical shear stress for fluid mud entrainment. The determination of this key parameter for Newport Bay is one the goals of this portion of the dissertation.

In the following sections, properties of the fluid mud, cohesive bed and lutocline, are reviewed. Then key sedimentation processes of cohesive sediment are surveyed along with experimentally derived mathematical formulations for these processes. In Chapter 6, a 1D vertical numerical model is presented that explores more complex sedimentation processes such as flocculated settling, turbulence damping of eddy diffusivity, and bed-shear induced entrainment to demonstrate whether there is a need for incorporating a set of complex parameters to predict suspended sediment

distributions above a cohesive sediment bed. In Chapter 7, critical shear stresses for bed samples collected in Newport Bay are calculated from erosion rates that were determined using a recirculating flume. These critical shear stresses are used in a 2D model to back-calculate entrainment parameters of the fluid mud overlying the consolidated bed sediments.

5.1 Fluid Mud

The fluid mud is a comparatively thin layer, sometimes on the order of a few centimeters. Near bed fluid mud results from the rapid deposition of suspended sediment or erosion of the consolidated bed. During deposition, if the rate of deposition exceeds the rate at which sediment develops structural integrity (effective stress), fluid mud will form. The upper interface of the fluid mud layer was found to correspond to the hindered flux (from settling) concentration in quiescent settling, and to the maximum net downward flux (sum of the settling and diffusive fluxes) when mixing occurred. This is nearly always the case for cohesive sediment at relatively high suspension concentrations because hindered settling result in decreasing settling flux with increasing concentrations (i.e. concentration $\geq$ 20 g/l). The concentration at which bed formation occurs, being high (e.g., 200 g/l), causes sediment to "bunch up" near the bed (Ross, 1988).

For fluid mud formation by rapid erosion (or fluidization), the rate at which bed material loses structural integrity must be greater than the rate at which sediment is entrained into the upper, well-mixed mobile suspension layer. For example, wave

action has been shown to result in fluid mud formation by rapid destruction of bed effective stress resulting in fluidization with little vertical entrainment (Ross, 1988). Measured total and pore pressures and concentrations under wave loading in a laboratory flume showed that destruction of effective stress occurred with little change in near bed concentration.

The fluid mud is composed of mobile and stationary layers that depend on the applied pressure gradient, internal shear stress, and rheological properties of the fluid mud. Stationary fluid mud suspensions are defined by Parker and Lee (1979) as assemblages of high concentration of sediment particles that are supported jointly by the water and the developing skeletal soil framework, and which have no horizontal movement. These suspensions, which are in the process of consolidation, have high water content and a very low, but measurable shear strength. Sediment concentrations in the fluid mud layer are typically usually in the range of 10-170 g/L with bulk density of about 1.03-1.30 g/cm^3 (Wells, 1983). There is a gradation of shear strengths transitioning from the upper, low sediment concentration suspension to the bed sediment. Krone (1962) demonstrated this gradation of fluid mud shear strengths in San Francisco Bay identifying six layers of fluid mud with shear strengths varying from 0.020 to 2.20 N/m^2.

5.2 Bed Formation and Consolidation

Sediment concentrations of 170-200 g/L define the transition from the fluid mud to the sediment bed. Partially consolidated sediment is defined by Parker and Lee

(1979) as assemblages of high concentration of sediment particles, having no horizontal movement, that are supported jointly by the water and the developing skeletal soil framework. These suspensions, which are in the process of consolidation, have high water content and a very low, but measurable shear strength. A structured matrix usually exists for bulk densities exceeding 1.1 g/cm^3 which corresponds to an approximate shear strength of 1.0 N/m^2 (Parker, 1987).

A cohesive sediment bed is formed when deposited particles and/or aggregates begin intergranular contacts thereby developing an effective stress which is transmitted by particle-to-particle contacts (Hayter, 1986; Parker, 1986). Deposited soils undergo self-weight consolidation where the overburden stress causes the soils matrix to collapse, expelling the interstitial fluid and resulting in a decreased void space which in turn creates a stronger soil matrix due to increased surface contact of the particles. The strengthening of a soil mass with depth is finite and approaches a steady state condition exponentially that will remain mostly constant assuming homogeneous soil composition. For heterogeneous soils, soil stratification will occur due to differential settling and depositional history (Teisson *et al.*, 1993). In the early stage of consolidation, the self-weight of the aggregates near the bed surface is balanced by the seepage force induce by the upward flow escaping from the underlying sediment. Thus, the effective stresses in this region are very small and, in general, not measurable. As the bed continues to undergo consolidation and the upward flux of pore water reduces, the self-weight of this near surface soil gradually turns into an effective stress. The surface stress may first crush the floc structures and then crush the aggregates them-

selves (Hayter, 1986). During consolidation, bed properties (density, effective stress) begin to vary with depth due to particle rearrangement and aggregates breakdown. For a fully consolidated bed, shear strengths are usually greater than 5 N/m^2 (Parker, 1986; Ross, 1988). The degree of bed consolidation strongly influences bed sediment erosion.

5.3 Lutocline

The transition from the upper water column to the fluid mud, sometimes characterized by a four- to five-order of magnitude sediment concentration gradient, is the zone of maximum settling velocity and minimum vertical mixing (Ross, 1988). This sharp sediment concentration gradient layer is termed the lutocline. The lutocline separates the water column into two reasonably well-defined zones: the near-bottom, non-Newtonian fluid mud characterized by high suspended sediment concentration, hindered settling, turbulence damping, and a sediment-modified velocity profile; and the overlying fluid suspension zone generally characterized with a suspended sediment concentration less than 10 g/L^3, free or flocculation settling, higher level of turbulence and near-Newtonian flow properties (Jiang, 1999).

Lutocline genesis, growth, and decay is governed by the dynamic interaction between the counteracting processes of turbulent mixing and gravitational settling. Lutoclines occur because sediment, being heavier than water, tries to settle out under quiescent conditions. Due to settling velocity differences between the flocculation and hindered settling regimes, fine sediment concentrates at a sharp, high concen-

tration interface. Turbulent eddies impinging on the interface exchange packets of sediment-laden fluid. However, vertical mixing is damped due to the buoyancy force because work must be done to raise heavy fluid packets and lower the lighter fluid packets. Due to the potential energy difference of each packet with its surroundings, they are returned to near origin levels with only modest mixing. Thus, additional work (the change in kinetic energy per unit mass) is required to keep the sediment in suspension and overcome cohesion and interactions between flocs. The resulting stable stratification, termed buoyancy or gravitational stabilization, causes damping of turbulent mass and momentum diffusion across the upper interface of the fluid mud layer resulting in minimal vertical mixing (Fischer *et al.*, 1979). When the magnitude of shear production exceeds the static stability of the fluid susupension due to vertical buoyancy flux, upward diffusion, which is dependent on the degree of stratification and relative turbulent intensity, becomes the dominant mixing mechanism. The diffusion process causes the lutocline to rise due to water entrained from above diluting the suspension (Kranenburg and Winterwerp, 1997).

Correct portrayal of the lutocline, the low-sediment concentration suspension layer in the upper water column that forms above the fluid mud, requires the concept of turbulence damping (or buoyancy stabilization). Buoyancy-induced stabilization of vertical mixing in the fluid mud reduces mass diffusion which is a function of vertical eddy diffusion. The most commonly applied expression of vertical variations in eddy diffusivity is the formulation given by Rouse (Vanoni, 1975). By following von Karman's assumptions of a linear shear stress distribution with depth leading

to a logarithmic velocity profile, the following expression for eddy diffusivity under neutral conditions is found:

$$\varepsilon_{zo} = \kappa u_* h \sigma (1 - \sigma) \tag{5.1}$$

where $h = \eta$-b is the depth of flow, κ=0.41 is von-Karman's constant, σ=(z-b)/h, and u_*=$\sqrt{\tau_b/\rho}$ is the shear velocity, with τ_b the bed shear strength and ρ the fluid density above the fluid mud. While this expression may be sufficient for describing turbulent-logarithmic, uni-directional flows, it does not describe highly oscillatory flows (Ross, 1988). When buoyancy-induced stabilization is a factor and assuming that eddy fluxes of mass can be related to mean gradients through a single eddy-mixing coefficient, the vertical eddy diffusion coefficient is modified using the approach described by Munk and Anderson (1948) shown in Eq. 5.2,

$$\varepsilon_z = \varepsilon_{zo} \left(1 + \alpha_1 R_i\right)^{-\beta_1} \tag{5.2}$$

where α_1 and β_1 are empirical coefficients and R_i is the Richardson number. The Richardson number is a measure of vertical stability based on the ratio of local density gradient (vertical buoyancy flux), which dampens turbulence, to mixing energy from turbulent shear stress (velocity shear), which generates turbulence. The Richardson number thus provides an index of the tendency of the water column to either mix (weak stratification) or resist mixing (strong stratification). The Richardson number is given by

$$R_i = \frac{-g}{\rho} \frac{\partial \rho}{\partial z} \left(\frac{\partial u}{\partial z} \right)^{-2} \tag{5.3}$$

Maa and Mehta (1987) found the eddy mass diffusion coefficient for the upper water column above the fluid mud layer ranged from 2 x 10^{-6} to 4 x 10^{-5} m^2/s. Within the fluid mud, the mass diffusion coefficient was found to be on the order of 1 x 10^{-6} m^2/s.

5.4 Erosion and Entrainment of Cohesive Soils

There is no comprehensive theory regarding the erosion and deposition of cohesive soils; erosion equations are all empirical. Principal factors controlling erosion of cohesive sediment beds are bed shear stress, sediment composition, pore fluid composition, eroding fluid composition and bed structure (deposition and stress history) (Hayter, 1983). During the increasing velocity periods of the ebb and flood tides, high bed shear stresses reduce effective stresses within the bed sediments leading to reduced shear strength of the bed sediments. If shear stresses are sufficiently large, continuous inter-particle contact ceases, effective stresses of the bed are destroyed and a fluid mud suspension is formed. Inasmuch as the hydrodynamic boundary effect is confined to a layer of relatively small height over the bed, the fluidized mud is not easily entrained into the upper water column unless a current-generated shear stress exceeds a critical value to entrain fluid mud into the upper water column. If shear stresses are sufficiently large, bed sediments are directly mixed into the upper water column (Ross, 1988).

After a fluid mud layer is formed, either from high erosion or deposition rates, re-entrainment of this high concentration sediment suspension can occur due to flow

shear at the upper fluid mud interface. The position of the interface between the upper low concentration layer and the fluid mud layer may change greatly due to re-entrainment and deposition. In a tidally influenced estuary, sediment is deposited, resuspended and deposited again without ample time for complete consolidation. The top several centimeters of the soil are critical, as this is generally the extent of the erosion over shorter time periods, e.g. days. For this situation, an increase in the bed shear strength with depth is significant, as opposed to riverine applications where a bed may be expected to undergo only erosion of a consolidated bed (Yan, 1995).

Research suggests that the critical entrainment stress threshold varies with the spring-neap cycle (Kirby, 1986; Clarke and Elliot, 1997). On the approach to neap tides where currents are less energetic, the erosion threshold was observed to increase due to consolidation of the sediment bed. The opposite was observed during the transition to spring tide. The cumulative effect of consolidation due to spring-neap tidal phasing was found to lead to net sedimentation, since the deposited material hardens with time and becomes less erodible. Once eroded from the bed, cohesive sediment is transported as suspended load by the estuarial flow. The transport is a result of advection, turbulent diffusion (driven by the spatial suspended sediment concentration gradients), and longitudinal dispersion (driven by spatial velocity gradients) (Ippen, 1966).

Ariathurai (1974) presented a formula for surface erosion rate by fitting experimental plots of erosion rate versus applied shear stress:

$$E = E_c\left(\frac{\tau_b - \tau_c}{\tau_c}\right)^n, \qquad (\tau_b \geq \tau_c) \tag{5.4}$$

where E_c and n are, respectively, the empirically derived surface erosion rate constant and power coefficient, τ_b is the applied bed shear stress, and τ_{cr} is the critical surface erosion shear stress for a consolidated bed.

One expression for the rate of entrainment for very soft, partially consolidated soils found in the upper few centimeters of the bed is:

$$E = E_o \exp[\alpha(\tau_b - \tau_{cr})^{0.5}] \qquad (\tau_b > \tau_{cr}) \tag{5.5}$$

where E_o and α are empirical coefficients, τ_b is the applied bed shear stress, and τ_{cr} is the bed shear strength for erosion of a partially consolidated beds (Mehta *et al.*, 1982; Parchure and Mehta, 1983).

Hwang and Mehta (1989) presented a relationship between critical shear stress for surface erosion and the wet bulk density of the bed,

$$\tau_b = a(\rho_{wb} - \rho_l)^b + c \tag{5.6}$$

where ρ_{wb} is the wet bulk density with a, b, c and ρ_l determined by field data. Nicholson and O'Connor (1986) proposed an expression for critical shear stress dependent upon the dry bulk density,

$$\tau_b = \tau_{ef} + A(\rho_b - \rho_f)^B \tag{5.7}$$

where τ_{ef} is the critical shear stress of a freshly deposited bed, ρ_f and ρ_f are the

dry bulk density of bed and freshly deposited bed, respectively, and A and B are empirically-derived constants.

5.5 Settling Velocity

Unlike cohesionless sediments where settling velocity is a primarily a function of particle diameter, the settling velocity of cohesive sediments depends on sediment concentration, salinity and turbulence, all of which affect the rate and degree of aggregation (Krone, 1962). Sediment concentration affects aggregation due to differential settling and Brownian motion. In saline conditions encountered in estuaries, repulsive electrochemical surface forces are suppressed and clay particles coagulate to form flocs. The systematic build-up of flocs as occurs in estuaries is defined as aggregation. Turbulence limits the size of aggregates as a result of fluid shearing (Mehta and Dyer, 1990).

The settling velocity, w_s, can be divided into three sub-ranges in terms of concentration. At low sediment concentrations, the rate of aggregation is negligible and individual sediment particles do not physically interfere with each other while settling. This is defined as free settling. For cohesive sediments, the free settling upper concentration limit is in the range of 300 to 500 mg/L (Krone 1962). For a particle with a diameter d settling in a viscous fluid with viscosity ν, the free settling velocity is

$$w_s = \left[\frac{4}{3}\frac{gd}{C_D}\frac{(\rho_s - \rho_w)}{\rho_w}\right]^{1/2} \tag{5.8}$$

where ρ_s and ρ_w are the sediment and fluid densities respectively and C_D the drag

coefficient which is function of the Reynold's Number ($R = w_s d/\nu$) and the shape of the particle. Fine sediment particles in dispersed conditions usually fall within the Stokes' settling range (R<0.1) and for spherical particles, $C_D = 24/R$. However, the shape of a cohesive sediment particle is generally plate-like, with a large ratio of surface area to volume. This results in a higher drag coefficient (Ross, 1988).

At moderate suspended sediment concentrations (approximately 400 to 3,000 mg/L), there is an increase of interparticle collisions in suspension that increases the likelihood that particles will coagulate into flocs. The three principal mechanisms of interparticle collisions are Brownian motion, internal shearing produced by local velocity gradients in the fluid, and differential sedimentation that results from the fact that particles of different sizes have different settling velocities. Settling velocity of flocs increase with increasing suspended sediment concentration due to the formation of stronger, denser and larger flocs (Hayter, 1986). This is the so-called enhanced or flocculated settling range, generally assumed to behave in a power-law form, i.e.,

$$w_s = k_1 c_s^{n_1} \tag{5.9}$$

where k_1 and n_1 are fitted constants. According to Teeter (1983) and Mehta (1986), n_1 should be in the range of 1 to 2 but should tend towards 4/3.

When sediment in suspension exceeds the flocculation settling range (about 3,000 to 10,000 mg/L), the mean sediment settling velocity begins to decrease with increasing suspended sediment concentration due to an aggregated particulate network of the fluid mud that inhibits the upward escape of the interstitial water present within

the fluid mud deposits. This region of increasing suspended sediment concentration defines the upper boundary of the fluid-mud where there is hindered settling and a corresponding decrease in the net downward vertical flux (Ross 1988). Richardson and Zaki (1954) account for the hindered settling velocity as follows,

$$w_s = w_{so}(1 - k_2 c_s)^{n_2} \tag{5.10}$$

where w_{so} is a reference settling velocity, k_2 and n_2 are empirical coefficients that depends on the sediment composition.

In the limiting case when sediment concentrations are small, the effects of flocculation settling can be ignored, and the eddy diffusivity for channel flow can be defined as Eq. 5.11, the steady-state vertical profile of suspended sediment is defined by the Rouse profile,

$$c_s = c_s^a \left(\frac{a(\eta - z)}{z(\eta - a)} \right)^{R_o} \tag{5.11}$$

where c_s^a represents the reference sediment concentration a distance a above the bed (typically 5 percent of the depth) and R_o=$w_s/\kappa u_*$ is the Rouse number. In the absence of buoyancy effects, the Rouse Number equals zero and c_s is computed to decrease smoothly with height above bottom. This is in agreement with conventional sediment transport theory where flocculation and hindered settling effects are ignored and lutocline formation above the bed is not predicted.

The boundary condition at the near-bottom reference elevation at z=a, corresponds to a prescribed flux condition,

$$- w_s c_s - \varepsilon_z \frac{\partial c_s}{\partial z} = E - D \tag{5.12}$$

At steady state, the deposition flux equals the entrainment flux, therefore the entrainment can be expressed as a function of the Rouse number:

$$E = c_s^a w_s \left(\frac{a(H-z)}{z(H-a)} \right)^{R_o} \tag{5.13}$$

5.6 Deposition

A relationship for the depositional flux related to the settling flux can be written as

$$D = p_D w_s c_s \tag{5.14}$$

where p_D can be interpreted as an attachment probability and represents the fraction of settling sediment within the fluid mud that is incorporated into the bed matrix (Krone, 1962). The attachment probability can be expressed as

$$p_D = 1 - \left(\frac{\tau_b}{\tau_{cd}} \right) \qquad (\tau_b \leq \tau_{cd}) \tag{5.15}$$

where τ_{cd} is the critical shear stress for full deposition.

Chapter 6

One-Dimensional Modeling of Sedimentation Processes Modified by Fluid Mud

The literature indicates that the occurrence of fluid mud is common in deep estuaries (Parker and Kirby, 1982; Kirby, 1986; Clarke and Elliot, 1998). Is there a minimum water column depth where the effects of fluid mud should be considered? That is, for a shallow estuary like Newport Beach, does a 2D evaluation of sediment transport need to consider modification of entrainment, mixing and settling parameters due to the existence of a fluid mud layer? To examine this question, a one-dimensional (1D) numerical model was developed that includes parameterization options for characterizing bed shear induced sediment entrainment, turbulence damp-

ing of vertical mixing, and free, flocculated or hindered settling velocity regimes. The 1D model was tested against known forms of the governing equation having exact solutions. Gridding requirements were checked for various combinations of linear and non-linear parameterization. Model predictions were verified using suspended sediment concentration profiles from the Severn Estuary, a deep estuary in England. Finally, the model examined Newport Bay, a shallow estuary to see if generation of a fluid mud layer would be expected to be produced.

6.1 Model Development

The 1D model predicts suspended sediment concentration in terms of a steady or unsteady balance between the upward flux of sediment as a result of turbulent mixing and the downward flux of suspended sediment due to the fall velocity of the sediment particles, with the fluxes modified appropriately in the presence of fluid mud. Changes in bed elevation or density changes in the fluid mud due to the processes of deposition and entrainment are not considered. Instead, a high sediment concentration is assumed at a reference level slightly above the bed which acts as a reservoir of material where sediment is deposited or entrained depending on the settling velocity, bed shear, and critical shear strength of the sediment. For a control volume $\mathcal{V}$ with surface $\mathcal{S}$, Reynolds transport equation applied to the mass of sediment gives the integral form of the sediment transport equation,

$$\frac{\partial}{\partial t}\int_{\mathcal{V}} c_s d\mathcal{V} + \int_{\mathcal{S}} \mathbf{F}_s \cdot \mathbf{n}\, d\mathcal{S} = 0 \tag{6.1}$$

where c_s is sediment concentration, $\mathbf{F}_s$ is the sediment flux through the control surface $\mathcal{S}$, and $\mathbf{n}$ is the unit outward normal vector. The sediment flux accounting for advection, settling and eddy diffusion is,

$$\mathbf{F}_s = (\mathbf{u} - w_s\mathbf{k})c_s - \mathbf{D}_s \nabla c_s \tag{6.2}$$

where $\mathbf{u} = u\mathbf{i} + v\mathbf{j} + w\mathbf{k}$, u, v, and w are the velocity components in the x, y, and z directions, respectively, $\mathbf{i}$, $\mathbf{j}$, and $\mathbf{k}$ are unit vectors in the x, y, and z directions, respectively, w_s is the settling velocity, $\mathbf{D}_s$ is the eddy diffusion second rank tensor for sediment, and ∇ is the gradient operator.

The eddy diffusion tensor is diagonal and its elements are ε_x, ε_y, and ε_z, where the subscript indicates the direction of each component. The differential form of the sediment transport equation is obtained by applying Gauss' divergence theorem to the second term on the left hand side of Eq. 6.1 to convert the surface integral to a volume integral and then grouping all terms under the volume integral. Since the integral must be zero for all $\mathcal{V}$ for which c_s is a continuous differentiable function, the integrand must be zero on a pointwise basis. That is,

$$\frac{\partial c_s}{\partial t} + \nabla \cdot \mathbf{F}_s = 0 \tag{6.3}$$

where $\nabla\cdot$ is the divergence operator. Expanding Eq. 6.3 into scalar form yields,

$$\frac{\partial c_s}{\partial t} + \frac{\partial}{\partial x}(uc_s) + \frac{\partial}{\partial y}(vc_s) + \frac{\partial}{\partial z}[(w - w_s)c_s] = \frac{\partial}{\partial x}\left(\varepsilon_x \frac{\partial c_s}{\partial x}\right) + \frac{\partial}{\partial y}\left(\varepsilon_y \frac{\partial c_s}{\partial y}\right) + \frac{\partial}{\partial z}\left(\varepsilon_z \frac{\partial c_s}{\partial z}\right) \tag{6.4}$$

The vertical component of the sediment transport equation (Eq. 6.3) is:

$$\frac{\partial c_s}{\partial t} - \frac{\partial}{\partial z}(w_s c_s) = \frac{\partial}{\partial z}\left(\varepsilon_z \frac{\partial c_s}{\partial z}\right) \qquad b < z < \eta \tag{6.5}$$

where b is the elevation of the top of the bed and η is the free surface elevation.

Boundary conditions and are required to solve the sediment transport equation. The vertical dimension is bounded from above by the air/liquid interface. The boundary condition at the air/liquid interface, $z = \eta$, corresponds to a no-flux condition,

$$-w_s c_s - \varepsilon_z \frac{\partial c_s}{\partial z} = 0 \tag{6.6}$$

The boundary condition at the bottom defined by the liquid/bed interface at $z = b$, corresponds to a prescribed flux condition,

$$-w_s c_s - \varepsilon_z \frac{\partial c_s}{\partial z} = E - D \tag{6.7}$$

where the sediment exchange consists of an upward flux of bed sediment, E, into the water column and a downward depositional flux D of suspended sediment returning to the bed sediment reservoir.

6.2 Numerical Solution Formulation

The vertical component of the sediment transport equation (Eq. 6.3) can be written as:

$$\frac{\partial C}{\partial t} + \frac{\partial F_a}{\partial z} + \frac{\partial F_d}{\partial z} = 0 \tag{6.8}$$

where the advective flux, F_a, is given by

$$F_a = -w_s C_s \tag{6.9}$$

and the diffusive flux F_d for sediment is given by,

$$F_d = -\left(\varepsilon_z \frac{\partial C_s}{\partial z}\right) \tag{6.10}$$

with ε_z the eddy diffusivity in the z-direction. A staggered grid is employed to solve the finite volume formulation of the sediment transport equation given by Eq. 6.8 where sediment concentrations, settling velocity, and density are calculated at the middle of each cell and advective and diffusive fluxes are calculated at the boundaries. Each cell is numbered at its center with index j and cell boundaries at half integer j+1/2. The upper boundary of the top cell defines the free surface. The lower boundary of the bottom cell defines the bed bottom (or reference elevation above the bottom). Diffusive fluxes are discretised by the finite difference method. Advective fluxes are discretised using flux limiters which are non-linear interpolations.

The discretization of the transport equation using the generic concentration and settling velocity parameters C and w respectively is:

$$\begin{aligned}&\frac{C_j^{n+1} - C_j^n}{\Delta t} + (1-\theta)\frac{F_{a_{j+1/2}}^{\ n} - F_{a_{j-1/2}}^{\ n}}{\Delta z} + (\theta)\frac{F_{a_{j+1/2}}^{\ n+1} - F_{a_{j-1/2}}^{\ n+1}}{\Delta z} \\ &+\frac{1}{2}\frac{F_{d_{j+1/2}}^n - F_{d_{j-1/2}}^n}{\Delta z} + \frac{1}{2}\frac{F_{d_{j+1/2}}^{n+1} - F_{d_{j-1/2}}^{n+1}}{\Delta z} = 0 \qquad 0 < \theta < 1\end{aligned} \tag{6.11}$$

where θ is the temporal weighting factor for advection, and

$$F_{a_{j+1/2}}^{\ n} = F_{a_{j+1}}^{\ n} - \frac{1}{2}\phi_{j+1}^n \delta F_{a_{j+1}}^{\ n} = F_{a_{j+1}}^{\ n} - \frac{1}{2}\phi_{j+1}^n \left(\frac{F_{a_{j+2}}^{\ n} - F_{a_j}^{\ n}}{2}\right) \tag{6.12}$$

$$F_{a_{j+1/2}}^{\ n+1} = F_{a_{j+1}}^{\ n+1} - \frac{1}{2}\phi_{j+1}^n \delta F_{a_{j+1}}^{\ n+1} = F_{a_{j+1}}^{\ n+1} - \frac{1}{2}\phi_{j+1}^{n+1} \left(\frac{F_{a_{j+2}}^{\ n+1} - F_{a_j}^{\ n+1}}{2}\right) \tag{6.13}$$

$$F_{d_{j+1/2}}^n = \varepsilon_{z_{j+1/2}}^{\ n} \frac{C_{j+1}^n - C_j^n}{\Delta z} = \frac{1}{2}(\varepsilon_{z_j}^{\ n} + \varepsilon_{z_{j+1}}^{\ n}) \frac{C_{j+1}^n - C_j^n}{\Delta z} \tag{6.14}$$

$$F_{d_{j+1/2}}^{n+1} = \varepsilon_{z_{j+1/2}}^{n+1} \frac{C_{j+1}^{n+1} - C_j^{n+1}}{\Delta z} = \frac{1}{2}(\varepsilon_{z_j}^{n+1} + \varepsilon_{z_{j+1}}^{n+1}) \frac{C_{j+1}^{n+1} - C_j^{n+1}}{\Delta z} \tag{6.15}$$

with ϕ, the flux limiter,

$$\phi = \frac{4(C_{j+1} - C_j)}{(C_{j+1} - C_{j-1})} \qquad 0 \leq \phi \leq 1 \tag{6.16}$$

Substituting these values into (Eq. 6.11) yields:

$$\begin{aligned}
C_j^{n+1} + \frac{\theta \Delta t}{\Delta z}[-w_{j+1}^{n+1} C_{j+1}^{n+1} + \phi_{j+1}^n \frac{1}{4}(w_{j+2}^{n+1} C_{j+2}^{n+1} - w_j^{n+1} C_j^{n+1}) \\
+ w_j^{n+1} C_j^{n+1} - \phi_j^n \frac{1}{4}(w_{j+1}^{n+1} C_{j+1}^{n+1} - w_{j-1}^{n+1} C_{j-1}^{n+1})] \\
- \frac{\Delta t}{4\Delta z^2}[(\varepsilon_{z_{j+1}}^{n+1} + \varepsilon_{z_j}^{n+1})(C_{j+1}^{n+1} - C_j^{n+1}) - (\varepsilon_{z_j}^{n+1} + \varepsilon_{z_{j-1}}^{n+1})(C_j^{n+1} - C_{j-1}^{n+1})] \\
= C_j^n - \frac{(1-\theta)\Delta t}{\Delta z}[-w_{j+1}^n C_{j+1}^n + \phi_{j+1}^n \frac{1}{4}(w_{j+2}^n C_{j+2}^n - w_j^n C_j^n) \\
+ w_j^n C_j^n - \phi_j^n \frac{1}{4}(w_{j+1}^n C_{j+1}^n - w_{j-1}^n C_{j-1}^n)] \\
+ \frac{\Delta t}{4\Delta z^2}[(\varepsilon_{z_{j+1}}^n + \varepsilon_{z_j}^n)(C_{j+1}^n - C_j^n) - (\varepsilon_{z_j}^n + \varepsilon_{z_{j-1}}^n)(C_j^n - C_{j-1}^n)] + 0
\end{aligned} \tag{6.17}$$

The two independent variables, z and t, denote the vertical space coordinate and time, respectively, using j subscript to represent z-directions grid index and n superscript to denote the number of time intervals that have elapsed where j, n = 1,2,3, etc.

Boundary Conditions

For the second cell below the free surface, assume F_a=0 and $w_s C$=0 above the free surface when computing the slope δF, then (Eq. 6.17) becomes

$$\begin{aligned}
C_{N-1}^{n+1} + \frac{\theta \Delta t}{\Delta z}[-w_N^{n+1} C_N^{n+1} + \phi_N^n \frac{1}{4}(-w_{N-1}^{n+1} C_{N-1}^{n+1}) \\
+ w_{N-1}^{n+1} C_{N-1}^{n+1} - \phi_{N-1}^n \frac{1}{4}(w_N^{n+1} C_N^{n+1})]
\end{aligned}$$

$$-\frac{\Delta t}{4\Delta z^2}[(\varepsilon_{z_N}^{n+1}+\varepsilon_{z_{N-1}}^{n+1})(C_N^{n+1}-C_{N-1}^{n+1})-(\varepsilon_{z_{N-1}}^{n+1}+\varepsilon_{z_{N-2}}^{n+1})(C_{N-1}^{n+1})]$$
$$=C_{N-1}^n-\frac{(1-\theta)\Delta t}{\Delta z}[-w_N^nC_N^n+\phi_N^n\frac{1}{4}(-w_{N-1}^nC_{N-1}^n)$$
$$+w_{N-1}^nC_{N-1}^n-\phi_{N-1}^n\frac{1}{4}(w_N^nC_N^n)]$$
$$+\frac{\Delta t}{4\Delta z^2}[(\varepsilon_{z_N}^{n}+\varepsilon_{z_{N-1}}^{n})(C_N^{n}-C_{N-1}^{n})-(\varepsilon_{z_{N-1}}^{n}+\varepsilon_{z_{N-2}}^{n})(C_{N-1}^{n})]+0 \tag{6.18}$$

For the top cell right below the free surface, assume F_a=F_d=0 at the free surface and the slope δF is limited assuming F=0 above the free surface. Then (Eq. 6.17) becomes

$$C_N^{n+1}+\frac{\theta\Delta t}{\Delta z}(-w_N^{n+1}C_N^{n+1})+\phi_{N+1}^n\frac{1}{4}(w_{N-1}^{n+1}C_{N-1}^{n+1})$$
$$+\frac{\Delta t}{4\Delta z^2}[(\varepsilon_{z_N}^{n+1}+\varepsilon_{z_{N-1}}^{n+1})(C_N^{n+1}-C_{N-1}^{n+1})]$$
$$=C_N^n-\frac{(1-\theta)\Delta t}{\Delta z}(-w_N^nC_N^n+\phi_N^n\frac{1}{4}(w_{N-1}^nC_{N-1}^n)$$
$$-\frac{\Delta t}{4\Delta z^2}[(\varepsilon_{z_N}^{n}+\varepsilon_{z_{N-1}}^{n})(C_N^{n}-C_{N-1}^{n})]+0 \tag{6.19}$$

For the first cell above the bottom boundary, assume

$$\delta F_a=F_{aj+1}-F_{aj} \tag{6.20}$$

$$\delta F_d=E-D \tag{6.21}$$

where D and E are the depositional and entrainment fluxes respectively. Then (Eq. 6.17) becomes

$$C_j^{n+1}+\frac{\theta\Delta t}{\Delta z}(-w_2^{n+1}C_2^{n+1}+\phi_2^n\frac{1}{4}(w_3^{n+1}C_3^{n+1}-w_1^{n+1}C_1^{n+1})$$
$$+w_1^{n+1}C_1^{n+1}-\frac{1}{2}(w_2^{n+1}C_2^{n+1}-w_1^{n+1}C_1^{n+1}))$$

$$
\begin{aligned}
-\frac{\Delta t}{4\Delta z^2}((\varepsilon_{z_2}{}^{n+1} + \varepsilon_{z_1}{}^{n+1})(C_2^{n+1} - C_1^{n+1}) + 2E^{n+1} - 2D^{n+1} \\
= C_1^n - \frac{(1-\theta)\Delta t}{\Delta z}(-w_2^n C_2^n + \phi_2^n \frac{1}{4}(w_3^n C_3^n - w_1^n C_1^n) \\
+ w_1^n C_1^n - \frac{1}{2}(w_2^n C_2^n - w_1^n C_1^n)) \\
+ \frac{\Delta t}{4\Delta z^2}((\varepsilon_{z_2}{}^n + \varepsilon_{z_1}{}^n)(C_2^n - C_1^n) + 2E^n - 2D^n
\end{aligned} \tag{6.22}
$$

6.3 Parameterization of Buoyancy-Induced Stabilization

The buoyancy-induced stabilization of vertical mixing in the fluid mud, as previously described in Equation 5.2 is,

$$\varepsilon_z = \varepsilon_{zo}\,(1 + \alpha_1 R_i)^{-\beta_1} \tag{6.23}$$

where R_i is the Richardson number, α_1 and β_1 are empirical coefficients, and ε_{zo} is the eddy diffusivity under neutral conditions given by the commonly applied expression of vertical variation in eddy diffusivity (Rouse, 1937) based on a linear shear stress distribution with depth leading to a logarithmic velocity profile,

$$\varepsilon_{zo} = \kappa u_* h \sigma (1 - \sigma) \tag{6.24}$$

For the mathematical expression for the Richardson number,

$$R_i = \frac{-g}{\rho}\frac{\partial \rho}{\partial z}\left(\frac{\partial u}{\partial z}\right)^{-2} \tag{6.25}$$

the local density gradient is discretised as

$$\frac{\partial \rho(j)}{\partial z} = \frac{(\rho_s - \rho_w)}{\rho_s} \frac{(C_j - C_{j-1})}{\partial z} \tag{6.26}$$

for ρ_s and ρ_w, the density of sediment and water, respectively. Velocity shear is parameterized as

$$\left(\frac{\partial u}{\partial z}\right) = (\hat{u}/H) \tag{6.27}$$

where $\hat{u}$ is the time-averaged velocity in turbulent flow parameterized as

$$\hat{u} = \bar{u}_0 \left(1 + \frac{(0.003)^{0.5}}{\kappa}\right) \tag{6.28}$$

$\bar{u}_0$ the maximum surface tidal stream velocity.

6.4 Model Testing

Special forms of the governing equations having exact solutions were used to test the accuracy of the numerical formulation.

Test Case 1: Harmonically-Varying Velocity Field with Constant Eddy Diffusivity

This numerical solution was first compared to an exact solution for the unsteady flow case derived by Dobbins (1952) that is based on the assumption of a harmonically-varying velocity field with a constant eddy diffusivity ε, constant settling flux w_s and

constant entrainment flux. The analytical solution to Eq. 6.5 is

$$c = Ae^{-wy/\varepsilon} + (c_o - A)e^{-0.5wy/\varepsilon} * \sum_{t=1}^{\infty} \frac{2\alpha_n^2 w \exp[-(\alpha_n^2\varepsilon + 0.25w^2/\varepsilon)t]Y_n}{(\alpha_n^2\varepsilon + \frac{w}{4\varepsilon})[(\alpha_n^2\varepsilon + \frac{w^2}{4\varepsilon})h + \frac{w}{\varepsilon}]} \tag{6.29}$$

where A is the concentration at the sediment bed at $t = \infty$, h is the depth of water, and α is defined in the following relationship:

$$2\cot(h\alpha) = \frac{h\alpha}{\frac{wh}{4\varepsilon}} - \frac{\frac{wh}{4\varepsilon}}{h\alpha} \tag{6.30}$$

where Y_n is given by:

$$Y_n = \cos\alpha_n y + \frac{w}{2\varepsilon\alpha_n}\sin\alpha_n y \tag{6.31}$$

The vertical component of the sediment transport equation given by Eq. 6.5 has four boundary conditions, two of which specify the conditions that prevail at the surface, z=η, and at the bed, z=0; and two that specify the original and the final distribution of the suspended sediment. There is no transport of material across the surface so the first boundary condition at z=η is:

$$\varepsilon\left(\frac{\partial c_s}{\partial z}\right)_\eta = -w_s c_\eta \tag{6.32}$$

At the equilibrium condition the rate of entrainment at the bed equals the rate of deposition $w_s c_0$ and the second boundary condition is:

$$\varepsilon\left(\frac{\partial c_s}{\partial z}\right)_0 = -w_s c_0 \tag{6.33}$$

where the minus sign accounts for the fact that the pickup is positive when the concentration gradient is negative.

For the third boundary condition, the initial vertical profile of suspended sediment is defined by the Rouse profile (see Eq. 5.11). The fourth boundary condition is the distribution of the sediment concentration as t approaches infinity. If it is assumed that ε is constant down to the top of the bed, the final concentration distribution is,

$$c = c_0 e^{-wz\varepsilon^{-1}} \tag{6.34}$$

where c_0 is the concentration at the bed (Dobbins, 1943) defined in this example as 2.0 kg/m^3. Buoyancy stabilization was simulated using Eq. 5.2 with α_1=0.5 and β_1=10. The mean particle diameter was defined as 10 μ. For the settling velocity/concentration relationships given by Equations 5.9 and 5.10, k_1= 0.51 $\times$ 10^{-3} m/s, n_1=1.29, w_{so}= 2.6 $\times$ 10^{-3}, k_2=0.80 $\times$ 10^{-2} and n_2=4.65. Eq. 5.5 was used for the bed entrainment with α = 2.5 (N/m^2)$^{-1/2}$ and E_o= 2.4 $\times$ 10^{-6} kg/m^{2}s. The critical shear stress for entrainment was defined as τ_{cr} = 0.20 Pa and the shear stress for deposition set at τ_{ci} as 0.10 Pa. The horizontal velocity was defined as a harmonic function with the maximum surface velocity of 1.5 m/s and mean water column depth of 21 meters. The numerically predicted concentrations with depth are plotted in Figure 6.1 against the Dobbins exact analytical solution for model durations of 10, 40, 100 and 400 seconds. The predicted results are identical to the exact solution for the model durations 40, 100 and 400 seconds.

Test Case 2: Steady Flow with Quadratic Eddy Diffusivity

The numerical model was then tested in a second case involving steady flow with a quadratic expression (Rouse profile) for eddy diffusivity (Equation 6.24). The

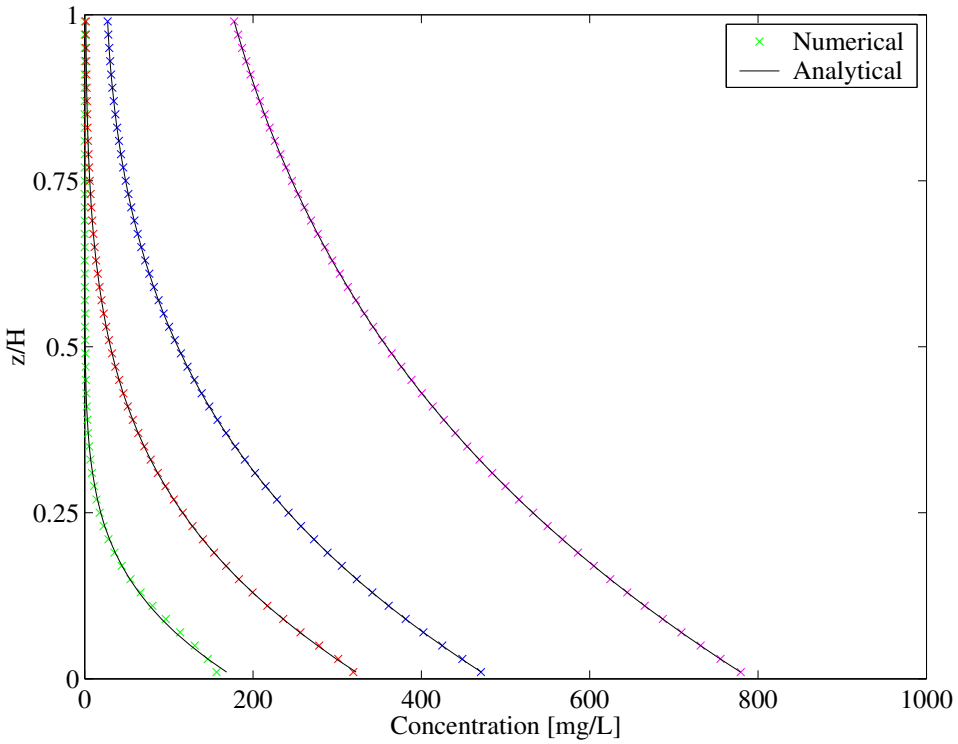

Figure 6.1: Case 1: The numerical model correctly predicts sediment concentrations at model durations of 10, 40, 100 and 400 seconds for an unsteady flow regime with constant eddy diffusivity.

quadratic form for the eddy diffusion is appropriate when sediment concentrations are small and the effects of flocculation settling can be ignored. For Case 2, the entrainment flux at the reference elevation, a, is assumed equal to the settling flux based on the particle velocity of the first grid cell. The model was run with a maximum surface tide velocity of 1.5 m/s, an initial sediment concentration of 1.0 kg/m^3 at a reference elevation of 0.001H, sediment settling velocity of 0.001 m/s, and a mean depth of the estuary of 21 meters. A modeling duration of 64,000 seconds was used with a time step of 25 seconds. Figure 6.2 shows that for an initial sediment concentration defined by the Rouse steady-state sediment profile (with number of grid cells N = 320), the numerical solution coincides with the exact solution.

Based on the model's success with these special forms, the next section examines the level of process representation needed to accurately simulate the development of the fluid mud.

6.5 Evaluation of Grid Resolution and Process Formulation

Toward the goal of determining whether a fluid mud layer in Newport Bay is an important feature relative to sediment (and FIB) transport, this section examines the relative importance of using entrainment, mixing and settling parameters modified to account for the existence of a fluid mud layer. The following six scenarios, consisting of various combinations of linear and non-linear processes (see Table 6.1), were con-

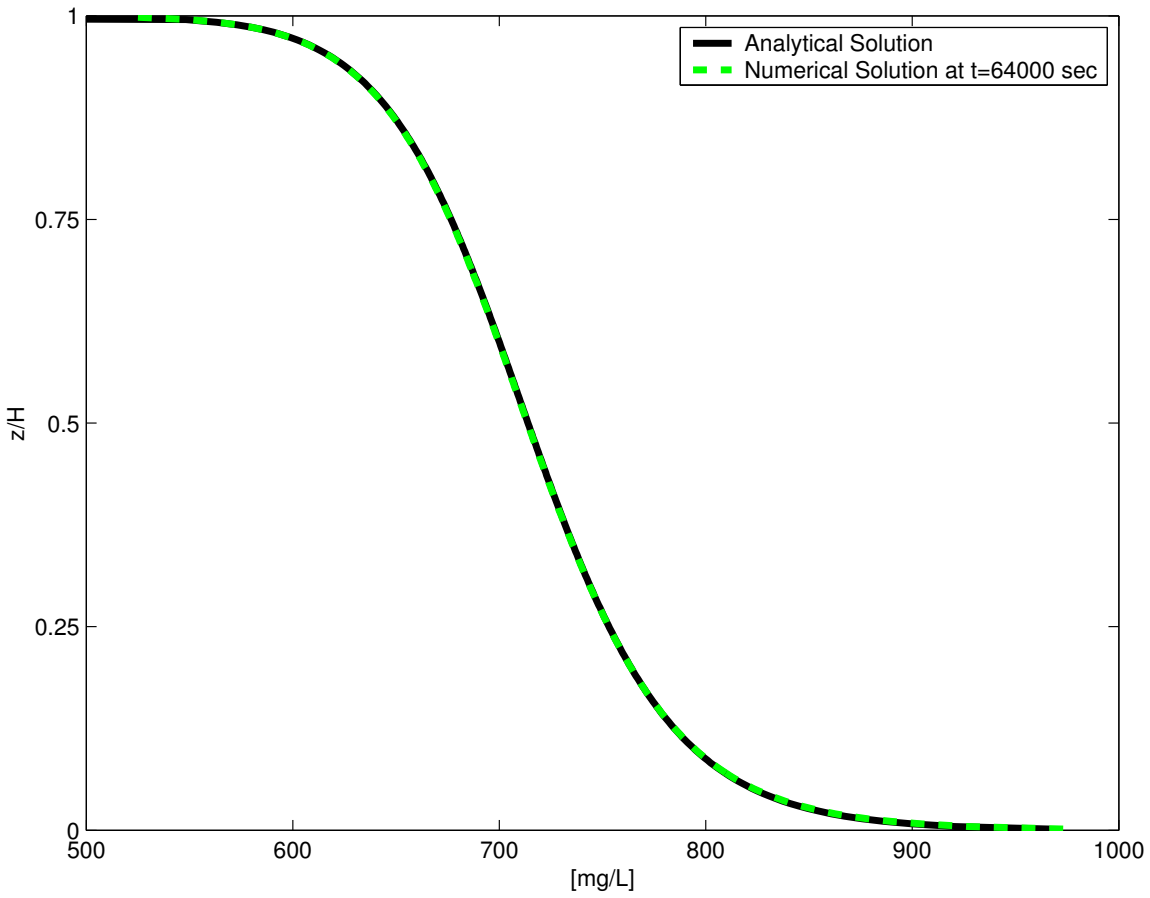

Figure 6.2: Case 2: The numerical model correctly predicts the suspended sediment concentrations for a steady flow regime with a quadratic parameterization for the eddy diffusion, a constant sediment settling velocity and a constant entrainment flux.

Sedimentation Process	**Linear Parameterization [1]**	**Non-linear Parameterization [2]**
Eddy Diffusion	Quadratic	Buoyancy-stabilized
Settling Velocity	Constant	Function of sediment concentration
Entrainment	Equal to settling flux	Function of bed shear

Table 6.1: Types of linear and non-linear parameterizations used in the 1D modeling for the processes of eddy diffusion, settling velocity and entrainment.

sidered. The numbers in brackets are used as a shorthand reference for characterizing each scenario.

1. Scenario A [1,1,1]: Quadratic eddy diffusion, constant settling velocity, and entrainment flux equal to the settling flux.

2. Scenario B [1,2,1]: Quadratic eddy diffusion, settling velocity a function of concentration, and entrainment flux equal to the settling flux.

3. Scenario C [1,1,2]: Quadratic eddy diffusion, constant settling velocity, and fluid mud entrainment/deposition a function of bed shear.

4. Scenario D [2,1,1]: Buoyancy-stabilized diffusion, constant settling velocity, and entrainment flux equal to the settling flux.

5. Scenario E [1,2,2]: Quadratic diffusion, settling velocity a function of sediment concentration, and fluid mud entrainment/deposition a function of bed shear.

6. Scenario F [2,2,2]: Buoyancy-stabilized diffusion, settling velocity a function of sediment concentration, and fluid mud entrainment/deposition a function of bed shear.

Two cases are considered: a steady velocity condition and a case with a harmonically-varying stream velocity, as follows.

Case 1: Constant Stream Velocity

The first case assumes a constant velocity of 1.5 m/s, stream depth of 21 meters, mean sediment diameter of 10 μm, a critical shear stress for entrainment of 0.2 Pa, and a critical shear stress for deposition of 0.1 Pa. For those scenarios involving entrainment as a function of bed shear, the entrainment parameterization for a partially consolidated bed case used Eq. 5.5 with E_o equal to 2.4×10^{-6} kg/m^{2}s and α_e equal to 2.5 (N/m^2)$^{-1/2}$.

Case 2: Harmonically-Varying Stream Velocity

Case 2 use the same values for all parameters as Case 1 with a harmonically-varying velocity (maximum velocity of 1.5 m/s).

Grid Resolution

Before considering the relative importance of each of these scenarios, grid resolution requirements were first examined. A reference solution was defined assuming that non-linear parameterizations for settling, entrainment and mixing are required, e.g., Scenario F, with a resolution of N=320 grid cells. Cases 1 and 2 were run five times with the following progressively finer grid resolutions: N= 10, 20, 40, 80 or 160. The results of each run were compared to the reference solution and the relative

Number of Grid Cells	Case 1	Case 2
10	4.7%	4.4%
20	4.0%	4.0%
40	3.2%	3.3%
80	2.3%	2.6%
160	1.3%	1.5%

Table 6.2: L2 errors using Scenario F parameters with a progressively finer grid resolution as compared to the reference solution (Scenario F, N=320).

errors was calculated as an L2-norm. (The L2 norm of a vector is the square root of the sum of the absolute values squared.) Results for Cases 1 and 2 are shown in Figures 6.3(a) and 6.3(b), respectively As expected, error progressively decrease with finer grid resolution. The L2 errors for the steady velocity case and the harmonically-varying velocity case with N=160 are approximately 1.3% and 1.5% respectively (see Table 6.2. For the process evaluations in the next section, grid resolution was set at N=320.

Processes Evaluation

The 1D model was then run to evaluate the process combinations defined as Scenarios A, B, C, D and E with a grid resolution of N=320. As before, the reference solution was defined as Scenario F run with N=320 grid cells. Table 6.3 shows the calculated L2 errors.

For Case 1, Scenario B, which incorporates settling velocity a function of concentration, shows a somewhat improved accuracy compared to the base scenario, Scenario A (L2 error equals 9.1% vs. 16.5%), which assumes a constant settling ve-

Scenario	**Case 1**	**Case 2**
Scenario A	16.5%	54.2%
Scenario B	9.1%	39.0%
Scenario C	160%	145%
Scenario D	16.5%	51.9%
Scenario E	1.5%	3.1%

Table 6.3: L2 errors of Scenarios A-E with N=320 as compared to the reference solution (Scenario F, N=320).

locity. There is considerable improvement under Scenario E (3.1%), which includes a non-linear parameterization for entrainment/deposition a function of bed shear in combination with settling velocity a function of concentration. Note that in Scenario C which has the non-linear parameterization for entrainment/deposition without the settling velocity a function of concentration, there is a L2 error higher than the base scenario.

Case 2 shows the same relative relationship among the scenarios. However, as opposed to Case 1 where even Scenario A provided a reasonably accurate prediction, only Scenario E for Case 2 provided good results. For the harmonically-varying velocity case, non-linear parameterization for entrainment/deposition and settling velocity as a function of concentration, are required as a minimum.

6.6 Model Verification Using Suspended Sediment Data from the Severn Estuary

The predictive ability of the vertical transport model was tested using suspended sediment concentrations measurements from a 1982 study of the Severn Estuary, Eng-

land (Kirby, 1986). Figures 6.4 and 6.5 compares model predictions with measured suspended sediment concentrations at Hours 0000, 0130, 0200 and 0300. Buoyancy stabilization was simulated using Eq. 5.2 coefficients selected for a bay mud: with α_1=0.5 and β_1=12 (Partheniandes, 1965). For the settling velocity/concentration relationships given by Equations 5.9 and 5.10, k_1= 0.66 $\times$ 10^{-3} m/s, n_1 =1.26, w_{so} = 2.6 $\times$ 10^{-3}, k_2=0.80 $\times$ 10^{-2} and n_2=4.65. Eq. 5.5 was used for the bed entrainment with α = 3.1 $(N/m^2)^{-1/2}$ and E_o= 3 $\times$ 10^{-6} kg/m^{2}s. The critical shear stress for entrainment was defined as τ_{cr} = 0.27 Pa and the shear stress for deposition set at τ_{ci} as 0.13 Pa. The horizontal velocity was defined as a harmonic function with the maximum surface velocity of 1.5 m/s and mean water column depth of 24 meters. The model correctly portrays the highly differentiated suspension with a dense suspended sediment layer formed adjacent to the bed during accelerating flows and an overlying water column virtually stripped of suspended sediment. At Hour 0130 the model simulates the beginning of the thickening of the lutocline which disappears by Hour 0300. Notice the irregularity of the bed entrainment with a very high sediment concentration layer that rises 1 to 3 meters above the bed with plumes of sediment with concentrations greater than 500 mg/L rising into the water column.

This model was then rerun using parameters that typify Newport Bay: mean water depth of 7 meters and maximum tide velocity of 1 m/s. The critical shear stress for entrainment was defined as τ_{cr} = 0.54 Pa (see Chapter 7). Entrainment coefficients for Eq. 5.2 were adjusted to be reflective of estuarial mud with α = 2.4 $(N/m^2)^{-1/2}$ and E_o= 2.5 $\times$ 10^{-5} kg/m^{2}s (Thorn and Parson, 1977).

Figure 6.6 shows that during a period of increasing tide velocities (during a spring tide), a suspended sediment concentration layer of ~ 50 mg/L, with thickness of about 10 cm layer, forms above the bed. In Figure 6.7, tide velocities are decreasing and the suspended sediment concentration layer above the bed disappears. It appears from this modeling that with increasing tide velocity, bed shear due to tides may be sufficient in Newport Bay to entrain bed sediments into the water column with subsequent deposition (at a different location due to transport) as tide velocities decrease.

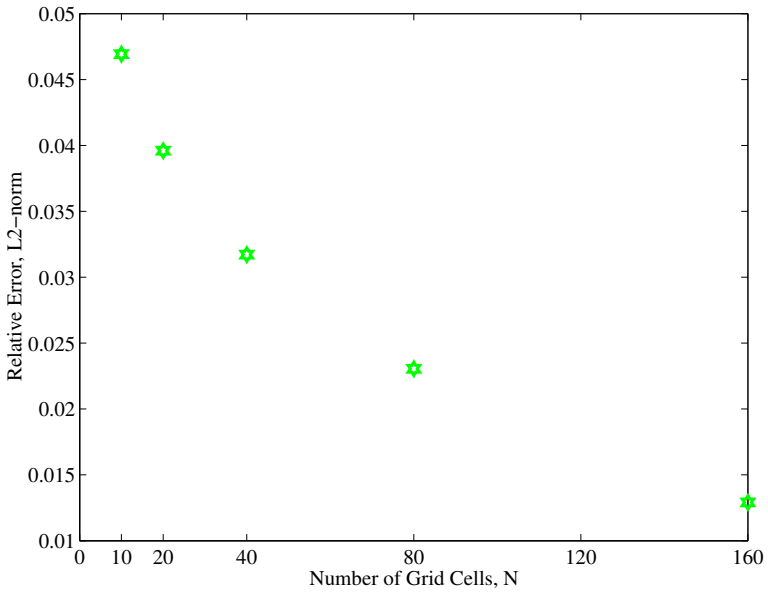

(a) Case 1: Steady Stream Velocity

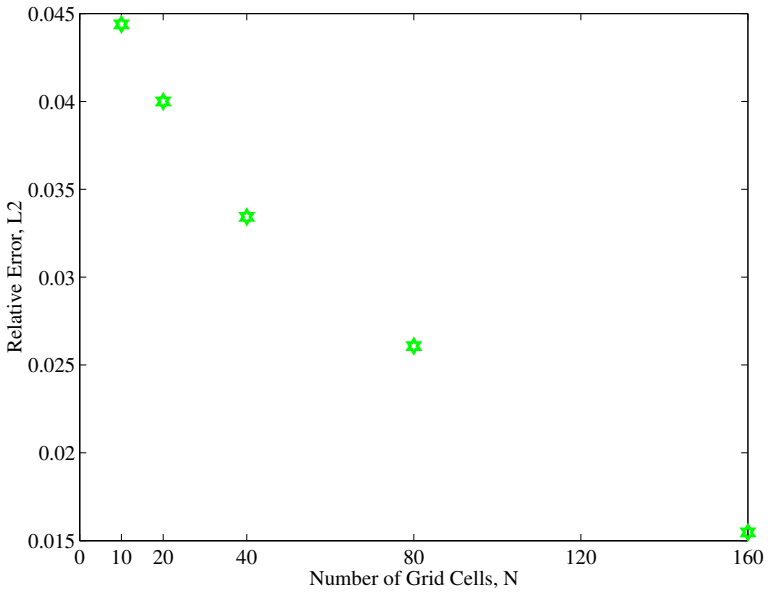

(b) Case 2: Harmonically-Varying Stream Velocity

Figure 6.3: Steady Flow: Relative error with respect to number of grid cells compared to Scenario F with N=320 cells for steady flow velocity (Case A) and harmonically-varying flow velocity (Case B).

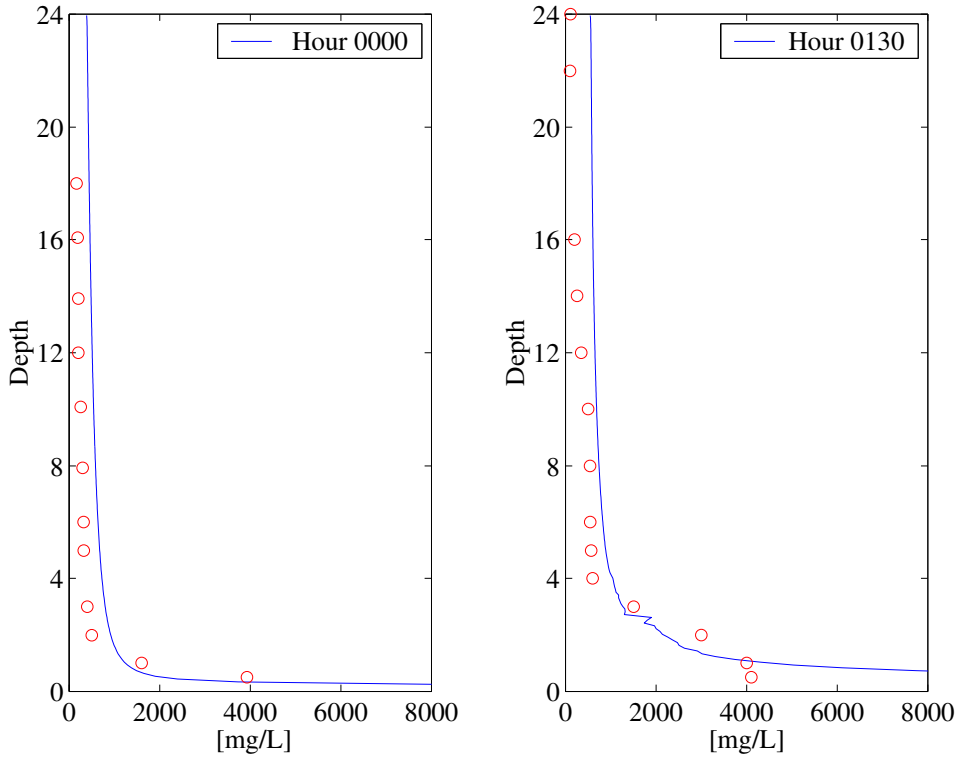

Figure 6.4: Predicted versus measured suspended sediment concentrations as Hours 0000 and 0100.

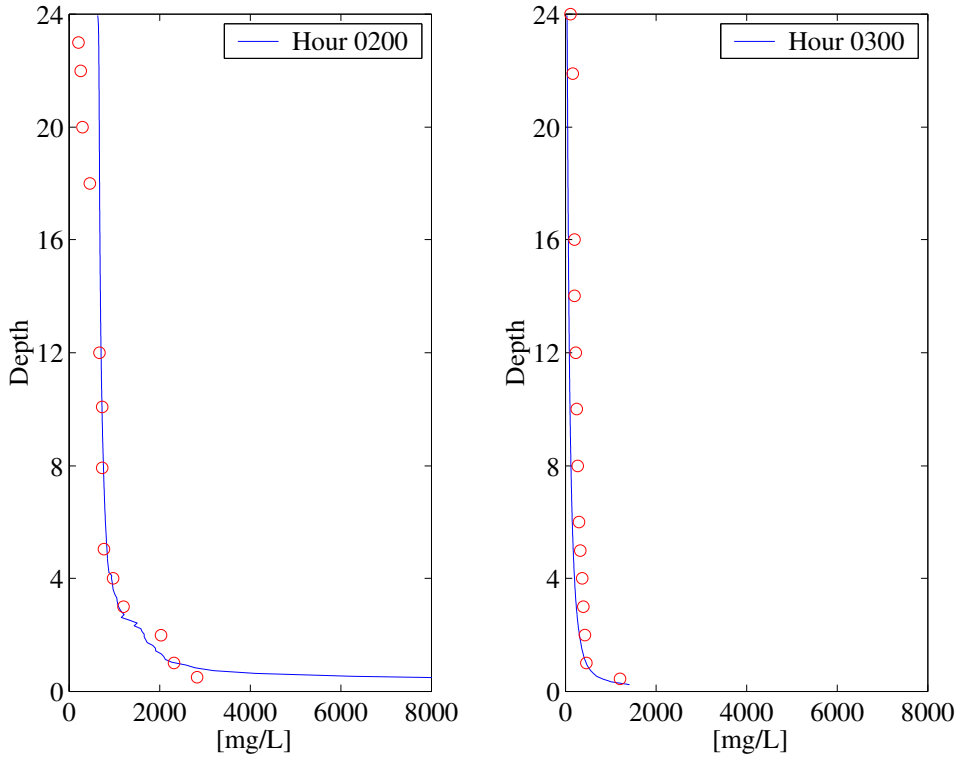

Figure 6.5: Predicted versus measured suspended sediment concentrations as Hours 0200 and 0300.

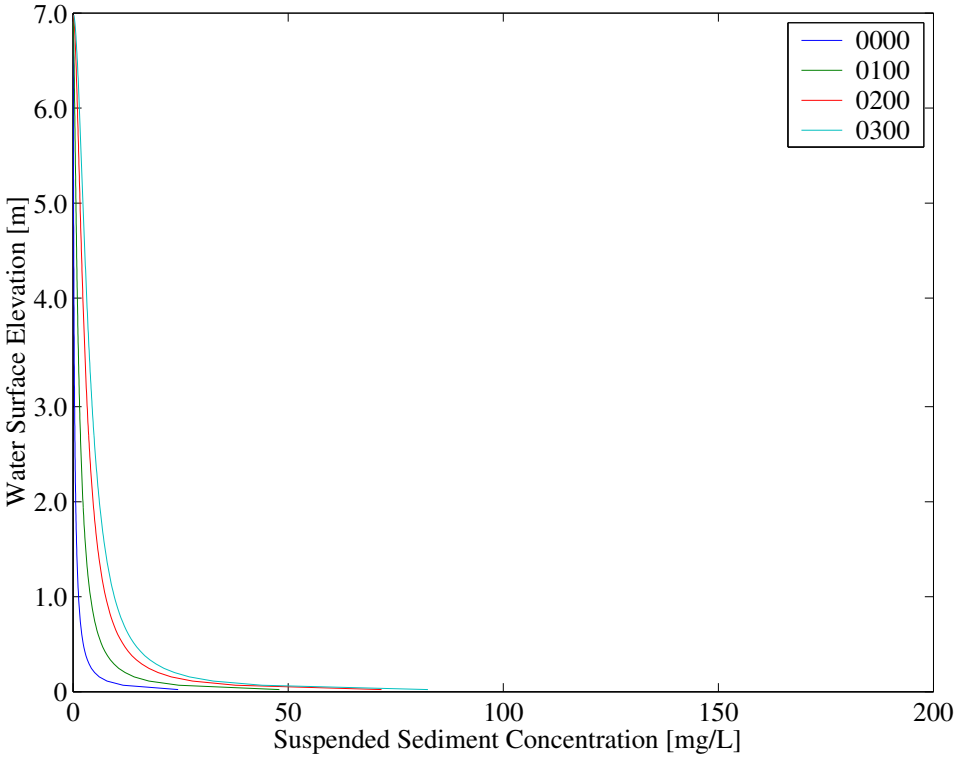

Figure 6.6: Predicted development of a layer of higher concentration suspended sediment above the bed as tidal flow velocity increases during a Spring tide for a water column depth of 7 meters and critical shear stress, τ_{cr}, equal to 0.54 Pa.

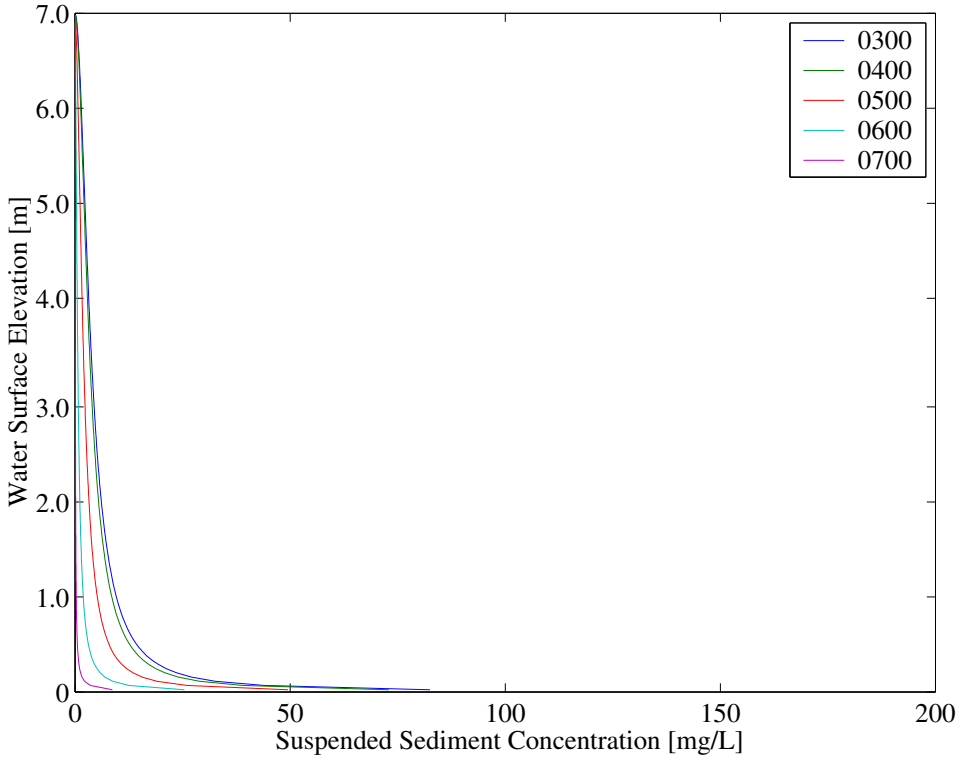

Figure 6.7: Predicted disappearance of suspended sediment layer with decreasing tidal velocity.

Chapter 7

Fine Sediment Entrainment in Newport Bay

This chapter examines two basic questions. Is sediment erosion an important contributor to dry-weather water quality, e.g, FIB, impacts? And if so, what reaches of the bay are subject to erosion and what areas of the bay are impacted by the transport of this material in suspension?

From an environmental perspective, the importance of quantifying dry-season entrainment of bed sediments into the water column is three-fold: (1) suspended sediments can be a water quality concern as turbidity caused by suspended sediment particles can restrict the penetration of sunlight to the detriment of aquatic biotic, e.g., eel grass, (2) heavy metals, pesticides and nutrients readily adsorb to fine sediment facilitating pollutant transport and potentially increasing pollutant bioavailability (Preston *et al.*, 1972; Kirby and Parker, 1973; Hayter, 1986; Yan, 1995), and

(3) studies have noted a complex web of processes that influence the distribution of bacteria in estuaries including sedimentation and resuspension, and regrowth on sediments, flushing by ocean water, die-off, predation, vegetation, and debris (Savage, 1905; Goyal *et al.*, 1977; Roper and Marshall, 1979; Jensen *et al.*, 1979; Labell *et al.*, 1980; Grimes *et al.*, 1986; Thomann and Mueller, 1987; Davies *et al.*, 1995; Oshiro and Fujioka, 1995; Anderson *et al.*, 1997; Byappanahalli and Fujioka, 1998; Solo-Gabriele *et al.*, 2000; Grant *et al.*, 2001).

Considerable advances in predicting cohesive sediment entrainment have been made in the past decades, however, one of the key difficulties in making accurate predictions is the difficulty of assessing the critical shear stress for esturial bed sediments. There has been no previous testing of bay sediments to evaluate erosion rates and bulk properties of bed sediments in Newport Bay. Previous modeling to predict sediment transport through the bay during a storm event used literature values for bulk density (US EPA, 2002). Therefore, to determine an appropriate critical bed shear stress needed for predicting entrainment in Newport Bay, four core samples (depth of 20-25 cm) were collected at the surface of the bed and an erosion rate study of these cores was conducted (Section 7.1-7.3). An additional field study collected suspended sediment data in the bay (Section 7.4). The 2D numerical model was then employed to mimic tidally induced bed shear and predict suspended sediment concentrations based on different combinations of critical shear stress and entrainment coefficients using an entrainment parameterization for partially consolidated bed sediments (see Eq. 5.5). Predicted suspended sediment concentrations were compared

with field measurements for determining an appropriate critical shear stress and associated entrainment coefficients (Section 7.5). In Sections 7.6 and 7.7, bed sediment erosion over the entire Bay is modeled and evaluated.

7.1 Collection of Bed Cores

Prior to field sampling, the 2D numerical model was run over a fourteen-day period to predict locations of the maximum bed shear stresses, τ_b, induced by tidal currents in Newport Bay in order assist in identifying potential critical sampling locations. For these numerical runs, bed shear was parameterized per Eq. 2.2.

Figure 7.1 shows two reaches within the main channel where the highest bed shears occur. One high shear reach is within the harbor from the jetty to the center of the harbor. The other reach starts at Coast Highway and extends two-thirds up the bay to Station BTO5.

To simplify the field work, sampling was focused on the second reach in Upper Bay where the bay is shallower. Four core sample sites were selected: Core 1 in the center of the harbor west of BTO9, Core 3 at the top of the bay opposite the outlet of San Diego Creek west of BTO4, Core 2 halfway up Upper Bay near the outlet of Big Canyon Creek between Stations BTO5 and BTO6, and Core 4 opposite the outlet of the Santa-Ana Delhi Channel near BTO5. (See Figure 7.2.) The sediment cores were collected with a push coring apparatus. The water depths varied between 1.37 and 4.85 meters at the time of coring. Detailed description on the core locations and core sampling methodology can be found in Appendix A.

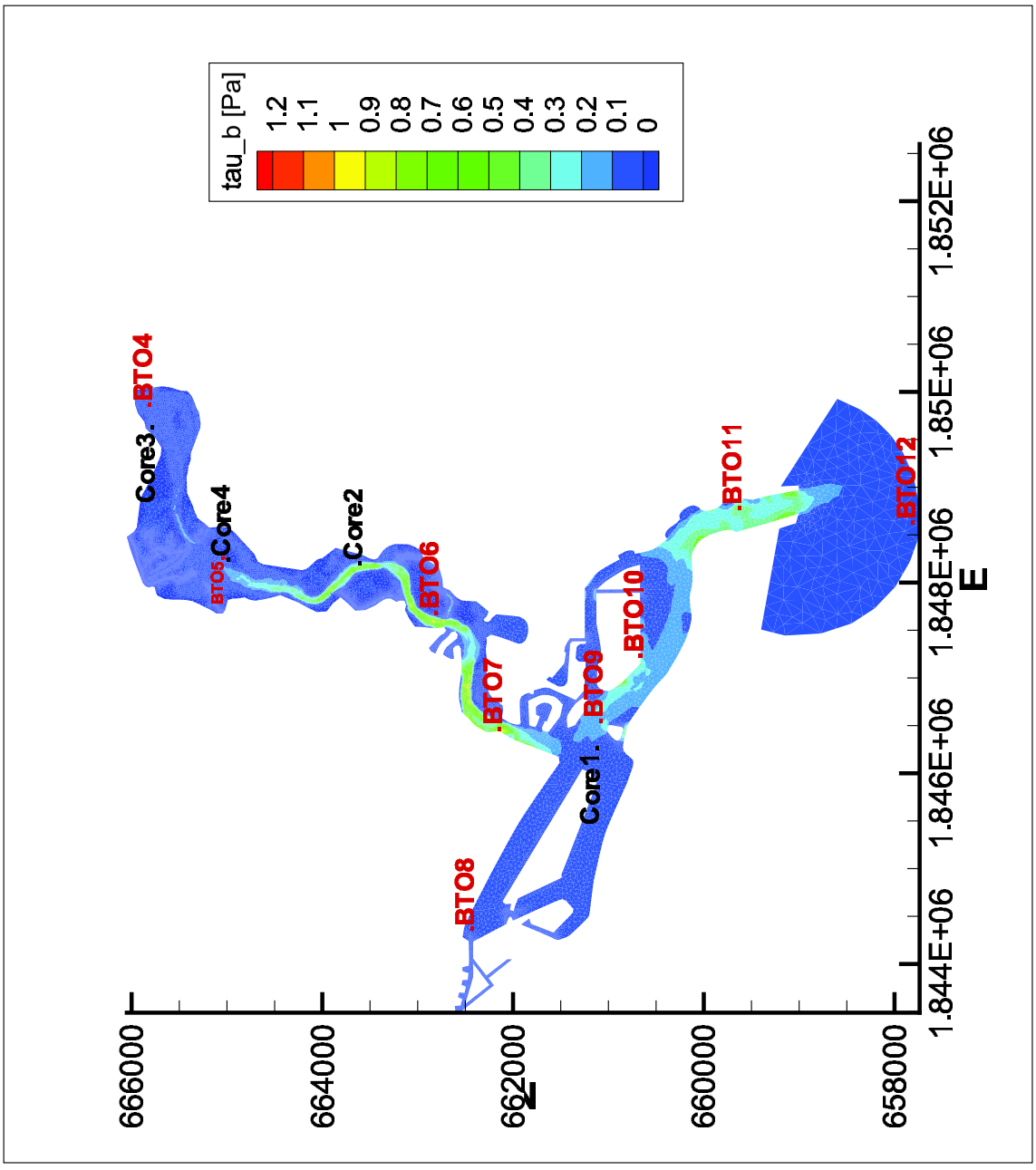

Figure 7.1: Tidally Induced Bed Shear with roughness coefficient n=0.020. Note that the highest bed shears are located in the reach between BTO6 and BTO7.

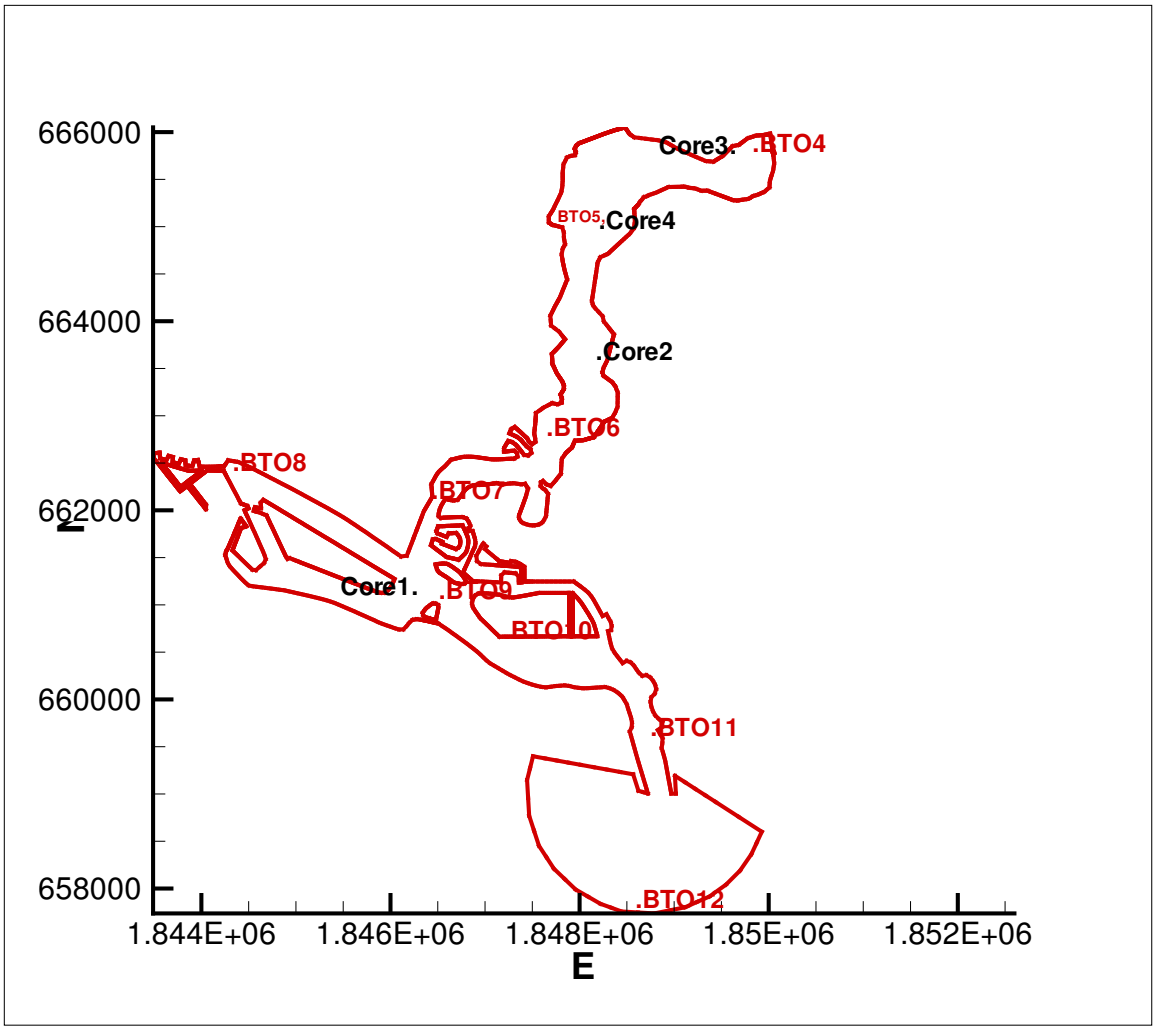

Figure 7.2: Location of Bed Sediment Samples

7.2 Measurement of Sediment Erosion Rates and Bulk Properties

A straight, recirculating flume, located at the Sea Engineering Laboratory in Santa Cruz, California, was used for measuring the erosion rates for each of these undisturbed bed sediment samples as a function of applied shear stress and eroded core depth (see Figure 7.3). The recirculating flume method, known at Sedflume (Sediment Erosion at Depth Flume), was developed by McNeil *et al.* (1996). The flume has a test section with an open bottom through which a rectangular coring tube (10 cm by 15 cm) containing a bay core sample was attached. The core sample was raised into the test section flume using the hydraulic jack until the sediment surface was even with the bottom of the flume channel. A measurement was then made of the core length. The flume was then run at a specific flow rate corresponding to a particular shear stress. As the sediment eroded from the surface of the core, the piston inside the core was raised to keep the sediment sample flush with the flume bed. Erosion rates were obtained by measuring the core length at different time intervals, taking the difference between each successive measurement, and dividing by the time interval. Details for the measurement methodology are provided in Appendix A.

The critical shear stress of a sediment bed, τ_{cr}, is defined quantitatively as the shear stress at which a very small, but accurately measurable, rate of erosion occurs. This rate of erosion has been practically defined as 10^{-4} cm/s. This represents 1 mm

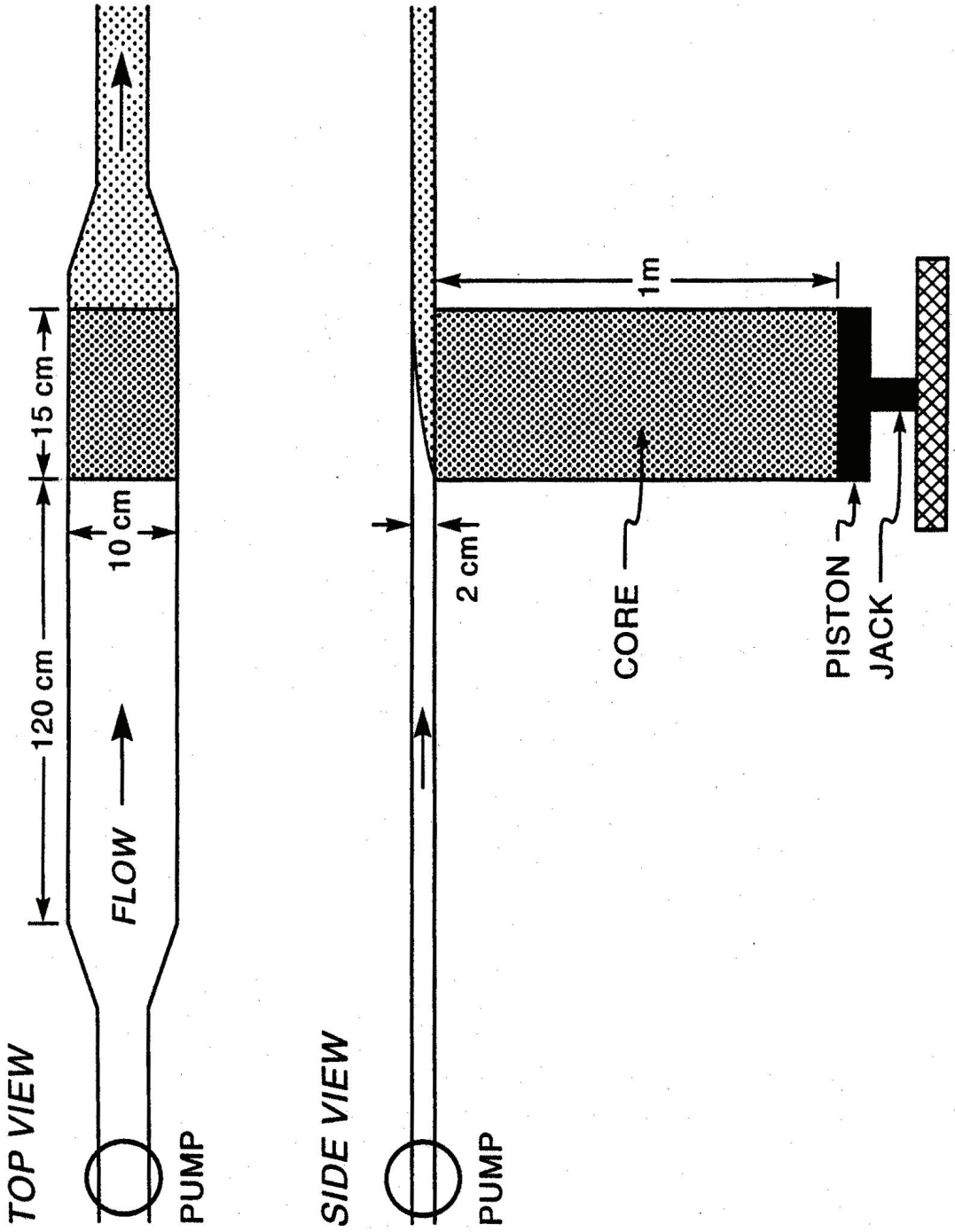

Figure 7.3: Sedflume Diagram

of erosion in approximately 15 minutes. Since it is difficult to measure τ_{cr} exactly at 10^{-4} cm/s, erosion rates were determined above and below 10^{-4} cm/s. The τ_{cr} was then determined by linear interpolation. The technique gives the τ_{cr} with at least a 20% accuracy (McNeil *et al.*, 1996; Roberts *et al.*, 1998).

Each core was also sub-sampled at vertical intervals to determine the water content, bulk density, and particle size distribution of the sediments. See Appendix A for details on the sampling and analysis methodology.

7.3 Evaluation of Core Sediment

All samples were found to be heterogeneous with depth with each core having its own character. Table 7.1 summarizes the measurement results. All core bulk densities were measured as 1.30 g/cm^3 or greater. Fluid mud has been defined as having bulk densities less than 1.30 g/cm^3, so this would indicate the core samples should be classified as partially-consolidated sediments. However, the low critical shear stresses fall within the range for a fluid mud.

Critical Shear Stress of Core Samples

Table 7.1 shows there is a range of critical shear stresses from 0.22 to 0.64 Pa for the top bed sediments. Table 7.2 compares the τ_{cr} of the top bed sediments at each of the mudcore locations to the numerically-predicted tidally-induced bed shear, τ_b, at each core location (from Figure 7.1). At all of the four core locations, tide-induced bed shear is insufficient to erode/entrain the top bed sediments. Note that

Core-1 (Mid-Harbor) Depth	D50 [μm]	ρ_b [g/cm^3]	τ_{cr} [N/m^2]
0-5.4 cm	13.6	1.32	0.26
5.4-10.5 cm	10.35	1.44	1.79
Core-2 (Big Canyon Depth	D50 [μm]	ρ_b [g/cm^3]	τ_{cr} [N/m^2]
0-6.9 cm	17.15	1.3	0.52
6.9-11.6 cm	212.9	1.86	0.24
Core-4 (Narrows) Depth	D50 [μm]	ρ_b [g/cm^3]	τ_{cr} [N/m^2]
0-6.5 cm	21.9	1.33	0.22
6.5-11.3 cm	21.13	1.5	0.16
Core-3 (Unit I/III) Depth	D50 [μm]	ρ_b [g/cm^3]	τ_{cr} [N/m^2]
0-5.4 cm	47.76	1.4	0.64
5.4-11.3 cm	61.73	1.77	0.32

Table 7.1: Sediment Properties for the Four Cores.

	Max τ_b [Pa]	Sedflow τ_{cr} [Pa]
Core 1	0.14	0.26
Core 2	0.38	0.58
Core 4	0.09	0.64
Core 3	0.11	0.22

Table 7.2: Critical shear stress versus bed shear.

all the core locations are located outside the main channel and therefore not subject to the higher bed shears. The direct implication is that sediment entrainment by tidal currents only occurs in the main channel during spring tides.

Bed Sediment Particle Sizes

Along with measuring erosion rates of the bed sediment, particle sizes were also determined. Figure 7.4 compares the particle sizes of the top 5 cm layer from each

	Clays [%]	Fine Sediment [%]	Coarser Sediment [%]
Core 1	11.2	77.0	11.8
Core 2	10.1	68.1	21.8
Core 4	6.6	49.0	44.4
Core 3	9.7	56.9	33.4

Table 7.3: Percentages of sediment size classes.

core. The two southerly-most bed samples, Core 1 and Core 2, have similar profiles with a significant amount of fines less than 10 μm. Core 2 has larger volume fractions of particles larger than 60 μm. Core 4, located near the outlet of the Santa Ana-Delhi Channel into Newport Bay, has significantly less fines with the peak volume fraction at about 200 μm. The northerly-most core, Core 3, has more fine sediment fractions than Core 4 (and similar to Cores 1 and 2), but a larger volume fraction of the large diameter particles. Table 7.3 shows the percentages of clays (<2 μm), fine sediments (<63 μm), and coarser materials, e.g., sands and gravels for each of the four core samples. There are higher percentages of clays and fine sediment in the downstream samples (Cores 1 and 2).

7.4 Suspended Sediment Field Data

A bacterial study conducted by Grant *et al.* (2006) involved the collection of surface sediment samples at the BTO stations in Newport Bay. These field data were used to check 2D model predictions for suspended sediment concentrations using an assumed critical shear stress within the range suggested by the mudcore evaluation. Samples were collected using a Wildco Ponar Petite Grab lowered approximately one

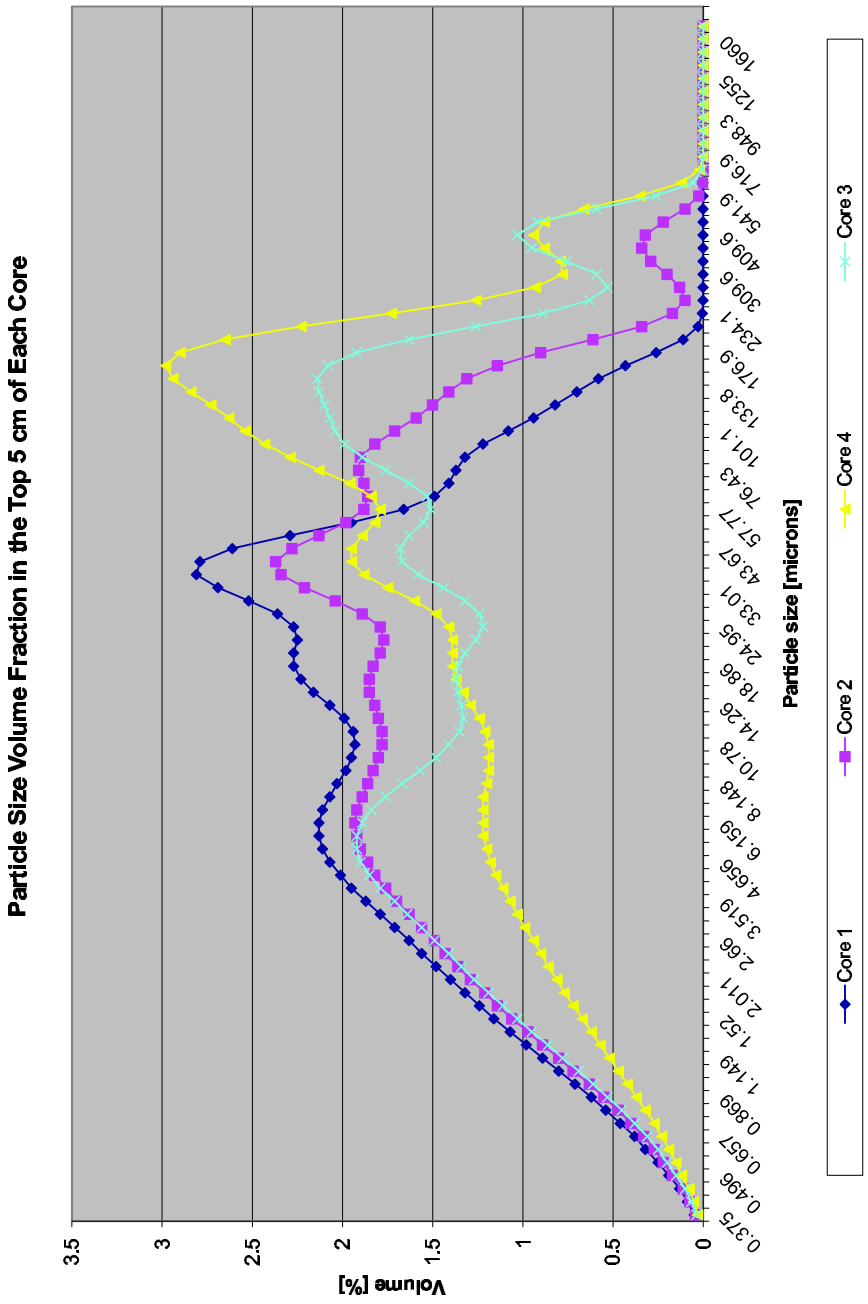

Figure 7.4: Volume fraction of sediment sizes in the top 5 cm of each core.

meter over the side of the boat with a mechanical davit. Sediment grab samples were emptied into a plastic tray on the deck of the boat and sub-sampled with a 50 mL sterile plastic centrifuge tube. The 50 mL tube was immediately capped and placed on ice in the dark. A total of four to eight samples were collected at each site over a ten month period. The samples were analyzed for grain size distribution as follows. Archived sediment samples were retrieved from the -85 °C freezer and defrosted overnight in the refrigerator. Approximately 30 grams of refrigerated sediment sample was suspended in 30 mL of 30% hydrogen peroxide and placed in the fume hood overnight to remove the organic fraction. Each sample was then centrifuged at high speed for 10 to 15 minutes and filtered through a 53 μm sieve to remove the sand fraction, diluted into DI water, and analyzed using a LISST-100 particle size analyzer (Sequoia Scientific, In., Bellevue, WA) in batch mode. Particle size were characterized into separate sediment size classes ranging for 1 to 230 μm.

The suspended sediment samples were collected during neap and spring tide periods. The time of the sample collection is not noted. Most of the suspended sediment samples collected (36 of the 40 samples) have filtered suspended sediment concentration between 7 to 60 mg/L (see Table 7.4). The remaining four filtered samples had elevated total suspended sediment concentrations ranging from 97 to 442 mg/L. These samples were collected during the rain season or after storm events so are likely not indicative of suspended sediment concentrations in the dry season.

The filtered samples were adjusted to compensate for the missing coarser sediment by observing the fraction of coarser sediment in the nearby mudcore samples. For

Station	Filtered Suspended Sediment Concentration (dry season) [mg/L]	Filtered Suspended Sediment Concentration (rain season) [mg/L]
BTO4	16-47	443
BTO5	19-58	
BTO6	10-60	
BTO7	19-58	158-248
BTO8	8-35	
BTO9	9-44	
BTO10	14-41	
BTO11	7-24	97

Table 7.4: Range of suspended sediment concentrations (filtered) from samples collected from January to October 2006. Samples were taken at the surface at BTO stations along Newport Bay thalweg.

instance, the coarse sediment fraction from Table 7.3, for Mudcore 1 is 0.12, while for Mudcore 2, the coarse sediment fraction is 0.22. Focusing on the suspended samples collected in September 2006 when the mudcore samples were taken, Table 7.5 shows the adjusted suspended sediment concentrations (SSC). Even with the adjustment, the suspended sediment concentration is low, ranging from 28 to 66 mg/L.

7.5 Representative Critical Shear Stress of Main Channel

The entrainment parameterization for a partially consolidated bed sediments can be expressed using Eq. 5.5:

$$E = E_o \exp[\alpha(\tau_b - \tau_{cr})^{0.5}] \qquad (\tau_b > \tau_{cr}) \tag{7.1}$$

where E_o and α are empirical coefficients, τ_b is the applied bed shear stress, and τ_{cr} is the bed shear strength for entrainment of the partially consolidated bed sediments.

The 2D model was run iteratively with different critical shear stress threshold, entrainment parameters and settling velocities. A range of settling velocities between 0.01 - 0.03 cm/s were used based on in-situ measurements made with a laser in-situ scattering and transmissometer (LISST-100, Type C) (Grant, 2008).

A first set of trials assumed a critical shear stress of $\tau_{cr} = 0.22$ Pa (the critical shear stress for Mudcore 3) using entrainment coefficients similar to those suggested by Thorn and Parson (1977 and 1979) for estuarial mud. The model predicted total suspended sediment mass concentrations considerably higher than measured concentrations. (See Table 7.6.) However, for a critical shear stress of 0.54 Pa (similar to the critical shear stress calculated at Core Location 2), total suspended sediment mass concentration predictions were reasonably close (but somewhat lower) to the adjusted total mass concentration (see Figure 7.5). While additional bed sediment samples should be collected in concert with suspended sediment concentrations within the water column, this first estimate of the critical shear stress within the main channel of the bay represents an important advance in our understanding of Bay sediment dynamics.

7.6 Sediment Resuspension, Transport and Deposition Processes in Newport Bay

The 2D model predicts that once the tidally-induced bed shear exceeds the critical shear stress of 0.54 Pa, the partially-consolidated bed sediments begin to be entrained

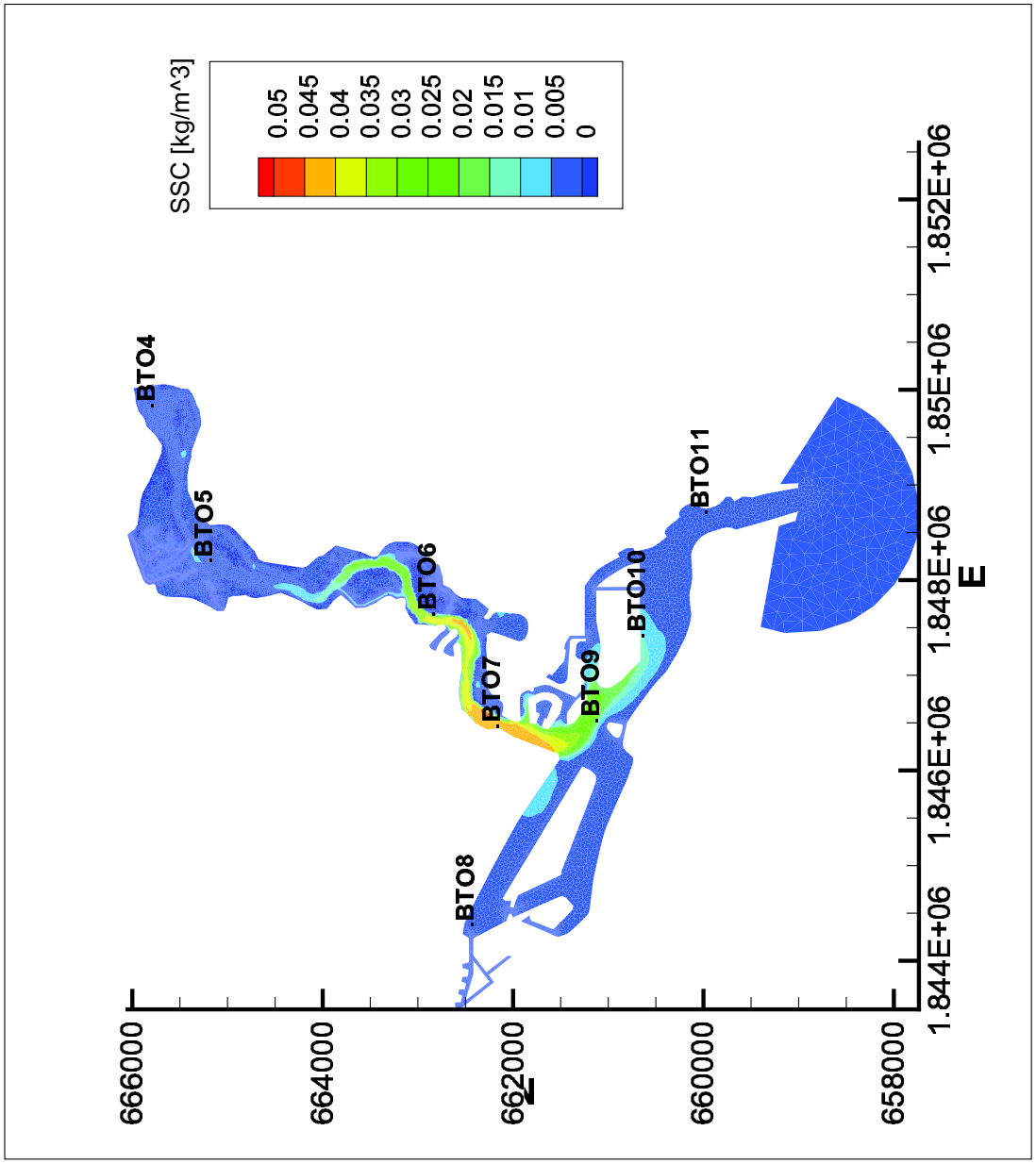

Figure 7.5: Assuming a critical shear stress of 0.54 Pa, suspended sediment concentrations during a spring tide reach 40 to 45 mg/L in the reach between BTO6 and BTO7 for assumed entrainment parameters E_o equal to 3.3×10^{-5} kg/m^{2}s and α equal to 4.2 (N/m^2)$^{-1/2}$.

Station	Filtered Total Mass Concentration [mg/L]	Coarse Bed Sediment Fraction [%]	Adjusted Total Mass Concentration [mg/L]
BTO5	19	44	44
BTO6	34	22	44
BTO7	58	12	66
BTO9	43	12	49
BTO10	25	12	28

Table 7.5: Suspended sediment concentrations (filtered) collected at the surface at BTO Stations in September 2006 with adjustments to account for filtered coarser sediment fraction based on evaluation of sediment bed cores collected nearby.

Trial	τ_c [N/m^2]	$E_o \times 10^5$ [kg/m^{2}s]	α [(N/m^2)$^{-1/2}$]	BTO5 [mg/L]	BTO6 [mg/L]	BTO7 [mg/L]	BTO10 [mg/L]
Measured				**44**	**44**	**66**	**28**
Modeled	0.22	7.0	5.0	300	300	250	200
Modeled	0.27	2.5	8.3	80	80	80	60
Modeled	0.30	2.0	6.9	70	50	60	50
Modeled	**0.54**	3.3	4.2	27	37	43	17

Table 7.6: Comparison of measured and predicted suspended sediment concentrations at selected BTO stations. Modeling indicates that the critical shear stress is approximately 0.54 Pa.

within an approximate 3,000 meter reach of the main channel from BTO7 to a point halfway between BTO5 and BTO6. Entrainment continues during a spring tide as the maximum bed shear approaches 1.1 Pa in some regions of the main channel. The entrained material is advected with the tides with a low-concentration sediment plume reaching the harbor jetty on the ebb tide and extending part way out into the ocean (see Figure 7.6). The model shows most of the sediment plume returning back into the harbor with the flood tide.

As the flood tide evolves, the suspended sediment plume advects up the harbor and is split at BTO9 with most of the suspended sediment flowing up the main

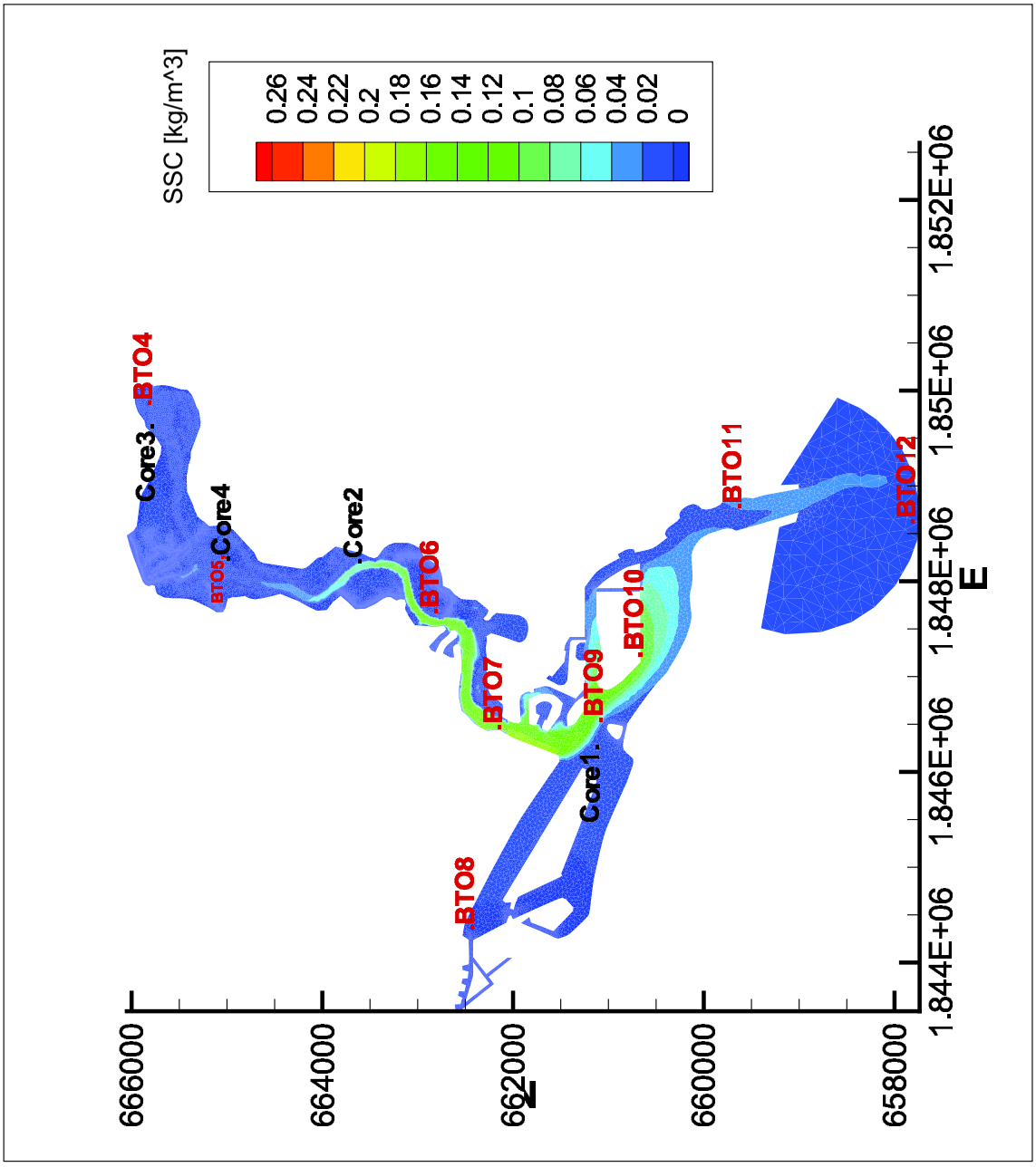

Figure 7.6: On a ebb tide, a sediment plume begins to escape our the harbor entrance.

channel toward BTO4 and a portion of the suspended sediment proceeding westerly toward BTO8 along the north side of Lido Island (Figure 7.7). Model predictions suggest that this slug of suspended sediment does not quite get to BTO8 on a single flood tide before the ebb tide pulls the plume back into the main channel.

The model predicts that during decelerating flow conditions, much of the suspended sediment settles back onto bed along the main channel. Apparently some sediment finds its way into the western harbor and other quiescent areas of the bay as these areas require periodic dredging. Mudcore 1, located in the center of the harbor somewhat west of the main channel, is composed of fine sediment with D50 sediment size ranging from 10 to 15 μm over the entire 35 cm core length. This sediment profile may be indicative of the settlement of fine sediment in the western area of the bay. Due to the small size and slow rate of settling, consolidation of these very fine sediments within the quiescent regions of the bay may be expected to occur slowly.

7.7 Discussion

Modeling results suggest that only the central section of the main stem of Newport Bay is subject to sediment erosion by tidal currents; currents elsewhere in the bay are too weak. Moreover, modeling results suggest that much of the suspension falls out during the same tidal cycle, in the vicinity of the main stem, although the finest particles may stay in suspension indefinitely and ultimately get mixed into the neighboring ocean. From a perspective of FIB transport, these results point to

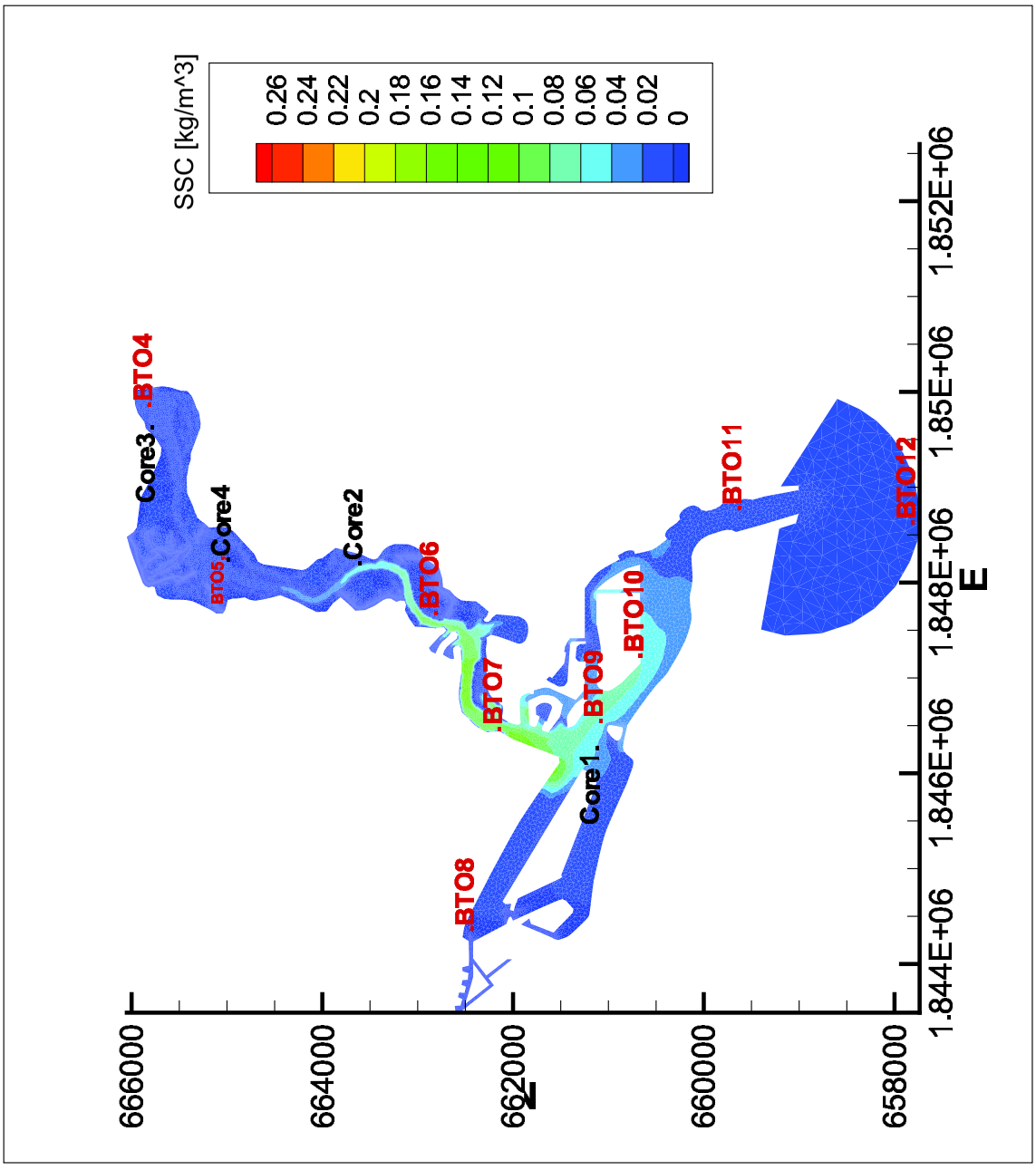

Figure 7.7: On a flood tide, the sediment plume splits; a portion is transported to the west end of the harbor and the remainder is advected North into Upper Bay.

sediment contamination within the central channel being a potentially important localized source for impacts to benthic community in that area and perhaps a potential contributor to bay-wide water quality impacts. On the other hand, contaminate sediments in quiescent parts of the harbor are unlikely to contribute to bay-wide "FIB impairment". An important caveat of the above analysis is that light, unconsolidated material (e.g., biofilms) may grow at the sediment-water interface. This can create a nutritionally favorable condition for bacterial regrowth in estuarine systems (Rheinheimer, 1968;Rheinheimer, 1992). These bacteria can then be mobilized throughout the bay by tidal currents either as free bacteria, or more likely, attached to particles or flocs (Kirchman, 1983; Geesey and Costerton, 1979; Goulder, 1976; Lind and Lind, 1991; Koske *et al.*, 1966; Cammen and Walker, 1982; Ferguson *et al.*, 1996), contributing to FIB impairment as has been shown in other marine wetlands (e.g., Sanders *et al.* 2005).

A more accurate dry season model of sediment entrainment, advection, and settling would require a more accurate assessment of characteristic critical shear stress for entrainment τ_{cr}, throughout the bay. Additional bed sediment cores would be needed within the main channel collected at key times of the lunar cycle, along with field study to measure the evolution of the suspended sediment concentrations during spring and neap tide periods just downstream of Coast Highway.

As a final thought, it should be stressed that the majority of sediment transport in Newport Bay is associated with storm events, not the dry-weather conditions which are the focus of this dissertation. Additionally, dredging is required on an ongoing

basis because high sediment loads are shed from the San Diego Creek Watershed resulting in significant deposits, particularly in upper Newport Bay. Nevertheless, the results of this study show that during dry-weather periods when water-contact recreation is heightened, the potential exists to suspend bed material and this may contribute to FIB impairment.

Summary

The objective of this dissertation is to advance a better understanding of two dry-weather distributed loading mechanisms in Newport Bay that will be central to future water quality management actions: (1) the magnitude of dry weather urban runoff from storm drains from the hundreds of watershed areas directly tributary into Newport Bay, and (2) the magnitude and spatial distribution of sediment resuspension during dry-weather periods in response to tidal currents. In addition to investigating these two dry-weather loading mechanisms, another objective of this dissertation is to improve the characterization of tidal circulation to better understand how this process acts to redistribute loads from storm drains and resuspended sediment.

From the investigations of this dissertation some fundamental aspects of Newport Bay have been revealed. First, salinity measurements along the main channel from Upper Bay to the Harbor Jetty indicate that the Bay is well mixed downstream of BTO 5 (see Section 2.6). This allows the deployment of a 2D numerical model which was calibrated with the salinity data. With salinity as tracer, the 2D modeling reveals an interesting bay-wide circulation pattern. The pattern involves the exchange

of water from the main stem of the estuary and the channel loop around Lido Island, on the western side of the bay. Successive flood and ebb tides create a residual circulation in the counter-clockwise direction around Lido Island, a complete circuit taking about 3 days during a Spring tide (Sections 2.7 and 2.8). In Newport Bay, this gives rise to a pattern of low and high salinity water parcels wrapped around Lido Island. Occurring on a shorter time-scale, a residual circulation in the clockwise direction can be observed around the Balboa Islands. These circulation patterns provide a clue of sediment and pollutant transport in the harbor.

In some estuaries, a majority of sediment load may be transported as fluid mud which can transport sorbed heavy metals, pesticides and nutrients. In Chapter 6, a vertical, 1D model was developed to analyze near-bed sediment dynamics with the goal of determining whether a fluid mud layer in Newport Bay may be an important feature relative to sediment (and FIB) transport. The 1D model predicts suspended sediment concentration in terms of a steady or unsteady balance between the upward flux of sediment as a result of turbulent mixing and the downward flux of suspended sediment due to the fall velocity of the sediment particles, with the fluxes modified appropriately in the presence of fluid mud. Model testing indicated the importance of a fine grid resolution with non-linear parameterizations for entrainment/deposition (as a function of bed shear), settling velocity (a function of fluid mud concentration), and eddy diffusivity (a function of buoyancy-stabilized diffusion). The predictive ability of the vertical transport model was tested using suspended sediment concentrations measurements from a 1982 study of the 21-meter deep Severn Estuary, England (Kirby,

1986). The 1D model correctly portrayed the formation and thickening of a dense suspended sediment layer formed adjacent to the bed during accelerating flows and subsequent disappearance of this layer as flow velocity decelerated (Section 6.6). The model was then rerun using parameters that typify the 7-meter deep main channel of Newport Bay. Modeling indicated that conditions in Newport Bay are not favorable for creating a significant fluid mud layer, however, bed shears developed during the high velocity portions of a spring tide appear large enough to entrain bed sediments within the main channel.

In Chapter 7, the importance of bed sediment erosion in Newport Bay as a potential contributor to dry-weather water quality, e.g., FIB, was evaluated including identification of reaches of the bay subject to erosion and areas of the bay impacted by the transport of this material in suspension. A key sediment parameter, the bed shear strength for entrainment of the partially consolidated bed sediments, τ_{cr}, was evaluated (Section 7.5) from measured erosion rates of core samples collected within the bay's main channel along with field measured suspended sediment concentrations. While additional bed sediment samples should be collected in concert with suspended sediment concentrations within the water column, this first estimate of the critical shear stress within the main channel of the bay represents an important advance in our understanding of Bay sediment dynamics. Using this critical shear stress value, 2D modeling results suggest that only the central section of the main stem of Newport Bay is subject to sediment erosion by tidal currents; currents elsewhere in the bay are too weak (Section 7.6). Moreover, modeling results suggest that much of the suspen-

sion falls out during the same tidal cycle, in the vicinity of the main stem, although the finest particles may stay in suspension indefinitely and ultimately get mixed into the neighboring ocean. From a perspective of FIB transport, these results point to sediment contamination within the central channel being a potentially important localized source for impacts to benthic community in that area and perhaps a potential contributor to bay-wide FIB impairment. On the other hand, contaminate sediments in quiescent parts of the harbor are unlikely to contribute to bay-wide water quality problems. An important caveat of the above analysis is that light, unconsolidated material (e.g., biofilms) may grow at the sediment-water interface. This can create a nutritionally favorable condition for bacterial regrowth in estuarine systems. These bacteria can then be mobilized throughout the bay by tidal currents either as free bacteria, or more likely, attached to particles or flocs, contributing to FIB impairment as has been shown in other marine wetlands.

As opposed to entrainment of pollutants in bed sediments, a more likely source of water quality in Newport Bay is direct inputs from urban runoff. In Chapter 3, an original empirical model was presented to predict the magnitude of these dry-weather flows as a function of drainage area (Sections 3.1 and 3.2). The empirical model is developed from a combination of storm drain flow measurements and a unique study of nearshore salinity using the 2D salinity transport model described in Chapter 2, along with an original "trap-and-release" model to describe the intermittent release of urban runoff from tidally flooded storm drains, to back-calculate discharge rates from individual storm drains. This discharge formula, when applied to the drainage

conveyances for every watershed tributary to Newport Bay indicates that the smaller watersheds, i.e. watersheds <100 acres, which account for 95% of number of watershed directly tributary to Newport Bay, contribute about one percent of the total dry weather flow discharging into the bay (Section 3.3).

While small drains account for only $\sim 1.0\%$ of the total freshwater volumetric flow into Newport Bay on a typical dry weather day, field and modeling results presented in Chapter 4 suggest that episodic freshwater discharges from small drains could be a significant source of nearshore fecal pollution at Lower Bay beaches during dry weather conditions (Section 4.3). This conclusion is supported by studies and modeling showing FIB concentrations in Lower Bay are typically high at the shoreline and low offshore, consistent with a beach-side bacterial source. The intermittent nature of FIB loading near storm drain outlets in Lower Bay was found by field testing to be highest at low tide when salinity is <30 ppt when drainpipe outlets are exposed, consistent with the idea of episodic discharges. As opposed to the continuous flow model, the trap-and-release model, developed in Chapter 3 for predicting storm drain dry-weather discharge, was more successful in showing tidal influence on FIB concentrations and simulating exceedances of detection limits and recreational standards for enterococci. The studies and modeling showed that upon release from small drains, FIB plumes are diluted by ambient turbulence and transported horizontally and vertically by tide- and wind-driven currents. Because the initial dilution step is characterized by relatively small eddy diffusivities ($\sim$0.001 m^2/s), FIB released from small drains may linger at the shoreline, where they are more likely to trigger water

quality exceedances. By comparison, tributaries e.g., San Diego Creek and Santa Ana-Delhi Channel, contribute relatively little to shoreline FIB pollution in Lower Bay.

The results of these studies indicate new ways for evaluating and estimating constituent loads to a receiving water especially dry weather runoff at enclosed beaches, and provide a basis for further investigations of water quality impacts within embayments.

List of Symbols

a, b, α, β, sediment-dependent empirical coefficients for settling velocity

b, top of fluid mud layer

c_s, concentration of suspended sediment

C_D, drag coefficient

C_m, a coefficient dependent on the granular density c_s, sediment concentration

$\mathbf{D}$, eddy diffusion tensor

d, sediment diameter

D, depositional flux

D_s, eddy diffusivity of sediment

$F(\theta)$, temperature function

E, erosion flux from a partially consolidated bed

E_o, bed erosion flux parameter

E_r, consolidated bed erosion flux parameter

F_a, advective flux

F_d, diffusive flux

$\mathbf{F}_s$, sediment flux through the control surface $\mathcal{S}$

$\mathbf{i}$, $\mathbf{j}$, and $\mathbf{k}$, unit vectors in the x, y, and z directions, respectively

h, depth of flow

k_1 and n_1, settling velocity coefficients for flocculated settling

k_2 and n_2, settling velocity coefficients for hindered settling

M_E, rate of interfacial entrainment

$\mathbf{n}$, unit outward normal vector

n and m, erosion flux calibration constants

p_D, attachment probability

R_o, Rouse number

Re, Reynolds number

Ri, Richardson number

$\mathcal{S}$ surface of control volume

u, v, and w, velocity components in the x, y, and z directions

u_*, turbulent bed shear or shear velocity

w_s, sediment settling velocity

w_{so}, reference settling velocity for hindered settling

$\mathcal{V}$, control volume

α_1 and β_1, eddy diffusivity empirical coefficients

α_2, entrainment flux empirical coefficient

∇, gradient operator

$\nabla\cdot$, divergence operator

ε_x, ε_y, and ε_z, eddy diffusivity where the subscript indicates the direction of each component

ε_{zo}, eddy diffusivity under neutral conditions

η, interface elevation between air and liquid

θ, temperature

κ, von-Karman's constant

ν, viscosity

ρ_s, sediment granular density

ρ_w, fluid density

ρ_b, dry bulk density, sediment mass per unit bed volume

τ_b or τ_o, bed shear stress

τ_{ci}, critical stress for deposition

τ_{cr}, critical shear stress for entrainment, bed shear strength for entrainment of the partially consolidated bed sediments

τ_p, critical stress for a partially consolidated bed

References

1. Allison D. and Sutherland I. W (1987) "The role of exopolysaccharides in adhesion of freshwater bacteria". Journal of General Microbiology, 133:1319-1327.

2. Anderson, S.A., Turner, S.J. and Lewis, GD. (1997) "Enterococci in the New Zealand Environment: Implications for Water Quality Monitoring". Water Science and Technology, 35(11-12), 171-174.

3. Ang, A. H-S. and Tang, W. H. (1990) Probability Concepts in Engineering Planning and Design. John Wiley and Sons.

4. Arega, F. and Sanders, B.F. (2004) "Dispersion Model for Tidal Wetlands". ASCE Journal of Hydraulic Engineering, 130(8), 739-754.

5. Ariathurai, R., (1974) "A Finite Element Model for Sediment Transport in Estuaries". Ph.D. Dissertation, University of California, Davis, California.

6. ASCE (2005) "Task Committee on Management of Fluid Mud". Management of

Fluid Mud in Estuaries, Bays, and Lakes.

7. Azevedo, I. C., Duarte, P. M. and Bordalo, A. A (2009) Draft Manuscript: "Influence of reiver discharge patterns on the hydrodynamics and potential contaminant dispersion in the Douro Estuary (Portugal)". Laboratory of Hydrobiology, Institute of Biomedical Sciences, Porto, Portugal.

8. Banks, H. O. (1984) "Ground Water Management - Irvine Area, Orange County, CA". In associations with Boyle Engineering Corp., Camp, Dresser & McKee, Inc., James M. Montgomery, Inc., and PRC Engineering. Prepared for the Orange County Water District.

9. Bechtel National. (2000) "Feasibility Study Report for Operational Unit 1-Marine Corps Air Facility Tustin".

10. Bechtel National. (2002) "Final Feasibility Study Report for Operable Unit 1B - Marine Corps Air Station Tustin".

11. Beck, M.B. (1987) "Water quality modeling: a review of the analysis of uncertainty". Wat. Resour. Res. 23, 1393-1442.

12. Begnudelli, L. and Sanders, B.F. (2006) "Unstructured Grid Finite Volume Algorithm for Shallow-water Flow and Transport with Wetting and Drying". ASCE Journal of Hydraulic Engineering, 132(4), 371-384.

13. Budd, R., Bondarenko, S. and Gan, J. (2005) "Survey for Synthetic Pyrethroids

within the San Diego Creek/ Newport Bay Watershed". Southern California SETAC Annual Meeting. Los Angeles, California.

14. Byappanahalli, M.N. and Fujioka, R.S. (1998) "Evidence that tropical soil environment can support the growth of Escherichia coli". Water Science and Technology, v. 38(12), No. 17 pp. 1-174.

15. Cammen, L.M. and Walker, J.A. (1982) "Distribution and activity of attached and free-living bacteria in the Bay of Fundy". J. Fish Aquat. Sci. 39, 1655-1663.

16. Camp, Dresser and McKee. (1985) "Shallow Groundwater Investigation-West Central Part of the Irvine Basin". Prepared for the Irvine Company.

17. City of Newport Beach. (2006) Aerial Photos of Newport Beach prepared from Lidar.

18. City of Newport Beach. (2008) "Flow Measurement from Ten Small Watersheds on the West Side of Newport Harbor". John Kappeler, Lead Investigator.

19. Clarke, L.B., Ackerman, D. and Largier, J. (2007) "Dye dispersion in the surf zone: measurements and simple models". Cont. Shelf Res. 27, 650-669.

20. City of Newport Beach. (2009) Central Orange County Integrated Regional and Coastal Water Management Plan - Phase 2. Prepared by Krista Slonowski (Connective Issues) and Bob Stein.

21. Clarke, S. and Elliot, A.J. (1998) "Modeling Suspended Sediment Concentrations in the Firth of Forth". Estuarine, Coastal and Shelf Science, V. 47, pp. 235-250.

22. Colford, J.M., Wade, T.J., Schiff, K.C., Wright, C.C., Griffith, J.F., Sandhu, S.K., Burns, S., Sobsey, M., Lovelace, G. and Weisberg, S.B. (2007) "Water quality indicators and the risk of illness at beaches with nonpoint sources of fecal contamination". Epidemiology 18, 27-35.

23. County of Orange. (2006) Flow rates from County monitoring stations on San Diego Creek at Campus Drive and the Santa Ana-Delhi Channel near Mesa Drive.

24. County of Orange. (2011) Field measurement of flow in Big Canyon Creek.

25. Davies, C., Long, J., Donald, M. and Ashbolt, N. (1995) "Survival of fecal microorganisms in marine and freshwater sediments". Applied and Environmental Microbiology". v. 61, 1888-1896.

26. Dobbins, W. E. (1952) "Effect of Turbulence on Sedimentation". Transactions, Paper No. 2218, American Society of Engineers, pp. 629-679.

27. Dorsey, J.H. (2010) "Improving water quality through Californias Clean Beach Initiative: an assessment of 17 projects". Environ. Monit. Assess. 166, 95-111.

28. Einstein, H. A. and Chien, N. (1955) "Effects of Heavy Sediment Concentration Near the Bed on Velocity and Sediment Distribution". MRD Series No. 8, Uni-

versity of California Institute of engineering Research and U.S. Army engineers, Missouri River, Omaha, Nebraska.

29. EOA, Inc. (2001) "Public Health Risk Assessment for the Newport Bay Watershed: Recreational Contact and Microbiological Risk". Prepared for California Regional Water Quality Control Board.

30. Everest International Consulting. (2006) "Large Storm Drain Flow Measurements". Prepared for the City of Newport Beach.

31. Ferguson, C.M., Coote, B.G., Ashbolt, N.J. and Stevenson. I.M. (1996). "Relationships Between Indicators, Pathogens and Water Quality in an Estuarine System". Water Research, vol. 30, no. 9. pp. 2045-2054, Sept. 1996.

32. Ferguson, D.M., Moore, D.F., Getrich, M.A. and Zhowandai, M.H. (2005) "Enumeration and speciation of enterococci found in marine and intertidal sediments and coastal water in southern California". J. Appl. Microbiol. 99, 598-608.

33. Fiandrino, A., Martin, Y., Got, P., Bonnefont, J.L. and Troussellier, M. (2003) "Bacterial contamination of Mediterranean coastal seawater as affected by riverine inputs: simulation approach applied to a shellfish breeding area". (Thau lagoon, France). Water Research 37, 1711-1722.

34. Fischer, H.B., List, E.J., Koh, R.C.Y., Imberger, J., Brooks, N.H. (1979) Mixing in Inland and Coastal Waters, Academic Press, New York.

35. Fletcher, T.D., Deletic, A., Mitchell, V.G. and Hatt, B.E. (2008) "Reuse of urban runoff in Australia: A review of recent advances and remaining challenges". J. Environ. Qual. 37, S116-S127.

36. Fletcher, T.D., Walsh, C.J., Bos, D., Nemes, V., RossRakesh, S., Prosser, T., Hatt, B. and Birch, R. (2011) "Restoration of stormwater retention capacity at the allotment-scale through a novel economic instrument". Wat. Sci. Technol. 64, 494-502.

37. Gallien, T.W., Schubert, J.E. and Sanders, B.F. "Predicting Tidal Flooding of Urbanized Embayments: A Modeling Framework and Data Requirements". Coastal Engineering, 58(6), 567-577, 2011.

38. Geesey, G.G. and Costerton, J.W. (1979) "Microbiology of a northern river: bacterial distribution and relationship to suspended sediment and organic carbon". Can. J. Microbiol. v. 25, pp. 1058-1062.

39. Geyer, W.R.; Signell, R.P. (1992) "A reassessment of the role of tidal dispersion in estuaries and bays". Estuaries 15, 97-108.

40. Goulder R. (1976) "Relationships Between Suspended Solids and Standing Crops and Activities of Bacteria in an Estuary During a Neap-Spring Tidal Cycle". Oecologia 24, pp. 83-90.

41. Goyal, S.M., Gerba. C.P. and Melnick, J.L. (1977) "Occurrence and Distribution of Bacterial Indicators and Pathogens in Canal Communities along the

Texas Coast". Applied and Environmental Microbiology, v. 34, pp. 139-149.

42. Grant, S. B., Sanders, B.F., Boehm, A., Arega, F., Ensari. S., Mrse, R., Kang, H.Y., Reeves, R., Kim, J.R., Redman, J., Jiang, S., Chu, W., Choi, S., Clark. C., Litz, L., Sutula, M., Noblet, I., Sobsey. M. and McGee, C. (2002) "Coastal runoff impact study phase II: sources and dynamics of fecal indicators in the lower Santa Ana River watershed". Report prepared for the National Water Research Institute, County of Orange, and the Santa Ana Regional Water Quality Control Board.

43. Grant, S.B., Sanders, B.F., Boehm, A.B., Redman. J.A., Kim, J.H., Morse, K., Chu, A. K., Gouldin, M., McGee, C., Gardiner, N., Jones, B.H., Svejkovsky, J., Leipzig, V., and Brown, A. (2001) "Generation of Enterococci Bacteria in a Coastal Wetland and its Impact on Surf Zone Water Quality". Environmental Science and Technology, v. 35(12), pp. 2407-2416

44. Grant, S. B., Sanders, B.F., Jeong, Y., Ritter, S., Reeves, R., Pednekar, A., Gates, H., Kim, J.H., Rekhi, N. and Candelaria, L.N. (2004) "The Contribution of Marinas to Fecal Indicator Bacteria Impairment in Lower Newport Bay, Southern California: A Report". Prepared for the City of Newport Beach and the Santa Ana Regional Water Quality Control Board.

45. Grant, S. B., Jiang, S.C., Sanders, B.F., McLaughlin, K., Ahn, J.H., Litton, R., Ho, L., and Moore, D. (2008) Draft Manuscript and laboratory data for the

"Newport Bay Fecal Indicator Bacteria Source Identification Project". Funded under a Proposition 13 Non-Point Source Pollution Control Brant Agreement between the California State Water Resource Control Board and the County of Orange (Agreement No. 04-198-558-2).

46. Grant, S.B. and Sanders, B.F. (2010) "Beach Boundary Layer: A framework for addressing recreational water quality impairment at enclosed beaches". Environ. Sci. Technol. 44, 8804-8813.

47. Grant, S.B., Kim, J.H., Jones, B.H., Jenkins, S.A., Wasyl, J. and Cudaback, C. (2005) "Surf zone entrainment, along-shore transport, and human-health implications of pollution from tidal outlets". J. Geophys. Res. 110 (C10) DOI 10.1029/2004JC002401.

48. Grant, S.B., Saphores, J-D., Feldman, D.L., Hamilton, A.J., Fletcher, T.D., Cook, P.L.M., Stewardson, M., Sanders, B.F., Levin, L.A., Ambrose, R.F., Deletic, A., Brown, R., Jiang, S.C., Rosso, D., Cooper, W.J. and Marusic, I. (2012) "Taking the *waste* out of *wastewater* for human water security and ecosystem sustainability". Science 337, 681-686.

49. Grimes, D.J., Atwell, R.W., Brayton, PR., Palmer. L.M., Rollins, D.M.. Roszak, D.B., Singleton, F.L., Tamplin, M.L. and Colwell, R.R. (1986) "The fate of enteric pathogenic bacteria in estuarine and marine environments". Microbiological Sciences, v. 3(11), pp. 324-329.

50. Haile, R.W., Witte, J.S., Gold,M., Cressey, R., McGee, C., Millikan,R.C., Glasser,A., Harawa, N., Ervin, C. and Harmon,P. (2009) "The health effects of swimming in ocean water contaminated by storm drain runoff". Epidemiology 2009 43, 4900-4907.

51. Halliday, E.; Gast, R.J. (2100) "Bacteria in beach sands: An emerging challenge in protecting coastal water quality and bather health". Environ. Sci. Technol. 45, 370-379.

52. Hayes, L. H. and Winkler, R. W. (1971) Statistics: Probability, Inference and Decision. Holt, Rinehart and Winston, Inc., New York.

53. Hayter, E. J. (1983) "Prediction of Cohesive Sediment Movement in Estuarial Waters". Ph.D. Dissertation, University of Florida.

54. Hayter, E. J. and Mehta, A. J. (1986) "Modeling cohesive sediment transport in estjarine waters". Applied Mathematical Modeling, v. 10, pp. 294-303.

55. Hibbs. T. and Lee. (2000) "Sources of Selenium in the San Diego Creek Watershed".

56. Hoag, B. L. (1983) "Channel Erosion as a Source of Sediment in Newport Bay, California".

57. Holm, S. (1979) "A simple sequentially rejective multiple test procedure". Scandinavian Journal of Statistics, 6, 65-70.

58. Hwang, K. N. and Mehta, A. J. (1989) "Fine sediment erodibility in Lake Okeechobee". Coastal and Oceanographic Engineering Department, University of Florida, Report UFL/COEL-89/019, Gainesville, Florida.

59. Ippen, A. T., Editor. (1966) Estuary and Coastline Hydrodynamics, McGraw-Hill, New York.

60. Jensen, P., Rola, I., and Tyrawski, J. (1979) "Tidal Wetlands and Estuarine Coliform Bacteria". Estuarine and Wetland Processes, Hamilton, P. and Macdonald, K.B. (ed.), pp. 385-399, Plenum Press, New York.

61. Jeong, Y., Grant, S. B., Ritter, S., Pednekar, A., Candelaria, L. and Winant, C. (2005) "Identifying pollutant sources in tidally mixed systems; Case study of fecal indicator bacteria in Newport Bay, southern California". Environ. Sci. Technol. 39, 9083-9093.

62. Jiang, J. H. and Wolanski, E. (1998) "Vertical Mixing by Internal Wave Breaking at the Lutocline, Jiaojiang River Estuary, China". Journal of Coastal Research, v. 14(4), pp. 1426-1431.

63. Jiang, J. (1999) "An Examination of Estuarine Lutoclne Dynamics". Ph.D. Dissertation, University of Florida.

64. Kashefipour, S.M., Lin, B., Harris, E. and Falconer, R.A. (2002) "Hydro-environmental modeling for bathing water compliance of an estuarine basin". Water Research 36, 1854-1868.

65. Katopodes, N. (2002) Free Surface Flow - Unpublished book manuscript.

66. Kendrick, M. P. and Derbyshire, B. V. (1985) "Monitoring of Near-bed Turbid Layers". Report SR 44, Hydraulics research, Wallingford, United Kingdom.

67. Kirby, R. (1986) "Suspended Fine Cohesive Sediment in the Severn Estuary and Inner Bristol Channel, U.K.". Report ETSU-STP-4042, Department of Atomic Energy, Harwell, United Kingdom.

68. Kirby, R. and Parker, W. R. (1977) "The Physical Characteristics and Environmental Significance of Fine Sediment Suspensions in Estuaries". Institute of Oceanographic Sciences, Tauton, England. Estuaries, Geophysics and the Environment, National Academy of Sciences, Washington, pp. 110-120.

69. Kirchman, D. (1983) "The production of bacteria attached to particles suspended in a freshwater pond". Limno. Oceanogr. V. 28, pp 858-872.

70. Koske, P.H., Krumm. H., Rheinheimer, G. and Szekielda, K-H. (1966) "Untersuchungen ber die Einwirkung der Tide auf Salzgehalt, Schwebstoffgehalt, Sedimentation und Bakteriengehalt in der Unterelhe". Kieler Meeresforsch, v. 22, (reported in Rheinheimer, G. (1992) Aquatic Microbiology, 4th Edition, John Wiley and Sons).

71. Kranenburg, C. and Winterwerp, J. C. (1997) "Erosion of Fluid Mud Layers". Journal of Hydraulic Engineering, V 123(6), pp. 504-511.

72. Krone, R. B. (1962) "Flume Studies of the Transport of Sediment in Estuarial Shoaling Process". Final Report, Hydraulic Engineering Laboratory and Sanitary Engineering Research Laboratory, University of California, Berkeley, California.

73. LaBelle, R.L., Gerba. C.P., Goyal, S.M., Melnick, J.L., Cech, I., and Bogdan, G.F. (1980) "Relationships between environmental factors, bacterial indicators, and the occurrence of enteric viruses in estuarine sediments". Applied and Environmental Microbiology, v. 39, pp. 588-596.

74. Largier, J. and Taggart, M. (2006) "Improving water quality at enclosed beaches: a report on the Enclosed Beach Symposium Workshop (Clean Beaches Initiative)". State of California State Water Resources Control Board, Clean Beaches Initiative.

75. Lee, G., Lee F., Taylor, S. (RBF) and County of Orange Public Facilities and Resources Department. (2001) "Newport Bay/San Diego Creek Watershed Study - Upper Newport Bay Water Quality Enhancement Project". Final Report, 319(h) Implementation Project Agreement Nos. 8-023-258-0 and 8-174-250-0.

76. Lind, O.T. and Lind, L.D. (1991) "Association of Turbidity and Organic Carbon with Bacterial Abundance and Cell Size in a Large, Turbid, Tropical Lake". Limnol. Oceanogr. v. 36, pp. 1200-1208.

77. Maa, P.-Y. and Mehta, A. J. (1987) "Mud Erosion by Waves: A Laboratory

Study". Continental Shelf Research, Vol. 7, Nos. 11/12, pp. 1269-1284.

78. Mallin, M.A., Cahoon, L.B., Toothman, B.R., Parsons, D.C., McIver, M.R., Ortwine, M.L. AND Harrington, R.N. (2007) "Impacts of raw sewage spill on water and sediment quality in an urbanized estuary". Mar. Poll. Bull. 54, 81-88.

79. Maurer, Don and Rozengurt, Michael (1997) "The Role of Watershed Modification in Water Quality and Living Resources in the Coastal Zone of off Orange County, California".

80. McNeil, J., Taylor, C. and Lick, W. (1996) "Measurements of erosion of undisturbed bottom sediments with depth". Journal of Hydraulic Engineering, 122(6), pp. 316-324.

81. Mehta, A. J. (1986) "Characteristics of Cohesive Sediment Properties and Transport Processes in Estuaries". Estuarine Cohesive Sediment Dynamics, A. J. Mehta, ed., Lecture Notes on Coastal and Estuarine Studies, No. 14, Springer-Verlag, New York.

82. Mehta, A. J. (1989) "Fine Sediment Stratification in Coastal Water". Proceedings of Third National Conference on Dock and Harbour Engineering, K.R.E.C., Surathkal, India, pp. 487-492.

83. Mehta, A. J., Parchure, T. M., Dixit, J. G., and Ariathurai, R. (1982) "Resuspension Potential of Deposited Cohesive sediment Bed". In Esturine Comparisons,

V. S. Kennedy, Editor, Academic Press, New York, pp. 591-609.

84. Mehta, A. J. and Dyer, K. R. (1990) "Cohesive sediment transport in estuarine and coastal waters, The Sea, Ideas and Observations on Progress in the Study of the Seas". Volume 9, Ocean Engineering Science Le Mehaute, B. and Hanes, D.M. (eds.), John Wiley and Sons.

85. Mehta, A. J. and Partheniades, E. (1973) "Depositional Behavior of Cohesive Sediments". Technical Report No. 16 Coastal and Oceanographic Engineering Laboratory, University of Florida, Gainesville, Florida, March.

86. Meixner, T., Hibbs, B., Sjolin, J. and Walker, J. (2004) "Sources of Selenium, Arsenic and Nutrients in the Newport Bay Watershed". SWRCB Agreement 00-200-180-01 Final Report of April 30th, 2004.

87. Munk, W. H. and Anderson, E. R. (1948) "Notes on the Theory of the Thermocline". Journal of Marine Research, Vol. 1, pp. 276-295.

88. Nitrogen Selenium Management Program Working Group (2006) "Sources and Loads and Identification of Data Gaps for Selenium Interim Report". OC Watershed, County of Orange.

89. NOAA (2006) Tide data from the Los Angeles monitoring station.

90. Noble, R.T., Weisberg, S.B., Leecaster, M.K., McGee, C.D., Ritter, K., Walker, K.O. and Vanik, P.M. (2003) "Comparison of beach bacterial water quality

indicator measurement methods". Environ. Monitoring and Assessment, 81, 301-312.

91. Noble, R.T., Griffith, J.F., Blackwood, A.D., Fuhrman, J.A., Greogory, J.B., Hernandez, X., Liang, X.L., Bera, A.A. and Schiff, K. (2006) "Multi-tiered approach using quantitative PCR to track sources of fecal pollution affecting Santa Monica Bay, California". Appl. Environ. Micrbiol. 72, 1604-1612.

92. Officer, C. B. (1981) "Physical Dynamics of Estuarine Suspended Sediments". Marine Geology, Vol. 40, 1981, pp. 1-14.

93. Orange County Coastkeeper and Candelaria, Linda. (July 2007) "Lower Newport Bay Copper/Metals Marina Study, Final Report. Prepared for the City of Newport Beach". Santa Ana Regional Water Quality Board.

94. Orange County Flood Control District (OCFCD). (1964) "An Investigation of Flood Control and Water Conservation Deficiencies within Orange County".

95. Orange County Flood Control District. (1967) "Engineer's Report Presenting a Program for the Control and Conservation of Flood and Storm Waters".

96. Oshiro, R. and Fujioka, R. (1995) "Sand, soil, and pigeon droppings - sources of indicator bacteria in the waters of Hanauma Bay, Oahu, Hawaii". Water Science and Technology, v. 31(5-6), pp. 251-254.

97. Parchure, T. M. and Mehta, A. J. (1983) "Erosive Shear Strength of Soft Muddy

Deposits". Journal of Hydraulic Engineering, ASCE, Vol. 3, No. 10, pp. 1308-1326.

98. Parker, W. R. (1986) "On the Observation of Cohesive Sediment Behavior for Engineering Purposes". Estuarine Cohesive Sediment Dynamics, A. J. Mehta ed., Springer-Verlag, Berlin.

99. Parker, W. R. (1987) "Observations on Fine Sediment Transport Phenomena in Turbid Coastal Environments". Continental Shelf Research, Vol. 7, Nos. 11/12, pp. 1285-1293.

100. Parker, W.R. and Kirby, R. (1982) "Time Dependent Properties of Cohesive Sediment Properties Relevant to Sedimentation Management - European Experience". Estuarine Comparison, V.S. Kennedy, Ed. Academic Press, New York.

101. Parker, W. R. and Lee, K. (1979) "The Behavior of Fine Sediment Relevant to the Dispersal of Pollutants". ICES Workshop on Sediment and Pollutant Interchange in Shallow Sea, Tecel, United Kingdom, pp. 28-34.

102. Pednekar, A. M., Grant, S. B., Jeong, Y., Poon, Y. and Oancea, C. (2005) "Influence of climate change, tidal mixing, and watershed urbanization on historical water quality in Newport Bay, a saltwater wetland and tidal embayment in southern California". Environmental Science and Technology, 39, 9071-9082.

103. Pohl, D. (2007) "Newport Coast Watershed Management Plan". Prepared for

the City of Newport Beach by Weston Solutions.

104. Preston, A., Jefferies, D. F., Dutton, J. W. R., Harvey, B. R. and Steele, A. K. (1972) "British Isles Coastal Waters: The Concentration of Selected Heavy Metals in Sea Water, Suspended Matter and Biological Indicators - a Pilot Survey". Journal of Environmental Pollution, Vol. 3, pp. 69-72.

105. Raudkivi, A. J. (1967) Loose Boundary Hydraulics, Pergamon Press, Oxford.

106. Reeder, Terri (2010) "Investigation of Selenium in Big Canyon Watershed". Prepared by the Santa Ana Regional Water Quality Board.

107. Reeves, R. L., Grant, S. B., Mrse, R. D., Oancea, C., Sanders, B. F. and Boehm, A. (2004) "Scaling and management of fecal indicator bacteria in runoff from a coastal urban watershed in southern California". Environmental Science and Technology, 38, 2637-2648.

108. Regional Water Resource Control Board (2008) NPDES Stormwater Permit - Section XII.E. - Low Impact Development.

109. Rheinheimer, G. (1992) Aquatic Microbiology. 4th Edition, John Wiley and Sons.

110. Richardson, J. F. and Zaki, W. N. (1954) "The Sedimentation of a Suspension of Uniform Spheres under Conditions of Viscous Flows". Chemical Engineering Sciences, March, pp. 65-72.

111. Rippy, M.A., Franks, P.J.S., Feddersen, F. and Guza, R.T. (2013) "Factors controlling variability in nearshore fecal pollution: the effects of mortality". Mar. Poll. Bull. 66, pp. 191-198.

112. Rippy, M.A., Franks, P.J.S., Feddersen, F., Guza, R.T. and Moore, D.F. (2013) "Physical dynamics controlling variability in nearshore fecal pollution: Fecal indicator bacteria as passive particles". Mar. Poll. Bull. 66, pp. 151-157.

113. Roberts, J., Jepsen, R., Gotthard, D. and Lick, L. (1998) "Effects of Particle Size and Bulk Density on Erosion of Quartz Particles". Journal of Hydraulic Engineering, December, pp. 1261-1267.

114. Roper, M. M. and Marshall, K. C. (1979) "Effects of salinity on sedimentation and of particulates on survival of bacteria in estuarine habitats". Geomicrobiology Journal, v. 1(2), pp. 103-116.

115. Ross, M. A. (1988) "Vertical structure of estuarine fine sediment suspensions". Ph.D. Dissertation, University of Florida.

116. Rouse, H. (1937) "Modern Conceptions of the Mechanics of Fluid Turbulence". Transactions, ASCE, Vol. 102, Paper No. 1965, pp. 463-543.

117. Sanders, B.F., Arega, F., and Sutula, M. (2005) "Modeling the dry-weather tidal cycling of fecal indicator bacteria in surface waters of an intertidal wetland". Water Research, v. 39, pp. 3394-3408.

118. Sassoubre, L.M., Nelson, K.L. and Boehm, A.B. (2012) "Mechanisms for photoinactivation of Enterococcus faecalis in seawater". Appl. Environ. Micro. 78, 7776-7785.

119. Savage, W.G. (1905) "Bacteriological Examination of Tidal Mud as an Index of Pollution of the River". Journal of Hygiene, v. 5, pp. 146-174.

120. Scarlatos, P. D. and Mehta, A. J. (1993) "Instability and entrainment mechanisms at the stratified fluid mud-water interface". In Mehta, A. J., (Ed.) Nearshore and Estuarine Cohesive Sediment Transport. Washington, D.C.: American Geophysical Union. pp. 205-233.

121. Sea Engineering, Inc. (2007) "Sedflume Analysis Upper Newport Bay, California".

122. Sercu, B., Van De Werfhorst, L.C., Murray, J. and Holden, P.A. (2009)"Storm drains are sources of human fecal pollution during dry weather in three urban southern California watersheds". Environ. Sci. Technol. 43, 293-298.

123. Skinner, J.F., Guzman, J. and Kappeler, J. (2010) "Regrowth of enterococci and fecal coliform in biofilm: studies of street gutters and storm drains in Newport Beach, CA., suggest causes for high bacteria levels". Stormwater 2010 July/August, 28-34.

124. Smith, T. J. and Kirby, R. (1989) "Generation, Stabilization and Dissipation of Layered Fine Sediment Suspensions". Journal of Coastal Research, SI 5, pp.

63-73.

125. Solo-Gabriele, N.M., Wolfert, M.A,, Desmarais, T.R., Palmer, C.A. (2000) "Sources of Escherichia cob in a Coastal Subtropical Environment". Applied and Environmental Microbiology, 66(1), pp. 230-237.

126. State Water Resource Control Board (2012) Special Protections for Areas of Special Biological Significance.

127. Steets, B.M., Holden, P.A. (2003) "A mechanistic model of runoff-associated fecal coliform fate and transport through a coastal lagoon". Water Research 37,pp. 589-608.

128. Teeter, A. M. (1983) "Investigations of Atchafalaya Bay Sediments". Proceedings of the Conference on Frontiers on Hydraulic Engineering, ASCE, Cambridge, Massachusetts, August, pp. 85-90.

129. Thomann, R.V. and Mueller, J.A. (1987) Principles of Surface Water Quality Modeling and Control. Harper Collins.

130. Thorn, M. F. C., and Parsons, J. G. (1977) "Properties of Grangemouth Mud" Report No. EX781. Hydraulics Research Station, Wallingford, United Kingdom, July, 1977.

131. Thorn, M. F. C., and Parsons, J. G. (1979) "Properties of Belawan Mud" Report No. EX880. Hydraulics Research Station, Wallingford, United Kingdom, April, 1979.

132. Trimble, Stanley (1998) "Historical Hydrographic and Hydrologic Changes in the Newport Bay/San Diego Creek watershed".

133. USGS topographic map - Tustin quadrant. (1965)

134. U.S. Army Corps of Engineers - Los Angeles District. (1972) "Flood Plain Information - San Diego Creek and Peters Canyon Wash, Orange County, California". Prepared for Orange County Flood Control District.

135. U.S. Army Corps of Engineers - Los Angeles District. (1999) "Newport Bay/San Diego Creek Watershed Reconnaissance Study Project Study Plan". Prepared for Orange County Public Facilities & Resources Department.

136. United States Environmental Protection Agency - Region 9. (April 12, 2002) "Total Maximum Daily Loads for Toxic Pollutants - San Diego Creek and Newport Bay, California".

137. United States Environmental Protection Agency (US EPA). (2012) "Recreational Water Quality Criteria, United States Environmental Protection Agency". Office of Water: Washington D.C., EPA 820-F-12-058.

138. van Leussen, W. and van Velzen, E. (1989) "High Concentration Suspensions: Their Origin and importance in Dutch Estuaries and Coastal Waters". Journal of Coastal Research, SI(5), pp. 1-22.

139. Vanoni, V. A. (1975) "Sedimentation Engineering". Report of Engineering Practice No. 54, American Society of Civil Engineers, New York.

140. Wade, T.J., Pai, N., Eisenberg, J.N.S. and Colford, J.M. (2003) "Do U.S. Environmental Protection Agency Water Quality Guidelines for Recreational Waters prevent gastrointestinal illness? A systematic review and meta-analysis". Environ. Health Persp. 111, 1102-1109.

141. Wells, T. J. and Kim, S. Y. (1991) "Trapping and Escape of Fine-grained Sediments: Neuse River Estuary, N.C.". Coastal Sediments '91, ASCE Specialty Conference on Quantitative Approaches to Coastal Sediment Processes, Nicholas Kraus *et al.* ed., June, pp. 775-788.

142. Weston Solution, Inc. (2007) Newport Coast Integrated Watershed Management Plan. Prepared for the City of Newport Beach.

143. Wolanski, E., Gibbs, R. J., Mehta, A. and King, B. (1992) "The Role of Turbulence in the Settling of Mud Flocs". Journal of Coastal Research, Vol. 8, pp. 35-46.

144. Wolanski, E., Chappell, J., Ridd, P., Vertessy, R. (1988) "Fluidization of Mud in Estuaries". Journal of Geophysical Research, v. 93, No. C3, pp. 2351.2361, March 15, 1988.

145. Wong, S.H.C., Monismith, S.G. and Boehm, A.B. (2013) "Simple estimate of entrainment rate of pollutants from a coastal discharge into the surf zone". Environ. Sci. Technol. 47, 11554-11561.

146. Yan, Y. (1995) "Laterally-Averaged Numerical Modeling of Fluid Mud Forma-

tion and Movement in Estuaries". Ph.D. Dissertation, Clemson University, 175 p.

147. Youngsul, J., Grant, S. B, Ritter, S., Pednekar, A., Candelaria, L. and Winant, C. (2005) "Identifying Pollutant Sources in Tidally Mixed Systems: Case Study of Fecal Indicator Bacteria from Marinas in Newport Bay, Southern California". Environmental Sciences Technology. 2005, 39, pp. 9083-9093.

Appendix A - Permission Letter

UNIVERSITY OF CALIFORNIA, IRVINE

BERKELEY • DAVIS • IRVINE • LOS ANGELES • MERCED • RIVERSIDE • SAN DIEGO • SAN FRANCISCO

SANTA BARBARA • SANTA CRUZ

THE HENRY SAMUELI SCHOOL OF ENGINEERING
DEPARTMENT OF CIVIL & ENVIRONMENTAL ENGINEERING

IRVINE, CALIFORNIA 92697-2175
949/824-5333
949/824-2117 Fax

September 22, 2014

Robert Stein, P.E.
Ph.D. Candidate
Henry Samueli School of Engineering
Engineering Tower Room 524
University of California, Irvine
Irvine, CA 92677-2575

Dear Mr. Stein:

Per Section 3 of the UCI Thesis and Dissertation Manual, I am writing this letter to grant you permission to include in Chapters 2, 3 and 4 of your dissertation the data and text from the report entitled, "Newport Bay Fecal Indicator Source Identification Project". Any journal publications that you prepare that includes text and data from the report would, of course, require additional permission from those responsible for the collection, analysis, and/or write-up of the data.

Sincerely,

Stanley B. Grant
Professor

Appendix B - Collection and Evaluation of Bed Core Samples

Appendix B - Collection and Evaluation of Bed Core Samples

As part of the bed sediment investigation, bed cores were collected at four locations in Newport Bay and then sediment properties and erosion rates evaluated under the supervision of Sea Engineering, Inc. The results of the evaluation appear in a summary report entitled "Sedflume Analysis Upper Newport Bay, California" (Sea Engineering, Inc., 2007). The following sections summarize the collection methodology and findings.

Core Locations and Sampling Methodology

Four bed sediment cores were collected from Newport Bay: one from the center of the harbor and three along the length of Upper Bay. (See Figure 7.2.) At each coring location, a GPS system was used for horizontal positioning. The following table provides the core sample designation, coring date and time, and the depth of water for the four cores obtained from the Newport Bay. Depths are measured from the water surface and are not referenced to any datum.

The cores were collected with a push core apparatus. A pole was attached with clamps to the 10 cm by 15 cm rectangular core barrel. A valve was temporarily affixed to the top of the core tube to provide suction when the core was pulled out of the sediment bed. The core was then lowered into the water and positioned perpendicular to the sediment bed. Pressure was applied by hand until at least 30 cm and no more

than 100 cm of the core penetrated into the sediment bed. Upon penetration of the core barrel into the bed, the valve opened upward allowing sediment to enter the core tube and water to exit without disturbing the sediment surface or deeper strata. When the barrel was lifted from the sediment bed, the valve was closed to retain sediment inside the core tube. During this sampling effort, core samples were immediately inspected visually for length and quality. Undisturbed surficial sediments were present for each core sample. The cores were sealed and transported upright to a laboratory in Santa Cruz, California for analysis. All cores arrived intact with sediment structure and surface preserved.

The first core, the southerly most core, was obtained near the center of the harbor near Bay Island just outside the main channel. The location is about 200 meters feet to the west of sampling point BTO9. This sample site was selected to be representative of sediments in the low shear stress areas of the harbor, e.g., the western portion of the harbor and perhaps the channel North of the Balboa Islands. The water depth at the time of coring was 4.85 meters. This core was difficult to pull because of the depth of the water. Subsequent cores were taken at depths less than 2 meters. Initial inspection of the core revealed 1-2 cm of light-colored silt over darker silt. Two large worms existed on the surface with smaller amphipods.

Core 2 was taken at the edge of the main channel just South of the mouth of Big Canyon Creek. The water depth at the time of coring was 1.37 meters. This core location is between Stations BTO5 and BTO6 approximately 1000 meters North of BTO6. Initial inspection of the core revealed a surface consisting of fine organic

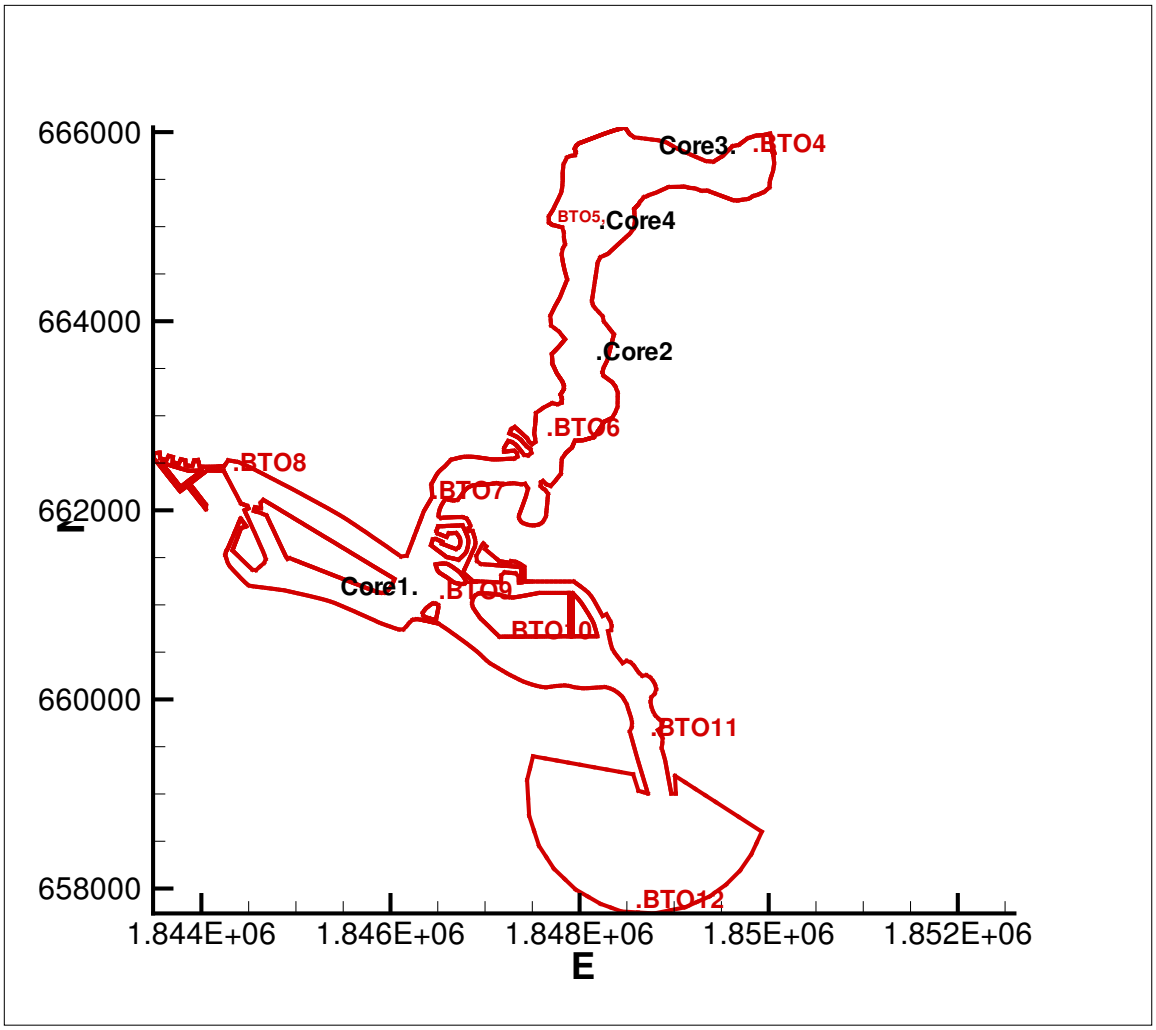

Figure A.1: Location of Bed Sediment Samples

Core No.	Latitude	Longitude	Coring Date	Depth [m]
1	N 33 36 29.0	W 117 54 27.6	01/04/07	4.85
2	N 33 37 51.0	W 117 53 10.0	01/04/07	1.37
3	N 33 39 04.2	W 117 52 17.0	01/04/07	1.45
4	N 33 38 35.0	W 117 53 13.7	01/04/07	1.68

Table A1: Core collection information.

material with some small visible worms, worm tubes and gravel pieces (<0.5 cm in diameter). There was a 1/2 cm light-colored fine silt layer over 5 cm of light and dark-colored clayey silt and sandy mixture. The remainder of the core consisted of light and dark-colored silt and sandy silt and some pockets of fine sand.

Core 3 was the northerly most core and was taken within the Unit I/III Basin South of the Jamboree Road bridge. This core was taken near the time of MHHW in order to get the craft well into the mudflat area. The water depth at the time of coring was 1.45 meters. This core location is about 250 meters west of Station BTO4. Initial inspection of the core revealed a mixed dark- and light-colored material. The top 1 cm was a silt and sandy silt layer over a layer of coarser silt and sandy silt. Shells existed on the surface.

Core 4 was taken on the bank opposite the outlet of the Santa Ana-Delhi Channel adjacent to the main channel of Newport Bay. This core is about 10 meters North of Station BTO5. The water depth at the time of coring was 1.68 meters. Initial inspection of the core revealed a mostly gray-colored silt and sandy silt material with some pockets of dark-colored silt.

Photos of each core are shown in Figures A.2, A.3, A.4, and A.5.

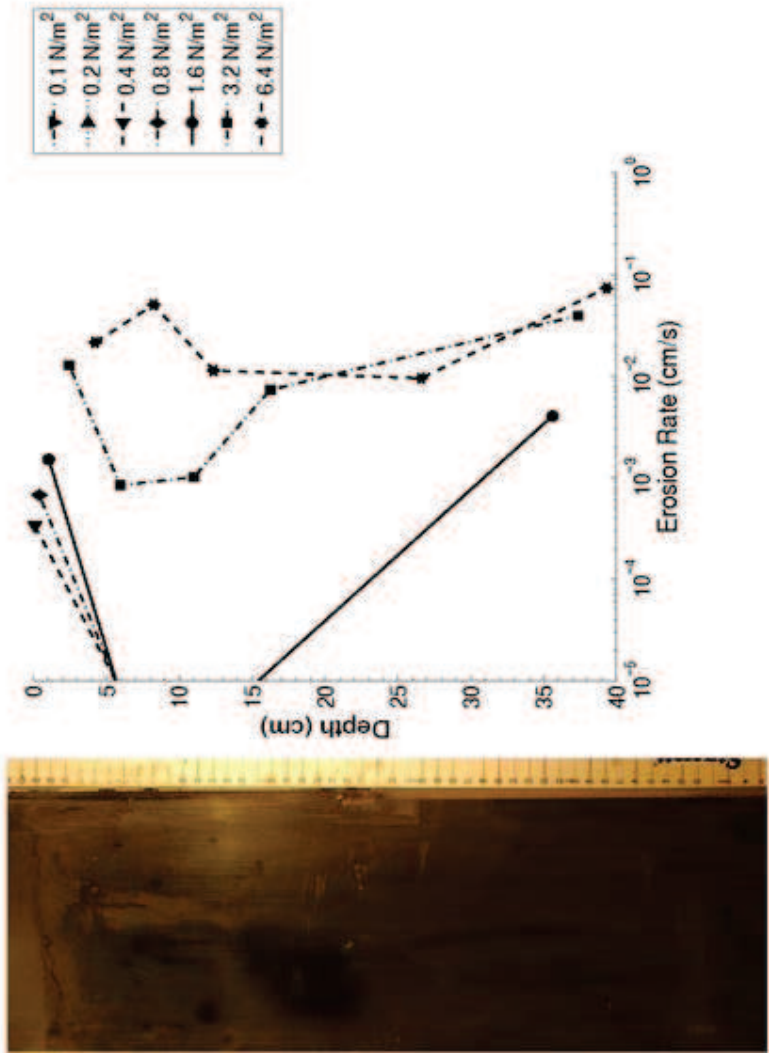

Figure A.2: Bed Sediment Sample (Core 1) Taken in the Harbor West of BTO9

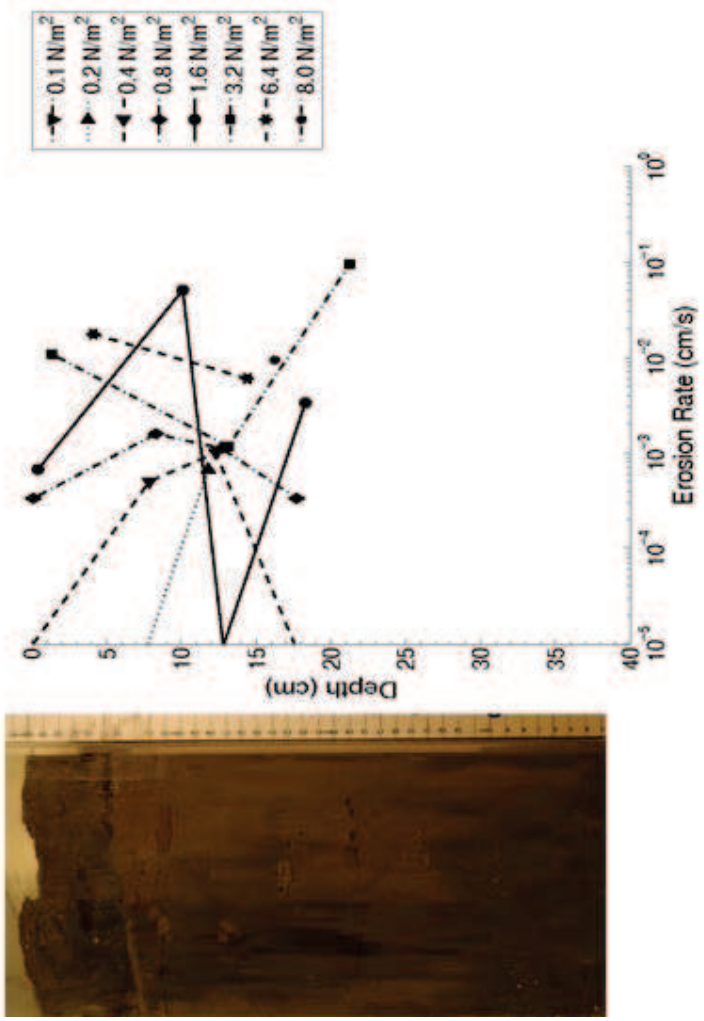

Figure A.3: Bed Sediment Sample (Core 2) Taken in Upper Bay near the Mouth of Big Canyon

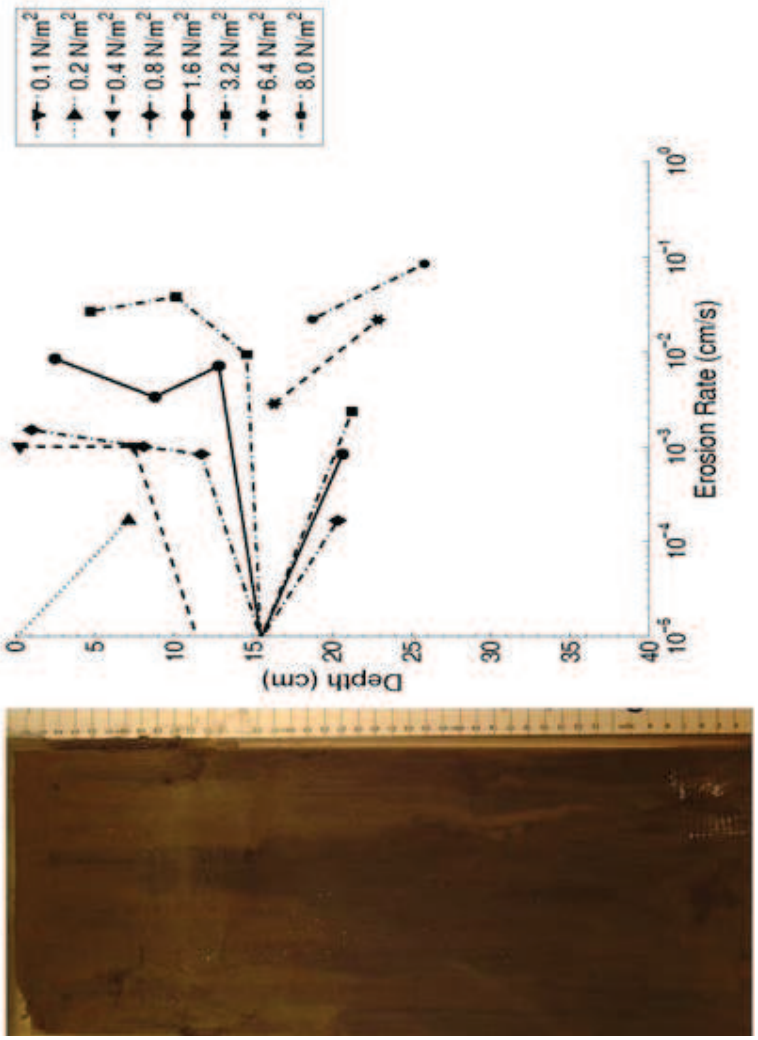

Figure A.4: Bed Sediment Sample (Core 3) Taken at the to of Upper Bay near the outlet of San Diego Creek

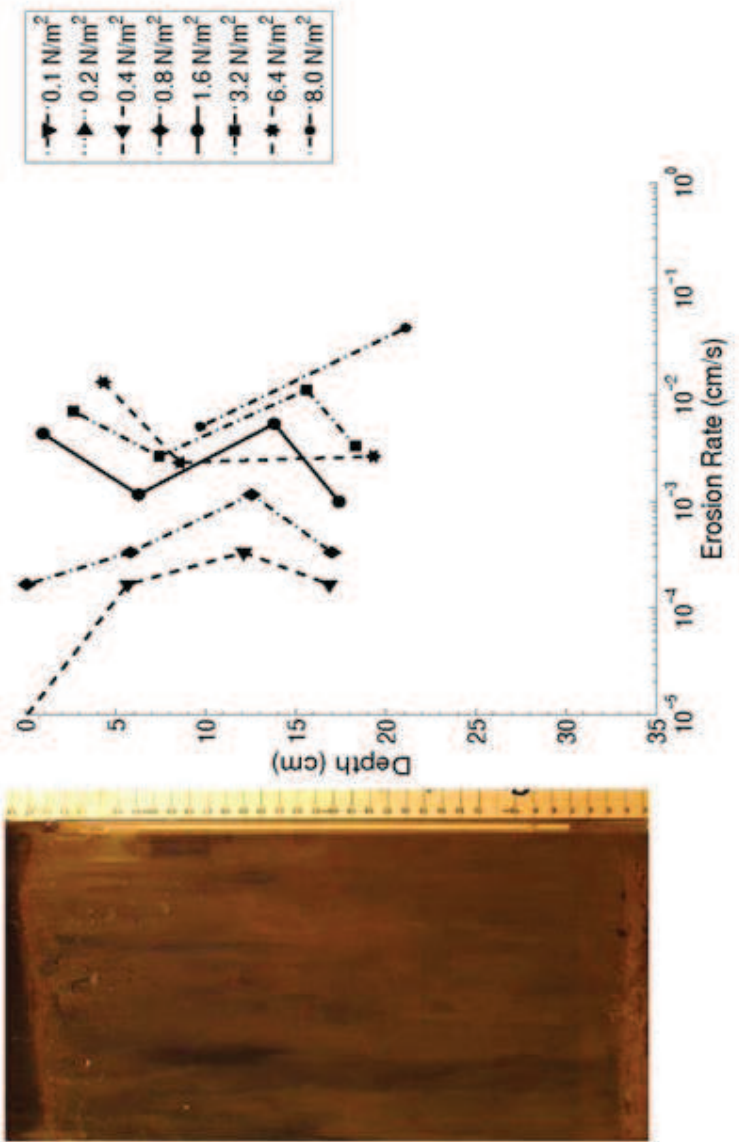

Figure A.5: Bed Sediment Sample (Core 4) Taken in Upper Bay near the Outlet of the Delhi Channel

Methodology for Measuring Erosion Rate and Sediment Bulk Properties

A straight, recirculating flume, located at the Sea Engineering Laboratory in Santa Cruz, California, was used for measuring the erosion rates for each of these undisturbed bed sediment samples as a function of applied shear stress and eroded core depth (see Figure A.6). The recirculating flume method, known at Sedflume (Sediment Erosion at Depth Flume), was developed by McNeil *et al.* (1996). The flume has a test section with an open bottom through which a rectangular coring tube (10 cm by 15 cm) containing a bay core sample was attached. The core sample was raised into the test section flume using the hydraulic jack until the sediment surface was even with the bottom of the flume channel. A measurement was then made of the core length. The flume was then run at a specific flow rate corresponding to a particular shear stress. As the sediment eroded from the surface of the core, the piston inside the core was raised to keep the sediment sample flush with the flume bed. Erosion rates were obtained by measuring the core length at different time intervals, taking the difference between each successive measurement, and dividing by the time interval:

$$E = \frac{\delta z}{T} \tag{A-1}$$

where E the rate of erosion, δ z the depth of core sample eroded, and T the sampling time.

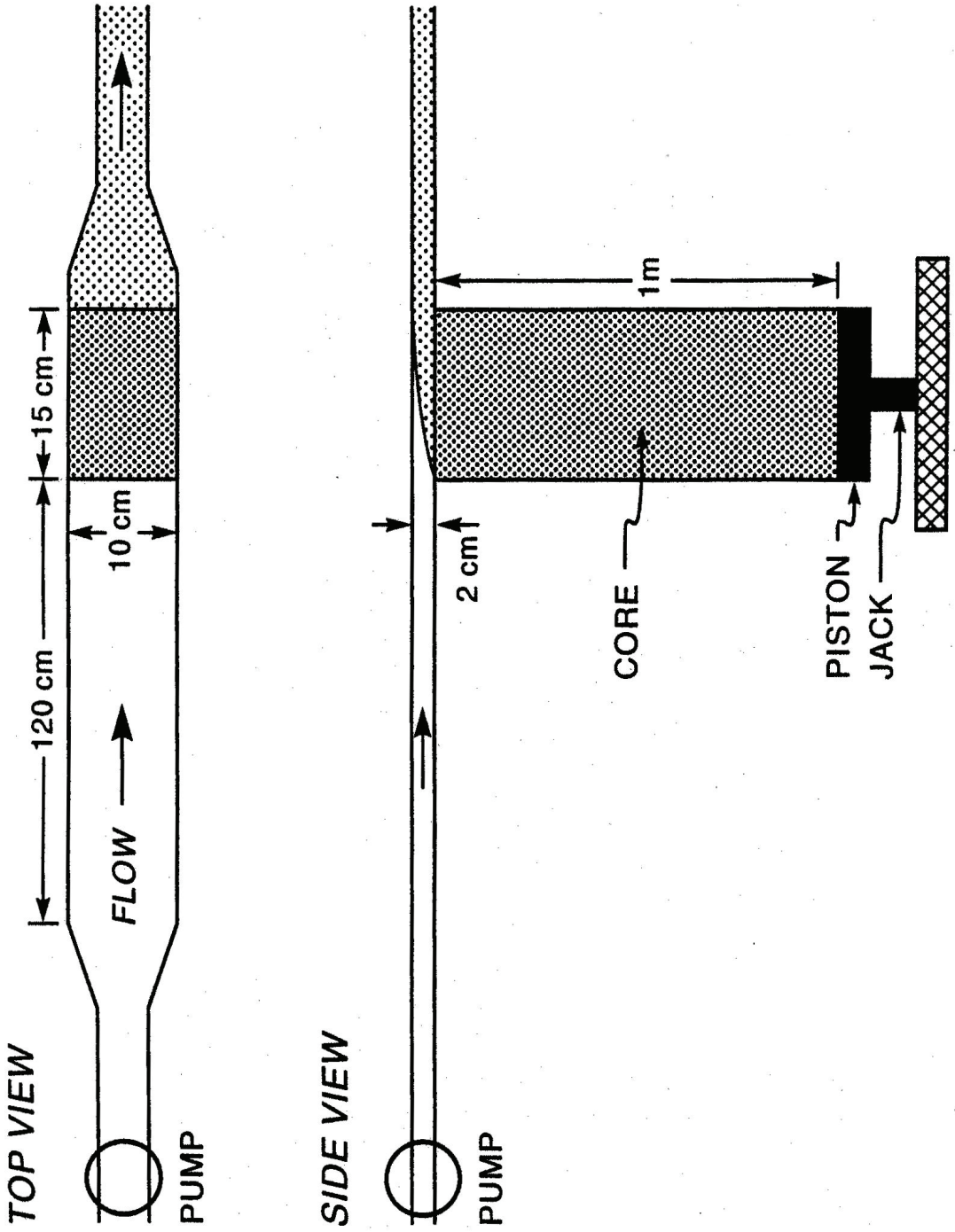

Figure A.6: Sedflume Diagram

In order to measure erosion rates at several different induced shear stresses for each core, the following procedure was used. Starting at a low shear stress, flow rates were increased to generate sequentially higher shear stresses such that each succeeding shear stress was twice the previous one. Generally about four flow rates were run sequentially in one shear cycle. Each flow rate was run for 10 minutes or until no more than 2 cm was eroded for that shear stress. The time interval was recorded for each run with a stopwatch. The flow was then increased to induce the next shear stress, and so on until the highest shear stress was run. This cycle was repeated until all of the sediment had eroded from the core. If after three shear cycles a particular shear stress showed a rate of erosion less than 10^{-4} cm/s, it was dropped from the cycle; if after many cycles the erosion rates decreased significantly, a higher shear stress was included in the cycle.

The critical shear stress of a sediment bed, τ_{cr}, is defined quantitatively as the shear stress at which a very small, but accurately measurable, rate of erosion occurs. This rate of erosion has been practically defined as 10^{-4} cm/s. This represents 1 mm of erosion in approximately 15 minutes. Since it is difficult to measure τ_{cr} exactly at 10^{-4} cm/s, erosion rates were determined above and below 10^{-4} cm/s. The τ_{cr} was then determined by linear interpolation. The technique gives the τ_{cr} with at least a 20% accuracy (McNeil *et al.*, 1996; Roberts *et al.*, 1998).

Each core was also sub-sampled at vertical intervals to determine the water content, bulk density, and particle size distribution of the sediments. Sub-samples were collected from the surface of the cores at the end of each erosion cycle. This procedure

typically allows 5 samples to be collected for analysis for approximately every 5 cm of core depth.

Bulk density was determined by water content analysis using methods outlined in Hakanson and Jansson (2002). This consisted of determining the wet and dry weight of the collected sample to determine the water content, W,

$$W = \frac{M_w - M_d}{M_w} \tag{A-2}$$

W = water content

M_w = wet weight of sample

M_d = dry weight of sample

With water content determined, the bulk density, ρ_b, is calculated:

$$\rho_b = \frac{\rho_w \rho_s}{\rho_w + (\rho_s - \rho_w)W} \tag{A-3}$$

ρ_w = density of water (1 g/cm^3)

ρ_s = density of sediment particle (2.65 g/cm^3)

Particle size distributions were determined using laser diffraction analysis. Samples collected from the core were prepared and inserted into a Beckman Coulter LS13-320. Each sample was analyzed in three 1-minute intervals and the results of the three analyses were averaged. This method is valid for particle sizes between 0.04 and 2000 mm. Any fraction over 2000 mm was weighed and compared to total sample weight to determine the weight percentage greater than 2000 mm. During the analysis no significant fraction over 2000 mm was sampled.

Evaluation of Core Sediment Samples

All samples are heterogeneous with depth with each core having its own character. Table A2 summarizes the results.

Core 1, collected in the harbor near Bay Island, became much stiffer with depth. Beneath a depth of 5 cm, erosion was only observed for applied shear stresses of 3.2 N/m^2 and 6.4 N/m^2, until a slight increase in the erosion rate at the deepest depths (Figure A.2. Critical shear stresses calculated from the erosion rates were low at the surface (0.26 N/m^2) but large at mid-depths (greater than 1.62 N/m^2). At the deepest shear cycle depth, the critical shear stress decreased to 0.82 N/m^2. The bulk densities increased from 1.32 g/cm^3 to 1.59 g/cm^3. The median particle sizes remained in the range of fine silt throughout the core (10.35 μm to 14.99 μm).

For Core 2, collected in Upper Bay downstream of Big Canyon, material stiffness varied greatly with depth. This was reflected in the fluctuating erosion rates with depth (Figure A.3. The critical shear stresses were largest at the surface and deepest shear cycle location (0.52 N/m^2), but smaller at mid-depths (0.24 N/m^2 and 0.12 N/m^2). The bulk densities increased from 1.30 g/cm^3 to 1.86 g/cm^3 before decreasing to a minimum of 1.65 g/cm^3 near the deepest sampling location. The median particle sizes fluctuated with depth as well. The surface value was 17.15 μm, increased to 212.9 μm, decreased to 33.02 μm and increased to 122.6 μm at the deepest sampling depth.

Core 3 was collected in Unit I/III Basin is the northerly-most coring station.

Similar to other cores collected in the upper bay, material stiffness and erosion rates fluctuated with depth (Figure A.4. The critical shear stresses were low near the surface (0.22 N/m^2 and 0.16 N/m^2), increased with depth to 0.45 N/m^2 and 3.31 N/m^2 before decreasing to 0.64 N/m^2. The bulk densities increased with depth from 1.33 g/cm^3 to 1.60 g/cm^3. Conversely, median particle sizes decreased with depth, from 21.90 μm at the surface to 11.19 μm near the deepest sampling location. Particle sizes were all in the range of fine silts.

Core 4, collected near the outfall of the Delhi Channel into Upper Bay, exhibited fluctuating stiffness with depth, but in a more uniform manner than the other Bay cores. The erosion rates decreased slightly beneath the surface, increased slightly at a deeper depth, and decreased again at the deepest shear cycle depth. The critical shear stresses were largest at the surface (0.64 N/m^2) and decreased with depth between 0.26 N/m^2 and 0.32 N/m^2. The bulk densities increased from a surface value of 1.40 g/cm^3 to 1.77 g/cm^3 before decreasing to 1.54 g/cm^3 at the deepest sampling location. The median particle size increased from 47.76 μm to 74.42 μm (the range of silts and very fine sands) before decreasing to 10.64 μm (fine silt) at the deepest sampling location.

Evaluation of Particle Size Distributions

Figure A.7 compares the particle sizes of the top 5 cm layer from each core. The two southerly-most bed samples, Core 1 and Core 2, have similar profiles with a significant amount of fines less than 10 μm. Core 2 has larger volume fractions of

particles larger than 60 μm. Core 4, located near the outlet of the Santa Ana-Delhi Channel into Newport Bay, has significantly less fines with the peak volume fraction at about 200 μm. The northerly-most core, Core 3, has more fine sediment fractions than Core 4 (and similar to Cores 1 and 2), but a larger volume fraction of the large diameter particles. It is interesting to note that almost each core sample has local maximum sediment volume fractions near 5.6 μm, 18 μm, 40 μm, 150 μm, and 410 μm. Table A3 shows the percentages of clays (<2 μm), fine sediments (<63 μm), and coarser materials, e.g., sands and gravels for each of the four core samples. There are higher percentages of clays and fine sediment in the downstream samples (Cores 1 and 2).

Figure A.8 compares the particles sizes for each of the cores at depths of 5 to 10 cm. Core 1 has substantially more fines than any of the other cores. Cores 2 and 4 have somewhat sediment distributions with Core 2 having a peak volume fraction at 340 μm and Core 4 a peak at 177 μm.

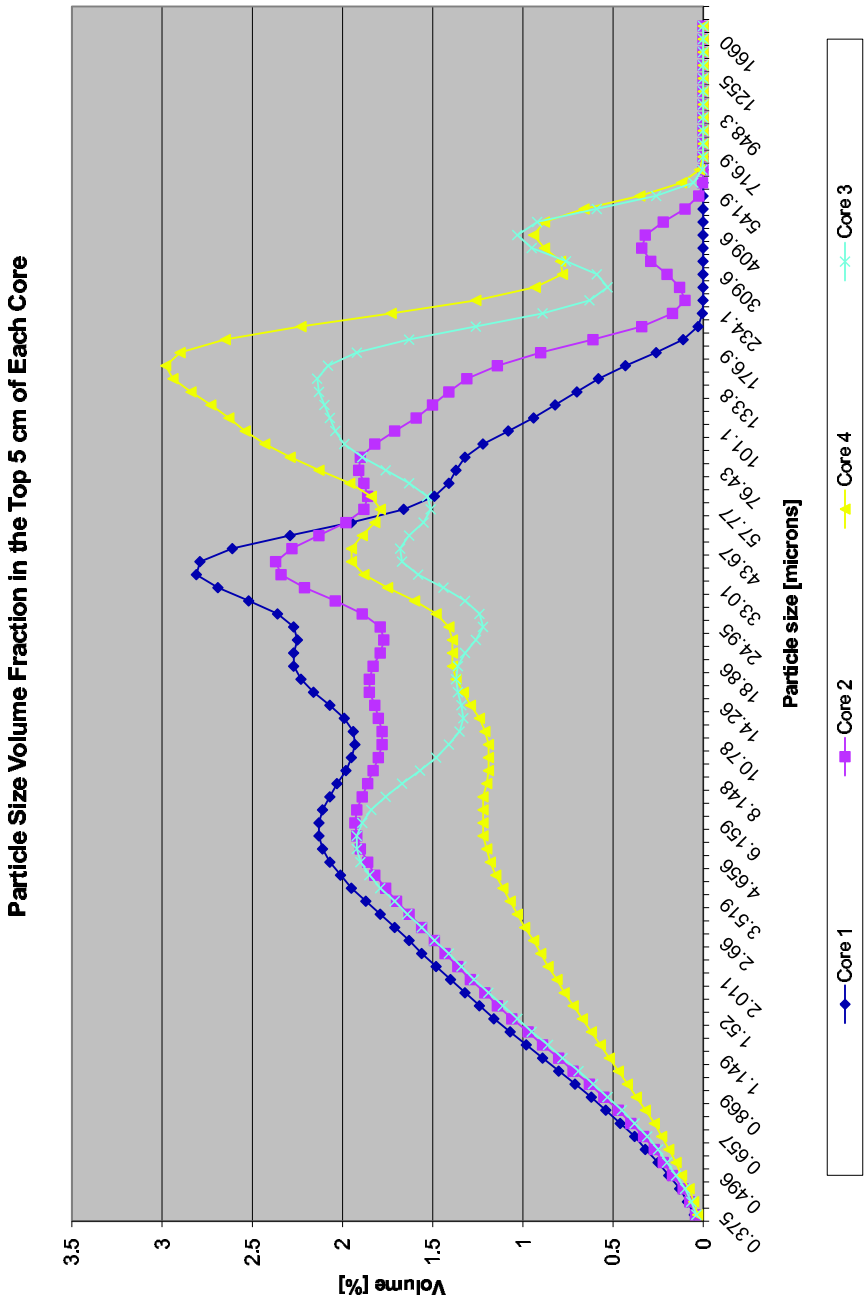

Figure A.7: Volume fraction of sediment sizes in the top 5 cm of each core.

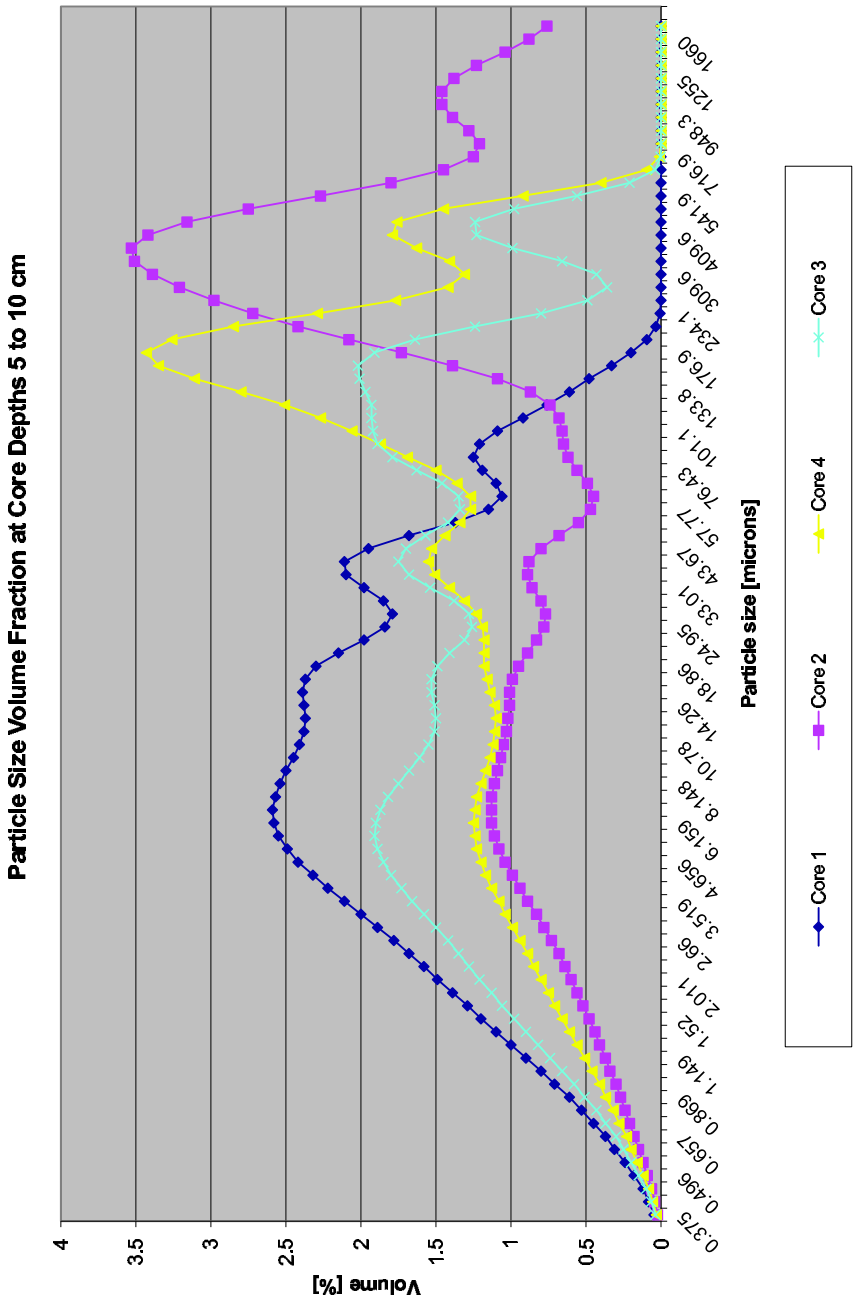

Figure A.8: Volume fraction of sediment sizes at depths 5 cm to 10 cm below surface of the bed sediment.

Core-1 Depth [cm]	D50 [μm]	ρ_b [g/cm^3]	τ_{cr} [N/m^2]
0	13.6	1.32	0.26
5.4	10.35	1.44	1.79
10.5	12.49	1.42	1.76
15.3	12.77	1.42	1.62
35	14.99	1.59	0.82
Mean	12.84	1.44	1.25
Core-2 (Big Canyon) Depth [cm]	D50 [μm]	ρ_b [g/cm^3]	τ_{cr} [N/m^2]
0	17.15	1.3	0.52
6.9	212.9	1.86	0.24
11.6	83.09	1.83	0.12
17.2	33.02	1.65	0.52
23.7	122.6	1.71	n/a
Mean	93.75	1.67	0.35
Core-4 (Narrows) Depth [cm]	D50 [μm]	ρ_b [g/cm^3]	τ_{cr} [N/m^2]
0	21.9	1.33	0.22
6.5	21.13	1.5	0.16
11.3	16.58	1.55	0.45
15.5	11.19	1.53	3.31
20.3	13.09	1.6	0.64
Mean	16.78	1.5	0.96
Core-3 (Unit I/III) Depth [cm]	D50 [μm]	ρ_b [g/cm^3]	τ_{cr} [N/m^2]
0	47.76	1.4	0.64
5.4	61.73	1.77	0.32
11.3	74.42	1.75	0.26
15.6	10.9	1.55	0.32
22.5	10.64	1.54	n/a
Mean	41.09	1.6	0.39

Table A2: Sediment Properties for the Four Cores.

	Clays [%]	Fine Sediment [%]	Coarser Sediment [%]
Core 1	11.2	77.0	11.8
Core 2	10.1	68.1	21.8
Core 4	6.6	49.0	44.4
Core 3	9.7	56.9	33.4

Table A3: Percentages of sediment size classes.